Preface

This Master of Science thesis is written as the conclusion of my study at the Faculty of Civil Engineering of Delft University. The research was carried out by order of the Hydraulic engineering section and Van Oord NV. The experiments that were conducted in the scope of my thesis were carried out in the Laboratory of Fluid Mechanics of Delft University of Technology.

Readers of this thesis who are mostly interested in the observations and conclusions of the experiment are referred to chapter 6. An overview of the research available regarding near-bed structures can be found in chapter 3.

During the process of writing my thesis I was supported by many people who gave helpful advise and practical assistance. I would like to express gratitude towards Mr. Verhagen, Mr. Fontijn and Mr. Stive from the Faculty of Civil Engineering and Mr. Stam from Van Oord for their guidance and support during the project. Also I would like to thank Mr. Van Gelderen and Mr. Smith from Van Oord who originally guided me in the initial phase of my research. Finally, I would like to thank the staff members of the laboratory for their assistance in building up the experiment and the measuring facilities.

Wouter Saers, November, 2004

Abstract

Most design methods in use today are based on a so-called critical shear stress applied on the stones derived from the water velocity. In practice the stones commonly are not allowed to move under design conditions. The question is whether or not a more optimal design method is possible.

A hypothesis is that when a structure deforms due to erosion it becomes stable after some time for a constant hydraulic load. With this hypothesis in mind and when some erosion is allowed a more optimal design is possible. This method can apply for rubble mound near-bed-structures (e.g. a pipeline cover) where erosion can be allowed but the functionality must remain. This implicates a need for erosion prediction for these structures.

The objective of this thesis is to investigate the deformation behaviour of near-bed structures under a long period of irregular waves and what aspects control this behaviour. An ultimate objective is to produce a rule or model to predict the deformation of such a near-bed structure. Only waves are considered in this thesis, steady currents are disregarded.

For this investigation the complex process of erosion of near bed structures under irregular waves was simulated with physical model tests. In the tests two aspects were examined for different hydraulic conditions: the influence of the number of waves and secondly, the influence of the initial structure height on the deformation. For all tests it was tried to create comparable wave conditions with similar shaped Jonswap spectra that describe the wave conditions.

The structure deformation (which could be seen in the physical model tests) is considered to be a function of dimensionless parameters describing the wave load, its duration (represented by the number of waves) and the structure geometry (represented by the initial structure height). As the structure is relatively low compared to the water depth, the flow is assumed to horizontally attacking the structure. The contraction of the flow lines at the structure slope is seen as the main cause for higher velocities at the structure crest. Compared to a larger initial structure height for equal slope angles this effect will be stronger and more erosion can be expected for the same wave field.

Two approaches, based on the results of the physical model tests, are used for the deformation prediction:

- 1. The eroded area from a profile was considered to be dependent of a mobility parameter based on a with linear wave theory derived velocity. The structure height was incorporated in the derived velocity; higher structures simulated larger velocities. It is shown that a logarithmical incorporation of the number of waves has better results for these tests than a square root function. The approach resulted in a prediction formula similar to the near-bed-structures erosion formula by Van Gent and Wallast (2001) but with a logarithmic incorporation of the number of waves.
- 2. The deformation is expressed in a relative structure height. The eroded area is related to the initial structure height; higher structures predict more absolute erosion. The relative structure height is expressed directly against the number

of waves for different values of the mobility parameter (a mobility parameter similar to the first approach but representing only the wave conditions).

For both approaches the test data for the lowest structures tested showed relatively minor erosion despite the way the initial structure height was incorporated. A dimensionless threshold value for the ratio of the slope length and the orbital wave motion, describing the extent of flow contraction, is suggested.

For a design method where erosion is allowed the first approach seems to have a better accuracy. Still a conservative margin is advisable for use in practice. In general more tests are needed, especially for the second approach with the relative structure height.

Table of contents

| PREF | ACE | l |
|----------------|---------------------------------------------------------|-----|
| ABST | RACT | I |
| TABL | E OF CONTENTS | IV |
| LIST | OF FIGURES | VI |
| | OF SYMBOLS | |
| 1 II | NTRODUCTION | 1 |
| 1.1 | Background | 1 |
| 1.2 | Subject analysis | |
| 1.3 | Objective | |
| 1.4 | General approach | |
| 1.5 | Outline | |
| | ~ | |
| 2 V | VATER PARTICLE VELOCITY AND STONE MOTION | V 7 |
| 2.1 | Wave Theory | 7 |
| 2.1.1 | Linear Wave Theory | 7 |
| 2.1.2 2.1.3 | ϵ | |
| 2.1.3 | boundary layer under waves | 14 |
| 2.2 | Forces on stones | |
| 2.2.1 2.2.2 | | |
| 2.2.2 | | |
| 2.3 | Initiation of motion or critical shear stress | 19 |
| 2.3.1 2.3.2 | | |
| 2.3.2 | initiation of motion under waves | 41 |
| 2.4 | Stone transport | |
| 2.4.1 2.4.2 | | |
| 2.4.2 | - T | |
| | | |
| 3 N | NEAR-BED STRUCTURES | 28 |
| 3.1 | Design aspects | 28 |
| 3.1.1 | Functions of near-bed structures | 28 |
| 3.1.2 3.1.3 | | |
| 3.1.3 | | |
| | - | |
| 3.2 | Predicting deformation of near-bed structures | 34 |
| 3.3 | Investigations on near-bed structures | |
| 3.3.1 | $\boldsymbol{\varepsilon}$ | |
| 3.3.2 | Explicit influence of wave load duration on deformation | |

| 4 P | HYSICAL MODEL TESTS | 44 |
|-------|--------------------------------------------------|-------------|
| 4.1 | Introduction | 4 4 |
| 4.1.1 | | |
| 4.1.2 | Parameters | 46 |
| 4.1.3 | Aspects of research | 47 |
| 4.2 | Model tests set-up | 48 |
| 4.2.1 | Granular material | |
| 4.2.2 | | |
| 4.2.3 | Test scheme | 53 |
| 4.3 | Measurements | 55 |
| 4.3.1 | Instruments | 55 |
| 4.3.2 | | |
| 4.3.3 | | |
| 4.3.4 | Additional observations | 62 |
| 1.4 | Accuracy of the measurements | 64 |
| 4.5 | Evaluation | 67 |
| | | . (0 |
| 5 A | NALYSIS OF THE EXPERIMENTS | 08 |
| 5.1 | Dimensional analysis | |
| 5.1.1 | 1 | |
| 5.1.2 | Dimensionless boundary conditions | 70 |
| 5.2 | Non-dimensional prediction parameters | |
| 5.2.1 | T - J | 72 |
| 5.2.2 | J 1 | |
| 5.2.3 | Incorporation of the initial structure height | 75 |
| 5.3 | Deformation prediction | 80 |
| 5.3.1 | | 82 |
| 5.3.2 | | |
| 5.3.3 | | |
| 5.3.4 | Example calculations based on the two approaches | 98 |
| 5.4 | Evaluation of deformation | |
| 5.4.1 | | |
| 5.4.2 | E | |
| 5.4.3 | Final remarks | 105 |
| 6 C | CONCLUSIONS AND RECOMMENDATIONS | 106 |
| 5.1 | Conclusions | 107 |
| 6.2 | Recommendations | 108 |
| | | |
| RFFF | FRENCES | 110 |

| APPENDIX A | : FLOW REGIME AND CRITICAL SHEAR STRESS. | 112 |
|--------------|------------------------------------------|-----|
| Flow regin | nes under waves | 112 |
| Critical sho | ear stress under waves | 113 |
| APPENDIX B | : TABLES OF THE PARAMETERS OF THE TESTS | 114 |
| APPENDIX C | : MEASURED HYDRAULIC CONDITIONS | 117 |
| Wave spec | tra | 117 |
| Wave exce | edance curves | 120 |
| APPENDIX D | : DATA GRANULAR MATERIAL | 124 |
| Rock gradi | ing | 124 |
| Rock densi | ity | 125 |
| Rock shape | e | 125 |
| APPENDIX E | : MEASURED DAMAGE PROFILES | 127 |
| APPENDIX F | PROVO ERROR ANALYSIS | 136 |
| PROVO pi | recision | 136 |
| Profile con | nparison accuracy | 137 |
| Carriage s | peed estimation | 138 |
| APPENDIX G | : EROSION AND RELATIVE HEIGHT IN TIME | 140 |
| APPENDIX H | : MATLAR SCRIPT LISTINGS | 149 |

List of figures

| Figure 1-1. Orbital motions: shallow/transitional water (A) and deep water (B) | 2 |
|---------------------------------------------------------------------------------------------------------------------------------------------|-------|
| | 3 |
| Figure 1-2. Comparison of current and wave velocity profiles. | 0 |
| Figure 2-3. Definitions linear wave theory | ð |
| Figure 2-4. Validity of wave theories (LeMéhauté, 1976; see Schiereck, 2001) | |
| Figure 2-5. Application of linear wave theory for bottom velocities (on a mild slope outside the limits of velidity (Schieragh et al. 1994) | - |
| | .11 |
| Figure 2-6. A wave signal in time, with registration of zero-down crossings and a defined wave height (H) in between | .12 |
| 8 () | . 1 4 |
| Figure 2-7. Normalized standard variance density spectra (equal area and peak frequency) | .14 |
| Figure 2-8. Horizontal velocity profile under a wave with rotational flow in the | . 14 |
| boundary layer (a). Horizontal velocity profiles for short waves at various phases in | |
| wave cycle (b). | |
| Figure 2-9. Forces on a stone due to a current | |
| Figure 2-10. Shields curve for steady flow | |
| Figure 2-11. Different levels of stability for the initiation of motion for bed material | |
| (Delft Hydraulics, 1972) | |
| Figure 2-12. Modified Shields curve for unsteady flow (Sleath, 1978) | 23 |
| Figure 3-13. A pipeline rock cover protection with a 50-200 mm rock grading (CUF | |
| | .28 |
| Figure 3-14 Standard fine grading classes by the Dutch standard NEN 5180 | |
| Figure 3-15 Example of a relation between wave height and return period based on | |
| | .32 |
| Figure 3-16. General construction methods for dumping rock; using a crane (a), side | e |
| stone dumping (b), using a split barge (c) or a fall pipe (d) | |
| Figure 3-17. Definition sketch of a deformed near-bed structure after erosion | |
| Figure 3-18 Damage of rubble mound structures in time (CUR report 169,2000) | .39 |
| Figure 3-19. Exponent b as a function of damage percentage, S_{1000}^* (Klomp and | |
| Lomonaco, 1995) | .41 |
| Figure 3-20. Deformation of a near bed structure under regular waves (Levit et al., | |
| 1997). The deformation slows down for increasing time as the 5 consecutive stages | |
| | .42 |
| Figure 3-21. Top two lines; measured and predicted (dotted line) damage for waves | , |
| only (Levit et al.,1997) | .42 |
| Figure 4-22 Side view on the flume with in detail a schematic representation of a | |
| structure | |
| Figure 4-23. Photos of the flume; left the flume, right the section where the structure | |
| were measured. | |
| Figure 4-24. Structure crest: the shape of the stones can be considered as 'irregular' | |
| material. | |
| Figure 4-25. Sieve curve of the material used for the tests. | |
| Figure 4-26. The water depth h[m] and wave height Hs [m] combination for each te | |
| code. The last digit represents the initial structure height h_c in cm | |
| Figure 4-27 Top view of 5 Provo lines. | .57 |
| Figure 4-28. 3-D view with 2 Provo lines and the reference bar. | .58 |

| Figure 4-29. The profile measurement of test 1a6 with five Provo lines; the red line | |
|----------------------------------------------------------------------------------------------------|------------|
| the profile after the last wave series. Below, on the right side, the relative eroded are | |
| $(A_0-A_e)/A_0$ is presented against the number of waves for each parallel Provo line | |
| Figure 4-30. A tested structure: on the left the structure before waves. Top right: aft | |
| 1000 waves. Down right: after 3000 waves | |
| Figure 4-31. PROVO probe measuring the structure profile. | |
| Figure 5-32. Test data with respect to S relatively to N=1000. Further a square root | |
| function ($\sqrt{N}/\sqrt{1000}$) and a logarithmic function ($\log N/\log 1000$) are shown to | |
| illustrate the trend. | |
| Figure 5-33. Example of the shape of the horizontal velocity components under the | |
| wave crest at the location of a near-bed structure. | .77 |
| Figure 5-34. Effect of the structure height on the water velocity at the crest with | |
| contracting streamlines of water particles during half a wave cycle. | |
| Figure 5-35. Test data with mobility parameter versus erosion parameter compared | |
| with the Van Gent and Wallast formula (blue line and after conversion from T _m to | |
| T _p) | |
| Figure 5-36. Graphs with θ_c on the horizontal axis and the parameter S/\sqrt{N} on the | e |
| vertical axis. The prediction formula in equation 5.10 is shown as a blue line | .84 |
| Figure 5-37. Graphs with θ_c versus S/logN for different number of waves and initial | 1 |
| structure heights. The prediction formula in equation 5.10 is shown as a blue line | .85 |
| Figure 5-38. The mobility parameter θ_c versus S/logN with a line fitted through the | . |
| maximal measured erosion data | |
| Figure 5-39. Procedure used to obtain the structure height after erosion (h_c) based of | |
| the eroded area (A_e) in a profile. | |
| - | |
| Figure 5-40. The measured test data expressed with the number of waves versus the relative height. | ; ວດ |
| Figure 5-41. Mobility level of 3c# with a line fitted through 3c5 and 3c6. | |
| Figure 5-42. Mobility level of 2b# and 1b# with a line fitted through 2b5 and 2b6. | |
| | .91 .91 |
| Figure 5-44. Lines fitted through the data representing different mobility values | |
| Figure 5-45. Accuracy of the tests with the erosion parameter approach | |
| Figure 5-46 Accuracy of the tests with the relative structure height approach | |
| Figure 5-47. Orbital motion compared with the structure slope length | |
| 1 15are 5 17. Orottal motion compared with the structure stope length | LUT |

List of symbols

| Symbol | Definition | |
|-----------------------------|--------------------------------------------------------------------------|--|
| \hat{a}_b | amplitude of horizontal water motion at the bottom [m] | |
| \hat{a}_{δ} | amplitude of horizontal water motion near the bottom [m] | |
| A_0 | initial profile area [m ²⁰] | |
| A_{e} | eroded profile area [m ²] | |
| b | exponent [-] | |
| B_c | structure profile crest length [m] | |
| C_D | drag coefficient [-] | |
| C_L | lift coefficient [-] | |
| C_{S} | shear coefficient [-] | |
| C_1 | coefficient [-] | |
| C_2 | coefficient [-] | |
| D | stone diameter [-] | |
| D_{50} | stone size | |
| D_* | dimensionless stone diameter $\left(\Delta g/v^2\right)^{1/3}D_{50}$ [-] | |
| D_{n50} | median nominal diameter $(=(W_{50}/g\rho_s)^{1/3})$ [m] | |
| $E_{\scriptscriptstyle PM}$ | spectrum shape defined by Pierson and Moskowitz [-] | |
| E | 1. spectrum variance density [m ² s] | |
| | 2. deformation parameter [-] | |
| f_m | JONSWAP scale parameter [-] | |
| f_w | friction factor by Jonsson [-] | |
| f | 1. friction coefficient between materials [-] | |
| | 2. wave frequency $(=1/t)$ [s ⁻¹] | |
| F_{D} | drag force on a stone [n] | |
| F_{L} | lift force on a stone [n] | |
| $F_{\scriptscriptstyle S}$ | shear force on a stone [n] | |
| g | gravitational acceleration [m/s ²] | |
| h | water depth [m] | |
| h_c | initial structure profile crest height [m] | |
| $h_c^{'}$ | structure profile crest height after erosion A_e [m] | |
| H | wave height [m] | |
| $H_{\scriptscriptstyle b}$ | wave height when breaking occurs [m] | |
| H_s | significant wave height (average height of 33% highest waves) [m] | |
| i_b | unity vector component in direction of bed slope [-] | |

```
bed roughness [m]
k_{s}
                wave number (2\pi/l) [m<sup>-1</sup>]
k
\boldsymbol{L}
                wavelength [m]
                structure profile bottom length [m]
L_{c}
                area beneath the energy spectrum curve [m<sup>2</sup>]
m_0
                slope angle (= inv \tan \alpha) [-]
                number of waves [-]
N
                stability number [-]
N_{\varsigma}
                volume of transport per unit width and per unit time [m<sup>3</sup>/m/s]
q_s
                critical volume of transport for design aspects [m<sup>3</sup>/m/s]
q_{s,cr}
                volume of transported bed material for a half wave period [m<sup>3</sup>/m/s]
q_{s,1/2}
                Reynolds number [-]
Re
                particle Reynolds number [-]
Re.
                wave steepness (=H/L) [-]
S
                wave steepness for deep water wave length (=2\pi H_s/gT_p^2) [-]
S_{op}
S
                erosion parameter [-]
                shape factor [-], for rubble mound rock: s_f \approx 0.6
S_f
                erosion after n waves [-]
S_N
                time [s]
                wave period (with the frequency f = 1/T) [s]
T
                mean wave period in a wave spectrum [s]
T_{m}
T_{p}
                peak wave period in a wave spectrum [s]
                steady current velocity [m/s]
и
                maximum horizontal velocity at the bottom [m/s]
\hat{u}_h
                peak velocity near the bed [m/s]
\hat{u}_{\delta}
                characteristic peak velocity based on a structure crest height [m/s]
\hat{u}_{\delta c}
                shear velocity [m/s]
u_*
                critical shear velocity [m/s]
u_{*_{cr}}
                stone volume [m<sup>3</sup>]
V
                stone gradation width [-]
W
                median stone weight [n]
W_{50}
                stone weight [n]
W_{\varsigma}
                horizontal coordinate [m]
х
                vertical coordinate [m]
Z.
                1. JONSWAP scale parameter [-]
\alpha
                2. structure slope angle [-]
γ
                1. JONSWAP peak enhancement function [-]
```

```
2. sediments natural angle of repose [-]
                 shape parameter with an average value in JONSWAP of 3.3 [-]
\gamma_0
δ
                 boundary layer thickness [m]
                 relative stone weight [-]
Δ
                 Von Karman constant (\approx 0.4) [-]
K
                 mobility parameter [-]
\theta
                 mobility parameter that includes the initial crest level [-]
\theta_{c}
                 wave direction [rad]
Θ
                 kinematic viscosity [m<sup>2</sup>/s]
ν
                 water density [kg/m<sup>3</sup>]
\rho_{\scriptscriptstyle w}
                 stone density [kg/m<sup>3</sup>]
\rho_{\rm s}
                 shape parameter with an average value in JONSWAP of 0.07 [-]
\sigma_{a}
                 shape parameter with an average value in JONSWAP of 0.09 [-]
\sigma_{b}
                 shear stress on grains on the bed [n/m^2]
\tau_{\scriptscriptstyle b}
                 critical shear stress [n/m<sup>2</sup>]
\tau_{b.cr}
                 maximum shear stress under oscillatory flow [n/m<sup>2</sup>]
\hat{	au}_{\scriptscriptstyle w}
                 critical maximum shear stress under oscillatory flow [n/m<sup>2</sup>]
\hat{	au}_{w,cr}
                 transport parameter [-]
                 transport parameter for half wave period [-]
\pmb{\phi}_{halfperiod}
W
                 mobility parameter [-]
                 Shields-parameter [-]
\psi_{cr}
                 critical mobility parameter for waves [-]
\psi_{w.cr}
                 Shields-parameter for generalized transport [-]
\psi_*
                 angular frequency of the wave (2\pi/T) [s<sup>-1</sup>]
ω
                 Proportional to [-]
```

1 Introduction

1.1 Background

Rubble mound rock is commonly used to protect offshore pipelines or sewage outfalls against damage caused by dragging fishing nets and anchors or as ballast to stabilise the pipeline. Depending on the construction method and water depth the rubble mound is placed on the sea-bed with a certain precision.

When using a fall-pipe vessel (see section 3.1.3), a large accuracy of rock placement, at a water depth of 20 meters or deeper, can be achieved but the stone size that can be placed is limited; the transport process on board of the fall pipe vessel only allows a certain rock weight to pass. There is a need to know what the limit is in water depth so that this stone size still can be used in a sound way with regard to the hydraulic conditions.

Cost effectiveness

Rubble mound rock structures can be designed conservatively meaning that there is no motion allowed for the rock. For cost effectiveness this might not be the most optimal design. For the use of rubble mound rock it is important to use the right size; not too small which causes a large amount of erosion and the pipeline looses its cover, not too large as this is much more costly and the construction method might be very costly. When the functionality of the structure is maintained, a certain extent of erosion can be allowed. When this approach is used, the prediction of the extent of the erosion is important. An optimal stone size for certain environmental conditions can be evaluated when the erosion behaviour of the rubble mound rock in a protection structure can be predicted. The erosion prediction can be combined with possibly more cost effective maintenance programs.

Transitional water depth

There is a specific need for erosion prediction in the "transitional water depth" zone. This zone can be specified as where (wind generated) waves feel the bottom and may influence erosion. Also a flow due to the tide can be felt. This investigation excludes breaking of waves as would be the case for a rubble mound shore protection. Also erosion prediction for deep water conditions, where wind generated waves hardly feel the bottom and tidal flow is dominant, are disregarded in this thesis. A typical case for transitional water depth is the relative shallow North Sea. When a storm occurs the waves will feel the bottom without severe breaking.

The hydraulic circumstances at the bottom depend on the wave characteristics and the water depth. There is a need to know to what depth a certain stone grading still can protect the structure, or what stone grading is needed for a certain water depth.

1.2 Subject analysis

In coastal engineering submerged rubble mounds can be subdivided into 1) low-crested structures and 2) near-bed structures of which the crest is relatively low such that occasional wave breaking does not have a significant influence (Van Gent and Wallast, 2001). This thesis will treat near-bed structures.

The type of hydraulic conditions that are investigated in this thesis regarding near-bed structures are defined as transitional water depth conditions. This means that, differing from the case with short waves; the waves passing the near-bed structures feel the bottom. On the other hand the wind waves that attack a near-bed structure cannot be seen as long waves as a clear orbital motion is still present. The aspect of waves feeling the bottom is shown in Figure 1-1. The transitional water depth condition is dependent on the ratio between the water depth and the wave length (defined in Table 2-1 in chapter 2).

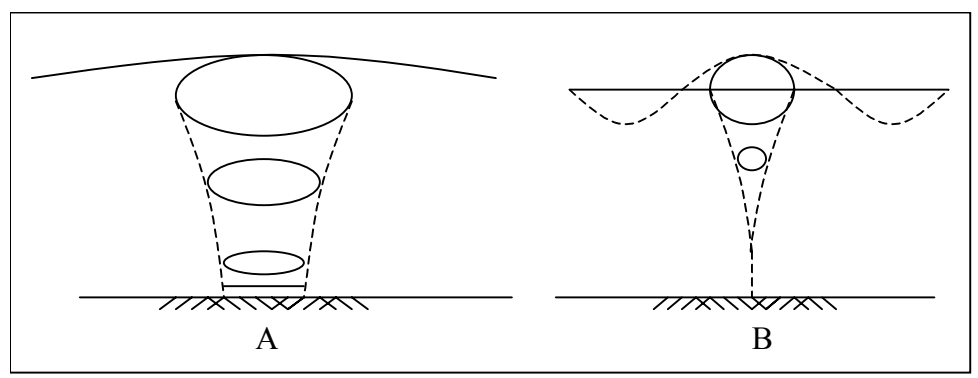


Figure 1-1. Orbital motions: shallow/transitional water (A) and deep water (B).

Contrary to breakwater stability analysis, the stability of rock with regard to near-bed structures deals with different processes. The waves passing a near-bed structure do not break in the way that a wave will break on the shore or at a breakwater. The occasional breaking or 'white capping' offshore on the water level above a near-bed structure will not influence the orbital velocities around the structure on the seabed.

Type of hydraulic load

For this investigation on near-bed structures can be chosen for:

- 1. A combination of quasi-steady current (tidal flow) and the orbital motion of waves feeling the bottom on one side.
- 2. Erosion of near-bed structures under non-breaking irregular waves only. Both flow types are schematically shown for a transitional water depth situation in Figure 1-2.

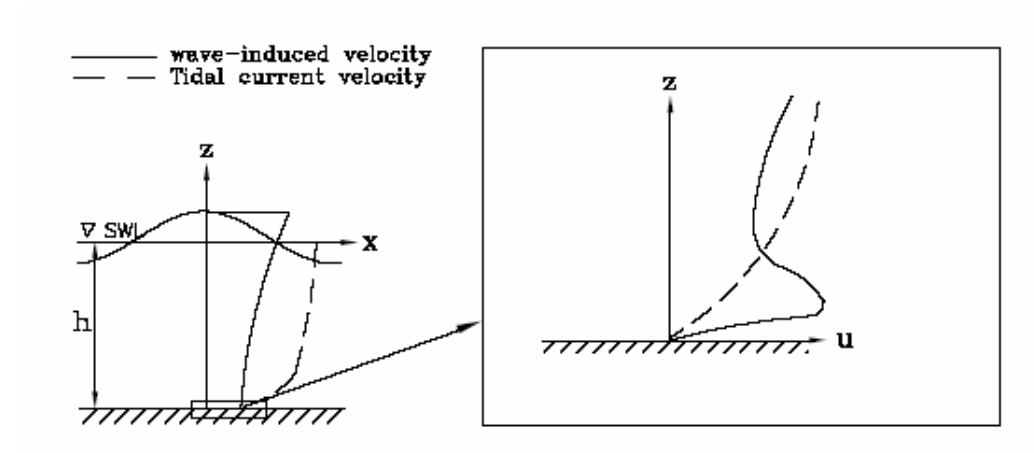


Figure 1-2. Comparison of current and wave velocity profiles.

In the research that has been done regarding a near-bed structures loaded with waves as well as a combination of waves and a superimposed current, it seems that the addition of a current does not show more erosion or reshaping of the structure:

- Klomp and Lomonaco (1995) conclude that the damage under combined current and waves is equal or even less compared to the damage found for waves only. A satisfactory explanation was not found. In 1997 Klomp and Lomonaco also found less damage with a superimposed current and they observed that the current made the waves less steep and smaller.
- By Levit et al. (1997) a model was used to find bed shear stresses with a
 derived velocity for waves with currents and waves alone. The model in the
 situation with waves alone was subject to larger peak bed shear stresses.
 However, the question why a model is unstable under waves and stable under
 waves and currents remained unanswered.
- Van Gent and Wallast (2001) found with a prediction method investigation that the erosion caused by the added current didn't result in a more accurate erosion prediction compared to waves alone.

The investigations mentioned above concerned near-bed structures such as pipeline covers, when the currents are not very strong and are never greater than the maximal orbital motion caused by waves. Only the wave load will be taken into account for this investigation. As for relatively low currents there doesn't seem to be a significant influence or more instability with regard to near-bed structures.

Dynamic stability

Specific parameters like the duration of a storm (represented by the number of waves) and the near-bed structure geometry are not very explicit in the used stability relations.

A rubble mound structure will strengthen itself during the first couple of waves when stones that have an unstable position will find a more stable one. Question is: how will the strengthening of an eroding near-bed structure proceed in time under

continuing hydraulic load? Is an equilibrium profile possible after erosion, where movement of stones can occur but the structure as a whole keeps its shape? A hypothesis that can be made is that a profile can reshape and reach, after a certain number of (irregular) waves, a situation where there still can be some stones moving back and fro but with a negligible deformation of the near-bed structure as a whole. So the situation changes from generally moving stones (back and fro) to a situation with no replacing stones or only occasionally replacement of stones. The latter situation can be defined as a dynamic stable situation. The hypothesis is based on the growing resistance against deformation in a period of (wave) load caused by the reshaped structure as a whole and the repositioned stones. For the design of a near-bed structure deformation can be allowed as long as the functionality remains. When the reshaping of the structure occurs within the boundaries of functionality, a more optimal design is possible.

1.3 Objective

This thesis targets the area between initiation of motion and transport of the rock resulting in failure of the functionality of near-bed structures such as pipeline covers or sewage outfalls. When a near-bed structure is subjected to a wave load, which causes erosion, a distorted profile will develop. Continuing wave load resulting in further erosion can affect the functionality of the structure.

Key question is: how will a geometrically defined rubble mound near-bed structure erode or under the influence of non-breaking irregular waves?

With 'geometrically defined' a specific situation of shape and stone size of a near-bed structure that is used for e.g. pipeline covers is meant. The erosion of a near-bed structure is investigated with the boundary condition that the wave load must be larger than the load causing the initiation of motion of the stones in a near-bed structure. If the erosion is expressed in the height of a near-bed structure, one can predict that the decreasing erosion in time will affect the height of the structure, which is the most important parameter as far as the functionality is concerned. When for example a pipeline cover is evaluated, the criterion will be a certain height of stones above the pipeline (cover to top of pipe).

The general objective of this thesis is: to investigate the deformation behaviour of near-bed structures under a long period of irregular waves and what aspects control this behaviour.

An ultimate objective is to produce a rule or model to predict the deformation of such a near-bed structure

1.4 General approach

How will the aspects brought forward in the subject analysis be studied? Several methods of investigation are possible: proto type measurements, physical modelling and numerical modelling with theoretical study.

Proto type measurements

With proto type measurements (e.g. measuring the erosion of a pipeline cover real time in the North Sea) the continuous measurement of the hydraulic conditions in (a period of) time is meant. Measuring local currents along the structure during a storm when stones could (start to) move and/or be transported. The hydraulic conditions measured can be linked to the hydraulic conditions to a response of the structure profile.

The measurements can or must take a long period of time because the hydraulic circumstances can't be influenced. One has to wait for a certain storm condition. Vidal et al. (2002) performed prototype erosion measurements on a near-bed structure and found that a mobility parameter based on regular waves compares reasonably well with erosion caused by a series of regular waves tested in the laboratory.

Numerical modelling

Numerical modelling based on mathematical equations is a low-cost method to estimate the damage of a near-bed structure.

The turbulent nature of the flow around the stones with accelerations in all directions is hard to describe mathematically. Also the stones can't be described mathematically, only if they are described in a mathematical form such as a sphere or cube. Change in geometry of the structure as a whole and repositioning of individual stones in time, affect the forces on the stones.

Also the factor of irregular wave load makes the situation even more complex. There are many simplifications necessary to obtain a numerical model that can deal with all the aspects at the same time.

Physical modelling

When performing model tests with a scaled situation, knowledge can be obtained of the development of a near-bed-structure under continuing wave load.

Apart from measuring errors and accuracy levels, scale effects can occur in the lab. These effects are artificial and have to be estimated before relating obtained data to a certain prototype.

Possible scale effects are treated in: Physical Models and Laboratory Techniques in Coastal Engineering (Hughes, 1993).

Choice between methods of investigation

A submerged structure under waves with turbulent flow, together with random particle size and shape, makes that initiation of motion is not pure deterministic, but also stochastic. The stochastic aspect is emphasized extra with irregular waves described by a wave spectrum. A numerical solution for a complete irregular wave field is still not possible for practical reasons, mainly due to the large number of calculation points in time and space. Because of the complex properties of the investigated subject there has been chosen for physical modelling, with a wave flume facilitated by the TU-Delft, as the method of investigation. This is a good tool to determine the relation between the development of erosion of a near-bed structure and the load/strength parameters.

1.5 Outline

The outline for the thesis will be presented here. In the next chapter the theoretical aspects will be treated. First the hydraulic conditions are evaluated, from the basic waves to irregular waves. Then the processes near the bottom will be focused upon the treatment of the boundary layer under waves. In chapter 3 near-bed structures are treated in general, from design aspects to an overview of near-bed structure investigations and resulting erosion prediction formulas. In chapter 4 the performed physical model tests are presented. Based on the data achieved in the physical model tests the experiments are analysed in chapter 5. After a dimensional analysis and the introduction of some non-dimensional parameters the data are used to construct ways to predict the deformation of near-bed structures. The first method that is used is an erosion parameter. The results are compared with a similar method used in literature. The second approach will use a relative structure height parameter and explicit time dependency. This method can be used to predict erosion in a graphical way. Eventually some aspects of the analysis are evaluated. In chapter 6 the conclusions of this thesis and recommendations for further investigation are given.

2 Water particle velocity and stone motion

This chapter describes the general theoretical aspects that can be found in literature and are the background for analyzing the stability of a near-bed structure under waves.

In this thesis the forces on a stone are considered to be governed by forces caused by the water velocity around a stone. The water velocity is a complex phenomenon and has a certain value defined at a certain time and place.

Another aspect than the velocity which can cause destabilising forces on a stone, is the acceleration of the flow. The acceleration of the flow is closely related to the velocity, it is its derivative in time at a certain place. Accelerations create pressure gradients that also try to move the grains from their initial position. Research on this aspect for non-breaking **regular** waves on a mild slope was executed by Tromp (2004). He found that stone stability was dependant on the combination of velocity and acceleration.

Possible acceleration aspects can be considered to be described in this thesis by wave parameters as the wave height H and the wave period T. The wave height influences the velocity near the bottom and the period determines how fast this velocity changes in time. So when the wave height and period are used in a transport prediction formula, the acceleration is incorporated implicitly.

The acceleration aspect is considered to be beyond the scope of this investigation and the velocity aspect is considered as cause of destabilising forces. The measurement of the influence of acceleration under irregular waves is considered to be more difficult than under regular waves.

First the cause of the water particle velocity that represents the hydraulic load on a near-bed structure is treated. In this thesis on near-bed structures only the orbital motion of waves is considered. Next the forces that determine the stability of a single stone are treated and the aspect of initiation of motion of a single stone is treated. A step further is the treatment of the erosion of rock and prediction methods for the erosion.

2.1 Wave Theory

2.1.1 Linear Wave Theory

The starting point for the Linear Wave Theory is the Navier-Stokes equations, neglecting boundary effects. Outside the boundary layer, growing during a wave period from the bottom (see section 2.1.3), viscosity can be neglected and the flow can be considered irrotational. In that case there are no Reynolds-stresses and a velocity potential, Φ , can be defined (here for two dimensions):

$$u = \frac{\partial \Phi}{\partial x} \qquad w = \frac{\partial \Phi}{\partial z}$$
 2.1

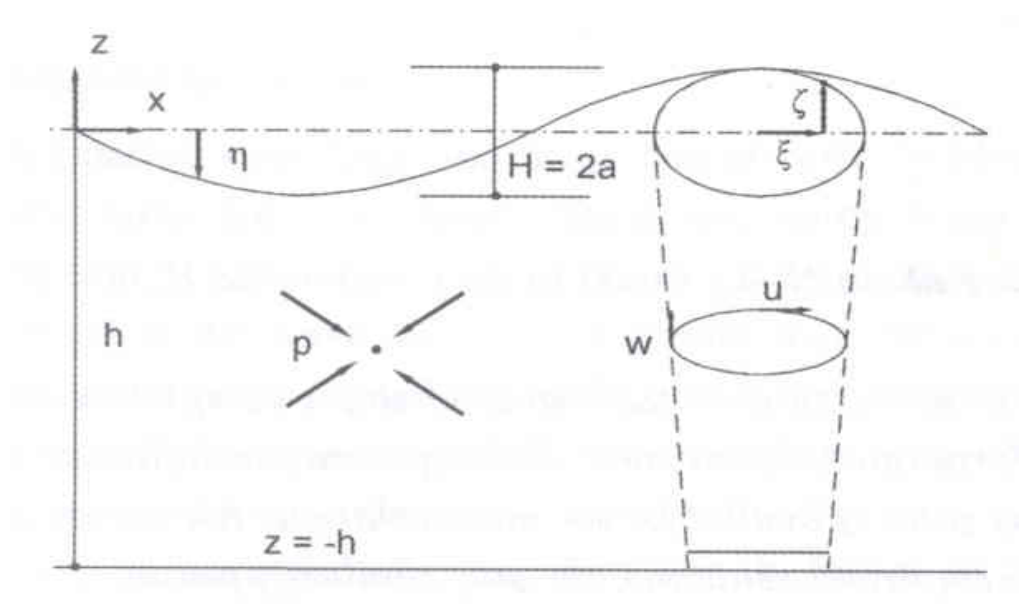


Figure 2-3. Definitions linear wave theory

The basic equations for Linear Wave Theory, which are not shown here, can be solved when a sinusoidal surface profile is assumed (See Figure 2-3) and the boundary conditions at the bottom and the surface are taken into account:

$$\eta = \frac{H}{2}\sin\left(\frac{2\pi t}{T} - \frac{2\pi x}{L}\right) = \frac{H}{2}\sin(\omega t - kx)$$
 2.2

The velocity potential becomes:

$$\Phi(x,z,t) = \frac{\omega a}{k} \frac{\cosh(h+z)}{\sinh kh} \cos(\omega t - kx)$$
2.3

where:

T is the wave period (with the frequency f = 1/T)

H is the wave height

t is the time

h is the water depth

k is the wave number $(2\pi/L)$

L is the wavelength

 ω is the angular frequency $(2\pi/T)$

z is the vertical coordinate, z = 0 represents still water level, z = -h and represents the bottom

x is the horizontal coordinate

All other quantities in the wave, as a function of x, z and t, can be derived from this expression for the velocity potential Φ .

In this thesis a situation of transitional water depth will be regarded. This is a situation where the waves feel the bottom. In a deep-water wave condition there is no velocity (caused to the deep-water waves) at the bottom and the water particles motion describe a circle. In a shallow water wave like a tidal wave there are no vertical velocities over the entire depth profile.

In the case of transitional water the water particles describe an elliptical orbit. From the water surface to the bottom the vertical displacement of the water particles reduces to zero while the horizontal displacement remains almost constant. The water particle movement at a certain point at the bottom can be expressed as a horizontally oscillating motion:

$$u_b = \frac{\omega H}{2} \frac{1}{\sinh kh} \sin(\omega t)$$
 2.4

$$u_b = \hat{u}_b \sin(\omega t) \tag{2.5}$$

$$\hat{a}_b = \frac{H}{2} \frac{1}{\sinh kh} = \frac{\hat{u}_b T}{2\pi}$$
with $\hat{u}_b = \frac{\omega H}{2} \frac{1}{\sinh kh}$

$$2.6$$

where:

 \hat{u}_b is the maximum horizontal velocity at the bottom

 \hat{a}_b is the horizontal displacement amplitude at the bottom

The maximum horizontal velocity and the maximum horizontal displacement near the bottom are considered to determine the hydraulic circumstances at near-bed structures. For the hydraulic load on a near-bed structure the horizontal velocities near the bed are important. The horizontal velocity is given based on equation 2.3.

| | Shallow water | Transitional water | Deep water |
|-----------------------------------------------|----------------------------------------------------------|--------------------------------------------------------------------------|-----------------------------------------------------|
| | h/L < 1/20 | $\frac{1}{20} < \frac{h}{L} < \frac{1}{2}$ | $\frac{h}{L} > \frac{1}{2}$ |
| horizontal water velocity component (u) | $u = \frac{H}{2} \sqrt{\frac{g}{h}} \sin(\omega t - kx)$ | $u = \omega \frac{H}{2} \frac{\cosh(h+z)}{\sinh kh} \sin(\omega t - kx)$ | $u = \omega \frac{H}{2} e^{kz} \sin(\omega t - kx)$ |

Table 2-1. Horizontal water velocity derived from linear wave theory

The water motion in short waves can be described as irrotational, excluding a thin boundary layer (see section 2.1.3). When the shape of the wave is represented in a more complicated form than a simple sine, relations differing from linear wave theory for the water motion are more appropriate.

Figure 2-4 gives an overview of the validity of various wave theories, based on various wave shapes (LeMéhauté, 1976; see Schiereck, 2001). The shape of waves with increasing steepness in transitional and deep water (upper right corner in Figure 2-4), can be described with more sine components, leading to more complex solutions of the equation of motion.

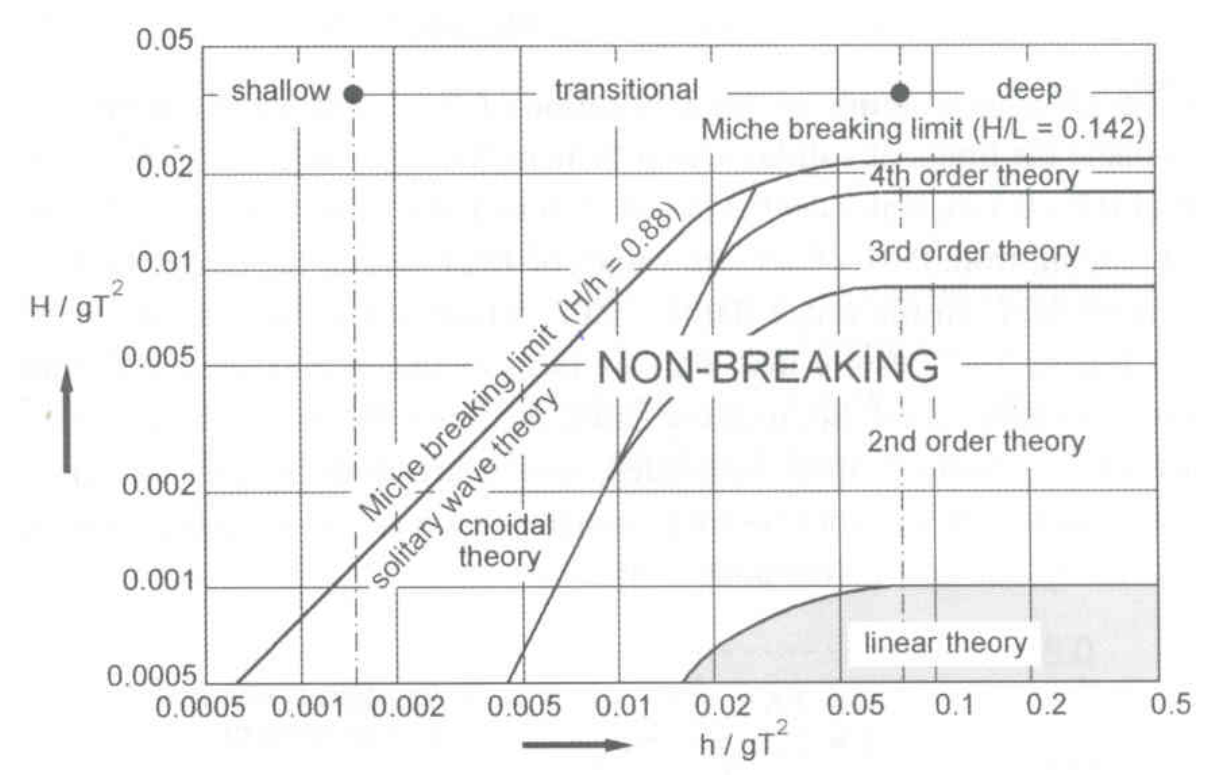


Figure 2-4. Validity of wave theories (LeMéhauté, 1976; see Schiereck, 2001)

Breaking occurs when a wave is too steep (on deep water), or when the water is too shallow or due to a combination of these reasons. Both limits are described with the breaking criterion by Miche (see Schiereck, 2001) also shown in Figure 2-4:

$$H_b = 0.142L \tanh\left(\frac{2\pi}{L}h\right)$$
 2.7

where:

 H_b is the wave height when breaking occurs

The linear wave theory is based on relatively small waves and the approximation of waves by a simple sine function is a crude simplification for predicting water pressures and velocities near the surface. The bottom velocity is considered in this thesis as the cause of the destabilising forces on the rock; linear wave theory gives a good approximation.

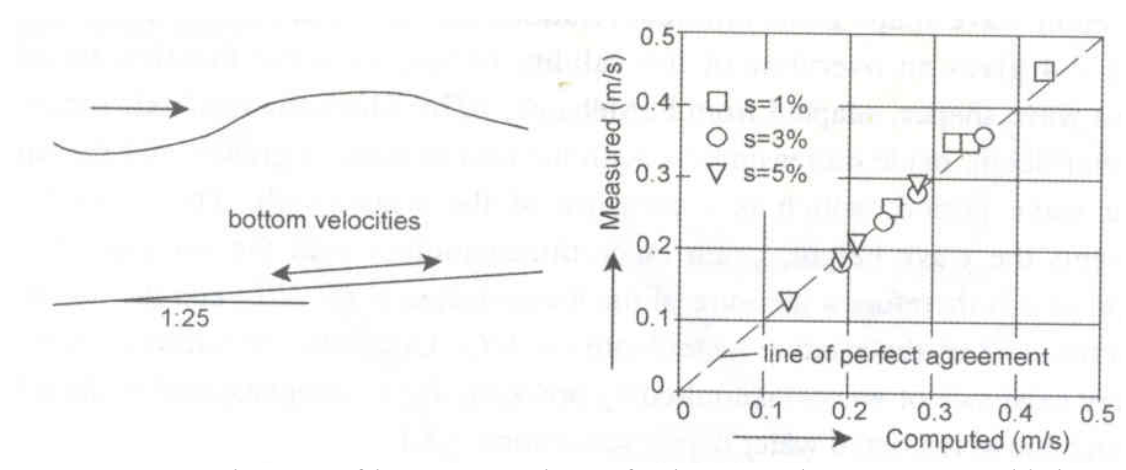


Figure 2-5. Application of linear wave theory for bottom velocities (on a mild slope) outside the limits of validity (Schiereck et al., 1994).

Figure 2-5 gives an example of the application of linear wave theory on a mild slope outside the limits of validity in Figure 2-4. The tests in Figure 2-5 by Schiereck et al.(1994) were performed with regular waves heights of 0.2-0.3 m, water depths of 0.4-0.6 m and a wave steepness (H/L) ranging from 0.01-0.05. The values of the dimensionless wave height (H/gT^2) are in the range 0.002-0.008 and those of the dimensionless water depth (h/gT^2) in the range 0.004-0.02, which is far outside the linear-theory range in Figure 2-4. Despite the fact that the tests of Schiereck et al. (1994) are outside this range of validity, the similarity between measured and computed values was good.

Although this example concerns waves on a mild slope, there is no reason why linear wave theory gives velocities on a flat bed that are less accurate. In this investigation only linear wave theory will be used. An overview of higher order theories, with more complex shapes than a single sine, is given by Sleath (1984) and Battjes (1991).

2.1.2 Irregular waves

Irregular waves are caused by wind, which has a turbulent character. In theory each wind velocity could make its own wave (period and height). All the wind velocity components together then make a very irregular water surface profile.

The wave period T and wave height H can be derived from the wave signal in time at a certain location. From a wave signal e.g. in Figure 2-6 a wave height and period can be defined. The wave period can be defined as the time between two zero down-crossings and the wave height as the maximum difference in water level between those zero down-crossings.

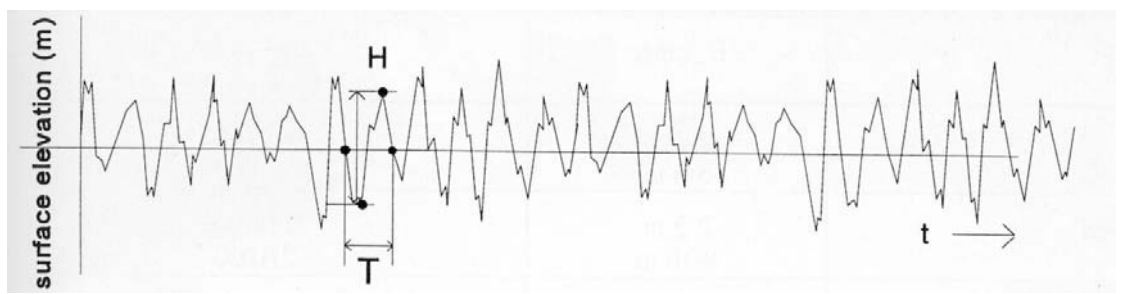


Figure 2-6. A wave signal in time, with registration of zero-down crossings and a defined wave height (H) in between

It has been found to be a very useful method to consider wind waves as a superposition of a lot of sinusoidal waves with different amplitudes, frequencies and phases, referred to as spectral components (Battjes, 1984). This representation with sinusoidal components makes use of random phases with a uniform probability. A spectral analysis (Fourier-transformation) of the surface elevation in one point as a function of time can be used to find a spectral variance density function E(f) in which f is the wave frequency. E(f) is defined such that its integral over all positive values of f, equals the variance of the surface elevation. The total average energy of the wave field per unit surface area can be found by multiplying the area beneath the spectral variance density (or energy spectrum) curve by $(1/2)\rho_w g$:

$$\overline{E} = \frac{1}{2} \rho_w g \int_0^\infty E(f) df$$
 2.8

where:

 ρ_{w} water density [kg/m³]

g gravitational acceleration [m/s²]

A characteristic period for a wave signal represented by the spectral variance spectrum is the peak period T_p (= $1/f_m$). The peak period is the period or frequency (f_m) at which the spectrum E(f), such as in Figure 2-7, has the maximum value.

As a characteristic wave height often the significant wave height H_s is used, which is defined as the average of the highest 1/3 of the waves.

$$H_s \equiv H_{1/3} \approx 4\sqrt{m_0} \tag{2.9}$$

where:

 m_0 is the area beneath the energy spectrum (E(f)) curve

 $H_{1/3}$ is the average of the highest 1/3 of the waves

 $H_{\rm s}$ is the significant wave height

Measured waves proved to be systematically smaller than the theoretical value predicts (Houmb and Overik, 1977; see Battjes, 1991). From measurements on deep water the following empirical relation was found:

$$H_{1/3} \approx 3.8 \sqrt{m_0}$$
 2.10

A specific spectrum shape ($E_{PM}(f)$) based on "fully grown" wind waves on relatively deep water was chosen based on measurements by Pierson and Moskowitz in 1964 (see Battjes, 1991):

$$E_{PM}(f) = \alpha g^{2} (2\pi)^{-4} f^{-5} \exp \left[-\frac{5}{4} \left(\frac{f}{f_{m}} \right)^{-4} \right]$$
 2.11

where:

 α and f_m are scale parameters.

The JONSWAP spectrum (Hasselman et al., 1973; see Battjes, 1991) applies to typical North Sea storms with undeveloped wind waves. The JONSWAP spectrum that was created based on tests on the North Sea will be used in this investigation. It is based on the Pierson and Moskowitz spectrum but has a sharper peak. The peak enhancement function has the following shape:

$$\gamma(f) = \gamma_0 \exp \left[-\frac{1}{2} \left(\frac{f - f_m}{\sigma f_m} \right)^2 \right]$$

$$\sigma = \sigma_a \text{ for } f < f_m$$

$$\sigma = \sigma_b \text{ for } f \ge f_m$$
2.12

where:

 σ_a is a shape parameter with an average value in JONSWAP of 0.07

 σ_b is a shape parameter with an average value in JONSWAP of 0.09

 γ_0 is a shape parameter with an average value in JONSWAP of 3.3

The JONSWAP expression becomes:

$$E_{IONSWAP} = E_{PM}(f) * \gamma(f)$$
 2.13

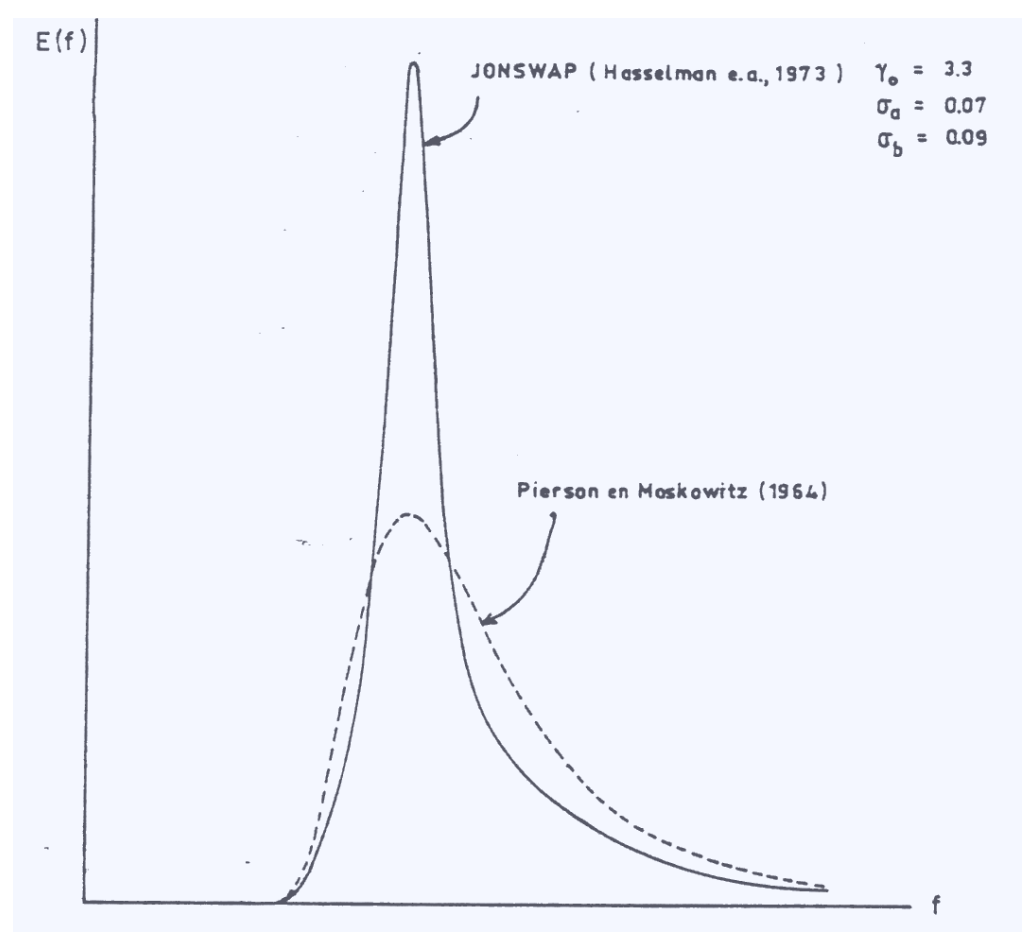


Figure 2-7. Normalized standard variance density spectra (equal area and peak frequency)

The shapes of the Pierson and Moskowitz and JONSWAP spectrum can be seen in Figure 2-7. For the tests in this investigation the JONSWAP spectrum will be generated with the shape factor values as in Figure 2-7.

2.1.3 Boundary layer under waves

This investigation is focused on the processes near the bottom when the influences of waves are present. This is the area where a near-bed structure has to withstand the hydraulic conditions.

According to boundary layer theory we should expect the actual velocity to be zero at the bottom. In a boundary layer near the bottom, with a velocity of exactly zero at the bottom, the flow is highly rotational and the assumptions on which wave equations are based are not valid. In the linear wave theory this boundary layer where the flow is rotational is neglected. The expressions \hat{a}_{δ} and \hat{u}_{δ} , instead of \hat{a}_{b} and \hat{u}_{b} from section 2.1.1, are used for the bottom. The boundary layer (or viscous sublayer) under waves can be expected in a relatively thin region near the bottom (see Figure 2-8). There is insufficient time in a wave period to develop a velocity profile over the entire depth as is the case in river flow or a tidal wave. The choice of the exact boundary layer thickness δ is somewhat arbitrary because there is no sharp transition from the

rotational to the irrotational flow (Figure 2-8 shows a sharp transition from rotational to irrotational flow but this is only a schematic view).

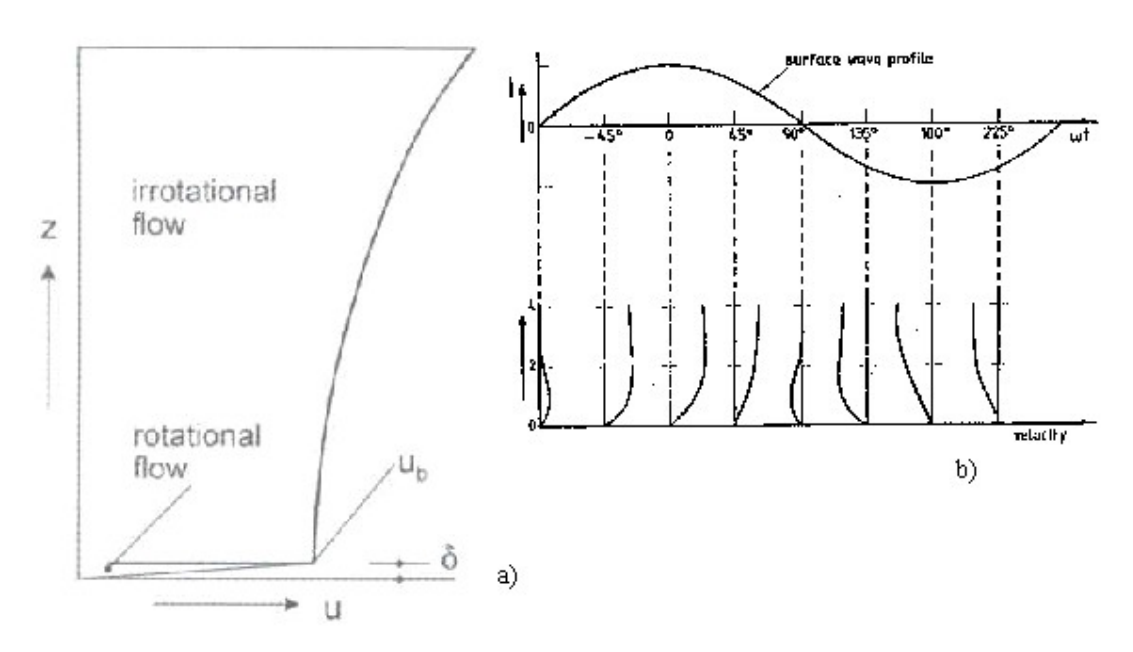


Figure 2-8. Horizontal velocity profile under a wave with rotational flow in the boundary layer (a). Horizontal velocity profiles for short waves at various phases in a wave cycle (b).

Jonsson (1966) measured in his experiments logarithmic velocity profiles near the bottom similar to those found for constant currents near the bed. Jonsson (1980) suggested that the maximum boundary layer thickness for waves (based on steady flow) should be:

$$\delta = 1/2\sqrt{v\pi T}$$

where:

 ν is the kinematic viscosity [m²/s]

Nielsen (1985; see Booij, 1992) suggested:

$$\delta = 1/2 f_{w} \hat{a}_{\delta}$$
 2.15

where:

 f_w is the friction factor according to Jonsson (1966) [-]

 \hat{a}_{δ} is the horizontal displacement amplitude near the bottom [m]

In waves the water accelerations are local: varying in time but not in place. The growth of the boundary layer can be approximated by (Booij, 1992):

$$\frac{d\delta}{dt} \approx \kappa u_* \approx 0.4u_*$$
 2.16

where:

```
\kappa is the von Kàrmàn constant (\approx 0.4) [-]
```

The growth of the thickness of the boundary layer, when a constant value for u_{δ} is assumed (in Figure 2-8(b) for y=0), can be considered to last half a wave period.

Example: For a wave with a period of 10 s; assume $\hat{u}_{\delta} \approx 2.0\,$ m/s; assume (according to Booij, 1992) $u_* \approx 0.1*u_{\delta}$, then with equation 2.16: $\delta \approx 0.4m$

Although the water motion induced by natural waves is not a simple harmonic, it is useful to use the simple harmonic oscillatory boundary layer as an approximation to natural wave boundary layers. The boundary layer calculation with equation 2.16 applies for a flat bed without irregularities such as a near-bed structure. The thickness of the boundary layer that is generated in front of the structure influences the horizontal velocity near the bottom. Therefore the hydraulic load on the stones of the near-bed structure is influenced by this boundary layer.

2.2 Forces on stones

This study treats the margin between initiation of motion and continuous transport of rubble mound stones considering near-bed structures. Generally the movement of a stone can be seen as a balance between load forces and the strength or resisting forces.

Hydraulic conditions give the load forces summarized in pressure forces due to gravity and skin forces due to the fluid motion. Resistance forces are particle inertia, friction between particles and interaction as a whole with aspects such as armouring, interlocking and sheltering.

2.2.1 Forces on a single stone

In this thesis the destabilising factor is thought to be the water velocity only. This water velocity is already a complex phenomenon. It varies in time and place.

Another aspect that can cause destabilising forces on a stone than the velocity, but closely related to the velocity, is the acceleration of the flow. Accelerations create pressure gradients that also try to move the grains from their initial position. The acceleration represents the change of velocity in time. Research on this aspect for non-breaking regular waves on a mild slope (shoaling) was executed by Tromp (2004). He found that stone stability was dependant on the combination of velocity and acceleration. The acceleration aspect is considered to be beyond the scope of this investigation.

The acceleration aspect is considered to be beyond the scope of this investigation. Measuring the influence of acceleration under irregular waves is considered to be more difficult than under regular waves.

In this thesis the forces on a stone are considered to be governed by forces caused by the water velocity around a stone. Possible acceleration aspects can be represented by wave parameters as the wave height H and the wave period T. The wave height influences the velocity near the bottom and the period determines how fast this velocity changes in time. So when the wave height and period are used in a transport prediction formula, the acceleration is incorporated implicitly.

When looking in detail to the forces acting upon a single stone, one can identify five forces. The forces are shown in the figure below:

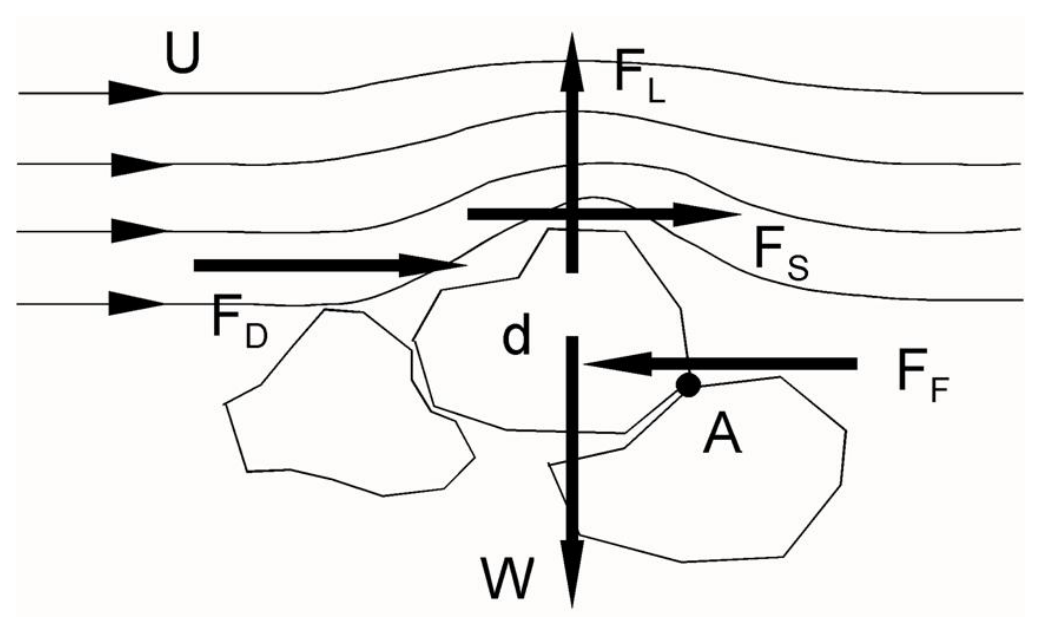


Figure 2-9. Forces on a stone due to a current

The five forces, due to water particle velocity in a current, are:

1. The drag force due to pressure differences over a stone,

$$F_D = \frac{1}{2} \rho_{w} C_D \overline{u}^2 D^2$$
 2.17

2. The lift force caused by the bending streamlines above the stone,

$$F_{L} = \frac{1}{2} \rho_{w} C_{L} \overline{u}^{2} D^{2}$$
2.18

3. The shear force: caused by the moving fluid along the stone

$$F_{S} = \frac{1}{2} \rho_{W} C_{S} \overline{u}^{2} D^{2}$$
 2.19

4. The gravity force: The weight of the stone under water

$$W_s = (\rho_s - \rho_w)gV \propto (\rho_s - \rho_w)gD^3$$
2.20

5. The friction force:

$$F_f = f * W_s 2.21$$

where:

u is the water particle velocity [m/s]

D is the stone diameter [m]

 C_D, C_L, C_S are coefficients [-]

V is the stone volume [m³]

g is the gravitational acceleration $[m/s^2]$

f is a weight friction factor [-]

The first three forces are the load forces responsible for moving a stone. These forces are all proportional to the squared water velocity. The latter two are the resisting forces keeping the stone on its place.

The lift force is balanced with the gravity force and the friction force is balanced with the drag force and the shear force. From the moment balance around the turning point of a stone (point A in Figure 2-9) it follows that, at the critical velocity when a stone starts to move, the proportionality relation is:

$$\rho_w u_{cr}^2 D^2 \propto (\rho_s - \rho_w) g D^3$$
 2.22

and for the critical velocity u_{cr} :

$$u_{cr}^2 \propto \left(\frac{\rho_s - \rho_w}{\rho_w}\right) gD = \Delta gD$$
 2.23

where:

 Δ is the relative stone weight

The critical velocity in equation 2.23 that causes a stone to move is proportional to the relative stone weight of a submerged stone. The precise relation of a (critical) velocity for certain hydraulic conditions and how it effects initiation of motion or transport can be determined experimentally.

2.2.2 Interacting stones

The position of stones in a structure relative to each other can be of influence on the stability of an individual stone. From the forces shown in Figure 2-9, especially the stabilizing friction force and the destabilizing drag force are sensitive to the earlier motioned sheltering and interlocking aspects. When a structure has a "smooth" top layer with stones that are tightly connected to one another, less drag force can be generated. If the stones also fit nicely into each other and make contact, the resistance against movement due to friction will increase.

The shape of certain elements in flow and their mutual position appear to be of large influence on the erodability (Carling et al., 1992). The magnitudes of the different stabilizing forces and eroding forces are greatly dependant of these aspects. In

particular the extent of sticking out of elements compared to their surroundings is very important (Wiberg and Smith, 1987) and can change not only the size of the different eroding forces, but also their proportionality.

When the aspect of element positioning influences the forces then positioning because of a continuing wave load in time should be part of predicting long-term erosion (Delft Cluster research; Behaviour of course granular structures).

2.3 Initiation of motion or critical shear stress

2.3.1 Shields and the initiation of motion

Several researchers studied the problem of initiation of motion. For uniform flow Shields (1936; see Schiereck, 2001) developed a relationship whether or not a particle is stable under given flow conditions. The stability of near-bed structures is determined by the rocks of which it is built and the environmental conditions. The movement of stones in water is often ascribed to the exceeding of critical values of velocity or shear stress. Commonly used design methods are empirical formulas based on this principle. Shields used a characteristic diameter D_{50} of the material and chose the shear force as destabilizing load force on a grain, where D_{50} is defined as the sieve openings where 50 % of the weight of the granular material falls through. The critical shear stress that causes a grain to move is defined by:

$$\tau_{b,cr} = \rho_w u_{*cr}^2 \tag{2.24}$$

where:

 $au_{b,cr}$ is the critical shear stress, for the initiation of motion , on grains on the bed. [N/m²]

 u_{*cr} is the critical shear velocity, where the shear velocity is generally defined as:

 $u_* = \sqrt{\tau_b/\rho_w}$ [m/s] where τ_b is the shear stress on grains on the bed.

Shields showed that a grain moves when the bed shear stress is larger than a critical value. The movement of a grain occurs when:

$$\psi > \psi_{cr}$$
 2.25

where:

$$\psi = \frac{\tau_b}{(\rho_s - \rho_w)gD} = \frac{u_*^2}{\Delta gD}$$
 is a mobility parameter

$$\psi_{cr} = \frac{\tau_{b,cr}}{(\rho_s - \rho_w)gD} = \frac{u_{*cr}^2}{\Delta gD}$$
 is the Shields-parameter

The result of his investigation was a graphical relation between the initiation of motion (described by the Shields-parameter) and hydraulic circumstances on the

bottom expressed in the Reynolds-number for grains Re_{*} (see equation 2.26). The Shields curve can be found in Figure 2-10.

The Reynolds number for grains:

$$Re_* = \frac{u_*D}{v}$$
 2.26

where:

 ν is the kinematic viscosity [m²/s]

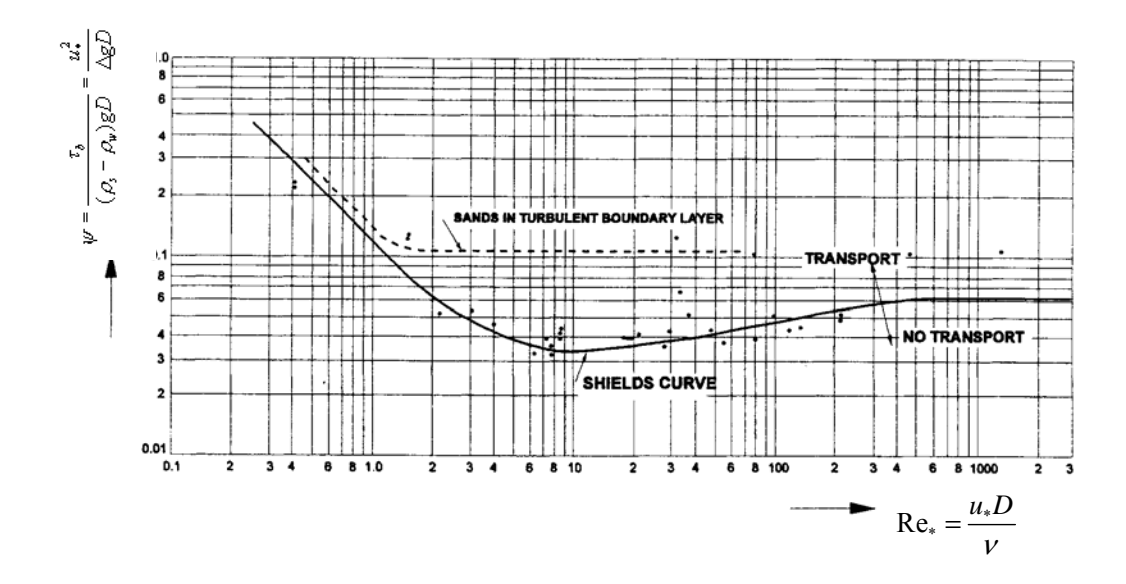


Figure 2-10. Shields curve for steady flow

For a mobility parameter smaller than the Shields parameter, the area under the curve in Figure 2-10, the grains show no movement. Above the curve there will be transport. Originally Shields did not display the transitional area between no motion and transport with a sharp line, but with a transition area for the threshold of motion. Shields obtained this area by extrapolating different levels of motion to zero. For this investigation the transport of rubble mound rock in near-bed structures such as pipeline covers is subject of research. This means larger stones, so for large values of the Reynolds grain number ($Re_* > 200\text{-}500$) the Shields parameter is independent of changes in Re_*

Delft Hydraulics (1972) has done more investigations on the initiation of motion for sediments. It was found that the transition between stability and movement wasn't as sharp as the Shields curve in Figure 2-10 displays. Movement of grains when the mobility parameter was smaller than the Shields parameter was seen. Delft Hydraulics defined 7 levels of stability with different intensities of movement (see Figure 2-11).

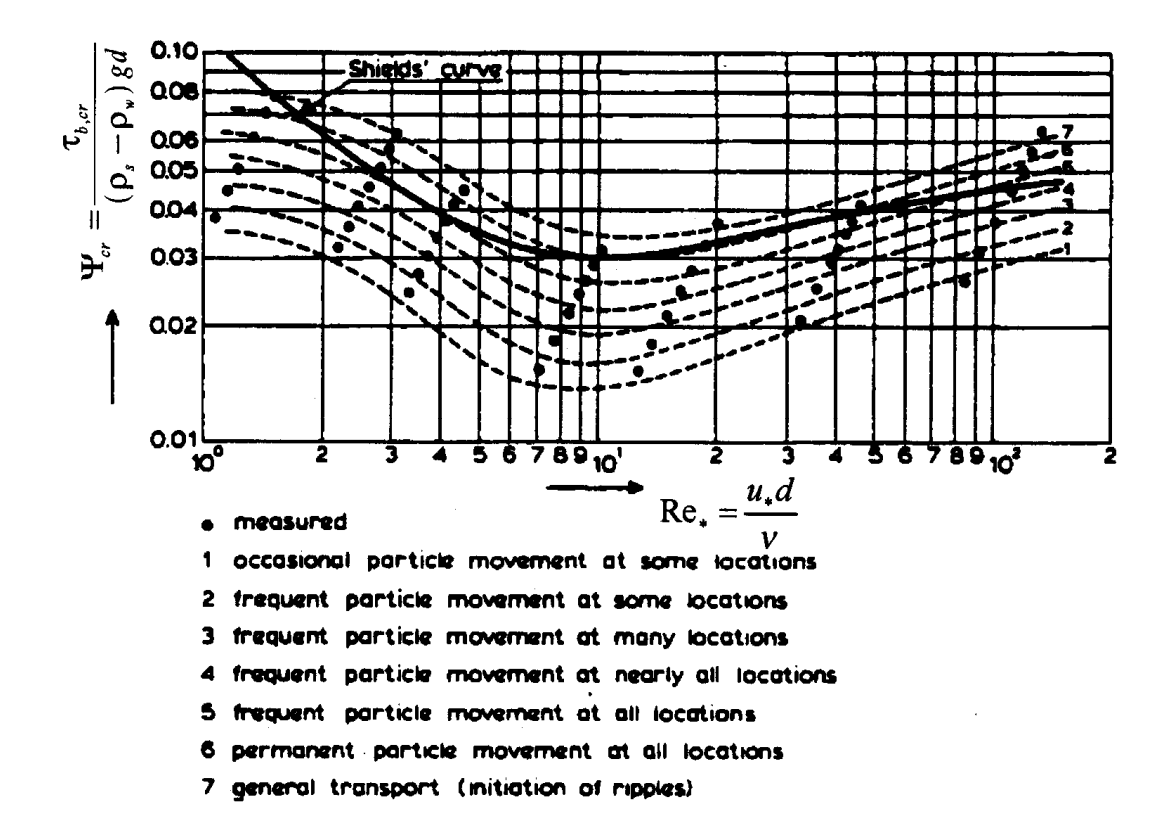


Figure 2-11. Different levels of stability for the initiation of motion for bed material (Delft Hydraulics, 1972)

The criterion that Shields defined as the initiation of motion agrees with level 5 of Delft Hydraulics: "Frequent particle movement at all locations". For design aspects a low mobility parameter is used in practice for stone stability, e.g.: $\psi = 0.03$. When for the functionality some motion or erosion is allowed a higher mobility parameter could be used. The area above the Shields curve defines transport of individual particles; however, the time aspect or the position of particles compared to each other isn't incorporated in the Shields parameter. It could, for example, be the case that when particles are instable with a low level of stability, but after some time become stable, a higher level of stability would apply to that case.

2.3.2 Initiation of motion under waves

The Shields criterion for the initial motion has been established from experimental observations in unidirectional steady flow. For very slowly varying flows, such as tidal flows in limited water depths, the flow can be regarded as quasi-steady. For short period waves, such as wind waves, the quasi-steady approach is no longer justified. Various investigators have addressed the phenomenon of initial motion under wave action.

Madsen and Grant (1975) and Komar and Millar (1975) have shown (see CUR/RWS Report 169,2000), independently, that the results obtained for the initiation of motion in unsteady flow are in reasonable agreement with the Shields curve for unidirectional

flow if the shear stress is calculated by introducing a wave friction factor according to Jonsson (1966):

$$\hat{\tau}_{w} = \frac{1}{2} \rho_{w} f_{w} \hat{u}_{\delta}^{2}$$
 2.27

where:

 $\hat{\tau}_{w}$ is the maximum shear stress under oscillatory flow

 f_w is a wave friction factor

 \hat{u}_{δ} is the peak velocity near the bed

The peak velocity near the bed can be determined, as an approximation, by linear wave theory. Swart (1974: see) has proposed the following empirical relationship for the friction factor, f_w , when the flow near the rough bed is turbulent:

for
$$a_{\delta}/k_{s} > 1.57$$
; $f_{w} = \exp\left[-6.0 + 5.2(a_{\delta}/k_{s})^{-0.19}\right]$
for $a_{\delta}/k_{s} \le 1.57$; $f_{w} = 0.3$

where:

 a_{δ} is the amplitude of horizontal wave motion near the bed, which equals $\hat{u}_{\delta}T/2\pi$ according to linear wave theory.

 k_s is the bed roughness for a flat horizontal bed.

Because it is not certain that unsteady flow results can be represented by steady flow conditions, a modified Shields criterion for unsteady flow has been established (Rance and Warren, 1968; Sleath, 1978) with dimensionless parameters based on forces other than skin friction of the Shields parameter. Sleath (1978) modified the Shields diagram for waves and stability of non-breaking waves, with use of Jonsson's values for $\hat{\tau}_w$ in equation 2.27. The actual results of various investigators for the initiation of motion in unsteady flow were used. This modified Shields function may be thought of as the ratio of the maximum fluid forces with the immersed weight.

In Figure 2-12 the critical value of the modified Shields function is plotted together with the experimental data against the non-dimensional grain size, D_* defined by:

$$D_* = \left\{ \frac{\rho_s - \rho_w}{\rho_w} \frac{g}{v^2} \right\}^{\frac{1}{3}} * D = \left(\Delta g / v^2 \right)^{\frac{1}{3}} * D$$
 2.29

and the Shields number for waves:

$$\psi_{w} = \frac{\hat{\tau}_{b,w}}{(\rho_{x} - \rho_{yy})gD}$$
 2.30

For comparison with experimental data a correction factor has been used to take into account the fact that different investigators have used different criteria for the initial motion condition. The correction factors are also shown in Figure 2-12.

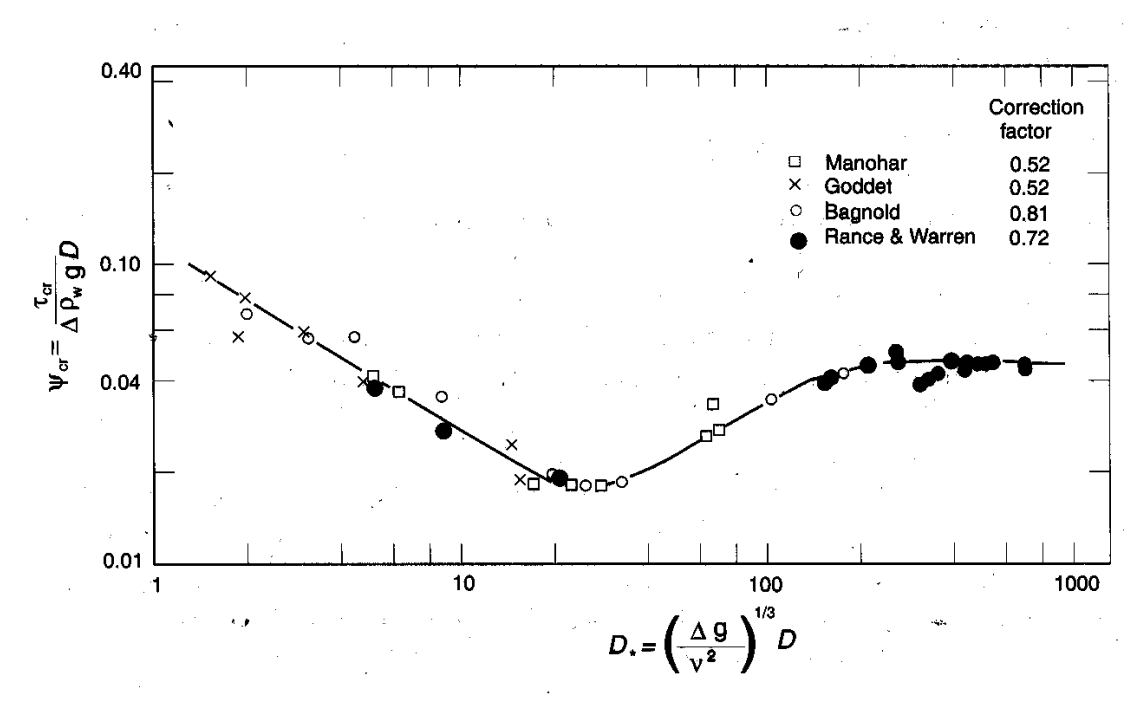


Figure 2-12. Modified Shields curve for unsteady flow (Sleath, 1978)

The original presentation of the Shields curve (Figure 2-10) has as disadvantage ,compared to the modified Shields curve by Sleath (Figure 2-12), which is that the shear velocity (u_*) is incorporated in the Shields parameter on the vertical axis, as well as in the Reynolds number on the horizontal axis. This implies that iteration is necessary to determine the shear stress velocity for a certain grain diameter. The aspect that every grain diameter has its own specific critical velocity was used by Sleath. The shear stress velocity is not incorporated in D_* on the horizontal axes in Figure 2-10 and the critical shear stress can be determined directly.

For the initiation of motion the maximum shear stress in orbital motion $\hat{\tau}_w$ based on the squared water velocity near the bottom (\hat{u}_{δ}^2) is used by Sleath. In section 2.2 it was shown that all the destabilizing forces are proportional to the squared water particle velocity. The use of the shear stress can be a justifiable method for the determination of stability. When an oscillatory water motion is the case, the use of the expressions of f_w and k_s is questionable. The bed or bottom roughness k_s is very difficult to measure in practice. For engineering purpose the scatter of k_s can be described by: $k_s/D_{90}=1-3$ (CUR/RWS Report 169, 2000) where the grain diameter D_{90} is defined by the size of the openings in a sieve through which 90 % of a sample by weight falls.

.

The value of k_s depends on how the stones are placed and movement of stones can change the k_s , e.g. repositioning can make a bed more smooth. Also the shape of a structure as a whole can influence the bed roughness.

2.4 Stone transport

Before treating the transport relations in literature that deal with transport of material under flow, the aspect of transport must be defined. Transport can be defined as the amount of stones or grains that passes a line per unit width and per unit time. In general the amount of material is expressed in volume or weight. The unity of transport depends on how it is defined and made dimensionless in an investigation. Sediment transported as "bed load" remains more or less continuously in rolling or sliding contact with the bed. In "suspension" the particles fall freely relative to the moving fluid. Transport as bed load applies for rubble mound rock and only the formulas in literature that regard bed load transport will be highlighted in this section.

Depending on the definitions there are different ways to make the transport dimensionless. Here the volume of transported material is used for the expression of the dimensionless transport parameter:

$$\phi = \frac{q_s}{\sqrt{\Delta g D^3}}$$
 2.31

where:

 ϕ is the transport parameter [-]

 q_s is the volume of transport per unit width and per unit time [m³/m/s]

The designer should not have high expectations of the absolute accuracy of transport formulas. The transport formulas for rubble mound structures can be used to provide a basic design methodology rather than to find absolute values for stone transport (CUR/RWS Report 169, 2000).

2.4.1 Transport formulas under general flow

There are several formulas where the mobility parameter ψ as defined in equation 2.25 is related to a transport parameter such as ϕ in equation 2.31. Sleath (1984) gives a clear and broad overview of these kinds of formulas.

When for design purposes transport of stones is allowed from a near-bed structure, a high (initial) mobility parameter can be allowed. After some duration of the load the mobility of the stones of a structure can decrease and a stable situation can be reached. This concerns aspects as changes in time, repositioning of individual stones and the change in the geometry of the structure as a whole. These aspects are not incorporated in the general transport formulas.

Paintal (1971; see Sleath, 1984) has performed similar tests as Shields but did not extrapolate his transport measurements to zero. For rather coarse material he found the following transport formula:

$$\phi = 6.56 * 10^{18} \psi^{16} \qquad \text{for } \psi < 0.05$$

$$\phi = 13 \psi^{2.5} \qquad \text{for } \psi > 0.05$$
2.32

Delft Hydraulics (see CUR/RWS Report 160, 2000) has corrected the Paintal formula for viscous effects:

$$\phi = 1.64 * 10^{10} \psi^{10.86}$$
 for $\psi < 0.085$ 2.33

The Paintal formula and Delft Hydraulics formula are the only formulas that predict the transport of rubble mound rock under steady flow. Most of the formulas available are based on tests for finer sediment and do often include sediment in suspension (see for example Sleath, 1984). The physical processes regarding the transport of grains under steady flow may be similar to transport under wave motion, the fluid motion causes instability of the grains, but the processes are not the same. The empirical formulas are often based on steady flow over a river bed. The physical processes here differ from the hydraulic load caused by waves on rubble mound stones on the sea bottom, which is investigated in this thesis.

2.4.2 Transport formulas under waves

The transport of grains is theoretically zero if the velocity at the bottom is oscillating symmetrical and when assuming a flat bed. During a half wave period the grains can show a net displacement, but during the next half wave period the transport rate in the opposite direction is theoretically the same. The investigation of Sleath (1978) is the only one on transport under an oscillating wave load with relatively coarse bed material. He found for the transport occurring during a half wave period:

$$q_{s,1/2} = 47\omega D^2 (\psi_w - \psi_{w,cr})^{\frac{3}{2}}$$
 2.34

where:

 $q_{s,1/2}$ is the volume of transported bed material (as used in equation 2.31) for a half wave period [m²/s]

 $\psi_{w,cr}$ is the critical mobility parameter for waves according to Sleath, as defined in Figure 2-12.

Sleath suggested that equation 2.34 might apply only to coarse sediments. The tests were done for grains with a diameter up to 4.24 mm.

Often the combination of current and waves is investigated. For this investigation, where waves only are investigated, the formulations where the current is set zero are

shown. To give a broader view on transport formulas under waves two other relations are given; the formulas in equation 2.35 (Bailard-Bagnold; see Levit et.al., 1997) and in equation 2.36 (Hallermeier; see Levit et.al., 1997). The Bailard-Bagnold formula originally included a superimposed current, which is set zero in equation 2.35.

Bailard-Bagnold (1985):
$$\Phi = \frac{0.05 f_w}{\tan \gamma \sqrt{(g \Delta D_{50})^3}} \left[\left| \hat{u}_{\delta} \right| \hat{u}_{\delta} - \frac{\tan \alpha}{\tan \gamma} \left| \hat{u}_{\delta} \right|^3 i_b \right]$$
 2.35

where:

 \hat{u}_{δ} is the maximum orbital velocity near the bed

 i_b is unity vector component in direction of bed slope

 γ is the sediment's natural angle of repose

 α is the bed slope angle

 D_{50} is the median grain diameter

Hallermeier (1985):
$$\Phi_{halfperiod} = \frac{\omega D_{50}^{2} (0.1 * \theta)^{1.5}}{\sqrt{g \Delta D_{50}^{3}}}$$

$$\theta = \frac{\hat{u}_{\delta}^{2}}{g \Delta D_{50}}$$
2.36

The Hallermeier formula was established for waves only and both investigations are based on equally sized or smaller particles than were tested by Sleath.

Bailards experiments were for sediments in a plane sloping beach and might not be representative for rock in near-bed structures.

The half period transport principle that is used, in the transport formulas with waves only, gives an indication of stone motion. When a near-bed structure is attacked, the oscillatory motion will not be symmetric which influences transport. The shape of the attacked near-bed structure as a whole also influences the transport of the stones of that near-bed structure.

The transport formulas containing a fixed threshold ψ_{cr} , such as in equation 2.34, involve the problem of a proper threshold value as treated in section 2.3.1 where several levels of stability were defined. Therefore the absence of a fixed threshold can be an advantage in a formula that predicts the reshaping of a near-bed structure. The transport formulas treated in this chapter don't generally incorporate the bed geometry aspect. Only the Bailard-Bagnold formula includes a bed slope. The relations are generally obtained for a flat bed situation. For design aspects of a near-bed structure attacked by an oscillatory water motion the transport relations of this chapter are unsuitable, as was mentioned earlier.

2.4.3 Investigations of general transport of stones in near-bed structures

The investigations on near-bed structures concern mainly the prediction of damage for design purposes. The investigations on deformation or reshaping of the near-bed structures of several investigators will be treated in chapter 3 Here the general transport of stones in a near-bed structure will be considered. Only a few investigators approached near-bed structures with a general transport analysis, these investigations will be treated here.

Levit et al.(1997) tested stones with an average diameter of 4.3 mm with a water depth of 0.5 m, a wave height up to 0.25 m and a period around 2 s. They found in their results that the Bailard-Bagnold formula for the transport of material (see equation 2.35) over predicted the transport for near-bed structures. The Hallermeier relation (see equation 2.36) seemed more accurate for the conditions tested.

Lomonaco and Klomp (1997) concluded that the stone size is not correctly incorporated in the available transport formulas (such as treated earlier this section) when considering near-bed structures. The difference in the overestimation between structures with the same slope is caused by stone size and structure size. It was concluded that parameters that include the stone size and shape should be in the denominator of a new formulation for transport computations.

The structure shape, height and slope, were compared with Paintal's formulations in equation 2.32 for structural over or under estimation. Different slopes, structure heights and stone sizes were tested and the results were compared with the formulations in equation 2.32. Then it was determined for each parameter whether it should be in the nominator or the denominator of a new adapted formulation. Based on the tests and with the use of a critical Shields-parameter a transport relation was formulated. This relation equation 2.37 includes the effect of the structure geometry and critical shear stress on the stones on the bed.

$$\Phi = \frac{A}{D_*} \left(\frac{h_c}{D_{50} n^a}\right)^b \psi^{2.5} \qquad \text{for } \psi > \psi_*$$

$$\Phi = \frac{B}{D_*} \left(\frac{h_c}{D_{50} n^c}\right)^d \psi^{10.86} \qquad \text{for } \psi < \psi_*$$

2.37

where:

 ψ is the Shields-parameter computed for the disturbed conditions

 ψ_* is the Shields-parameter for generalized transport, is a function of the stone size and may be influenced by geometry

 h_c is the structure height

 D_{50} is the stone size and D_* is the dimensionless stone size and equal to $\left(\Delta g/v^2\right)^{1/3}D_{50}$

n is the structure slope.

In equation 2.37 A and B are dimensionless constants and a, b, c, and d are exponents to be computed using regression analysis. The relation can be seen as an applied Paintal formula for near-bed structure with the incorporation of parameters that describe the geometry of the structure.

3 Near-bed structures

Here the aspects of transport, deformation and the time aspect in reshaping are treated with regard to the investigation made on near-bed structures.

In this chapter first general design aspects with regard to near-bed structures are treated. Rather than looking for a situation where the near-bed structure is completely stable, a situation where some erosion is allowed can be defined. Then the deformation prediction of near-bed structures is treated. The last part of this chapter is an overview of investigations and results specifically regarding near-bed structures.

3.1 Design aspects

3.1.1 Functions of near-bed structures

The main function of a near-bed structure in practise is pipeline or transmission protection. When the Southern North Sea situation is regarded, the pipelines differ in depth between 15 m up to 100 m. For different depths different gradations of rock are used. The waves that represent the hydraulic load on the structure, feel the bottom, are irregular and non-breaking. Rubble mound structures under breaking waves such as breakwaters and outfalls on the shoreline are subjected to different physical processes and are out of the scope of this investigation.

The cover over a pipeline on the sea bottom protects the pipe against fishing gear and ship anchors or as ballast to prevent the pipeline from destabilising. Also a ship wreckage, sinking scrap or illegally dumped objects could damage an unprotected pipeline. This calamity will have a great effect on nature; the release of the contents of a pipeline causes a serious environmental impact. Furthermore, the downtime of the pipeline will be costly and repair of it will be difficult. A rubble mound cover layer can provide protection. The thickness of the cover layer has a minimum for which the near-bed structure is still considered functional (see Figure 3-13).

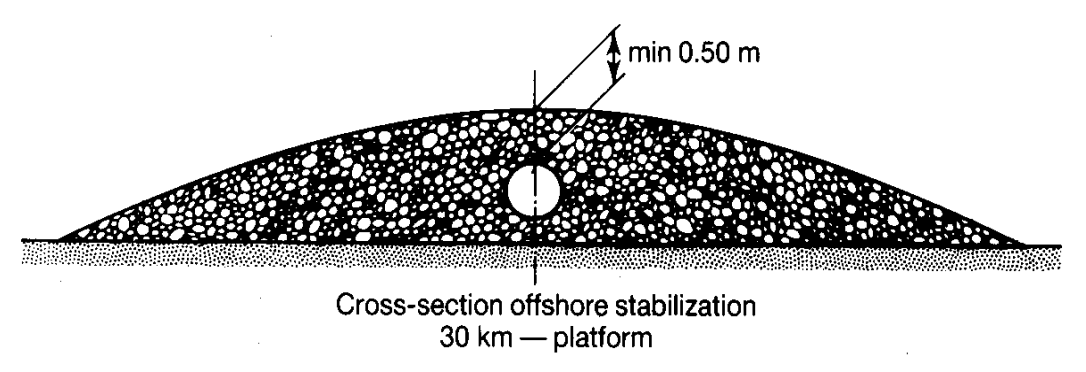


Figure 3-13. A pipeline rock cover protection with a 50-200 mm rock grading (CUR Report 169, 2000).

The near-bed structure, e.g. a pipeline cover, is considered to have "failed" when the thickness of the cover layer measured above the pipe centre is smaller than a minimum value.

In general the transition area between a sand bed to rubble mound structure gives erosion of the sand due to local accelerations. A rubble mound near-bed structure constructed on sand must be flexible enough to resist eroding sand around the structure. This is often done with one (or more) filter layer(s) as a transition between the rubble mound rock used for near-bed structures (size 50-150 mm) and the much smaller sand grains (0.2-2.0 mm).

This investigation will focus only on the stability of the near-bed structure alone and will disregard the erosion of the bottom layer and the possible filter on which it is built.

3.1.2 Rubble mound rock

Rubble mound rock is a product of nature and is won in a quarry where the rock is blasted, and sorted out. The density of the rubble mound rock can differ. The rock commonly used in the North Sea varies from 2.5-2.7 ton/m³ (limestone) to 3.1 ton/m³ (basalt). The rock doesn't have a constant size and is divided in different sort ranges.

A characteristic parameter for a stone sorting is the median stone weight W_{50} . The W_{50} is defined as the stone weight where 50% of the individual stones have a lower mass. The D_{n50} , the nominal median diameter, is the size of a rib of a cube with the same volume as the W_{50} stone and can be directly derived from the M_{50} and the density of the material:

$$D_{n50} = \sqrt{\frac{W_{50}}{g \cdot \rho_s}} \tag{3.1}$$

For smaller material (like sand, gravel and smaller stones) is worked with the D_{50} ; the characteristic sieve diameter (square openings). This diameter corresponds with the sieve diameter through which 50 % of the mass of the stone sample falls through. The sieve diameter (D) can be used to calculate the D_n with a shape factor:

$$D_n = \sqrt[3]{s_f} * D \approx 0.84 * D$$
 3.2

where:

 s_f is the shape factor [-], for rubble mound rock: $s_f \approx 0.6$

In a sample of quarried rock there will be a range of rock sizes. The particle weight distribution is most conveniently presented in a percentage lighter by weight cumulative curve, where W_{50} expresses the block weight for which 50 % of the total sample weight is of lighter blocks and W_{85} and W_{15} are similarly defined. The overall steepness of the curve indicates the grading width. A popular quantitive indication of

grading width is the W_{85}/W_{15} ratio or its cube root, which is equivalent to the D_{85}/D_{15} ratio determined from the cumulative curve of the equivalent cube or sieve diameters of the sample. In CUR report 169 the following grading widths are described:

| Gradation | D_{85}/D_{15} | W_{85}/W_{15} |
|---------------------------|-----------------|-----------------|
| Narrow | 1.2 - 1.5 | 1.7 - 3.4 |
| Wide | 1.5 - 2.5 | 3.4 – 16.0 |
| Very wide or "quarry run" | 2.5 – 5.0 + | 16 – 125 + |

It is noted here that it isn't advisable to use very wide graded rock in a near-bed structure. Reason for this is that de-mixing can take place during transport, processing and dumping.

When the stone sizes of the gradings are considered, the "fine gradings" apply for near-bed structures on the bottom of the southern part of the North Sea. With "fine gradings" is meant: such a size that all pieces can be processed by production screens with square openings (in practise this means stone sizes less than around 200 mm). A scheme for standard fine grading classes (Dutch standard NEN 5180) can be found in Figure 3-14.

| Grading class | Class l | imit defii | nition D (| (mm) | | | | |
|------------------------------------------------------|---------|------------|--------------|------|---------------|------|-------|------|
| designition (mm) | 30/60 | mm | 40/100 | 0 mm | 50/15 | 0 mm | 80/20 | 0 mm |
| sieve Cumulative mass passing sieve as percentage of | | | | | e of total ma | iss | | |
| opening size (mm) | min. | max. | min. | max. | min. | max. | min. | max. |
| 250 | | | | | | | 95 | 100 |
| 180 | | | | | 90 | 100 | 50 | 100 |
| 125 | | | 90 | 100 | ` | | 10 | 50 |
| 90 | | | | | 10 | 50 | | |
| 63 | 90 | 100 | 10 | 50 | | | 0 | 10 |
| 45 | 30 | 70 | | | . 0 | 10 | | |
| 31.5 | 0 | 20 | 0 | 10 | | | | |
| | | | | | | | | |

Figure 3-14 Standard fine grading classes by the Dutch standard NEN 5180.

The near-bed structures regarded in this investigation consist of rubble mound rock with only one type of rock grading without filter layers inside the near-bed structure.

3.1.3 General design methods

'No movement' and 'limited movement' design method

A traditional design method defines qualitative levels of instability. These design levels are expressed in terms of the Shields number (see equation **2.25**). The two design levels commonly applied are the 'no movement' and 'limited movement' method.

The mobility parameters (ψ) of the two levels of instability are related to the following critical Shields values (ψ_{cr}) for Re_{*} > 500 (see Figure 2-10):

 $\psi_{cr} = 0.03$ 'no movement' design level $\psi_{cr} = 0.05 - 0.055$ 'limited movement' design level

This method is widely used nowadays for the stability of rubble mound rock structures and is based on the movement of an individual stone without the incorporation of the duration of a (wave) load. For coastal protections with a sharp definable "failure point" (breakthrough of a dam) this method is often applied.

Critical transport design method

In the critical transport design method movement of stones is allowed. This method is based on the idea that the transport of stones doesn't directly mean the failure of the structure.

The mobility parameter (ψ) as used by Shields can be used to predict a level of stone transport q_s (see equation 2.31), which represents the transported volume per unit width and per unit time [m³/m/s]. The parameter q_s is based on bed transport and is predicted in relations such as the Paintal formulas treated in paragraph 2.4. No time aspect or structure geometry is taken into account. When a critical amount of transported volume $(q_{s,cr})$ is defined (depending on the designer's demands) a relation similar to the one in equation 2.25 can be stated:

$$q_{s} < q_{s,cr}$$
 3.3

For near-bed structures the "failure point" is based on how the functionality is defined (see figure Figure 3-13) and what stone transport then can be allowed (with a certain value for parameter $q_{s,cr}$).

The probabilistic aspect in the design of a structure becomes more important with a non-deterministic method as a critical transport design method. In the probabilistic process for the design of a near-bed structure the main parameter is a damage prediction parameter. Also the wave load in time, which forms a part of the damage prediction parameter, has a probabilistic character.

When estimating the wave load on a structure, often a design storm is used which is assumed to be representative for the local wave conditions. A storm can be characterised by a significant wave height (H_s), a characteristic wave period and a return period. Based on measurements a relation with a return period is made. From this probabilistic approach a design wave height can be chosen. For an example of a relation between wave height and return period see Figure 3-15.

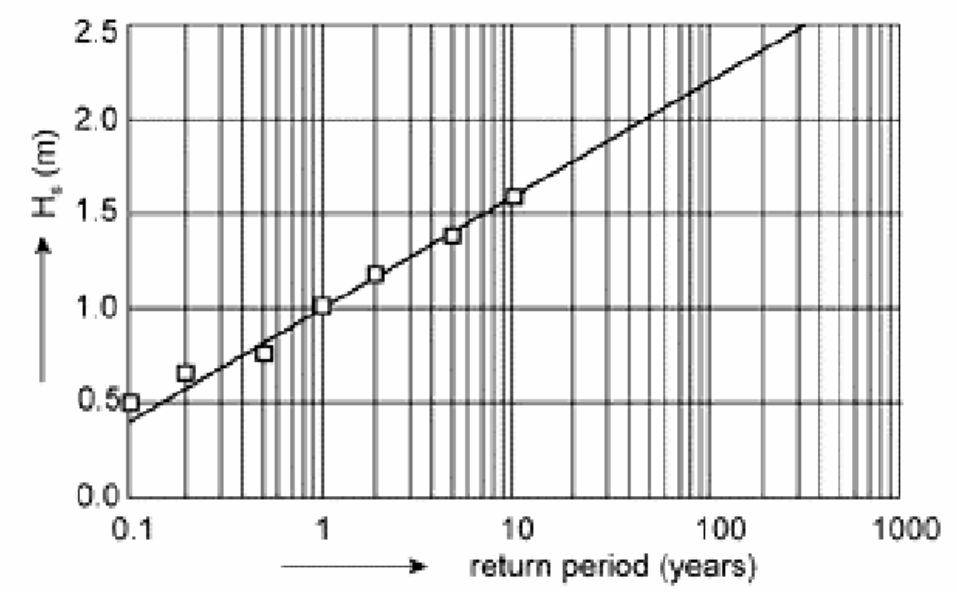


Figure 3-15 Example of a relation between wave height and return period based on measurements at a certain location.

The difference of the critical transport method with the 'no movement' and 'limited movement' design method is that the design can be optimized, so the functional demands of a structure can be achieved with less cost.

In this thesis the erosion of stones from a near-bed structure is treated and the critical transport approach will form the background of this investigation.

3.1.4 Construction and maintenance strategy

Construction methods

The rubble mound rock can be dumped on the sea-bed in several ways. For the deeper parts (over 20 m water depth) a fall pipe vessel is generally used. With a fall-pipe more precise rock dumping is possible but the stone size that can be dumped is limited. Depending on the exact dumping process the maximum stone size will be around 250 mm. An overview of generally applied construction methods is shown in Figure 3-16.

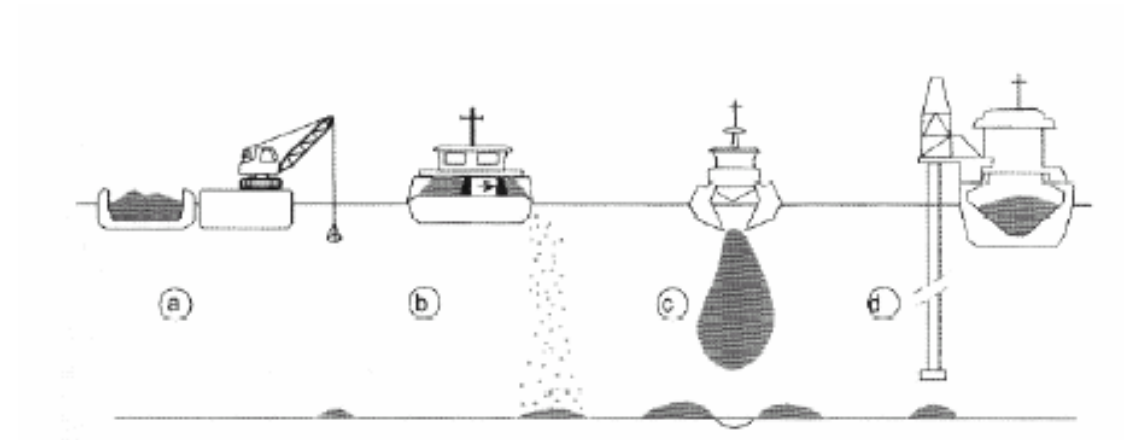


Figure 3-16. General construction methods for dumping rock; using a crane (a), side stone dumping (b), using a split barge (c) or a fall pipe (d).

The accuracy between the methods differs; dumping from the water line is a rather inaccurate method, which depends on the water depth. Bringing the rock under the water line and placing near the bottom is more accurate. For pipeline covers with a water depth around 20 m or deeper a fall pipe can be used.

Any influences of the construction method possible that depends on the construction method, like the resulting porosity of the structure after a certain dumping-method and breaking of the stones when dumped, will be disregarded in this thesis.

Maintenance strategy

With the critical transport method the erosion of a near-bed structure is accepted to a certain extent. The erosion can not be allowed to disable the functionality of a pipeline cover structure. Maintenance can be incorporated in the design of a pipeline cover. The maintenance strategy is a cost optimisation aspect. A design that has a very high probability to endure any condition possible during its functional period might not always be optimal as relatively large stones have to be used. The costs depend on aspects such as the availability of equipment, where and under what conditions the possible maintenance has to be performed.

When some transport or erosion of rock is allowed in the design of the near-bed structure, there are generally three maintenance strategies:

- Continuous strategy
- Extreme conditions strategy
- Preventive strategy

Continuous strategy

A continuous strategy means that maintenance is performed on a regular basis. This could be applied when the design conditions occur regularly. The maintenance costs must be sufficiently low for this strategy.

Extreme conditions strategy

When an extreme conditions strategy is used there will be maintenance after every extreme storm. The design conditions are relatively rare and the structure has to be monitored after the storm.

Preventive strategy

This strategy implies an over-dimensioning of a structure and the allowance of considerable erosion without the need of maintenance (within a certain probability) within its life period. Extra rubble mound rock will be dumped creating a buffer zone that is allowed to erode under the design conditions. This strategy could be very cost effective when maintenance is expensive compared with the extra needed stones.

The preventive strategy with the critical transport design method forms the background of this investigation as stated in chapter 1. A possible extra effect of the preventive strategy is that the over-dimensioning allows possible reshaping of the structure in a way it can better resist the design conditions.

3.2 Predicting deformation of near-bed structures

Compared with bottom protections and breakwaters a relatively small amount of research has been done with regard to deformation prediction of near-bed structures. For a near-bed structure under waves the level of transported stones can be defined in relation to the geometry of the structure. To express the deformation of a near-bed structure not the transported volume q_s is used but the eroded area (A_e) from a structure profile (see Figure 3-17).

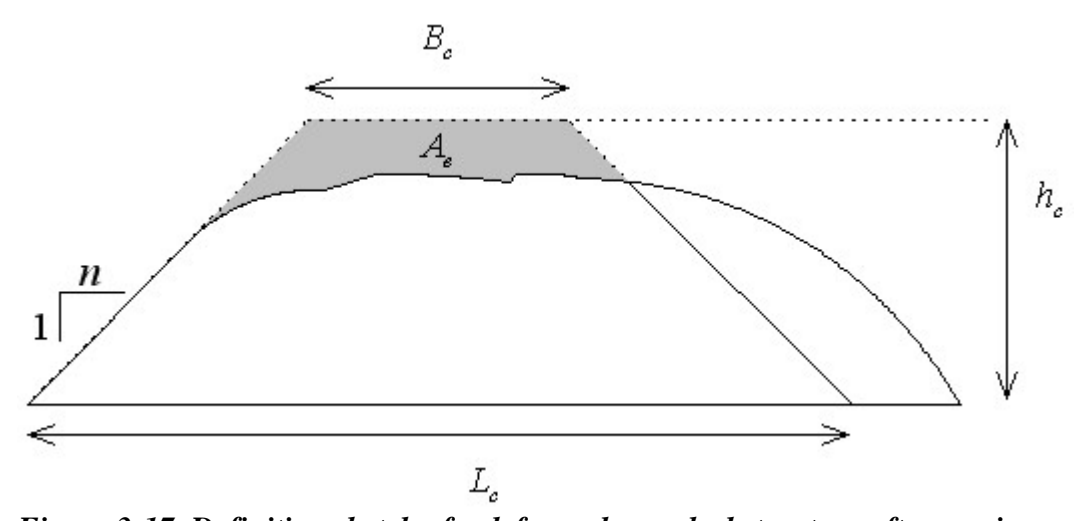


Figure 3-17. Definition sketch of a deformed near-bed structure after erosion.

A critical eroded area from a profile can be defined by a designer similarly as in equation 3.3. The difference of the area A_e compared with q_s is that a specific profile with boundaries is defined and the geometry of the structure is taken into account. So a balance of net stone erosion is made differing from the case with q_s where only the

transport intensity (volume) passing a line is regarded. This is useful for the specific case of predicting erosion from a near-bed structure.

A dimensionless damage level S of the structure can be expressed with the use of A_e as shown in the following equation by Van der Meer (1992):

$$S = \frac{A_e}{D_{n50}^2}$$
 3.4

where:

S is the erosion number [-]

 A_e is the eroded area of a profile [m²]

The parameter S can be seen as an erosion number representing the number of stones lost from a profile (with a width of D_{n50}) as in Figure 3-17. In the investigations on near-bed structures, S is often used as a dependent variable that results from conditions under which a near-bed structure is tested. When the conditions are divided in three aspects; hydraulics, structure geometry and the time aspect, then S can be described as a function of those environmental parameters:

$$S = f$$
 (hydraulics, structure geometry, time) 3.5

In the investigations specifically done on near-bed structures several parameters are used to relate hydraulic and environmental conditions to the deformation of a structure described by the damage parameter S. The structure geometry is often incorporated together with the hydraulics in a parameter describing the deformation.

Hydraulic conditions

Several parameters to describe the hydraulic conditions used by several investigators for determining the deformation of near-bed structures are:

• Stability number with, as hydraulic load, the significant wave height of a spectrum:

$$N_s = \frac{H_s}{\Delta D_{n50}}$$

• Shields-parameter as mobility parameter based on the shear stress on a stone:

$$\psi = \frac{\tau}{\rho g \Delta D_{n50}}$$

• Mobility parameter based on the maximum orbital velocity near the bottom:

$$\theta = \frac{\hat{u}_{\delta}^2}{\Delta g D_{n50}}$$

• Mobility parameter based on ratio of loading and resistance to lifting (see equations **2.18** and **2.22**):

$$\frac{F_L}{\cos\alpha\,W_{\rm s}}$$

Structure geometry

The structure geometry of a near-bed structure can be defined by the definition sketch in Figure 3-17. In the figure the symbols B_c , h_c and L_c (respectively the crest width, structure height and the length of the structure bottom) define the (symmetrical) structure profile shape.

In the mobility parameter based on the lift force that can be used as a parameter in equation 3.5 the structure geometry is incorporated in one of the slope steepness $n = (inv \tan \alpha)$ of the near-bed structure. The erosion seems to concentrate at the crest with accretion at the downhill slope for most near-bed structures.

Time aspect

Not much research has been done on the influence of the time aspect for near-bed structures. For rock stability the duration of wave load is often incorporated into the parameter N, which represents the number of waves. Data on rock slopes of breakwaters by Thompson and Shuttler (1975; see Van Gent and Wallast, 2001) indicated that the influence of the number of waves can be estimated using the following parameter:

$$S/\sqrt{N}$$

This was confirmed by tests by Van der Meer (1988; see Van Gent and Wallast, 2001). Lomonaco and Klomp (1997) found a roughly similar dependency on the number of waves for the prediction of erosion of near-bed-structures. In this way the dependent parameter S (S can be seen as the result of the hydraulics, structure geometry and time influences) from equation 3.5 is combined with the time aspect represented by the number of waves (N).

In the two following paragraphs the investigations on deformation will be treated. First with general formulas for predicting deformation, second the investigations on the explicit time aspect will be dealt with.

3.3 Investigations on near-bed structures

3.3.1 Several investigations on deformation of near-bed structures

Vidal et al.

Vidal et al. (1998) tested regular waves and compared different parameters representing the tested conditions as approaches for damage assessment. Every test consisted of 230 regular waves, so no time dependency was tested. Water depths from 0.2 m up to 0.61 m, wave periods from 1.2 s up to 2.8 s and wave heights from 0.05 m up to 0.33 m were tested. The structures had slopes of 1/3 with a crest height (h_c) and crest width (B_c) of 0.06 m. The test circumstances were coupled to the number of displaced stones.

First the stability number N_s was used to represent the wave load. The crest height and water depth were also incorporated in $(h-h_c)/h$. As a second approach, with use of a Morrison Forces analysis, a drag parameter was used to asses the damage S. Finally the Shields-parameter as a mobility parameter was used. The structure geometry was only implicitly incorporated in the drag parameter with different velocities for different structure heights. All the assessment approaches used the following form:

$$S = f(parameters used in approach)$$

The Shields-parameter was found to give the best results. Also a change in the relation from linear for lower damage levels to exponential for higher damage levels was identified for the different approaches. For low damage levels the movement stabilizes in the first part of the wave trains. For the higher damage regime stones still eroded at the end of the tests. It was expected that the stones never would find a definitive stable position and the damage depended on the number of waves. Finally it was concluded that the change from linear to exponential in the relation between the damage (S) and the used Shields-parameter as mobility parameter (ψ) is a clear indication that new parameters should be added to describe the transported stones.

As these test concerned regular waves and no time incorporation was used, the results can't be directly applied to the design of a near-bed structure in nature that is allowed to reshape. The methodology of the damage assessment used here is useful, however, for predicting damage to a near-bed structure. Further, are the number of waves not incorporated in the deformation prediction methods, only a qualitative indication is made with the assumption that the stabilisation of the stone transport only accounts for low damage levels.

Lomonaco and Klomp

The research of Lomonaco and Klomp (1997, irregular waves with JONSWAP spectrum) was focused on damage measurement and related the data to an empirical formula. Wave heights (H_s) between 0.15 m and 0.25 m, and periods (T_p) between 1.5 s and 2.5 s with a wave steepness (s_{op}) of around 0.03 were tested. Water depths varied between 0.5 m and 0.9 m and particle sizes varied from 3 mm up to 10 mm with structure heights between 0.03 and 0.25 m. The transport of stone was very low and was neglected. Only the reshaping of the structure was investigated. A mobility parameter with peak bottom-velocity was used to estimate the damage with an empirical formula from Klomp (1995):

3.6

$$S_{1000} = \frac{21.4}{n} \theta^{2.25}$$
 3.7

Equation 3.7 represents a formulation for damage level after 1000 waves which incorporates the hydraulic load in the mobility parameter. Furthermore the structure geometry aspect is incorporated in the slope (n) of the, initially symmetrical, near-bed structure. The development in time is disregarded; how the damage develops in the first 1000 waves and for a number of waves greater than 1000 is not predicted directly. Of course an indication can be made for the damage development when the damage after 1000 waves is predicted.

Van Gent and Wallast

Van Gent and Wallast (2001) tested near-bed structures under current and waves with a JONSWAP spectrum and compared different parameters to predict the erosion number S (see equation 3.4). For an overview of the conditions tested see Table 3-1.

| Slope angle(tanα) | 1:8 – 1:1 | A steady current (u) | 0 - 0.74 m/s |
|--------------------------------|----------------|----------------------------|---------------|
| Crest height (h _c) | 0.03-0.25 m | Stone diameter (D_{n50}) | 3.1 - 8.3 mm |
| Crest width (B _c) | 0.06 - 0.25 m | Damage levels (S) | 1-1360 |
| Wave height (H _s) | 0.07 - 0.27 m | Wave steepness (s=H/L) | 0.03 - 0.07 |
| Water depth (h) | 0.37 - 0.90 m | Number of waves (N) | 1000 - 3000 |

Table 3-1. Parameter ranges tested by Van Gent and Wallast (2001).

The time dependency was incorporated in the damage number S with the number of waves (N). Comparison of several prediction parameters led to the mobility parameter in equation 3.8 that was used to assess their data and the data of Lomonaco (1994). It was found that this mobility parameter θ_c , based on the use of the maximum velocity at the near-bed-structure crest in the test situations without a steady current, gave the best results.

$$\theta_c = \frac{\hat{u}_c^2}{g \Delta D_{n50}}$$

$$\hat{u}_c = \frac{\pi H_s}{T_m} \frac{1}{\sinh k(h - h_c)}$$
3.8

where:

 h_c is the initial structure crest height

 T_m is the mean wave period derived from the JONSWAP spectrum

The initial crest height h_c influences the value of the mobility parameter θ_c . In this way the geometry is incorporated together with the hydraulics. The characteristic velocity used (\hat{u}_c^2) is the peak bottom velocity at the crest. The use of this parameter resulted in the prediction formula in the following equation:

$$S/\sqrt{N} = 0.2\theta_c^3$$
 3.9

This relation was the best fit through the data where the currents were neglected for the range of the data, so the relation is based on the wave orbital velocity only.

3.3.2 Explicit influence of wave load duration on deformation

General duration influence

A rock cover for underwater pipelines can be defined as a dynamically stable submerged breakwater (Lomonaco, 1994). A near-bed structure allowed to be reshaped in time by wave attack can be defined in a similar way. The aspect of dynamic stability means that after some time the reshaped structure has a larger resistance against the wave load. This definition of deformation or reshaping of a near-bed-structure implies a significant amount of erosion, resulting in a different shape of the structure as a whole after some time.

When the hydraulics present and the geometry of a near-bed structure are described there is a third aspect; the duration of the load. The duration can be represented by the number of waves (N). When some erosion is allowed, as is the case in a 'critical transport' design method (see paragraph 3.1.3), the question is how the erosion will develop in time. Will a structure become more stable with less and less erosion or will the erosion remain constant. In Figure 3-18 some general examples of (relative) damage S are related to the number of waves.

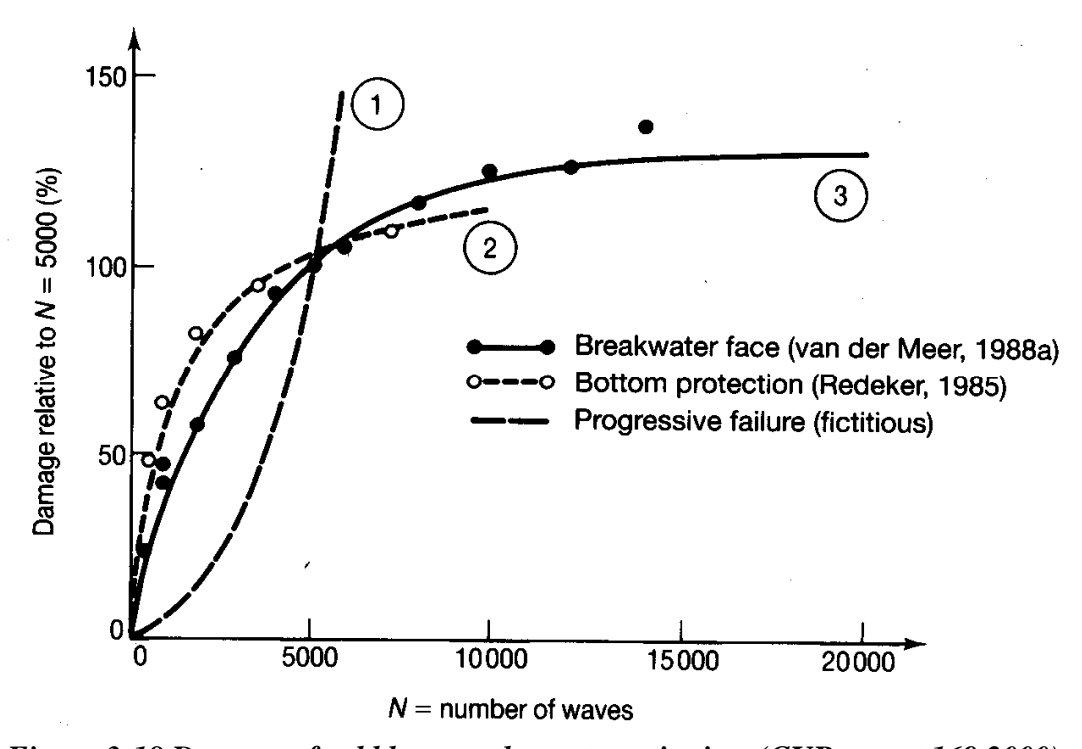


Figure 3-18 Damage of rubble mound structures in time (CUR report 169,2000).

The lines in Figure 3-18 are for a breakwater (line 3) and a bottom protection (line 2) but can be compared with a near-bed structure. The trend is that the structures become more stable and less erosion occurs in time

Investigations on predicting deformation with wave load duration

Most research with regard to near-bed structures has been done for damage with a limited duration of regular and irregular waves. The existing data is limited to 3000 or occasionally 4000 waves. For design purposes near-bed structures often withstand a greater number of waves in a wind-generated spectrum within its required period of functioning.

For the influence of the number of waves an indication can be given with the parameter S/\sqrt{N} . Van Gent and Wallast used S/\sqrt{N} as can be seen in equation 3.9 and incorporated the time aspect (through N) implicitly. Most prediction methods predict or are based on initial damage where the number of waves are incorporated in the damage as \sqrt{N} . This seems reasonably accurate for numbers up to two or three thousand waves.

Klomp and Lomonaco (1995) performed two wave series of 1000 waves to incorporate time dependency based on the damage after 1000 waves. A relation of the following form was assumed:

$$S_N = S_{1000} (N/1000)^b 3.10$$

where:

b = exponent[-]

N = number of waves [-]

 $S_N = \text{damage after N waves [-]}$

The value of exponent b is an indication of the reduction of damage in time. To incorporate the effect of profile deformation use is made of a relative damage parameter defined as:

$$S_{1000}^{'} = A_e / (D_{n50} * B_c)$$
 3.11

The damage number S_{1000} can be interpreted as the number of eroded layers with the thickness of one stone diameter after 1000 waves.

Based on the results in Figure 3-19 the following relation for b was established:

$$b = 1 - S'_{1000} / 200$$
 for $S'_{1000} \le 100$
 $b = 0.5$ for $S'_{1000} > 100$

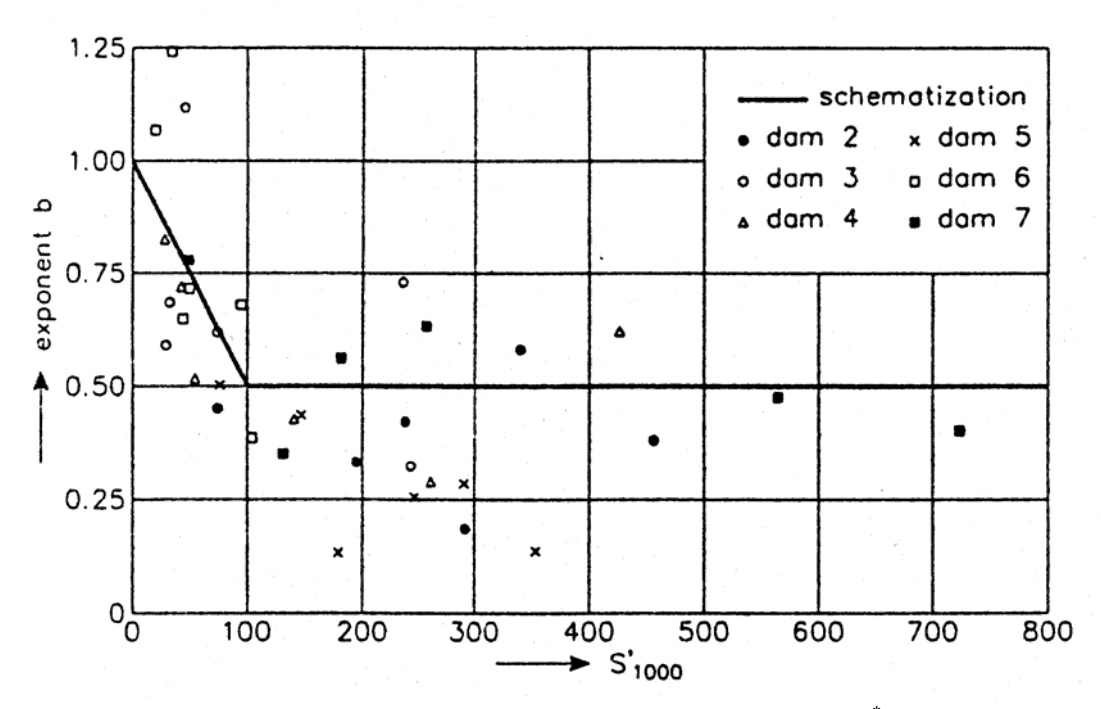


Figure 3-19. Exponent b as a function of damage percentage, S_{1000}^* (Klomp and Lomonaco, 1995)

Lomonaco and Klomp found in 1997 that the stones become more or less stable and much less motion is observed. This stable condition became visible before the end of a first wave series of 1000 waves and during the next 1000 waves almost no damage occurred. Only three tests were performed measuring the erosion change after the first 1000 waves, so tests with more waves were recommended for further research.

The investigation by Levit et al (1997) tested near-bed structures under currents and regular waves. The stone sizes varied from 2-4 mm with a D_{n50} of 4.3 mm. Two slopes were tested: 1:5 and 1:2 with a structure height of 0.1 m and a crest width (B_c) of 0.2 m. The water depth was 0.5 m, the wave height 0.25 m and the wave period 2 s. The typical deformation pattern in time (see Figure 3-20) was that the upstream slope remained practically unchanged. Only the area near the crest was eroded. The downhill slope shows accretion of displaced material. The material comes mainly from the crest of the near-bed structure.

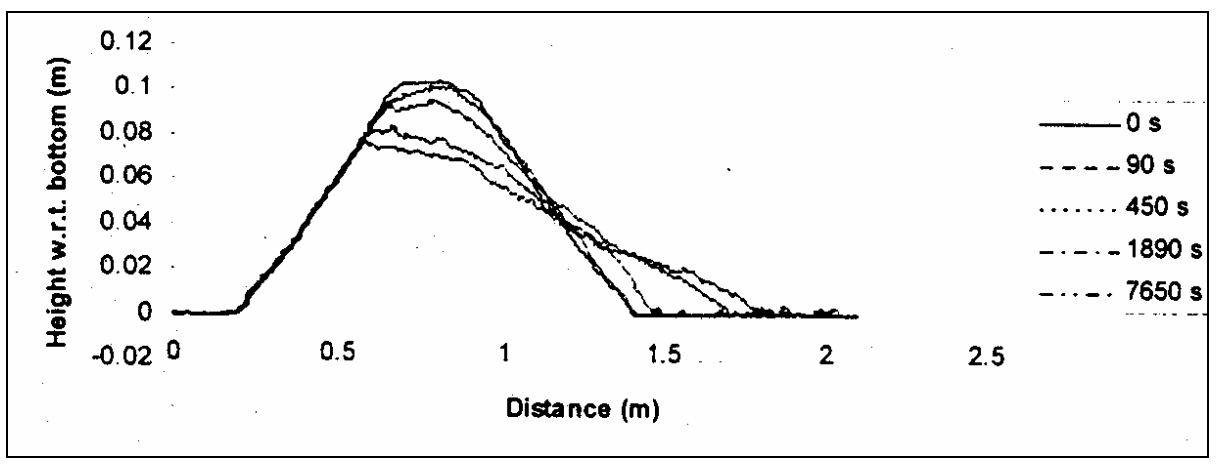


Figure 3-20. Deformation of a near bed structure under regular waves (Levit et al., 1997). The deformation slows down for increasing time as the 5 consecutive stages indicate.

When the duration of wave load on near-bed structures is regarded, the test results show that the erosion curve becomes very flat after 4000 waves when compared with the often used square root relation (see Figure 3-21). The figure is based on the measured eroded areas and the predicted damage line (dotted) is based on the theory given by Klomp and Lomonaco (1995). Equation 3.11 and 3.12 are used for the theoretical damage.

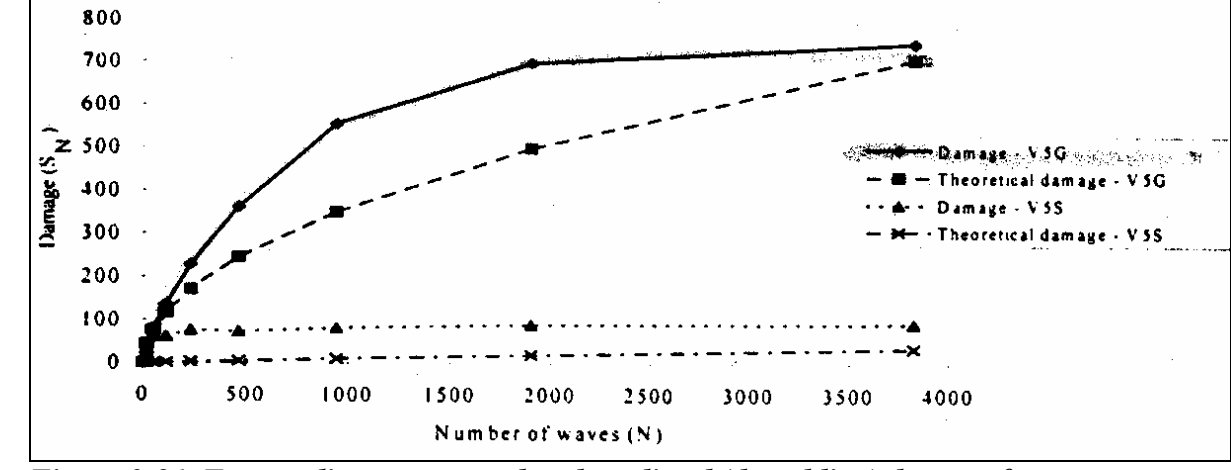


Figure 3-21. Top two lines; measured and predicted (dotted line) damage for waves only (Levit et al., 1997).

From the tests in Figure 3-21 it clearly can be seen that the measured damage grows faster than the theoretical damage values by Klomp and Lomonaco predicts. As the number of waves increases, the measured damage line becomes flatter and flatter.

Evaluation of the time aspect of a wave load that (initially) causes erosion

It may be possible that the theoretical damage shown in Figure 3-21 will be larger than the measured damage. This can be due to the incorrect incorporation of the reshaping and the time aspect of the wave load in the prediction formula. A wave load that causes erosion and has a long duration will displace a great number of stones. When the erosion curve is flattening, it could be that the stones have found new and more stable positions and (when they are not transported outside the boundary of the structure) are still contributing to the functionality of the structure. Stabilizing effects of a structure under continuing wave load can occur at two levels:

- 1. First the structure as a whole can reshape such that it lets the fluid flow pass more smoothly.
- 2. Locally the individual stones can find more stable positions with aspects as sheltering and interlocking, interaction with the direct neighbour-stones, and can withstand a greater load than before a hydraulic load.

The two levels can also interact; when a near-bed-structure has reshaped more, individual stones possibly can find more stable positions with a higher level of sheltering and interlocking than when the near-bed-structure as a whole had a more "blunt" shape.

4 Physical model tests

The North Sea environment, where near-bed-structures can be applied, is characterised by its randomness, non-linearity and turbulence. So any investigation dealing with these aspects has to simplify the problem and make a schematisation. When doing physical model tests generally empirical formulations based on the model tests are constructed next to theoretical analysis. The range of applicability is based on the range of characteristics of the tests when empirical relations are concerned. This chapter will treat the physical model tests that were done for this investigation.

First an introduction with the test facilities and a parameter inventarisation is treated in this chapter. Then the aspects that will be focused on are given. After the test set-up where the environmental conditions are considered and quantified, a test scheme that defines the test-plan is given. The instrumentation is treated next and the test procedure is explained. Then the measured conditions are given with an estimation of the accuracy. Finally an evaluation of certain aspects can be found.

4.1 Introduction

4.1.1 Test facilities

The tests were performed in the "Sediment transportgoot" of the Fluid Mechanics Laboratory of the TU Delft. The flume is 39 m long, 0.8 m wide and 0.85 m high. At one end of the flume a hydraulically driven wave board with a stroke length of 60 cm is present. The flume with the structure is presented schematically in Figure 4-22. In the area where the structures were built small grains (1mm-2mm) were glued to the bottom of the flume. This roughness prevented the stones at the toes of the structure sliding unrealistically easily.

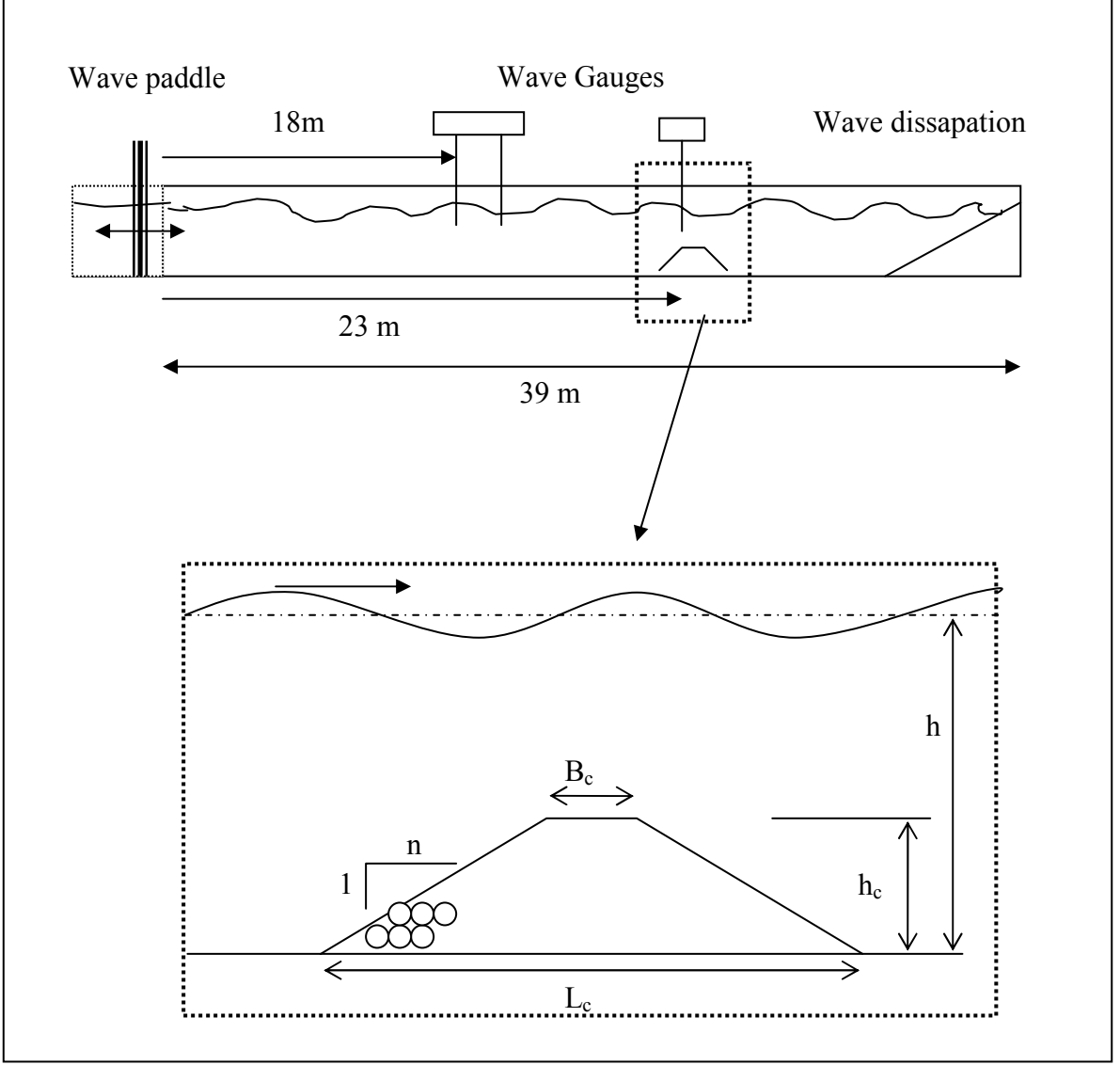


Figure 4-22 Side view on the flume with in detail a schematic representation of a structure.

The wave paddle was controlled by a steering file which creates a certain wave spectrum. The steering file was created with the program "Delft Auke" where the characteristics for a JONSWAP spectrum (for the spectrum shape, see equation 2.13) were filled in. When the steering file was uploaded to the wave machine, the wave paddle moved back and fro to generate waves with different frequencies and heights. With these waves, each with an individual length and height and in a random sequence, the JONSWAP spectrum from the steering file was built.





Figure 4-23. Photos of the flume; left the flume, right the section where the structures were measured.

The most important limitation of the test facilities was the limited stroke length of the wave paddle of 60 cm. The maximum significant wave height (H_s) that could be generated from the steering file was about 22 cm with a peak period of the spectrum (T_p) of around 2.17 s as input parameter. With these values in the steering file the paddle used the maximum stroke length for the largest waves in the spectrum. As some severe breaking occurred directly after the wave paddle, the measured spectrum will reproduce a lower H_s than the input H_s .

4.1.2 Parameters

To investigate the erosion of stones in a certain situation, all relevant parameters must be looked upon. The parameters that can influence the erosion of the stones of a near-bed-structure can be found in Table 4-2.

| Parameter | Symbol | Unit | |
|-------------------------------|-----------|------|--|
| | | | |
| Structure geometry | | | |
| slope angle | n | [-] | |
| crest length | B_c | [m] | |
| crest height | h_c | [m] | |
| | | | |
| Material properties | | | |
| stone characteristic diameter | D_{n50} | [m] | |

| stone gradation width | W_s | [-] |
|----------------------------|---------------------------------|---------|
| stone density | $ ho_{s}$ | [kg/m3] |
| Environmental conditions | | |
| water depth | h | [m] |
| wave height | H | [m] |
| wave length | L | [m] |
| wave period | T | [s] |
| wave direction | Θ | [rad] |
| water density | $ ho_{_{\scriptscriptstyle w}}$ | [kg/m3] |
| kinematic viscosity | ν | [m2/s] |
| gravitational acceleration | g | [m/s2] |
| Time | | |
| number of waves | N | [-] |

Table 4-2. Parameter overview. The marked parameters are varied in the tests.

The problem will be seen as a 2-dimensional process, so the parameter describing the wave direction will be excluded from this analysis. The tests will consist only of waves attacking the structure perpendicularly to its length axis. Furthermore, the water density, kinematic viscosity and gravitational acceleration will be assumed constant for the tests. Also only one stone type will be used, so the material properties are also assumed constant for the tests. The parameters varied for the investigation will be treated in section 4.1.3.

In order to keep similarity with real conditions, characteristic non-dimensional parameters were used and evaluated before constructing the measuring set-up. The non-dimensional parameters are constructed with the use of the parameters in the overview in Table 4-2. Which dimensionless parameters were evaluated for the tests, will be treated in section 4.2. When the tests are to be compared with a situation in nature, or with each other, the flow characteristics must be similar. Different flow situations are uniform if the relevant dimensionless parameters are equal (Battjes, 1990). For a dimensionless parameter analysis see chapter 5.

4.1.3 Aspects of research

Not all aspects of the erosion of rock of a near-bed structure can be investigated because of the limited time to be spent on a graduation thesis. Only a limited set of parameters can be varied to learn about the influence of each individual parameter. Two aspects that influence the erosion of a near-bed structure are the influence of the structure height and the influence of the duration of a certain hydraulic load. The hydraulic load is assumed here to be described completely by the environmental parameters from the parameter overview in Table 4-2. When the influence of the initial structure height and the duration of the wave load become clearer, a better prediction of the reshaping of a near-bed structure can be made.

4.1.3.1 The influence of the initial structure height

The initial structure height (h_c) can be seen as the main geometry component. The three aspects describing the geometry as defined in Table 4-2 can be seen as derivatives from the structure height. The declination of the structure height during a wave load can be seen as a flattening of the slopes (n) or as an increase of the structure profile crest-length (B_c) . So obviously the aspects that determine the geometry of the structure are intertwined and are a matter of definition. The initial structure height is considered to be a good representative for the total structure geometry as the other parameters describing the structure geometry can be derived from the (change in) height. It is also determining for the functionality of the structure as for a pipeline a minimum cover thickness (or structure height) is demanded. When the remaining initial geometry parameters are held constant, the question is what the effect will be of different structure heights on rock motion and deformation of the structure. In the experiments three structure heights were tested as structure geometry characteristics. A higher structure is assumed to influence the load on the stones at the crest, because the crest of the structure will be closer to the water surface and therefore theoretically suffers greater water velocities.

4.1.3.2 The influence of the time aspect

The second aspect of research is the influence of the duration of the wave load. The duration of the wave load can be represented with the number of waves N. The question is how the structure will deform in time. Will the erosion rate decrease and will the stones in a structure eventually become stable for a constant hydraulic load that initially caused stone movement?

For each test the structure was loaded with three series of waves with the same JONSWAP spectrum for each wave series. After each series the deformation of the structure is measured. The number of waves of the next series can be added to the former series so the deformation at a certain point in time can be expressed. In this way the wave series can be added up and a development of the structure in time can be seen.

4.2 Model tests set-up

To test the aspects of this research, stated in the former section, a model test set-up had been made. The aim of this testing plan was to successfully investigate the influence of the initial structure height and the influence of the duration of the wave load on the deformation of a near-bed structure. The similarity of the hydraulic load of the tests mutually and with a situation in nature, must be present when investigating the influence of structure geometry and wave load duration. In this section the granular material used for the tests and the wave conditions for the different test will be treated. Finally the test scheme will be given.

4.2.1 Granular material

The same stones are used for each structure. Three colours were used for painting the stones: red, white and black. Because of the small size of the stones the layer of paint was a significant part of the stone weight. The painted stones had a lower density than the unpainted stones, and therefore had a relatively low density value (see Table 4-3). Normally rubble mound rock has values between 2.6 g/cm³ and 2.7 g/cm³.

| Rock density based on 23 tests with painted rock samples of about | | | | |
|-------------------------------------------------------------------|-----------------------|--|--|--|
| 80 g | | | | |
| Mean | $2,47 \text{ g/cm}^3$ | | | |
| Stdev. (standard deviation) | 0.09 g/cm^3 | | | |

Table 4-3. Painted rock density.

The shape of the material used for the tests is comparable with rubble mound rock used for a pipeline cover. The shape of the material used for the tests (see Figure 4-24) can be typified as the stone shape that is defined as 'irregular (IR)' in Appendix D. The stones used in practice for a pipeline cover on 20 m depth or deeper have sizes up to a D_{n50} of 110 mm and are still relatively sharp in comparison with larger rock.

The shape of the stones was irregular with some unrealistic shapes; one spatial dimension of some stones was very small so the stone was "disk" shaped. These splinters were removed when seen during the construction of the near-bed structure. But the number of these stones was small and these stones have a relatively small influence on the volume and weight of a structure.

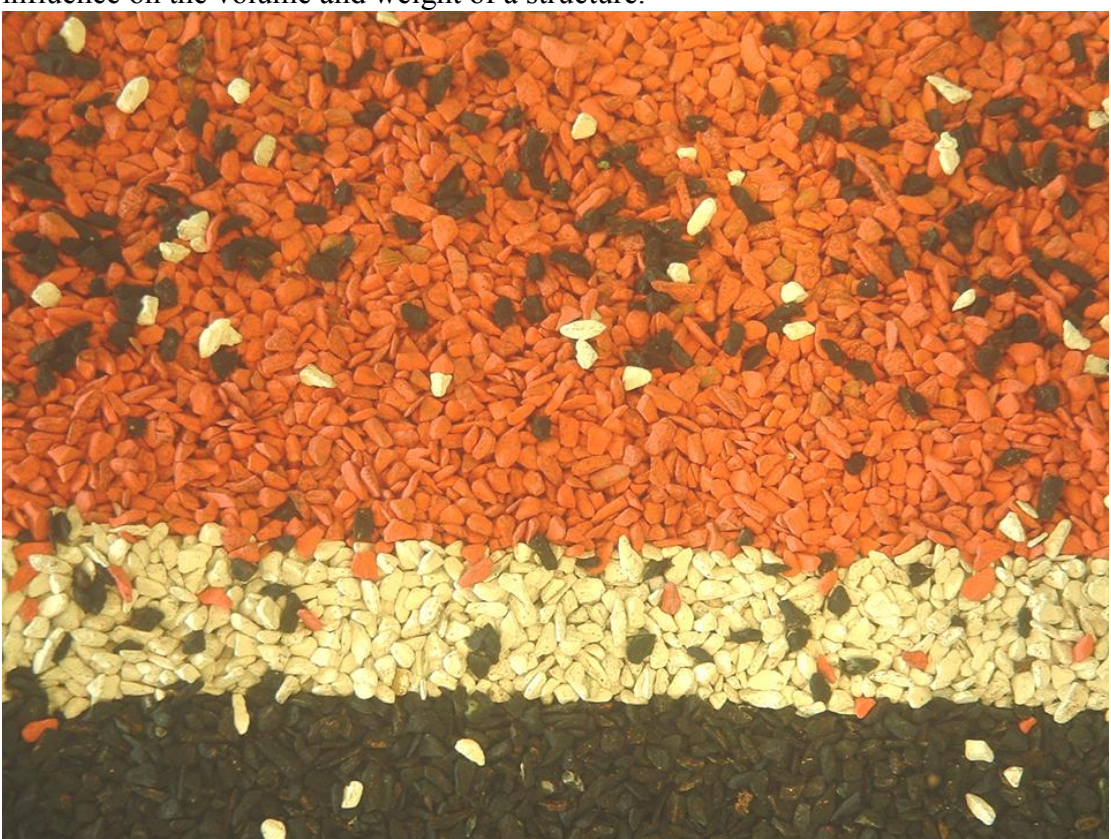


Figure 4-24. Structure crest: the shape of the stones can be considered as 'irregular' material.

The stone-properties are only represented in this thesis by the D_{n50} (based on the sieve curve) and the stone density (more details can be found in Appendix D). The sieve curve and stone diameters can be found in Figure 4-22 and Table 4-4, respectively.

| Sieve (mm) | % of total weight on the sieve | Diameter [mm] | | |
|------------|--------------------------------|----------------------------------------------|------------------|--|
| 5,6 | 0 | | | |
| 4 | 77,2 | D_{10} | 2,5 mm | |
| 2 | 22,5 | $egin{array}{c} D_{10} \ D_{50} \end{array}$ | 2,5 mm 4,4 mm | |
| < 2 | 0,3 | D_{90} | 5,3 mm | |
| Total | 100 | | | |

Table 4-4. Sieve percentage.

For the sieve curve three sieves and a residue sieve were available. From the square sieve openings fall-through percentages are derived. The nominal median diameter can be obtained with the relation in equation 3.2. For these tests the D_{n50} has a value of: $4.4 \text{ mm} * 0.84 \approx 3.7 \text{ mm}$.

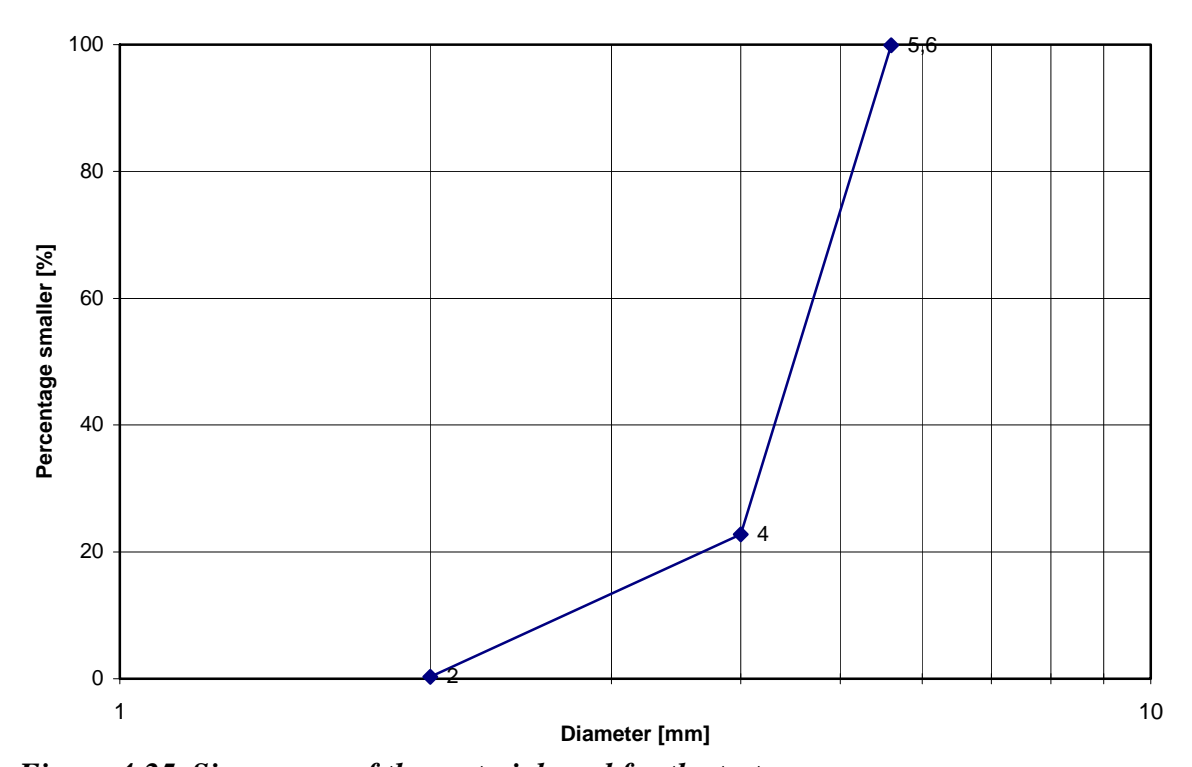


Figure 4-25. Sieve curve of the material used for the tests.

Influences of the gradation width (W) of the used rubble mound stones and individual stone shapes are neglected in this thesis.

The stones used in the model tests were chosen based on two requirements. Firstly the stones must be small enough to be eroded under the range of hydraulic loads that are possible in the flume. The orbital water velocities created by the wave machine must result in a measurably reshaped structure. Secondly the stone diameter must be large enough to guarantee hydraulically rough conditions in order to reduce scale effects. Hydraulic roughness depends on the size of the stones in the fluid motion and the fluid speed, when the conditions aren't hydraulically rough, the roughness of the

structure will not only depend on the stones but also on the fluid velocity itself. The hydraulic conditions where the viscous shear stresses do not influence the different situations in the model tests are related to the wave Reynolds number ($\text{Re} = \hat{u}_{\delta} a_{\delta}/v$) and a relative roughness (a_{δ}/k_s with $k_s = 2.5 D_{n50}$). The value of 2.5 for k_s was used by Jonsson (1966) and can be seen as an average value for bed roughness. The rough turbulent zone as defined by Jonsson (1966) applies in the model. How the rough turbulent zone is defined can be found in Appendix A.

In real conditions, such as a pipeline cover in the North Sea, the flow around near-bed structures is almost always turbulent. The Reynolds number for waves defines turbulent flow when it is larger than 10.000; never a lower Reynolds number was achieved in the test series (see Appendix A).

4.2.2 Wave conditions

This set-up for the wave conditions copes with two issues. First the characterisation of the irregular wave spectrum by certain parameters. These wave parameters then can be compared with the mutual tests and a situation in nature. Secondly, how to create, with the characteristic wave parameters, similar conditions for the mutual tests and a situation in nature such as a North Sea storm. The physical processes described with the wave parameters must be similar.

4.2.2.1 Wave spectrum characteristics

The waves in this investigation are irregular with a JONSWAP spectrum entered in the steering file for the wave paddle. From the measured spectrum some characteristics have to be defined to describe the form for which the wave characteristics were derived. The input parameters of the wave spectrum are the significant wave height (H_s) and the peak wave period of the spectrum (T_p) . These two parameters are assumed in this thesis to describe the wave field. How the peak period and the significant wave height are derived from the spectrum can be found in chapter 2.

The two hydraulic parameters representing the wave spectrum, H_s and T_p , together with the water depth (h), govern the load on the structure with a given structure geometry and material properties. Ultimately these three parameters govern the fluid velocity near the bottom that is responsible for the forces on the stones. With the use of linear wave theory the characteristic horizontal velocity near the bottom becomes:

$$\hat{u}_{\delta} = \frac{\pi H_s}{T_n} \frac{1}{\sinh kh}$$
 4.1

So, with different combinations of significant wave height, wave period and water depth, describing the irregular wave field in the flume, it will be possible to test different hydraulic load situations.

4.2.2.2 Wave climate similarity

To achieve similar physical conditions with a pipeline cover in nature (North Sea conditions) the shape of the waves is tried to held constant through the input parameters, with changing structure geometry (different initial crest heights) and wave load duration. For the tests similar conditions as in a prototype North Sea situation were aimed to be tested in the flume. Two general demands can be stated for the tests:

The wave spectrum that will be measured must have a typical JONSWAP-shape. Severe breaking in the flume can conflict with this demand.

The flow at the height of the structure crest must be horizontally orientated. When for transitional or deep water the structure height relative to the water depth becomes too high, the vertical velocity component of the water particles, predicted by linear wave theory, can have a significant influence on the erosion.

Both aspects will be treated now before the measurement test scheme with the planned hydraulic conditions.

1. Wave spectrum shape similarity

A non-breaking wave climate must be ensured so that the measured waves will result in a spectrum that can be characterised as a JONSWAP-type wave spectrum, which is the input for the wave paddle. There are two different conditions that will cause a wave to break: the wave is too steep or the water is too shallow. For a spectrum these conditions can be characterised by the wave steepness s_p (see equation 4.2) and the relative water depth H_s/h .

Wave steepness.

The input parameters of the significant wave height of the wave spectrum (H_s) and the peak period of the spectrum (T_p) are linked and chosen in a way that they result in a not widely varying wave steepness (s_p) for each test. So the individual influence of T_p or H_s is not investigated. The wave steepness for deep water and the peak period T_p can be expressed with linear wave theory as:

$$s_p = \frac{2\pi H_s}{gT_p^2} \tanh\left(2\pi h/L_p\right)$$
 4.2

where
$$L_p$$
 is derived through iteration: $L_p = \frac{gT_p}{2\pi} \tanh\left(2\pi h/L_p\right)$

For the tests it is tried to keep a low variation of wave steepness between the tests. Also a wave steepness typical for a North Sea storm situation was chosen.

Relative water depth.

An individual wave breaks when the water is too shallow and the H/h parameter has a value of 0.8-0.9. For a characteristic wave height of a spectrum the relative water depth H_s/h when breaking occurs is 0.4-0.5.

The tests are performed for approximately the same relative water depth. A value higher than 0.5 for H_s/h will give severe breaking and the measured spectrum will be significantly different. A lower value will not give different hydraulic conditions, but for the tests the flow velocity must cause erosion for the used stone size. So for the tests a constant value (and maximum value for a non-breaking wave climate) for H_s/h was used. This maximum value was used for most of the tests.

2. Similar flow around the structure

When the wave breaking is minimal and the wave climate is mutually comparable between the tests and a North Sea situation, the horizontal flow can be compared as the mean hydraulic load. When the waves feel the bottom the water particles will follow elliptic paths near the bottom. At the bottom the water particles theoretically only move horizontally, so without a significant vertical velocity component. This situation is typical for transitional water depth, as is the case in the North Sea with a design storm. The dimensionless parameter defining transitional water depth is the h/L ratio. For transitional water depth this ratio lies between 1/20 and ½. (see chapter 4).

The relative structure height h_c/h in the tests must be sufficiently low for the assumption that the flow is horizontally orientated. When this ratio is too high, under the given condition of transitional water depth, then a physically different situation can be defined where there is a significant vertical velocity component of the orbital motion under the waves. This would especially be the case at the crest, as it is nearer to the water surface, where erosion is first expected. So when a transitional water depth situation is present the ratio h_c/h must be sufficiently low to assume similar flow attack for all situations.

4.2.3 Test scheme

All the environmental parameters that were varied in the tests are given in Table 4-5 with the range in which they varied. The shape parameters n and B_c are not varied. The construction was build aiming for a slope n of 2.5 and a crest width B_c of 4 cm.

| Water depth h [m] | Wave height | Wave period | Number of | Initial structure |
|-------------------|-------------|-------------|-------------|---------------------------|
| | $H_s[m]$ | $T_p[s]$ | waves N [-] | height h _c [m] |
| 0.55(0) | 0.22 (a) | 2.17 | 1000 | 0.04 (4) |
| 0.50(1) | 0.20 (b) | 2.07 | 3000 | 0.05 (5) |
| 0.45 (2) | 0.18 (c) | 1.96 | 6000 | 0.06 (6) |
| 0.40(3) | 0.16 (d) | 1.85 | | . , |

Table 4-5. The varying test parameters with test codes. Example for "test 0a6": h=0.55m, $H_s=0.22m$ and $h_c=0.06m$.

Not all combinations of the water depth, wave period and wave height given in Table 4-2 were tested. For the tests 4 significant wave heights, with corresponding wave periods to achieve a wave steepness s_p of around 0.03 (which is a typical value for a North Sea design storm) were tested. These different combinations of significant wave heights and peak wave periods were combined with four water depths in the tests. Most of the tests were performed with a total of 6000 waves, which were performed in three series of 1000, 2000 and 3000 waves.

| Water depth h[m] Wave height H _s [m] | 0.55 (0) | 0.50 (1) | 0.45 (2) | 0.40 (3) |
|-------------------------------------------------|-------------|------------------------------|-------------------|-------------------|
| 0.22 (a) | 0a6 0a6s | 1a6 1a6 her 1a4 1a5 | 2a6 | |
| 0.20 (b) | | 1b4 1b6 | 2b4 2b5 2b6 | |
| 0.18 (c) | | | | 3c4 3c5 3c6 |
| 0.16 (d) | | 1d6 | | |

Figure 4-26. The water depth h[m] and wave height Hs [m] combination for each test code. The last digit represents the initial structure height h_c in cm.

The tests are chosen mainly near a limit of the H_s/h parameter of around 0.44 as can be seen in the test overview in Figure 4-26. The test codes in Figure 4-26 with the first two digits 1a, 2b and 3c have around the same value for H_s/h , where H_s is the chosen input parameter for the wave paddle. For the shallow parts in the North Sea during a typical storm this value for H_s/h of 0.44 is considered a maximum value. Usually H_s/h is smaller for the average North Sea water depth. For these tests this value of H_s/h , with the granular material used and the limited input for the significant wave height for the wave paddle, was the limit where erosion was possible without severe wave breaking. The test 1d6 (see Figure 4-26) was a boundary condition where a very low level of motion was visible, so a lower significant wave

height and a water depth without breaking of the waves don't result in a water velocity near the bottom that causes erosion.

With the wave steepness and relative water depth in these tests the tested range of h_c/h is sufficiently low (a maximum in the test scheme of 0.15) to assume that the (turbulent) flow is horizontally orientated at the height of the structure crest. When this is the case linear wave theory will not predict a large vertical velocity component (disregarding local and incidental turbulence) that can attack the near-bed structure. In a North Sea situation the values for h_c/h under similar wave steepness are generally lower so the flow is horizontally orientated at the height of the structure crest.

4.3 Measurements

For each test the following general aspects were determined:

- The water depth
- The wave signal in time at three locations
- The duration of each wave series
- Several structure profiles in the direction of the flume to measure the deformation after each wave series and before the start of the first wave series.

4.3.1 Instruments

In this section the instruments used for measuring the parameters will be treated. Then the procedure and the measured conditions will be presented. Finally something will be said about accuracy of the measurements and the calibration of the instruments and the key test elements will be evaluated.

4.3.1.1 PROVO

The shape of the structure was measured with a Provo instrument. The Provo is an instrument which measures vertical coordinates with millimetric accuracy. It contains a probe attached to cogwheels. At the end of the probe the electrical resistance is measured which depends on the distance to a non-conducting surface. The electrical resistance is held constant and therefore a certain constant distance from the surface is maintained. The measuring carriage moves horizontally on the flume at constant speed. The probe will follow the surface of the structure keeping a pre-adjusted distance (of about 5mm) so the surface elevation is followed. Every 0.05 second a voltage corresponding with the up or down moving probe is registered. Within one Provo measurement multiple lines are measured by replacing the Provo on the carriage for the measurement of parallel lines. The different positions of the Provo on the carriage were marked so the Provo could be placed in a consistent and accurate way.

4.3.1.2 Provo measuring carriage

The measuring carriage carrying the Provo is responsible for the horizontal coordinates registered via the Provo to a data file. One speed setting was used corresponding with 0.60 cm/s. On a display from which the speed could be read, the speed was oscillating around 0.61 cm/s varying rapidly but consistently between 0.59 cm/s and 0.63 cm/s. The speed necessary for the horizontal coordinates was not directly measured but derived from fixed points detected by the Provo. The speed was calculated from the distance between the points and the elapsed time. This calculation was done for each test with the calculation program MATLAB to include speed variation and to obtain the horizontal coordinate as accurate as possible. This procedure of the speed estimation can be found in Appendix H.

4.3.1.3 Wave gauges

The wave gauges consist of two parallel electrodes placed in the water. The electric resistance against an electric current is derived from the water height between the electrodes. Every 0.05 sec the electric resistance is registered and translated into a water height. As can be seen in Figure 4-22, a wave signal in time was recorded at three different locations.

4.3.1.4 Other instruments

When filling the flume the water height was set with a ruler taped on the glass. For building the structures also rulers and a lath was used. On both sides of the flume the three different profiles were marked on the glass and with the rulers the borders of the structures were marked. The duration of the waves were measured with a stopwatch.

4.3.1.5 Visual documentation

The structure was divided in three sections; the upstream slope (slope nearest to the wave paddle with black stones), the crest (white stones) and the downstream slope (slope farthest from the wave paddle with red stones). The different colours of the stones for the three different sections (upstream, crest and downstream) made visual observations possible.

Photographs were taken from certain tests before and after a wave series. In this way the number of stones that moved can be estimated. Also it can be seen from what area (upstream slope, crest or downstream slope) the stones were coming from. Video recording was performed for one test: the recorder zoomed in on the structure to record the process of the movement of the stones. The processes of the to-and-fro

4.3.2 Test procedure

moving rock could then be analysed.

For each test a structure was built in dry conditions with the profile drawn on the glass on both sides of the flume as reference. The toes on the glass were connected with a line and the volume, marked by the profile on the glass and the line, was filled by dropping stones sliding over a plate. The structure was filled with too small amount of

stones so the filling up to the correct height could be executed more accurately by hand. For the final part of the construction a ruler, connecting the drawn profiles on both sides of the flume, was used to check the height at different points. At the locations with a "gap" stones were dropped from the hand. When constructing the next structure with a different height, the already placed stones were used. For the next structure stones were added or removed. In order to get the same consistency in stone placement the stones of the former structure were stirred; so stones would still be randomly placed and not be influenced by a wave series of the previous test. In this way possible effects like compaction of the stones in the structure were prevented. Then the structure was completed with new stones for the test.

After the structure was build the flume was filled slowly so that the stones kept their position. Then the initial profile of the structure was measured with the PROVO. A carriage on the flume carried the PROVO to and fro over the structure. This was done multiple times in the direction of the flume for one line. A reference bar (see Figure 4-28) was used to compare profiles before and after a wave series to a set point. This point before each profile is used as reference point to compare the data from each measured profile.

The first series were carried out by measuring three different lines, in latter tests five lines were measured as can be seen in Figure 4-27 and two example lines in Figure 4-28. The Provo was placed on the measuring carriage on marked points with 5 cm space in between.

After each wave series the same lines were measured with the PROVO and the damage area could be derived from the difference between profiles of successive wave series.

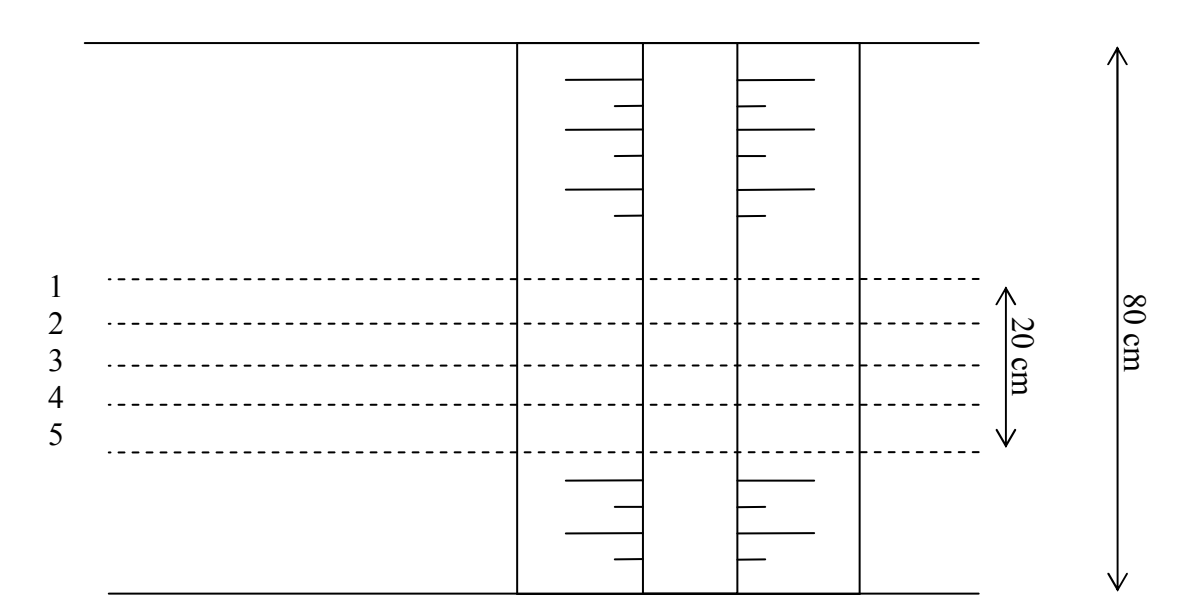


Figure 4-27 Top view of 5 Provo lines.

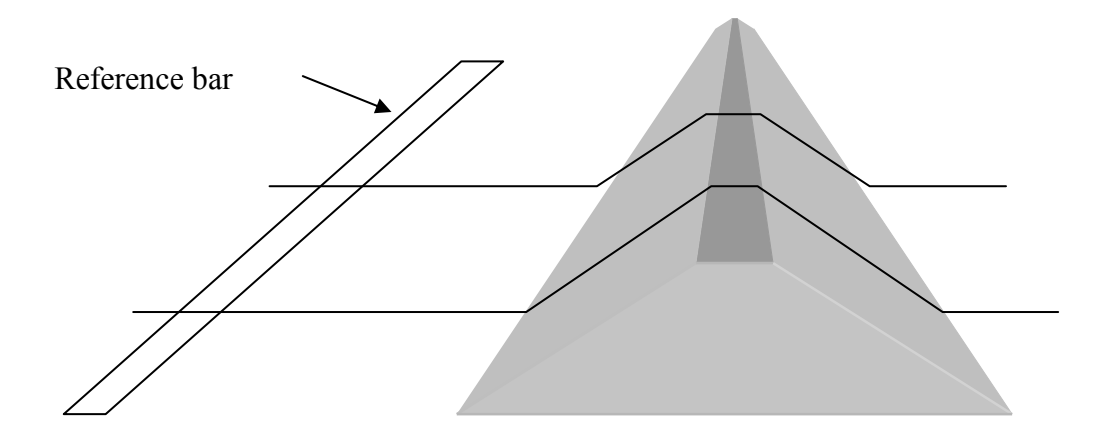


Figure 4-28. 3-D view with 2 Provo lines and the reference bar.

The wave parameters for each test were exported from a steering-file to the wave machine. Within one test three durations of waves were generated; first 1000 than 2000 and finally 3000 waves all with identical input parameters. After each wave duration PROVO measurements were executed.

4.3.3 Measured Conditions

There is a difference between input conditions like structure dimensions as designed or as measured. In the former sections of this chapter general input values were pointed out. The measured values will not give the same values as the input values for the steering file.

The values that will be analysed in chapter 5 will be conditions measured in the model tests.

4.3.3.1 Wave conditions

The water elevation in time was registered with the "Dasylab" program for the different wave gauges. Two wave gauges were placed in front of the structure to measure the wave climate and were used to separate incident and reflected irregular wave spectra. Also one wave gauge was placed above the crest of the structure for each test. This gauge recorded the wave climate above the structure but without the ability to separate incident and reflected waves at that position in the flume.

Wave reflection

Determination of incident and reflected irregular wave spectra can be accomplished by analysing time series records collected using spatially separated wave gauges (Hughes, 1993). Two wave gauges between the structure and the wave paddle were used to estimate the incident wave signal and the reflected wave signal.

The reflection could be separated into the reflection from the structure and the reflection from the wave dissipater. The computer program "Waves" estimated the distance range between the wave gauge closest to the structure and to the one in front of it, required for the Matlab program "Reflec" to separate incident and reflected waves. A distance between the wave gauges, within the margin indicated by "Waves", was set for each test. This distance was an input for "Reflec". The programmes used to obtain the incident and reflected spectrum are based on the Goda and Suzuki Method for spatially separated wave gauges (see Hughes, 1993). The incident waves only were considered to be responsible for the erosion. The reflection was considered to be sufficiently low to neglect (see spectra in Appendix C)

Wave measurements

Three series of waves were performed for each test. First 1000 waves, then 2000 waves and finally a series of 3000 waves. The wave conditions are constant, only the duration changed. The hydraulic conditions can be found in Table 4-6.

| Test | Test code | Water depth h (m) | Wave height H _s (m) | Peak Period T _p (s) | Wave steepness s_{op} (-) |
|------|-----------|-------------------|--------------------------------|--------------------------------------|-----------------------------|
| 1 | 0a6 | 0.55 | 0.198 | 2.14 | 0.0277 |
| 2 | 0a6s2.6 | 0.55 | - | - | - |
| 3 | 1a4 | 0.50 | 0.199 | 2.13 | 0.0281 |
| 4 | 1a5 | 0.50 | 0.199 | 2.13 | 0.0281 |
| 5 | 1a6 | 0.50 | 0.199 | 2.13 | 0.0281 |
| 6 | 1a6 her | 0.50 | 0.199 | 2.13 | 0.0281 |
| 7 | 1b4 | 0.45 | 0.171 | 2.04 | 0.0263 |
| 8 | 1b6 | 0.45 | 0.171 | 2.04 | 0.0263 |
| 9 | 2a6 | 0.45 | - | - | - |
| 10 | 2b4 | 0.45 | 0.163 | 2.04 | 0.0251 |
| 11 | 2b5 | 0.45 | 0.163 | 2.04 | 0.0251 |
| 12 | 2b6 | 0.45 | 0.163 | 2.04 | 0.0251 |
| 13 | 3c4 | 0.40 | 0.142 | 2.01 | 0.0225 |
| 14 | 3c5 | 0.40 | 0.142 | 2.01 | 0.0225 |
| 15 | 3c6 | 0.40 | 0.142 | 2.01 | 0.0225 |
| 16 | 1d6 | 0.50 | - | - | - |

Table 4-6. Measured hydraulic conditions.

The wave values from Table 4-6 are based on the incident spectrum from the wave paddle. For the fields without values only the combined spectra of incident and reflected waves are available.

No H_s higher than 0.22 m was possible because of the limitations of the wave generator. The highest waves measured in the test where a H_s of 0.22 was an input parameter, were about 0.26 m (see Appendix B). With a water depth of 0.60 m or

greater combined with the maximum H_s the stones showed very little or no movement.

In Appendix C the incident and reflected wave spectrum for each test can be found as well as the wave height distribution.

4.3.3.2 Structure deformation

For each test three or five Provo lines were measured. From the data two points were marked at a certain distance, so the average speed of the measuring carriage and thus the average distance step was known. In Figure 4-29 the first five graphs show the development of the profiles against an increasing number of waves. The horizontal and vertical axis are given in centimetres. The red line is the profile after the last wave series. The last graph below on the right side gives the relative eroded area $(A_0 - A_e)/A_0$.

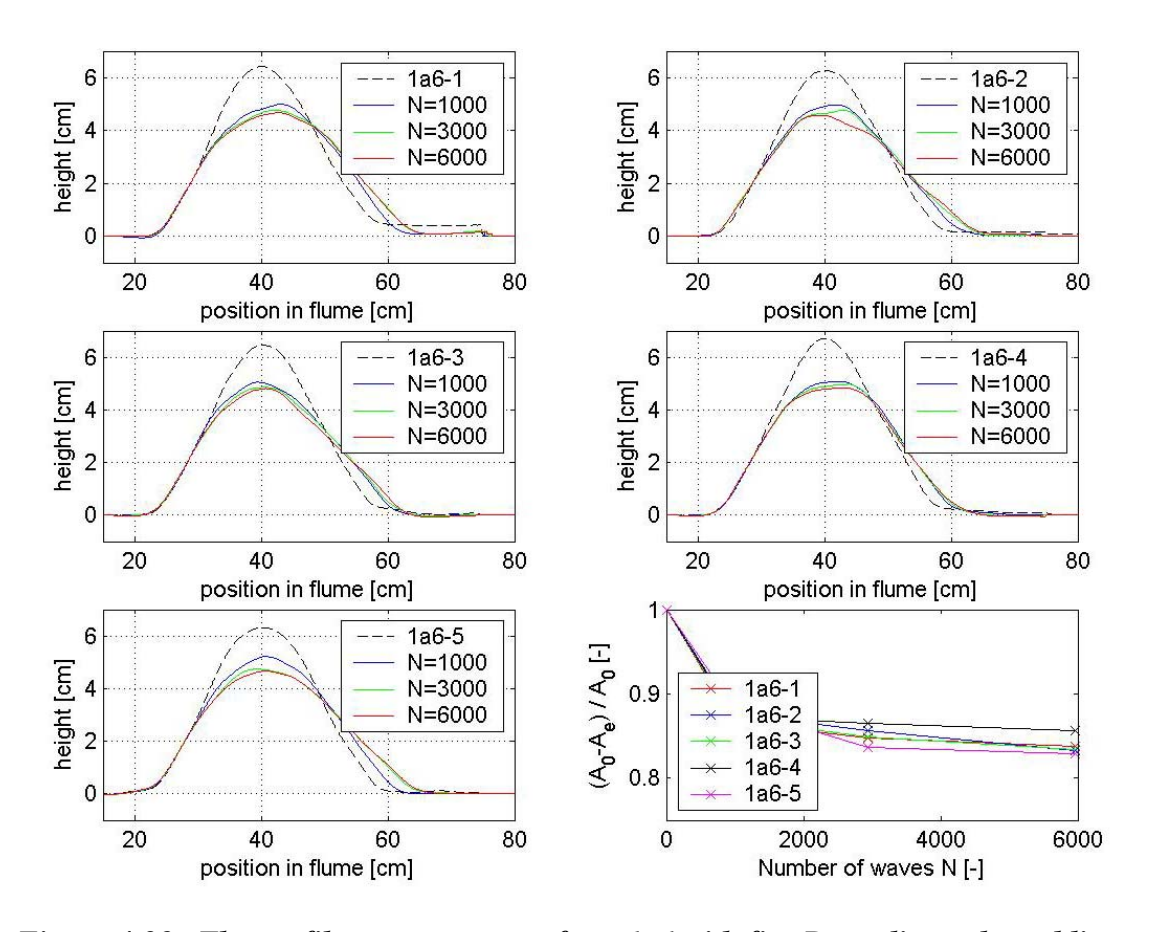


Figure 4-29. The profile measurement of test 1a6 with five Provo lines; the red line is the profile after the last wave series. Below, on the right side, the relative eroded area $(A_0$ - $A_e)/A_0$ is presented against the number of waves for each parallel Provo line.

All profile lines for each test and the relative area for each line can be found in **Appendix** E.

The structure height for each test is directly derived from the initial area A_0 and the prism shape defined by the structure slopes n and the crest width B_c (see Figure 3-17 and equation 4.3). The initial structure height h_c is the only unknown structure geometry and can be derived when shape and area are known. The heights, defined as the highest points measured by the Provo for a profile line, varied between individual lines. Less variation was seen in the structure area of different profile lines.

$$A_0 = (nh_c)h_c + B_ch_c \rightarrow h_c = \frac{-B_c + \sqrt{B_c^2 + 4(nA_0)}}{2n}$$
 4.3

The initial area and the derived height are averages over the measured Provo lines. The initial area (before wave load) and the derived initial structure height can be seen in Table 4-7.

| Test | Test code | Initial Area A ₀ | Initial structure |
|------|-----------|-----------------------------|----------------------------|
| | | [cm2] | height h _c [cm] |
| 1 | 0a6 | 113,5 | 5,98 |
| 2 | 0a6s2.6 | 112,76 | 5,96 |
| 3 | 1a4 | 68,108 | 4,48 |
| 4 | 1a5 | 80,83 | 4,94 |
| 5 | 1a6 | 127,06 | 6,37 |
| 6 | 1a6 her | 112,72 | 5,96 |
| 7 | 1b4 | 61,024 | 4,20 |
| 8 | 1b6 | 101,75 | 6,04 |
| 9 | 2a6 | 114,56 | 6,02 |
| 10 | 2b4 | 59,028 | 4,12 |
| 11 | 2b5 | 85,136 | 5,09 |
| 12 | 2b6 | 115,03 | 6,03 |
| 13 | 3c4 | 62,053 | 4,25 |
| 14 | 3c5 | 87,814 | 5,18 |
| 15 | 3c6 | 112,58 | 5,96 |
| 16 | 1d6 | 109,86 | 5,88 |

Table 4-7. Geometry of the structures.

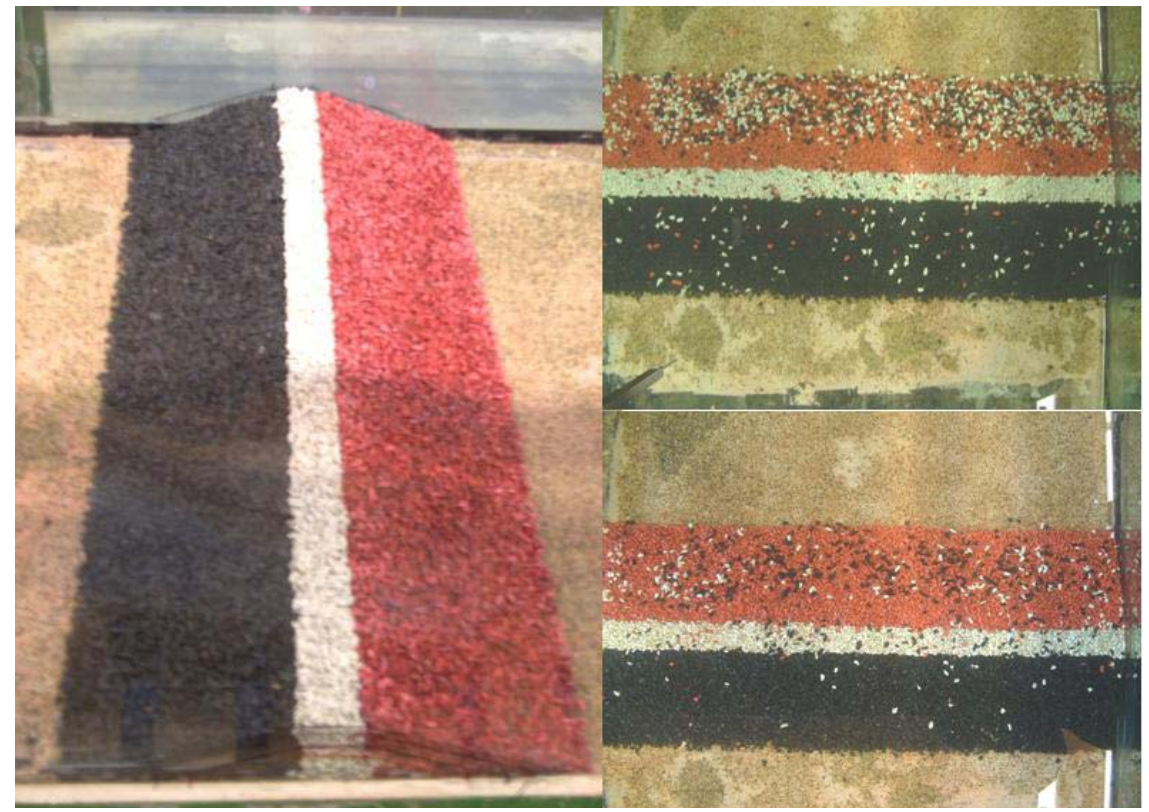


Figure 4-30. A tested structure: on the left the structure before waves. Top right: after 1000 waves. Down right: after 3000 waves

The area values of the individual lines and other measured geometry parameters can be found in Appendix B.

4.3.4 Additional observations

Some general observations are important for the analysis and further understanding of the tests. Certain environmental conditions were typical for all tests. The characteristic behaviour of the tested structures is mentioned below. The observations are divided in wave and erosion observations

Wave observations

The wave reflection caused by the structures was very low. Tests have been done in the flume without structure to compare the resulting spectra with the spectra of the tests. The presence of the structure showed no difference in the incoming or reflected spectra. The measured wave spectra and exceedance curves can be found in Appendix C.

For all tested conditions there still was occasionally breaking and white capping of the waves. This was primarily caused by a locally too high wave steepness. In the irregular wave spectrum the individual wave components travel at different speeds and due to wave interfering locally white capping occurred whereas individual waves would not break. The water depth had a minor influence on the breaking along the

flume. Different water depths showed the same observed breaking in the flume and it can be seen from the wave spectra exceedance curves of two water depths of the tests 0a6 and 1a6 that the wave characteristics do not differ significantly. Further observations showed also that white capping or breaking did not intensify in the area directly after the structure from which the assumption can be made that the waves were not "feeling" the bottom of the flume in a critical way.

In general the wave profile shows a clear non-linear behaviour, a sharp crest and a long through. The lowest part of the through is closer to still water level and the wave crest amplitude is higher than the significant wave amplitude.

Stone erosion observations

In general at the beginning of a test, the stones start moving at the top of the structure. The movement of the stones was always rolling and sometimes bouncing. The stones followed an oscillatory path where some stones travelled from the upstream slope over the crest to find the downstream slope. The opposite movement was observed less as the stones from the downstream slope remained on the crest or the upper part of the upstream slope.

The eroded stones were deposited mainly on the downstream slope of the structure. The upstream slope would lose a limited amount of stones but these occasionally created gaps in the slope were filled with surrounding stones and stones rolling back from the crest. As can be seen e.g. in Figure 4-29 and in Appendix E for all tests, the border of the lower part of the upstream slope keeps its slope angle. The net erosion or accretion of the lower part of the upstream slope is very low under the tested environment.

Only a small amount of transport outside the structure boundaries (toes of the slopes) could be seen. Almost no stones would find a stable position at the bottom on the upstream side of the structure apart from a few flat-shaped stones. Sometimes stones rolled in front of the structure but later they rolled back up the upstream slope or were left at its toe. The stones that left the border of the structure on the downstream side either found a stable position in the rough bottom area or, when they reached the smooth bottom, were transported further down the flume. After the last tests the stones were collected from the flume. All off them reached the breaker zone in the end, and were weighed to give an indication of the amount of transport. For the 15 tests where transport was seen (1d6 only minor repositioning) a quantitative estimation is made through the following calculation:

the structure initial volumes, derived from the average profile area in Table 4-7, lie between 4,700 and 9,200 cm^3. With an assumed porosity of 0.4, a rock density from Table 4-3 of 2,47 g/cm and the flume width of 80 cm the weight of an average structure in the flume is about 11 kg. The total weight of the transported stones during all tests was a little over 0.7 kg. This was for 15 tests, so for one test this means 0.7/15 on average. This is less than 50; so, for the tested conditions on average less than 0.5 % of the structure weight per meter is transported outside the downstream boundary of the structure.

The contribution of transport to the reshaping of the structure can be considered as relatively small compared with repositioning of individual stones to the downstream slope and the compaction of the structure as a whole.

After some time, when more waves had passed, the stones became more stable and less motion was observed. When occasionally stones moved it was observed that they often moved as a group of 3 to 5 stones at the same time.

At the end of each test the structure stiffness as a whole and the position of individual stones was measured in a qualitative way. The structure was smoother after the wave series. The interlocking forces in the direction of the flume was simulated by lightly stroking the crest of the structure under water with the fingertips. When this was done on stones in a structure that wasn't loaded by waves, the surface felt more rough and the stones rolled easily along the fingertips. The same situation was present for a tested structure where the stones on the slopes where easily moved. Whereas the crest stones, down to the curves to the slopes, showed no movement. The stones in the top layer interacted and could withstand a much greater load from the fingertips than the slope stones. When the top layer was removed the stones directly under the top layer were moved as easily with the fingertips as the stones on the slopes.

4.4 Accuracy of the measurements

The character and reliability of the measurements depend on the accuracy and precision provided by the instruments with the operator's dependability and skill (Hudson, 1979).

The extent, to which instrument and operator's errors impact the results, depends of course on the magnitude of the error. Quantifying these errors is very important, in order to establish the reliability of the experiments.

Deviations in measured data which can arise due to external factors that cannot be controlled, like the inability to repeat exactly a flow condition, can be found during the test. There will always be deviations in the results for the model tests, even when the instruments have an error that is zero. The analysis of the measurements and the results will be treated in chapter 5.

Other errors, like reading errors and incorrect instrument usage can only be eliminated through careful and continual checking of the experiments (ASCE, 2000).

Profile measuring errors

Measuring the damages is a key aspect in the investigation. The profile measurements by the Provo instrument are translated directly into the damages that are related to the properties of the wave field. The profile measuring system consists of three basic elements that can be an error source:

- 1. Measuring carriage
- 2. The positioning of the Provo on the carriage
- 3. Provo system itself

Comment on the three elements:

- 1. The measuring carriage has a left and right going speed which slightly differs. The difference of the mean speed in left and right direction of the car has to be taken into account to calculate the profile length in the flume direction. It trembles a bit and showed changes in velocity which are up to 3% of the mean speed (0.61 cm/s) which can give errors on a slope. These peak changes in velocity have a period of less than half a second, so on average the error will be small.
- 2. The Provo is placed on the car and is put into position by hand. Its own weight keeps it in place, the Provo doesn't move visually, even when a turning point is reached. Before each test the Provo had to be placed as exact as possible, so the probe would have the same position for a measured line as it had in the former measurement. This placement was done by marking the position with two points on the carriage. In this way the probe could measure the same line after a wave attack with an error smaller than 1 mm.
- 3. The probe of the Provo keeps a constant distance above the rock and delivers a line which is seen as the boundary of the measured near-bed structure. The Provo signal sometimes showed a jump (of the average signal) of about 1 mm or less (see Appendix F). A second error source is that, when the constant distance from the probe to the rock was too large (6-7 mm), the distance from the structure crest was smaller than the distance from the flume bottom.

Also the shape of the top layer can change the measured top level. A rough top layer can cause the probe to detect the highest point and then has little time to find gaps in between. When the surface is smoother, as can be the case after a wave load, there are less and smaller gaps which can result in a smaller area of the top layer of stones. This aspect is shown in Figure 4-31.

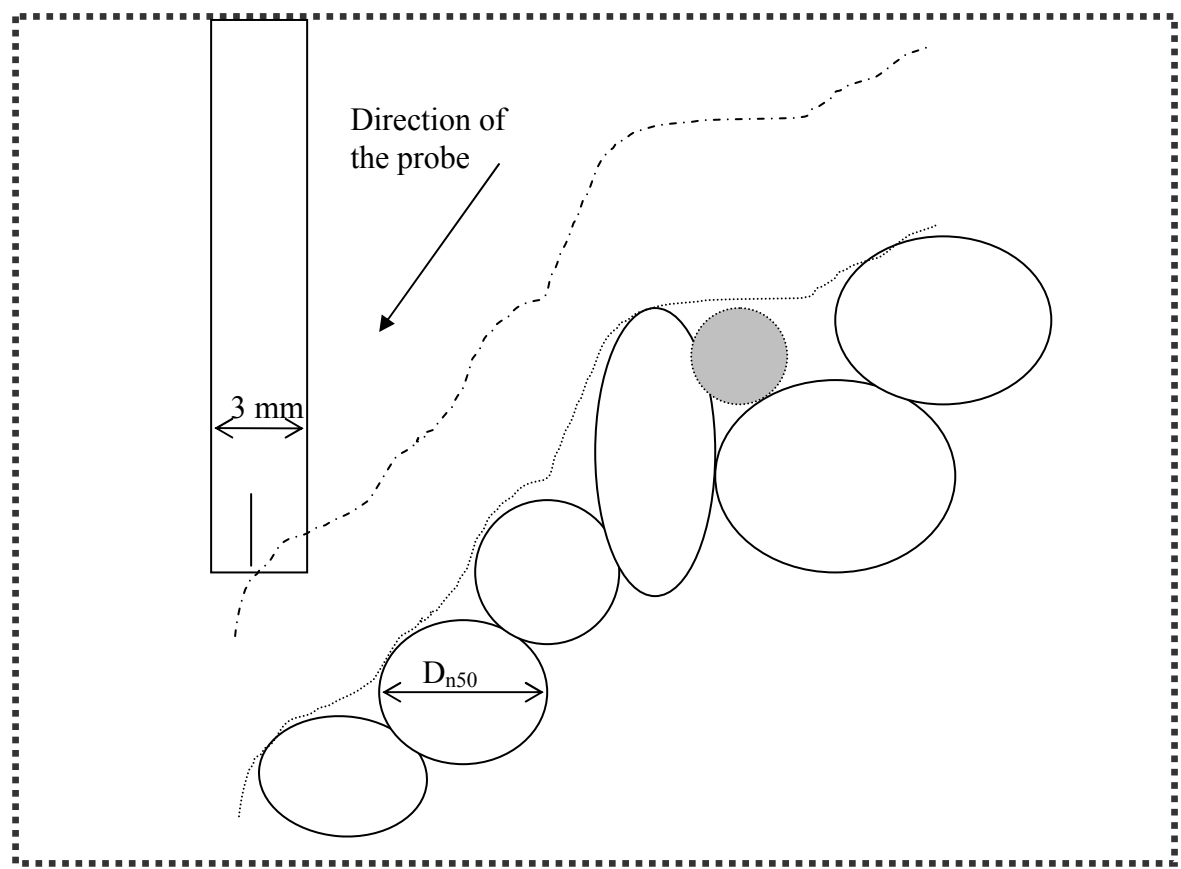


Figure 4-31. PROVO probe measuring the structure profile.

Calibration of the measuring carriage speed

It was found that the velocity on the display turned out to be an underestimation of the actual carriage speed. The speed of the carriage was found to be constant during one test, but proved to deviate for different tests. When according to the profile data for test 1a4 the carriage speed was 6.3 cm/s after the wave series of 1000 waves, the carriage speed for the second series of 2000 waves turned out to be 6.8 cm/s. As no carriage speed was directly recorded the speed of each profile measurement was estimated based on the profile data. For the calibration of each individual test two set points with a known distance were needed. The first point was the centre point of the reference bar. The probe would pass the reference bar again after the switch of the carriage turned for the left going measurement of the profile. When turning at the switch point the carriage had a pause of around 5 seconds. This turning time accuracy was found to show a large deviation of up to 0.5 seconds. So the reference bar for the second time as second point was found unsuitable.

The second point used was the uphill slope of the structure. This slope, nearest to the wave paddle, showed no visual erosion near the bottom of the structure. The centre points of the structures were built always at the same position in the flume. With this centre point as second reference point the velocity of the first profile measurement before erosion could be calibrated accurately. The uphill slope at a height of half the initial structure height was assumed to keep its position after wave attack. So after a wave series the data of the next structure profile was calibrated in a way that the uphill slope kept the same position. Then the carriage speed was calculated and the same derived distance step (carriage speed * time step) was used for the eroded area (A_e) calculation. The precision and accuracy of the profile measuring system will be analysed based on the measured signals during calibration and can be found in Appendix F.

Quantified errors

The error values measured from the experiments and used for the analysis and derivation of characteristic parameters must be quantified. These errors can then be evaluated in the analysis of the experiments in chapter 5 and compared with the deviations in the measurements. The measuring errors due to the used instruments are estimated in Table 4-8

| Instrument | Used for measuring | estimated error | |
|-------------|----------------------------------|----------------------------|--|
| Provo | Structure profile | Accuracy ±1.5 mm | |
| Wave gauges | Water level registration | Accuracy ±0.2 cm | |
| Tapeline | Dimensions of flume, still water | Accuracy & reading errors; | |
| | level | ±1 mm | |
| Balance | Stone density | Accuracy & reading errors; | |
| | | $\pm 0.1 \text{ g/cm}^3$ | |

Table 4-8. Error estimations for the instruments.

The errors in this section are based on the measurements. As pointed out earlier, even with perfect measurements there will always be deviation in the results. The complexity of individual stone position and the turbulent water flow will lead to the fact that no measurement can be done under exactly identical circumstances. The deviation of the results and the measurement errors both influence the accuracy of

deformation prediction based on the test results. The test result accuracy will be treated in section 5.3.3.

4.5 Evaluation

For all tested conditions there still was occasionally breaking and white capping of the waves. In the irregular wave spectrum the individual wave components travel at different speeds and due to waves interfering locally white capping occurred whereas individual waves would not break. In Appendix B all the directly measured parameters and derived parameters are given in order to give an overview of the numeric results.

Wave measurements

The wave measurement is important for the comparison of the different tests. The spectrum is based on the time signal from the wave gauges. From this spectrum all the parameters that describe the hydraulic conditions are derived. These derived parameters are used in the next chapter for the analysis of the experiments. The severe breaking of the waves mostly occurred at or directly beyond the wave paddle. This transmission of the steering file on the water is therefore not perfect and obviously the highest waves that the paddle intends to create are the first to break. This influences the measured spectrum and, maybe more important for erosion, the wave exceedance curve. The breaking of the highest waves will cause the peak waves to break into waves with less height and a large group of waves will be present with a same maximal height. The spectra and the wave exceedance curves for the tests can be found in Appendix C.

Provo measurements

The calibration of the instruments was done before the tests when the different signals were checked. An important error source turned out to be the measuring carriage speed. The method of calibration of the speed of the measuring carriage (Appendix F) is important for the accuracy of the results of the profile measurements. A reference point is the uphill slope at half the initial structure height. The assumption that this structure boundary keeps its position is important. The fact that most erosion occurs at the crest supports this assumption. From the profile data it can be seen that the uphill slope keeps its angle after erosion, at least up to half the initial structure height. This observation also supports the assumption that the uphill slope keeps its position in the flume.

The background of this problem and the calibration procedure can be found in Appendix F.

5 Analysis of the Experiments

In this part of the thesis the results from the measurements are analysed. The aim of this chapter is to find a way to predict the deformation of near-bed structures under irregular waves based on the test results.

First the relevant parameters used are described in general and dimensionless quantities and boundary conditions are defined. To asses the damage through dimensional analysis non-dimensional parameters are treated to predict the deformation of the tested structures. Two approaches to predict the deformation are used and an example calculation for the prediction of a situation in nature is given. Finally some aspects of the test results are evaluated.

5.1 Dimensional analysis

Vidal et al. (1998) identify three approaches applied by scientists and engineers to asses the damage of rubble mound structures:

- Dimensional analysis: The damage is expressed as a function of some non-dimensional parameters. The experimental data are used to obtain the function that gives the better fit between calculated and measured damage. This approach is the most widely used in the assessment of rubble mound breakwaters
- Quasi-empirical approach: This approach makes use of the knowledge of the flow around and inside a rubble mound structure. With a flow model and a formulation for the hydrodynamic forces the quasi-empirical model is based on the assumption that the damage should be a functional of some nondimensional parameters that represent the hydrodynamic forces acting on the units.
- Dynamic analysis: This approach is similar to the quasi-empirical approach as it uses an analytical model of the flow. Once the flow is known, also the vector forces over the units are expressed, including the interlocking forces between the units. This approach allows the study of the dynamics of the armour stones in real time. The state-of-the-art of the analytical knowledge of flow and interlocking forces does not allow its use for the design of structures.

It is difficult to measure or describe the flow around the stones, especially when irregular waves are concerned. In these tests no direct flow measurements are performed. The water velocities near the bottom can be derived from the measured wave signal. In this thesis the dimensional analysis is used as approach to assess the damage due to the environmental conditions tested.

For the dimensional analysis and the prediction of deformation the parameters are divided into three categories:

- 1. hydraulic conditions present
- 2. duration of the hydraulic load
- 3. geometry of the near-bed structure

With the first category, hydraulic conditions, is meant the circumstances that "attack" the near-bed-structure and determine the stability of one stone. The hydraulic conditions are defined here as if there was no rubble mound near-bed-structure present (without the influence of the size and shape of the structure as a whole). The parameters that follow from the three categories are dealt with in the next section.

5.1.1 General parameters in deformation analysis

The deformation of a near-bed-structure can be expressed as *E*, which represents the level of erosion of a measured profile. The (initial) porosity of the structure and the individual stone shapes are disregarded here. When, furthermore, the structure is considered to be geometrically defined as in **Figure 3-17**, the parameter *E* can be seen as a function of the parameters that describe the environmental conditions and has the following form:

$$E = f(n, B_c, h_c D_{n50}, W, \rho_w, \rho_s, \nu, h, H, T, g, N)$$
5.1

where:

E is the dependent deformation parameter [-]

In equation 5.1 α , B_c , h_c describe the initial geometry of the structure, D_{n50} , W, ρ_w , ρ_s , v, h, H, T, g represent the hydraulic conditions and N describes the time aspect. The parameters are defined in the overview in **Table 4-2**.

The incorporation of the structure geometry parameters for predicting erosion is difficult. The difficulties can be divided in two basic problems:

- 1. How the structure geometry is defined when the structure is eroding in time.
- 2. The aspect that the erosion changes the geometry and therefore influences future erosion.

A near-bed-structure can be defined as a prism with a certain crest-width, crest-height and slope angle (see **Figure 3-17**). The most evident geometry influence seems to be the structure height as other geometry parameters can be derived from a change in structure height. The decline of structure height can be seen as a flattening of the structure, an increase of the crest width B_c and/or a decline of the slope n. Levit et al. (1997) tested two slopes (1:2 and 1:5) and found that the different slopes had no significant influence on the erosion of the structures. The structure can be defined by a prism with area A, with the only varying parameter h_c . So erosion can be expressed directly in a derived h_c .

The second part of the problem, the influence of erosion on future erosion, can be handled by regarding the structure geometry as starting conditions for the erosion process. When the structure height can represent the structure geometry, then for the prediction of following erosion it can be seen as a starting condition. For a prediction formula the structure geometry is represented in this analysis by the initial structure height. The height is derived from the measured area and the defined

structure shape. The procedure of deriving the structure height from the measured profile area can be found in section **4.3.3**. The analysis of the structure height will be treated further in section 5.2.3.

In these tests only one stone gradation is used, so possible results due to variation in stone gradation (W) or size (D_{n50}) have not been tested.

The wave height and period are assumed to be described by a JONSWAP Spectrum and incorporated through the significant wave height H_s from m_0 by equation **2.10** and the peak period T_p . When considering that the flow above the stones causing erosion is rough turbulent for all tests (see **Appendix** A), a change in Reynolds number does not affect the drag on the stones and the influence of the kinematic viscosity ν can be neglected in a damage prediction formula.

Based on the former statements, equation 5.2 can be simplified to the following expression:

$$E = f(h_c D_{n50}, \rho_w, \rho_s, h, H_s, T_n, g, N)$$
 5.2

The parameters that are considered to describe the structure deformation process in equation 5.2 can be found in Table **5-9**.

| Parameter | Symbol | Unit |
|-------------------------------|---------------------------------|----------------------|
| crest height | h_c | [m] |
| stone characteristic diameter | D_{n50} | [m] |
| | | |
| stone density | ρ_s | $[kg/m^3]$ |
| water density | $ ho_{_{\scriptscriptstyle w}}$ | [kg/m ³] |
| | | |
| water depth | h | [m] |
| wave height | H_s | [m] |
| wave period | T_p | [s] |
| gravitational acceleration | g | $[m/s^2]$ |
| | | |
| number of waves | N | [-] |

Table 5-9. Parameters considered describing the structure deformation process. The marked parameters were varied in the tests.

5.1.2 Dimensionless boundary conditions

Based on the parameters that describe the environmental conditions some general dimensionless parameters can be derived. These parameters can be seen as boundary conditions for the physical processes governing a relation between deformation and non-dimensional parameters. When comparing the model circumstances with those in nature, these parameters can be used to test the similarity of the physical processes. To compare the conditions in the model with a situation in nature the conditions must be similar. That similarity can be described by dimensionless boundary conditions

that describe the physical processes of irregular waves attacking a rubble mound nearbed-structure in transitional water depth.

The boundary conditions for the experiments can be expressed in the following dimensionless ratios:

• Reynolds wave number and relative roughness: $\frac{\hat{u}_{\delta}a_{\delta}}{V}$, $\frac{a_{\delta}}{k_{s}}$

These parameters were used by Jonsson (1966) to determine the turbulent character of the flow around the stones. To compare the model tests with the situation in nature the flow must be in the rough turbulent zone to exclude viscous influences on the tests.

• Ratio between water depth and wavelength: h/L

A condition for a similar vertical velocity profile in the model as in nature is that the h/L ratio that is analysed in nature must be similar to the value in the model. In the model the situation is described as transitional water depth meaning: $1/20 < h/L < \frac{1}{2}$ and defines transitional water depth. In the model h/L is about 1/8. This means that the velocity profile from linear wave theory has a similar shape around the bottom when in practice also transitional water depth is the case.

• Wave steepness and the ratio between wave height and water depth:

$$s_p = \frac{2\pi H_s}{gT_p^2} \tanh kh, \ \frac{H_s}{h}$$

These parameters determine the state of the waves with regard to breaking aspects and wave spectrum shape. When the wave steepness in two situations is very different, then the comparison of the type of wave load is difficult. The ratio between wave height and water depth cannot be too large, otherwise the highest waves in the spectrum will break. The objective in the experiments was to keep the variation of the wave steepness s_p as small as possible to keep the wave spectra comparable. The influence of the wave steepness is not tested in this investigation.

• Ratio between structure height and water depth: $\frac{h_c}{h}$

To fit the geometry in the hydraulic boundary conditions the structure height can be made dimensionless with the water depth (h). This parameter can be used to determine similar flow around the structure. When this parameter has a sufficiently low value, the water flow, attacking the structure, can be considered to be horizontally orientated and a relatively low vertical component of the orbital water movement is present.

Also dimensionless boundary conditions specifically for the structure geometry can be defined:

• Dimensionless crest width: B_c/D_{n50}

This ratio can be seen as the number of stones covering the crest in a profile of a nearbed structure. • Dimensionless structure height: h_c/D_{n50}

This ratio can be seen as number of layers of the near-bed-structure.

• Slope angle: *n*

This is the angle of both slopes of the tested near-bed-structures

These dimensionless boundary conditions for the structure geometry define the number of stones in a near-bed-structure and determine the ability of the stones in the structure to interact. When, theoretically, a structure consists of only one stone no interlocking or sheltering is possible. When the crest (profile) consists of a large number of stones, the stones have more possibilities of finding a stable position with the same dimensionless hydraulic conditions.

5.2 Non-dimensional prediction parameters

To use the model results for the damage prediction of near-bed-structures, the deformation parameter E can be expressed in non-dimensional parameters. Non-dimensional parameters can be used to translate the results of physical model testing to a prototype situation. Different current situations can be compared if the relevant dimensionless parameters are equal (Battjes, 1990). When the flow situation in the laboratory and a proto-type situation are similar and the same physical processes are present, the transformation of the results of the physical model tests to near shore/offshore conditions in nature is valid. When the relevant parameters are incorporated, they should have the same value in nature as in the model, if in both cases the same physical processes are present. In this way the situation in nature can be predicted from the model.

With the use of the parameters in the former section non-dimensional parameters can be constructed and the deformation parameter E can be expressed as:

$$E = f$$
 (non-dimensional parameters)

The function will vary every time the geometry of the structure changes the hydrodynamics and the gravity or interlocking forces involved in the movement of the units.

5.2.1 Time dependency

The dimensionless representation of the duration of the wave load can be expressed in N, the number of waves attacking the structure. When all the waves attacking the structure are equal in height and in period the summation is a very trivial operation. When dealing with irregular waves this is a bit more difficult. But if the wave spectrum describing the waves is considered constant in time, then the waves occurring with a certain duration can be summated. Two completely different wave fields with a different spectrum shape and area (wave height) can not be summated to

5.3

describe the erosion in time. An hour of swell and an hour of waves with a shorter wave period don't simply represent two hours of waves.

A necessity for the wave registration is that the wave paddle must have enough time to "fill" the spectrum with all its typical wave components. A value of around 1000 waves can be considered a representative number of waves in a spectrum.

The problem is that in nature a constant wave spectrum doesn't occur; a spectrum develops in time. When regarding several storms with different wave spectrum properties and thus with different parameters H_s and T_p representing the hydraulic conditions, the waves can't be summated without complications because of the internal differences in N. So the use of N is bounded by only one hydraulic situation. A possibility to avoid this problem is to seek one hydraulic condition that is considered representative for the storm situation over a certain period. For the model tests the same hydraulic conditions for the three wave series were used within each test, so the number of waves N could be summated to represent the wave load duration

The erosion per time unit is expected to become less when time passes under the same hydraulic conditions. This aspect of decreasing erosion in time can be incorporated by using an exponent for N smaller than one.

Thomas and Schuttler (1975; see Van Gent and Wallast, 2001) suggested to incorporate N for an erosion prediction formula with a square root. When looking at equation 5.2 and when the erosion parameter S is used for E, the parameter N has the following dependency:

$$E = S \propto \sqrt{N}$$
 5.4

This relation is often used in breakwater research (Van der Meer, 1991; see Van Gent and Wallast, 2001) and seems satisfactory for the hydraulic conditions concerning the near-bed structure investigation by Van Gent and Wallast (2001) which included the data of Lomonaco (1994). In their investigation the number of waves N and the deformation parameter S are combined to one parameter: S/\sqrt{N} .

When a near-bed structure is exposed longer with values of N over 3000 waves, S/\sqrt{N} doesn't seem to fit the trend (Levit et al., 1997).

In the test series of this investigation a trend in the erosion in time shows a "flatter" trend than the square root of N (Figure 5-32).

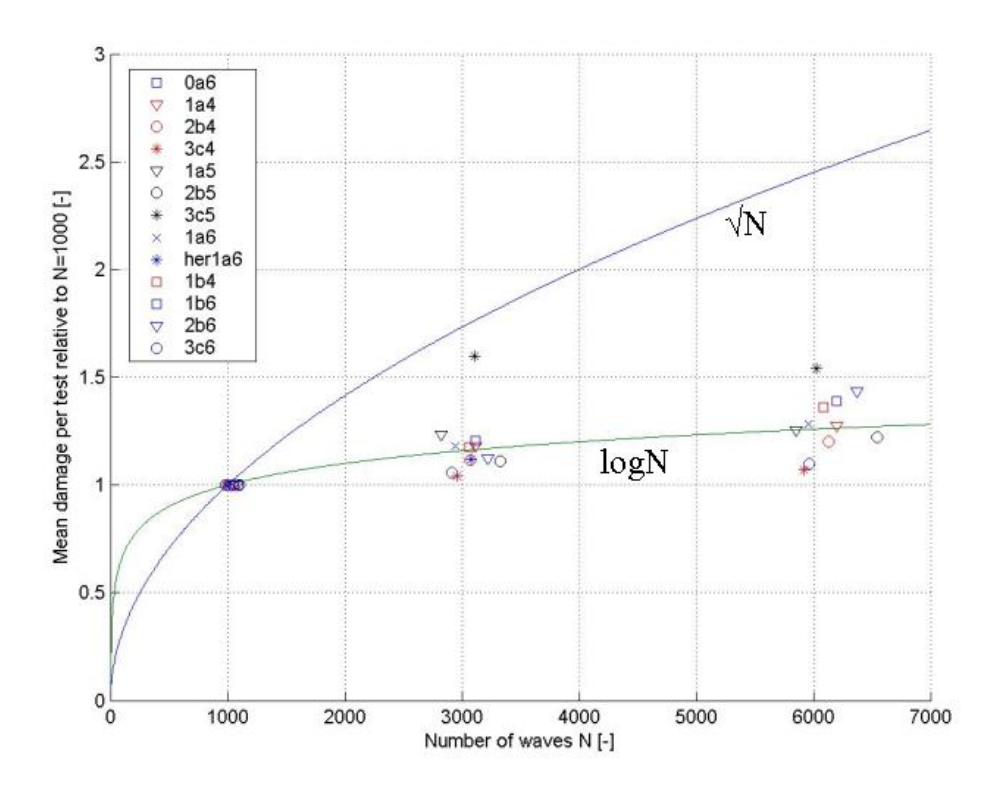


Figure 5-32. Test data with respect to S relatively to N=1000. Further a square root function ($\sqrt{N}/\sqrt{1000}$) and a logarithmic function ($\log N/\log 1000$) are shown to illustrate the trend.

In Figure **5-32** the relative erosion (erosion normalised to the erosion after 1000 waves) for all the tests is shown. A profile line measured by the Provo is regarded as a single independent test. For each test 3 to 5 parallel profile lines were measured which are considered independent of each other, e.g. when one profile line shows erosion this erosion is assumed not to influence the line next to it. The relative erosion reaches a certain level relatively quickly and then follows a flat trend upward for all the tests. To incorporate the relation between S and N in a damage prediction formula a log N rather than \sqrt{N} is suggested here. In Figure **5-32** can be seen that the logarithmic gives a good estimation of the influence of the number of waves. For the data analysis where also the different hydraulic conditions are incorporated, a comparison will be made between the parameters S/\sqrt{N} and $S/\log N$ in section 5.3.1.

5.2.2 Hydraulic conditions: mobility parameter

The hydraulic conditions can be put into a mobility parameter as non-dimensional parameter. In this parameter the time effect and structure geometry are not incorporated and has the following form:

Mobility parameter =
$$f(D_{n50}, \rho_w, \rho_s, h, H_s, T_p, g)$$
 5.5

This mobility parameter represents the intensity of the hydraulic load; when it has a larger value there will be more stone mobility or erosion.

The hydraulic conditions can be described with the Shields parameter as mobility parameter. The Shields curve for unidirectional flow is then used and the peak shear stress $\hat{\tau}_w$ under oscillatory flow is calculated introducing the wave friction factor according to Jonsson (see equation 2.27).

For the shear stress $\hat{\tau}_w$ use is made of the characteristic velocity \hat{u}_δ and a wave friction factor (f_w) . The latter requires expressions for the bed roughness (k_s) and a characteristic amplitude of the oscillatory horizontal wave motion at the bed (a_δ) . The expressions for f_w and k_s are not very accurate in general, so a description based on the bed roughness might be inappropriate.

Considering the limitations in the accuracy of the determination of the shear stress $\hat{\tau}_w$ for stone stability, it might be more appropriate to express the destabilizing load directly in the squared water velocity \hat{u}_{δ}^2 near the bottom. This aspect is also treated in chapter 3 where the investigations on near-bed structures are treated. This characteristic velocity can be considered to be able to describe the hydraulic conditions.

To investigate a near-bed structure with the aim to predict its erosion in real conditions that can be compared with those in the Southern North Sea, a mobility parameter similar as earlier defined can be used:

$$\theta = \frac{\hat{u}_{\delta}^{2}}{g \Delta D_{n50}}$$

$$\hat{u}_{\delta} = \frac{\pi H_{s}}{T_{p}} \frac{1}{\sinh k(h)}$$
5.6

where:

 θ is a mobility parameter based on the bottom velocity \hat{u}_{δ} [-]

The mobility parameter θ in equation 5.6 (with a spectrum-based velocity) must be combined, together with the time aspect, with a parameter that represents the structure geometry. The incorporation of a structure geometry parameter in a deformation prediction formula will be treated in section 5.2.3. The hydraulic conditions are represented by θ and can be scaled to real conditions. All parameters from equation 5.5 are represented in the mobility parameter θ .

5.2.3 Incorporation of the initial structure height

Here the incorporation of parameters that represent the initial structure height is treated. An inventory of dimensionless parameters that can describe the influence of the initial structure height is given. These parameters are evaluated to represent the structure geometry in a deformation prediction formula. A choice is made how to incorporate the structure geometry for deformation prediction.

5.2.3.1 Initial structure height and velocity at the structure crest

The influences of change in initial structure height on the flow around a near-bed structure are analysed here. The initial structure height is a starting condition for the deformation or reshaping process. The change of the crest level in time itself influences further deformation. The decline of crest height has a stabilizing effect on the structure as a whole; the water can flow more smoothly over it. The h_c -parameter is regarded to represent the geometry and its influence should be incorporated in a formula describing the deformation or reshaping of a near-bed-structure. The initial structure height h_c is seen in this thesis as the governing geometry parameter representing the structure geometry.

The influence of the initial structure height is complicated, as it interacts with the hydraulic conditions. Differences in initial height influence the water velocity at the stones on the structure crest and therefore the erosion. Two (or a combination of two) basic processes can cause the increase of velocity at the structure crest compared to the velocity near the bottom of the flume:

- 1. Wave theories predict higher (orbital) velocities nearer to the water surface.
- 2. The structure causes streamlines to go around it and the streamlines contract above the slope resulting in a higher water velocity at the crest.

These two aspects will be treated below.

1. Higher velocities nearer to the surface

There is a velocity profile which changes with the structure height. Near the bottom the orbital (elliptic for transitional water depth) motion becomes flatter to a purely horizontally orientated motion at the bed disregarding local turbulence. The vertical velocities of the orbital water motion are theoretically zero at the bottom. A velocity profile with a near-bed-structure is shown in Figure 5-33.

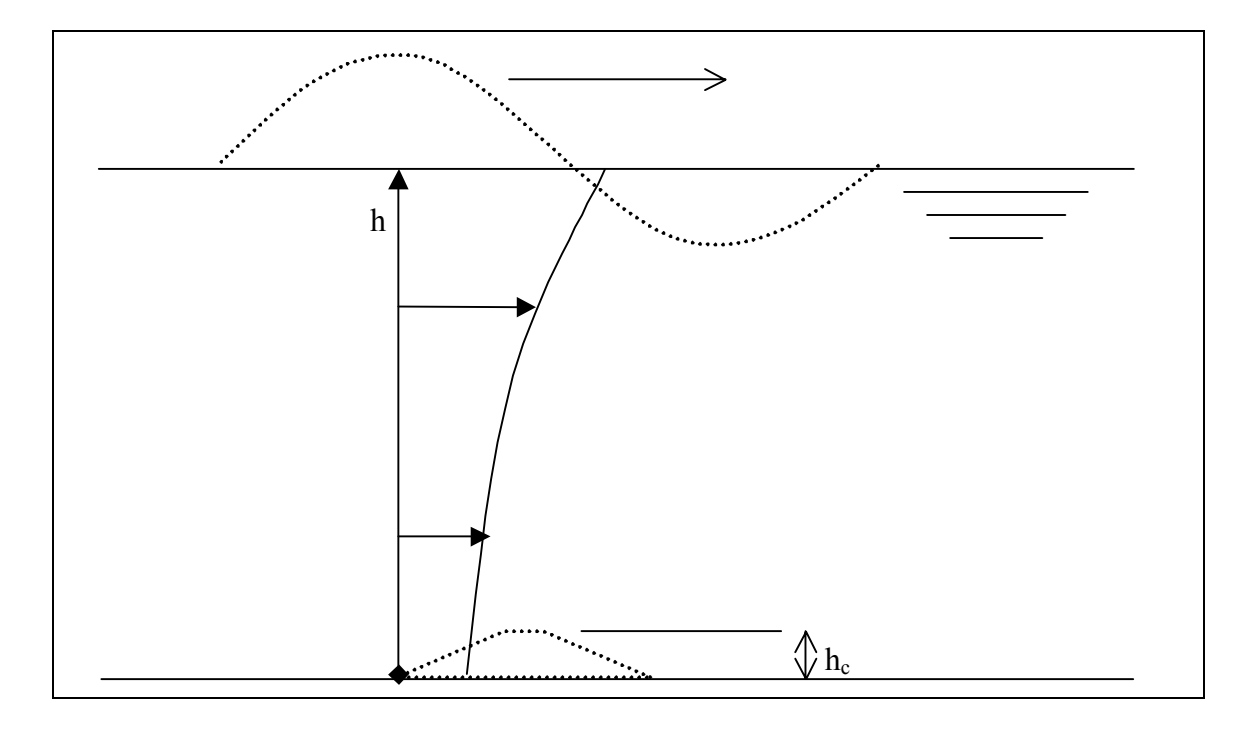


Figure 5-33. Example of the shape of the horizontal velocity components under the wave crest at the location of a near-bed structure.

There are vertical velocities and accelerations present because of the turbulent water flow around the stones but these influences on the mobility of the stones are assumed to be incorporated by the horizontal velocity component from linear wave theory. The horizontal velocity amplitude near the bottom \hat{u}_{δ} is used for the mobility parameter θ .

When the ratio between structure height and water depth is low (in the tests h_c/h is always smaller than 0.15), the velocity from linear wave theory shows minimal changes for different initial structure heights. In the logarithmic profile of Figure 5-33, the horizontal velocity at the bottom has almost the same value as the theoretic velocity at the crest height. So, for all the tests with the values of h_c/h below 0.15 it is assumed that the differences in velocity at the bed level and at the crest level (in a vertical velocity profile according to linear wave theory) are negligible when no structure is present. The velocity profile (when no structure is present) near the bottom will be assumed to be equal for all water depths up to the crest level; a vertical profile near the bottom.

2. Streamline contraction

With a prism, with a certain initial structure height representing the structure geometry, the horizontal flow near the bottom would be diverted more to the crest and a higher velocity can be expected at the crest compared with the situation without a structure. A higher structure, with identical environmental conditions, means a greater mobility or loss of stones at the crest because of the described contraction of streamlines above the area of the structure slope (Figure 5-34). This effect can be labelled as shoaling. The structure slope decreases the water depth which results in higher velocities at the crest (disregarding flow through the structure that is considered to be relatively low).

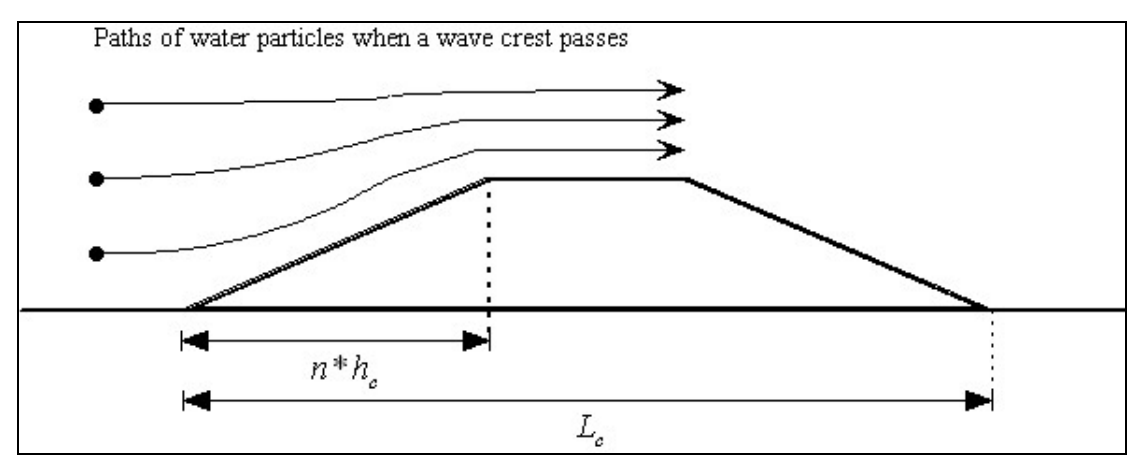


Figure 5-34. Effect of the structure height on the water velocity at the crest with contracting streamlines of water particles during half a wave cycle.

The length of the streamlines in Figure 5-34 are of the same order of magnitude as the profile bottom length (L_c). With a longer slope length ($n*h_c$), as result of a higher initial structure height, the flow contracts more. At the crest the stones are subjected to larger hydraulic forces than would be the case at a smaller initial structure height.

Based on the two effects treated in the former part, the increase of velocity for a higher structure crest is assumed to be primarily caused by the streamline contraction due to the shoaling as result of the structure slope. The velocity profile (when no structure is present a logarithmic profile) is assumed to be vertical near the bottom.

5.2.3.2 Parameters incorporating initial structure height

For the prediction of damage the initial structure height can be incorporated in dimensionless form. Combined with the dimensionless parameters for the hydraulics and the duration of the load this will result in the following general expression:

$$E = f$$
 (dimensionless h_c)

The question is how to incorporate the influence of the initial structure height h_c . When the initial structure height is larger than a reference design height and all other conditions are identical, the wave load on the crest stones is larger. A parameter that represents the initial structure height must include this effect and should be derived with the physical processes in mind.

For the incorporation of the initial structure height into a deformation prediction formula the following dimensionless parameters are considered:

• Initial structure height/stone diameter h_c/D_{n50}

The parameter h_c/D_{n50} can be seen as the number of the number of layers in a structure with the thickness of one stone diameter. But an increase of the layers can't be explained as a more instable situation. It can be considered as a boundary condition that creates possibilities for moving stones to find a more stable position (see section 5.1.2). When the structure would consist of e.g. one layer, then the sheltering and interlocking forces would have less chance.

In the tests the only varying structure-geometry parameter was the initial structure height. The parameter D_{n50} was constant for the tests.

So incorporation of the initial structure height can only be compared for situations with identical stone sizes. But the aim for this investigation is to use model tests to predict erosion in nature. The stone sizes will be 10 to 25 bigger for a pipeline protection in practise.

• Initial structure height / Water depth: h_c/h

The parameter gives a relation between the geometry and the hydraulic conditions and is named as relevant parameter in the investigation of Vidal et al. (1998) in combination with the stability parameter N_s . The problem with this parameter combined with a parameter representing the hydraulics like θ is that the water velocity is already defined. When comparing different h_c with the same water depth, the initial structure height has effect in deformation prediction formulas. But a change

5.7

in water depth (implicating a different h_c/h) has no influence on the situation because the velocity near the bottom (\hat{u}_{δ}) is already defined in θ .

• Initial structure height incorporated in a mobility parameter The initial structure height can also be incorporated in a mobility parameter such as θ . A higher value for the initial structure height must give a higher mobility parameter. The velocity part of θ can be given a higher value for increasing initial structure height. As can be seen from the velocity profile from linear wave theory, the difference between the theoretic velocity at the crest height and the bottom is negligible for values of h_c/h smaller than 0.15. A different parameter must be used to express a larger initial structure height in a larger velocity \hat{u}_{δ} .

A similar approach can be used as Van Gent and Wallast (2001); the crest level is used as the bottom level to simulate a higher velocity with linear wave theory. For the determination of the alternative speed in the mobility parameter a lower water depth of $h - h_c$ is used:

$$\theta_c = \frac{\hat{u}_{\delta,c}^2}{g\Delta D_{n50}}$$

$$\hat{u}_{\delta,c} = \frac{\pi H_s}{T_p} \frac{1}{\sinh k(h - h_c)}$$
5.8

where:

 θ_c is the mobility parameter that includes the initial crest level h_c [-]

In equation 5.8 $\hat{u}_{\delta,c}$ is a characteristic near-bed velocity based on the maximum horizontal velocity from linear wave theory. The initial structure height h_c is incorporated to simulate a larger velocity for a larger value of h_c . The effect of a larger value for h_c is that a lower water depth is simulated which results in a higher value for $\hat{u}_{\delta,c}$. This incorporation of the initial structure height means that for increasing crest level the mobility parameter θ_c will increase significantly. So the hydraulic load increases when the initial structure height increases, as was aimed.

Relative structure height as deformation parameter

A way of incorporating the initial structure height in a parameter is to relate the initial structure height to a structure height after erosion. This relative structure height can be derived from the relative profile erosion:

$$A_{rel} = \frac{A_0 - A_e}{A_0} \propto \frac{h_c - h_e}{h_c}$$

From the profile area after erosion and the profile area before erosion a relative structure height can be defined as deformation parameter:

$$h_{rel} = \frac{h_c - h_e}{h_c} = \frac{h_c'}{h_c}$$

where:

 h_e is the height of the eroded area [m]

 h_c is the structure height after erosion [m]

This is a way, other than the erosion parameter S, to relate the erosion area from a profile to the initial structure height.

Choice of parameters for deformation prediction

The parameters h_c/D_{n50} and h_c/h can be seen as boundary conditions for the process of an eroding near-bed structure on transitional water depth and are not considered to be able to incorporate the structure geometry in a deformation prediction formula. These parameters do not represent the streamline contraction. The initial structure height is made dimensionless with the stone size D_{n50} or the water depth h. But the change in the parameters h_c/D_{n50} and h_c/h must be combined with a hydraulics parameter like θ . With θ the hydraulic conditions for the stones at the structure toe (so at the bottom before the shoaling effect or streamline contraction depending on h_c with constant slope angle) are known.

For the incorporation of the initial structure height two different approaches are used:

- 1. Approach with the parameter θ_c that combines the structure height and the hydraulics in one parameter. The erosion number S is used as deformation parameter. The basic equation will be: $E \equiv S = f(\theta_c, N)$
- 2. Approach with the relative structure height h_{rel} as deformation parameter which will include the initial structure height. The mobility parameter θ , without the incorporation of the structure geometry, will be used to represent the hydraulic conditions. The former can be described as: $E \equiv h_{rel} = f(\theta, N)$

Two approaches for deformation prediction are executed in the next section, which deals with the deformation prediction, and are based on the two ways to incorporate the initial structure height in this section. In these approaches the data available from the tests will be analysed and used for deformation prediction.

5.3 Deformation prediction

The tests codes analysed for the deformation prediction are marked in Table **5-10**. The incident wave spectra from these tests are available (**Appendix** C). From the unmarked tests in Table **5-10** (0a6s2, 2a6 and 1d6) only the combined spectrum (incident and reflected) was obtained.

| h[m] | | | | |
|--------------------|-------------|------------------------------|-------------------|-------------------|
| | 0.55(0) | 0.50(1) | 0.45 (2) | 0.40(3) |
| H _s [m] | | | | |
| 0.22 (a) | 0a6 0a6s | 1a6 1a6 her 1a4 1a5 | 2a6 | |
| 0.20 (b) | | 1b4 1b6 | 2b4 2b5 2b6 | |
| 0.18 (c) | | | | 3c4 3c5 3c6 |
| 0.16 (d) | | 1d6 | | |

Table 5-10. The tests that are marked grey were used for the erosion analysis.

In this chapter two approaches for deformation prediction will be used. First the approach with the parameter θ_c will be treated. This parameter was also used by Van Gent and Wallast (2001) and a comparison will be made with their prediction formula and the data from this investigation. This mobility parameter θ_c , earlier defined in equation 5.8, has the following shape:

$$\theta_c = \frac{\hat{u}_{\delta,c}^2}{g\Delta D_{n50}}$$

$$\hat{u}_{\delta,c} = \frac{\pi H_s}{T_p} \frac{1}{\sinh k(h - h_c)}$$

For the second approach the parameter h_{rel} will be used to express the data and construct a prediction formula. This approach uses the relative structure height to predict the deformation of near-bed structures and uses a slightly different mobility parameter (θ) as the first approach and defined as:

$$\theta = \frac{\hat{u}_{\delta}^{2}}{g\Delta D_{n50}}$$

$$\hat{u}_{\delta} = \frac{\pi H_{s}}{T_{p}} \frac{1}{\sinh k(h)}$$

This mobility parameter, earlier defined in equation 5.6, incorporates structure height influence.

After the two approaches to predict the deformation of near-bed structures, the accuracy and limitation of the tests will be treated. Finally example calculations for the use of both approaches will be given.

5.3.1 First approach: erosion parameter

A prediction formula with the mobility parameter θ_c based on the available data of the tests is the aim of this first approach. Here the erosion parameter S will be used for the deformation parameter E:

$$S = \frac{A_e}{D_{n50}^2} = C_1 * (\theta_c^{C_2}) * f(N)$$
 5.9

where:

 C_1, C_2 are coefficients to fit the available data

In this first approach the dependency of S on the influence of the initial structure height and the number of waves are analysed.

5.3.1.1 Comparison with Van Gent and Wallast

Van Gent and Wallast (2001) used the erosion parameter S and the mobility parameter θ_c in their investigation. The time aspect was incorporated as a square root of N.

The difference with the parameter θ_c of Van Gent and Wallast is that they used the mean wave period T_m instead of the peak period T_p (see equation 3.8) which is used for the data in this thesis (see equation). To convert the original prediction formula from Van Gent and Wallast the assumption (based on the spectra they measured) that $T_m \approx 0.9 * T_p$ is used (in Schiereck (2001, p. 173) a range in values of 0.7-0.9 T_p is suggested depending on the spectrum shape). Using this value for T_m the following formula is obtained:

$$S = 0.11 * \theta_c^3 * \sqrt{N}$$
 5.10

The factor 0.2 in the original formula turned into 0.11 with the use of T_p . Their data was expressed with θ_c on the horizontal axis and the parameter S/\sqrt{N} on the vertical axis. Using the same parameters for the data analyzed in this thesis gives the graph in Figure 5-35.

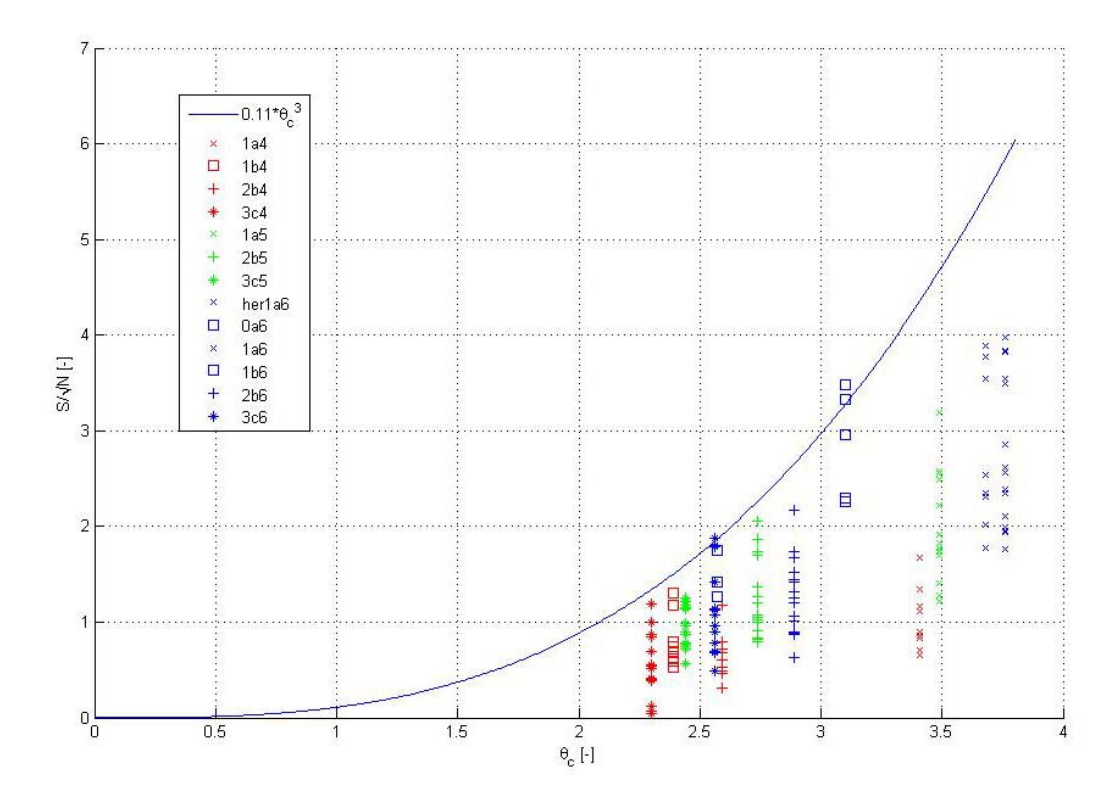


Figure 5-35. Test data with mobility parameter versus erosion parameter compared with the Van Gent and Wallast formula (blue line and after conversion from T_m to T_p).

It has to be remarked that the formula by Van Gent and Wallast is based on different dimensionless boundary conditions compared to the test conditions of this investigation. Most important difference is that the ratio between structure height and water depth (h_c/h) in their investigation is much higher (see section 3.3.1). This ratio has values up to 0.15 for the present tests, where the same ration in the tests of Van Gent and Wallast has values between 0.25 and 0.33. The test conditions here are considered more appropriate for comparison to a pipeline cover attacked by waves in a North Sea storm. When h_c/h has a relatively high value in transitional water depth conditions, a negligible vertical component of the orbital water movement can not be assumed and different processes apply.

5.3.1.2 <u>Influence initial structure height and N</u>

The formula by Van Gent and Wallast in equation 5.10 is also plotted in Figure 5-35. The relation from Van Gent and Wallast generally predicts a larger deformation. Instead of plotting all the data in one figure, the available data is grouped in the three tested wave series (N = 1000, 2000 and 3000, totally 6000 waves) and in the three

initial structure heights (h_c of around 4, 5 and 6cm) resulting in an overview of nine graphs (Figure **5-36**).

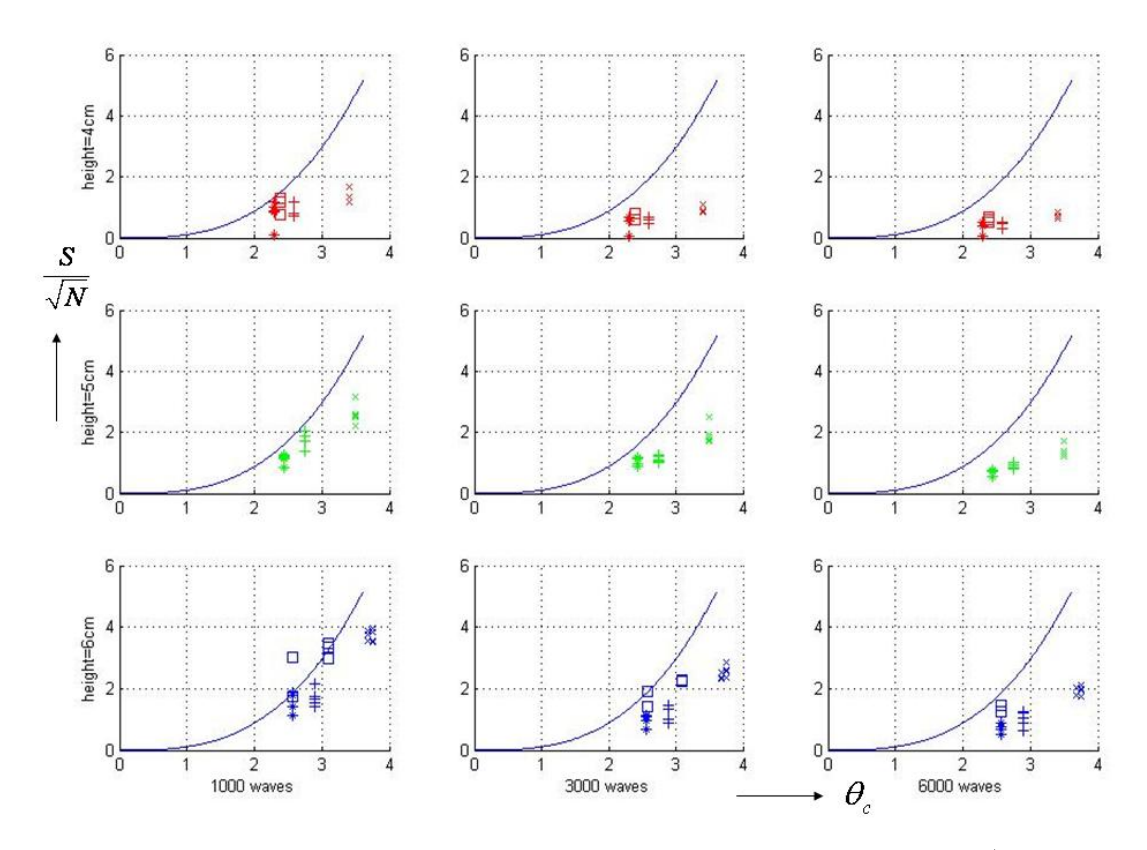


Figure 5-36. Graphs with θ_c on the horizontal axis and the parameter S/\sqrt{N} on the vertical axis. The prediction formula in equation 5.10 is shown as a blue line.

The top three graphs in Figure **5-36** are filled with the data for an initial structure height of around 4 cm, the second row applies to an initial structure height of 5 cm and the bottom row to an initial structure height of 6 cm. The left column represents data after 1000 waves, the second after 3000 waves and the right column after 6000 waves. The damage S is influenced by different values for N and for the initial structure height. This indicates that the parameter S/\sqrt{N} , which incorporates the number of waves, doesn't represent the conditions for the tests correctly. It can be concluded that the number of waves must be incorporated in a different way and that the incorporation of the initial structure height in θ_c seems to be insufficient for the data with structure heights of around 4 cm. The 5 and 6 cm structures in Figure **5-36** have similar values, but the 4 cm structures (red) deviate from the other two parts of the data.

5.3.1.3 <u>Incorporation of N</u>

The dimensionless parameter N is already incorporated but the parameter S/\sqrt{N} gives structurally lower values for different numbers of waves that have attacked the near-bed-structure. In section 5.2.1 the data was already analysed and a square root relation and a logarithmic relation with regard to N were compared. The logarithmic relation showed better agreement with the data than the square root. When N is incorporated

with a logarithmic function, a damage prediction formula then would have the following shape:

$$S = C_1 * (\theta_c^{C_2}) * \log N$$
 5.11

The available data was processed in the same way and the graph in Figure 5-37 was obtained.

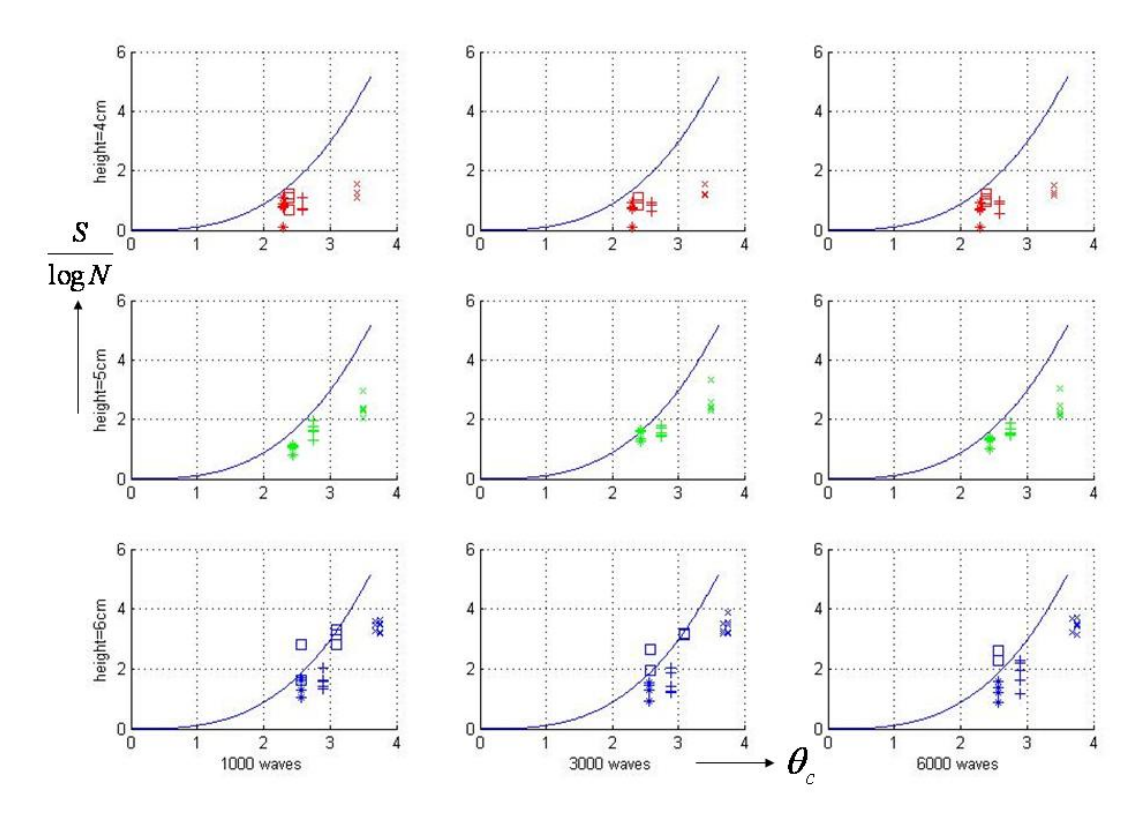


Figure 5-37. Graphs with θ_c versus S/logN for different number of waves and initial structure heights. The prediction formula in equation 5.10 is shown as a blue line.

From Figure 5-37 it can be seen that for the parameter S/logN the different number of waves gives the same relation meaning that S/logN is more or less independent of N and this N is better incorporated in S/logN than it was in S/ \sqrt{N} . In Figure 5-37 the data for the different number of waves is horizontally similar for each initial structure height.

5.3.1.4 <u>Prediction formula based on the erosion parameter</u>

The coefficients C_1 and C_2 in equation 5.11 can be chosen in a way that follows the data of this investigation. It can be seen that the relation by Van Gent and Wallast in equation 5.10 overestimates the erosion, especially for a higher value of θ_c .

With a lower value for the exponent C_2 of 2.5 (instead of 3) a better fit is possible. The value 2.5 for C_2 gives the formula a Paintal-like shape for high transport rates (equation 2.33). Only here the structure geometry (in θ_c) and the time aspect (in N) are incorporated. The fitted line is expressed in the following formula:

$$S = 0.8 * \theta_c^{2.5} * \log N$$
 5.12

This relation is plotted through the data in Figure 5-38.

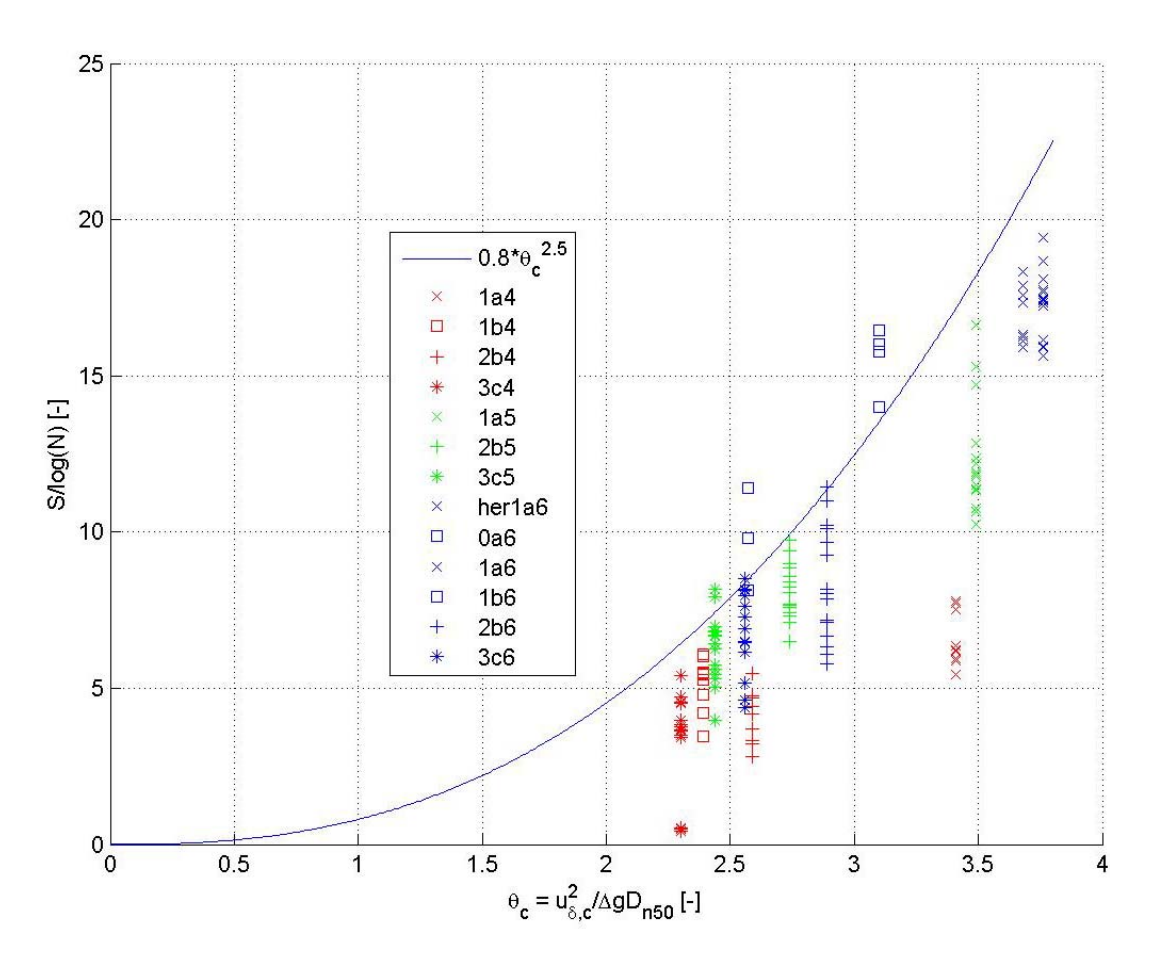


Figure 5-38. The mobility parameter θ_c versus S/logN with a line fitted through the maximal measured erosion data.

The incorporation of the initial structure height in the mobility parameter θ_c doesn't seem to be accurate for all test circumstances. The lower structures with an initial structure height of around 4 cm have much lower damage levels than the other heights. The influence of the structure height will be evaluated in section 5.4.2.

A possible explanation for the higher values of S/logN for tests 0a6 and 1b6 is that the lower value for H_s/h causes less breaking of the (highest) waves. This aspect influences the dependency of the number of waves N. With less breaking higher peaks are possible in a certain wave load duration. So for these tests the dependency of the erosion on the number of waves can have a less flat curve than a logarithmic relation.

5.3.2 Second approach: Relative structure height and direct time dependency

In this approach there are two main differences compared with the approach using the erosion parameter (S) in the former section.

The erosion of the near-bed-structure profiles will be expressed with a relative structure height parameter (h_{rel}) based on the change in the measured profile areas. The dependent parameters from the general deformation expression in equation 5.2 will also be present in the expression with the relative structure height instead of the erosion number S for the deformation parameter E. The relative structure height will be expressed in the mobility parameter θ (defined in section 5.2.2) and the number of waves N. The mobility parameter θ is used instead of θ_c (defined in equation 5.7), because the initial structure height is already incorporated in h_{rel} . In this way the hydraulic conditions and the structure geometry are separated.

Both parameters will be expressed in a different way then was done in the first approach. The parameter N will be set explicitly on the horizontal axis versus the relative height on the vertical axis. The relations for different values of θ will be plotted to achieve a method such that from h_{rel} directly a structure height after erosion (h_c) can be derived.

5.3.2.1 Expressing reshaping in relative height

For predicting erosion of a pipeline the most important parameter is the structure height. If erosion is allowed, the decline of the structure height determines for example the protection that is left above the pipeline.

An alternative way of expressing the deformation of a near-bed-structure, not applying the erosion number S, can be with a relative decline of the original profile area. The relative area can be derived from the eroded area A_e (also used for the damage number S). The relative area of a profile after deformation can be defined in dimensionless form:

$$A_{rel} \equiv \frac{A_0 - A_e}{A_0} \tag{5.13}$$

where:

 A_0 is the initial area of the profile [m²]

 A_e is the eroded area from the profile [m²]

From the measured profile area the structure height can be derived directly when the initial profile area and the eroded area are defined as prisms. The prisms are assumed to be equivalent in shape as the parameters n and B_c are constructed to be the same for the different tests. The procedure of deriving the height from the structure profile is explained graphically in Figure 5-39.

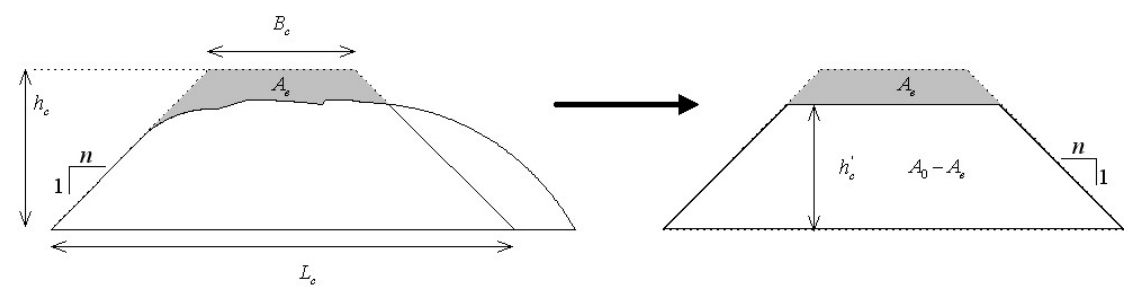


Figure 5-39. Procedure used to obtain the structure height after erosion (h_c) based on the eroded area (A_c) in a profile.

The same procedure can be followed as shown in equation 4.3 to derive the structure height after erosion. The abc-formula can be used to determine the profile area and translate it in a derived structure height after erosion:

$$h_c' = \frac{-B_c + \sqrt{B_c^2 + 4(nA_0)}}{2n} - \frac{-B_c + \sqrt{B_c^2 + 4(nA_e)}}{2n}$$
 5.14

where:

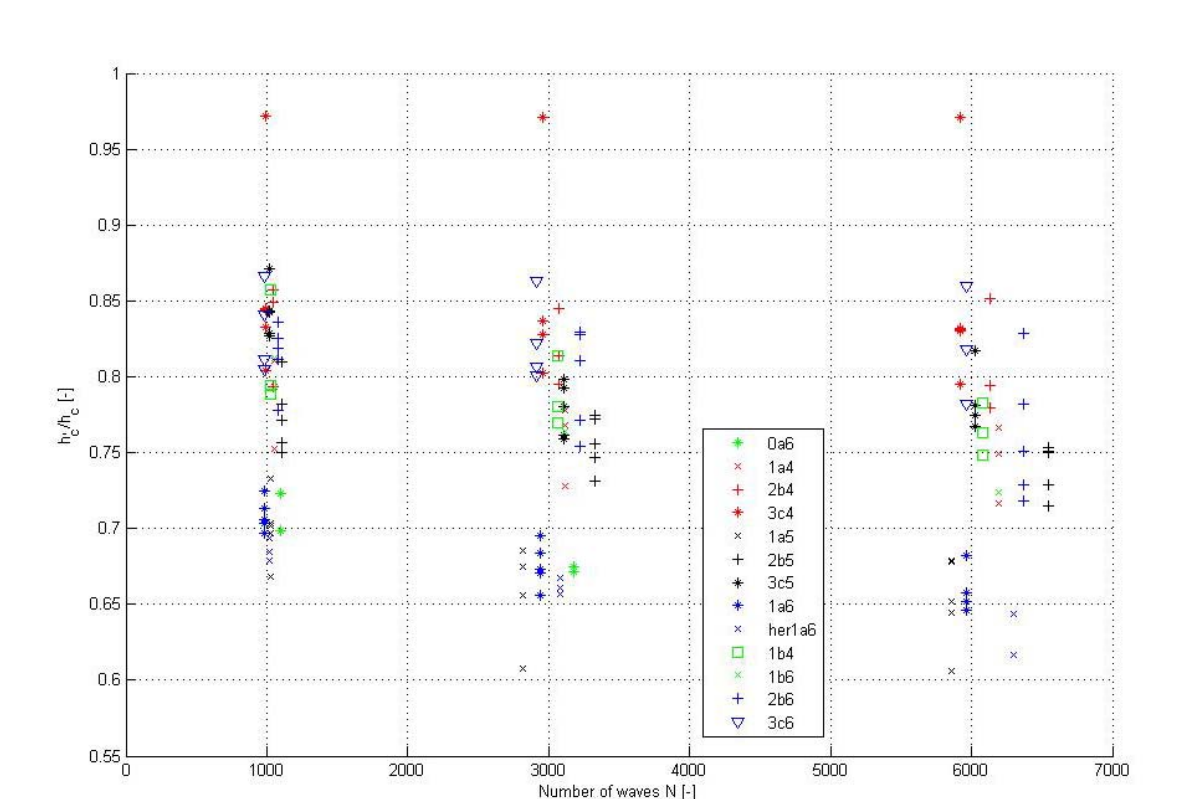
 h_c is the derived structure height after erosion A_e [m]

In equation 5.13 the height of the eroded prism is subtracted from the initial structure height. This method gives a good estimation of a representative height which can be used to estimate the functionality of a near-bed-structure. The eroded area is always similar to the area in Figure 5-39 as can be concluded when looking at the different reshaped profiles in **Appendix** E. If the loss of stones would occur in a different part of the profile, e.g. the crest would hold its position and only the front slope would lose stones, then this method would not apply. It is assumed here that the deformation shape is general and is valid in the model as well as in practice. The structure deformation is considered to be similar to crest erosion in this investigation. The deformation parameter E is expressed in the relative height which has the following shape:

$$E \equiv h_{rel} \equiv \frac{h_c}{h_c} = f(\theta, N)$$
 5.15

The relation in equation 5.15 contains the mobility parameter θ without incorporation of h_c . The initial structure height h_c is expressed in the relative height. From a first look on the deformed structures (**Appendix** E) one can see that the decline of the structure's crest levels is relative to its initial level. This relative erosion is also a way to incorporate the structure geometry, different from the methods treated in section 5.2.

Another difference from the approach in the former section, is the explicit use of N. Contrary to using N implicitly in a deformation prediction relation with a logarithmic or a square root function, it can also be set explicitly along an axis.



The data is expressed in h_c/h_c and can be found in Figure **5-40**

Figure 5-40. The measured test data expressed with the number of waves versus the relative height.

From Figure **5-40** can be seen, just as in the first approach with the erosion parameter, that the tendency of the data with respect to the number of waves has the logarithmic shape as treated earlier in this chapter (with the parameter $S/\log N$).

With regard to the use of θ , instead of θ_c , the data with different initial structure height tend to give similar values of h_{rel} . Compare, for example, the data from 1a5 and 1a6 and from 2b5 and 2b6 (both comparisons have identical values for N and θ) in Figure **5-40**.

For these tests the values for h_{rel} are similar. When θ_c is used, h_{rel} will be different for similar hydraulic conditions. For the expression of the data the combination h_{rel} and θ fit the tests results better than the combination of h_{rel} and θ_c .

Each test in Figure **5-40** has its own mobility parameter θ (tests with identical first two digits, the tests codes starting with 1a, 2b and 3c, have the same θ) and the issue here is to demonstrate the mobility-parameter trend graphically. The aim is to group the data for different mobility parameters to show the influence of θ on the relative structure height h_{rel} . This will be treated in the following part of this section where the mobility parameter θ is expressed graphically.

5.3.2.2 Graphical expression of the mobility parameter

For the graphical expression three different levels are distinguished in the following three figures.

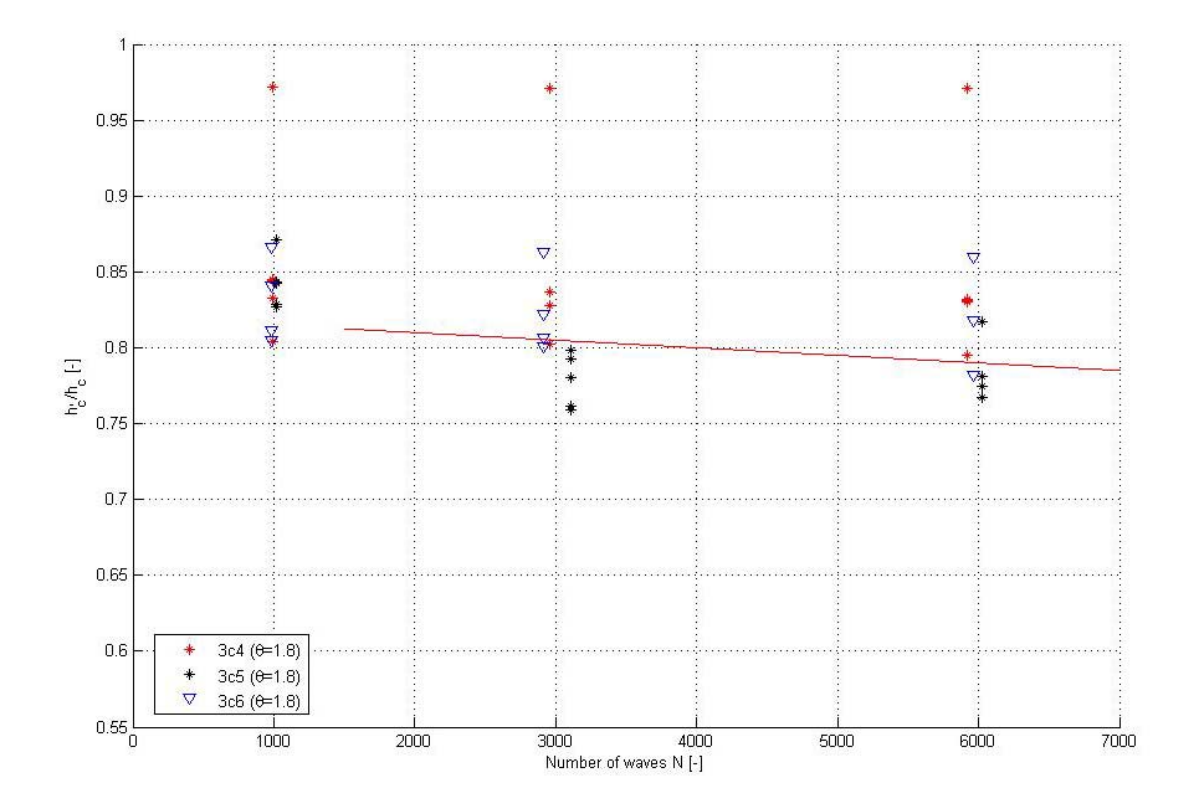


Figure 5-41. Mobility level of 3c# with a line fitted through 3c5 and 3c6.

The reason for the extremely low damage of one of the profiles (of test 3c4) with 4 cm height in Figure **5-41** (the profiles can be found in **Appendix** E) could be that the stones in this profile had already reasonably high interlocking forces. This could be a coincidence when the stones were placed with a possibly higher level of compaction or with better sheltering conditions. Another possible reason is that the stones in that particular profile (one of the 5 measured in test 3c4) found a stable position coincidentally fast after moving.

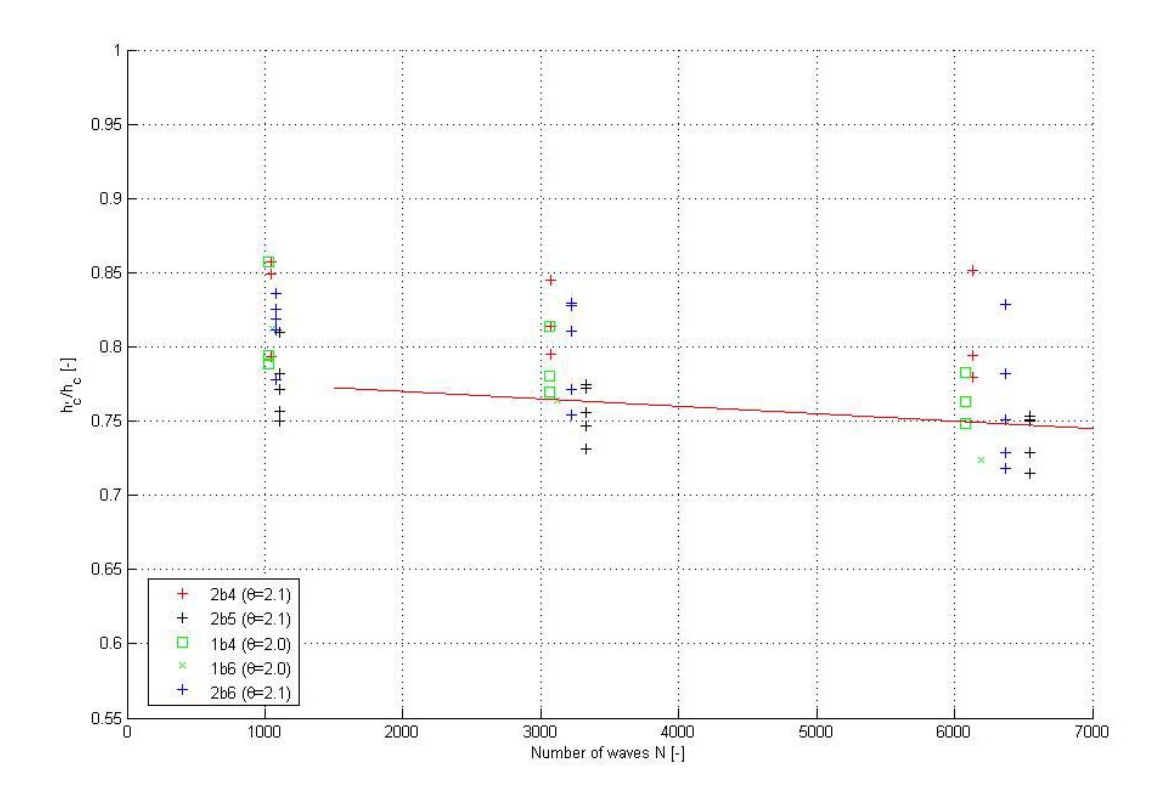


Figure 5-42. Mobility level of 2b# and 1b# with a line fitted through 2b5 and 2b6.

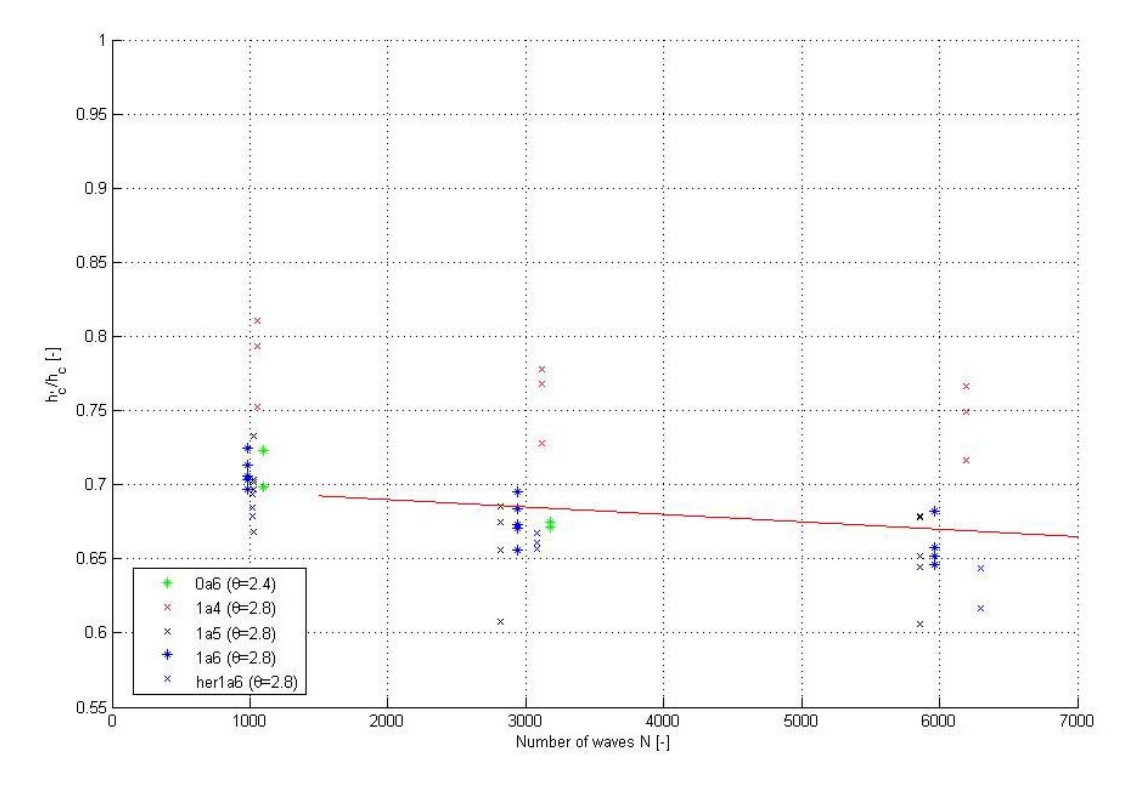


Figure 5-43. Mobility level of 1a# with a line fitted through 1a5 and 1a6.

In the former three figures a choice has been made to fit lines of equal θ . The 5 and 6 cm were fitted to represent the mobility parameter. It can be seen (primarily in

Figure **5-43**) that initial structure height of the data between the "4 cm" structures on the one side and the "5 and 6 cm" structures on the other side differ. For the same mobility parameter the erosion values expressed in h_{rel} for the "4 cm" structures are lower. The same aspect was seen in the former section where the structure geometry was incorporated through θ_c .

Furthermore, the data of 0a6 and 1b6 and 1b4 tend to follow the values for the test codes 1a# and 2b#. It seems that the greater water depth doesn't influence the hydraulic load. For the higher erosion levels there is a significant difference. The 1b4 and 1b6 tests have similar values as the 2b test-codes for θ (2.0 against 2.1, see Figure 5-42). Only 0a6 has a significant different value of 2.4 compared to the 1a test codes which have a θ -value of 2.8 (see Figure 5-43). There is no clear explanation based on possible test boundary conditions. It seems that the difference in water levels (0.55 m for code 0a6 and 0.50 m for test codes 1a#) has little influence on the hydraulic conditions. More tests are needed to give a clearer view on the relative structure height parameter h_{rel} .

5.3.2.3 Prediction formula based on the relative height

As pointed out earlier, for the graphical method it is chosen here to use the data for 5 and 6 cm to fit the three different levels of mobility parameters. So, for the lower structures of around 4 cm in height the resulting fitted relation is an overestimation of the structure deformation. The aspect of the difference in relative structure height after erosion for the lower structures will be treated in section 5.4.2.

When looking at one level of hydraulic conditions, there is one mobility parameter θ for all the erosion data and h_{rel} is only a function of N. From Figure **5-40** it can be concluded that the trend of data becomes flat. This transition occurs somewhere between 1000 and 3000 waves. After 1500 waves it can be considered reasonable to describe the data with a straight line for one mobility parameter θ :

$$h_{rel} \equiv \frac{h_c^{'}}{h_c} = -aN + b$$
 for $N > 1500$ 5.16

The constants a and b in equation 5.16 for the different mobility parameters are given in Table **5-11**.

| Test code | h [m] | H_s [m] | θ [-] | a [-] | b [-] |
|-----------|-------|-----------|-------|---------|-------|
| 1a* | 0.50 | 0.20 | 2.8 | 5.0*E-6 | 0.70 |
| 2b* | 0.45 | 0.19 | 2.1 | 5.0*E-6 | 0.77 |
| 3c* | 0.40 | 0.18 | 1.8 | 5.0*E-6 | 0.82 |

Table 5-11. Values for the constants a and b for the three chosen mobility levels.

The coefficient a can vary considerably and different values for each θ does not contribute to the accuracy, so there is chosen for one value. A value that causes the relative height to go down for larger N is considered to be justified according to the test results. Each test shows (a small) a consistent decrease of the relative structure height as can be seen in Appendix G.

0.95 0.9 $oldsymbol{ heta}$ =1.8 (3c#) $m{ heta}_{=2.0\text{-}2.1\ (2b\#)}$ 1a4 2b4 Π 7 1a5 2b5 2.4-2.8 (1a#) × 1a6 her1a8 1b4 2h6 3c6 0.55 L 2000 3000 4000 5000

The relation in equation 5.16 is expressed graphically with the data in these tests in Figure **5-44**.

Figure 5-44. Lines fitted through the data representing different mobility values.

For the practical use of the expression in equation 5.16 the constants a and b must be estimated for other values of θ . Linear interpolation for the values in Table **5-11** will be used for the estimation:

| | b (0 <b<1) [-]<="" th=""></b<1)> |
|--------------------------|----------------------------------|
| for $\theta < 1.8$ | > 0.82 |
| for $1.8 < \theta < 2.1$ | $-0.13*\theta+1.05$ |
| for $2.1 < \theta < 2.8$ | $-0.11*\theta+1.0$ |
| for $\theta > 2.8$ | < 0.70 |

These interpolation functions for θ give only rough predictions of the relative structure height. The variations within one test are often already outside the interpolation areas. In the next section the accuracy of the prediction formulas obtained in both approaches will be treated.

5.3.3 Accuracy and limitations of the deformation prediction

Next to the measuring errors treated in section **4.4** There will always be a deviation in the results of the erosion process. This will also be the case when the measurements are perfect and flawless. The deviations have two origins for the two approaches in the sections 5.3.1 and 5.3.2.

No flow situation in one test is identical due to the complex aspects of eroding stones. Local turbulences of the fluid flow and the randomness of the positions of the stones and their individual sizes, shapes and densities always will cause deviation. When interpreting the measurements and relating erosion to a hydraulic load, the theoretical parameters describing the physical processes can be incomplete or certain effects are incorporated incorrect.

In the following part of this section the accuracy of the two approaches will be estimated.

Accuracy of the prediction with the erosion parameter

The dependent parameter is the erosion parameter S. It consists of an erosion area and the squared D_{n50} . The errors that influence the accuracy are schematically dealt with in the following table:

| Prediction | | Error | Background | |
|----------------------|----------------------|---------------|---------------------------------------------------------------------------------------------------------------------------------------------------------------------------------------------------------|--|
| parameters | | | | |
| $S/\log N$ | A_{e} | +/- 10-20% | Range of standard deviations of the tests (based on the measured variations.). This estimation includes the Provo error measurements of A_e | |
| | D_{n50} | +/- 5% | Based on the measured sieve curve | |
| | N | +/- 1%. | Based on the counting procedure with a Matlab script | |
| | | | | |
| $oldsymbol{	heta}_c$ | $\hat{u}_{\delta,c}$ | +/-10% | This error is based on the grid of the used spectra. The value of T _p can show some deviation. Most important is the fact that the velocity is a derived parameter and not directly measured | |
| | Δ | +/-2.5% | Based on the density measurements | |
| | g | - | Negligible error | |
| | D_{n50} | +/- 5% | Based on the measured sieve curve | |

Table 5-12 Erosion parameter error quantification and background.

The deviations in the measurements of A_e give the most important inaccuracy for the dependent parameter $S/\log N$. The influences of D_{n50} and N are neglected in this analysis. The deviations of the tests will be displayed graphically. When assuming that the deviations are normally distributed, then a 95% confidence interval can be obtained by the following relation: $1.65*\sigma$. The parameter σ is the standard deviation of a normal distribution. This is displayed in Figure 5-45 where the error bars per test have total length of $2*1.65*\sigma$.

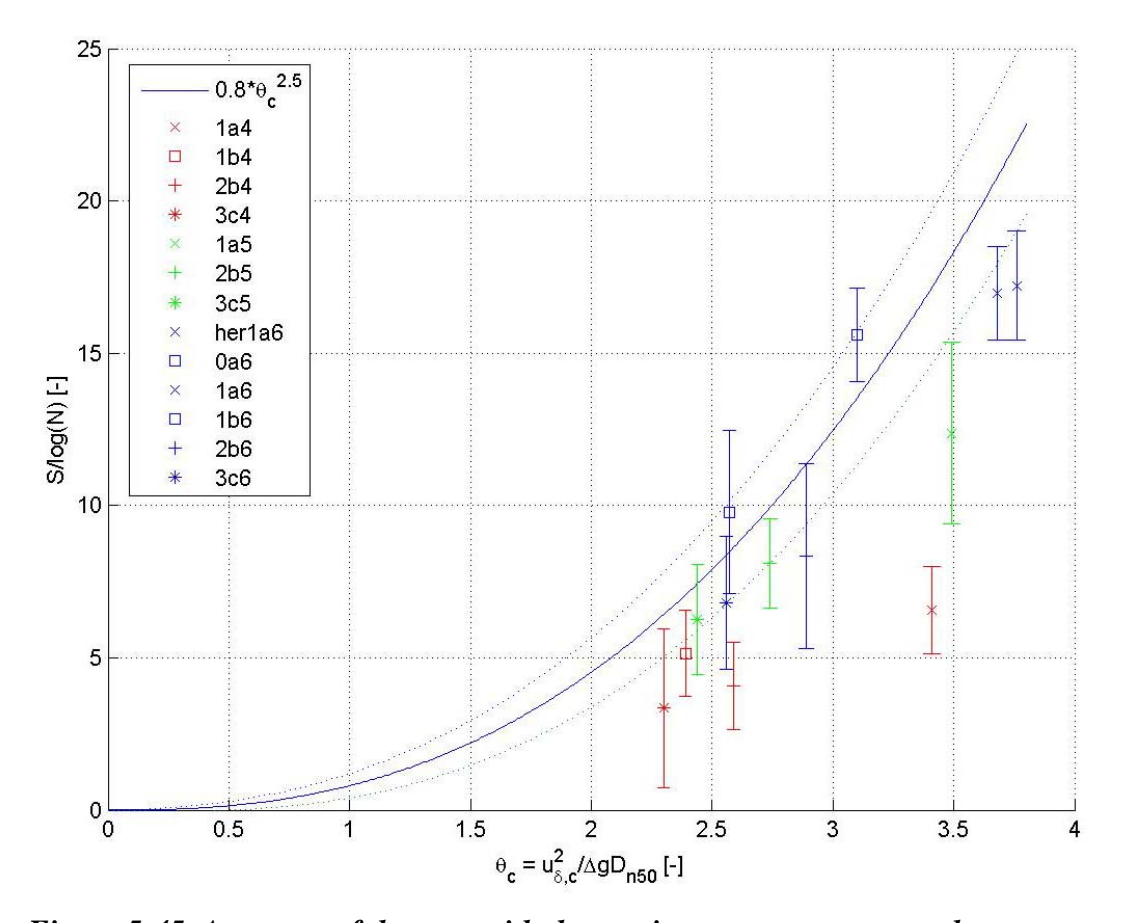


Figure 5-45. Accuracy of the tests with the erosion parameter approach.

The second error source in table Table **5-12** is the parameter θ_c . This parameter can also show deviations. The error in the water velocity $\hat{u}_{\delta,c}$ is considered to represent the total inaccuracy θ_c . The influences of D_{n50} and Δ are neglected compared to the velocity. This error was estimated at+/-10% in Table **5-12**; this means an error of approximately 20% in θ_c as the squared velocity is used. To estimate a possible error in $S/\log N$ caused by θ_c , the derivative of the function in equation 5.12 is used. With this derivative the error of 20% $(0.2*\theta_c)$ is translated to a linearised interval expressed as:

error interval:
$$0.8*\theta_c^{2.5} + \underbrace{\left(0.2*\theta_c}_{\text{error}} * \underbrace{\left(2.5*0.8*\theta_c^{1.5}\right)}_{\text{derivative}}\right)$$

This error interval, caused by the estimated variation in θ_c , is shown in Figure **5-45** by the dotted lines and can be added to the variation in $S/\log N$.

It is possible, for example, that the error in $S/\log N$ and the error in θ_c both occur simultaneously in an unfavourable way. This happens when for the erosion prediction a θ_c is calculated that is too low, with the maximal error. This means that the deformation will be underestimated. When at the same time also the deformation in practice occurs at the edge of the 95% confidence interval, an extreme total error

occurs. The chance that these two events coincide is small. When both effects are maximally incorporated in a prediction function, this would be very conservative.

Accuracy of the prediction with the relative structure height

For the relative structure height a similar approach as with the error estimation of the erosion parameter is used here. For the dependent parameter $h_c^{'}/h$ this results in identical error margins in the following table:

| Prediction parameters | | Error | Background |
|-----------------------|----------------------|---------------|------------------------------------------------------------------------------------------------------------------------------------------------------------------------------------------------|
| $\frac{h_c^{'}}{h}$, | A_e | +/- 10-15% | Range of standard deviations of the tests (based on the measured variations.) This estimation includes the Provo error measurements of A_e |
| | h_c | +/- 5% | Based on the measured sieve curve. |
| | | 1 | |
| N | | +/- 1%. | Based on the counting procedure with a Matlab script |
| | | | |
| θ | $\hat{u}_{\delta,c}$ | +/-10% | This error is based on the grid of the used spectra. The value of T_p can show some deviation. Most important is the fact that the velocity is a derived parameter and not directly measured |
| | Δ | +/-2.5% | Based on the density measurements |
| | g | - | Negligible error |
| | D_{n50} | +/- 5% | Based on the measured sieve curve |

Table 5-13 Relative structure height error quantification and background.

Similarly as for the accuracy estimation of the erosion parameter, the deviations in the measurements of A_e give the most important inaccuracy for the dependent parameter $h_c^{'}/h$. The influences of h_c and N are neglected in this analysis. With regard to h_c , the highest point of a profile structure can differ in the range of +/-0.5* D_{n50} . But h_c is a derived parameter based on the initial structure volume: the deviations in the initial structure height h_c are small as can be seen in Appendix C.

The deviations of $h_c^{'}/h$ for the tests will be displayed graphically. When, again, assuming that the deviations are normally distributed, then a 95% confidence interval can be obtained by the following relation: $1.65*\sigma$. This is displayed in Figure **5-46**.

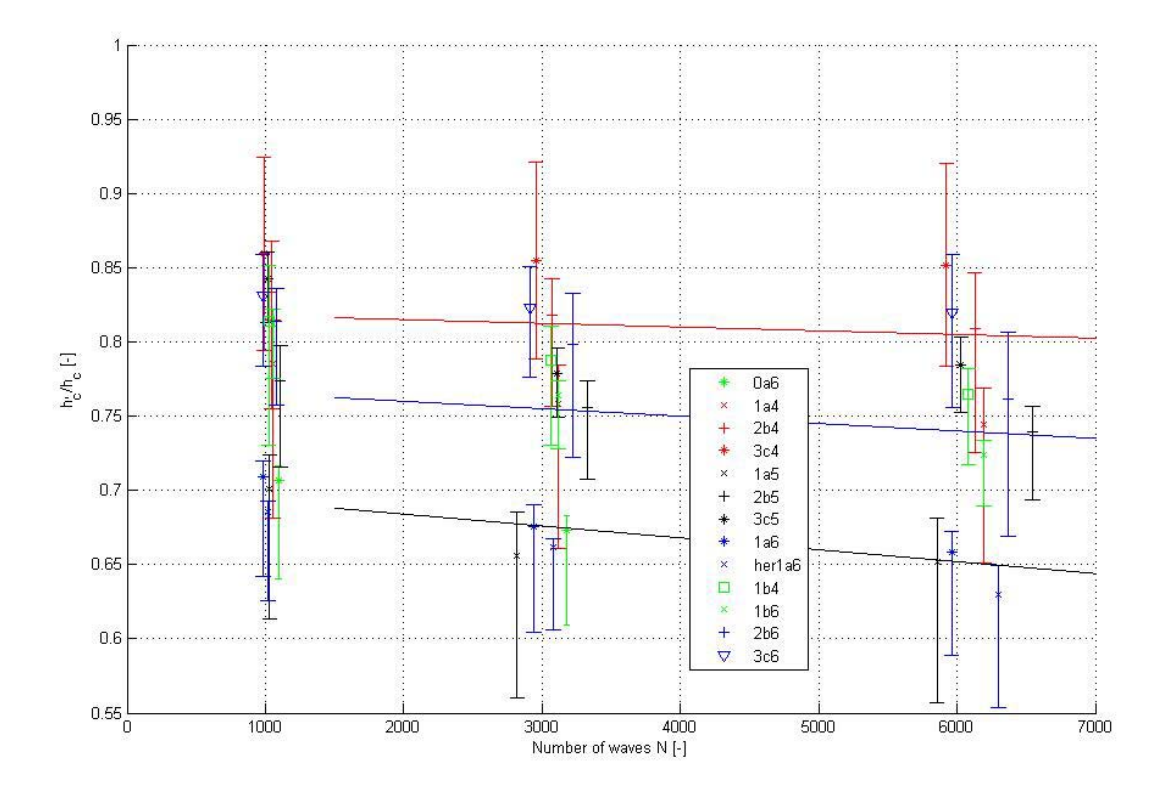


Figure 5-46 Accuracy of the tests with the relative structure height approach.

The standard deviation times the factor 1.65 for each test was only displayed in Figure 5-46 for the upper error compared to the mean values (higher values for $h_c^{'}/h_c$ implicates less erosion).

The error based on θ in the prediction formula is difficult, it is only implicitly incorporated. For the lower error the standard deviation in h_c'/h_c for each test was added with the factors based on the graphical errors in θ in Table **5-14**. This results in a generally larger estimated inaccuracy (see Figure **5-46**) for the lower side which can be considered the "safe side" for erosion prediction.

| Prediction parameters | | Graphical lower | Background |
|-----------------------|----------------------|-----------------------------------------|--------------------------------------------------------------------|
| | | error | |
| θ | $0 < \theta < 1.8$ | - | Based on the values for θ Figure 5-44 . |
| | $2.0 < \theta < 2.1$ | $+/-0.025*h_c/h_c$ | $\frac{2.1-2.0}{2.1} \approx \text{interval of 5\%} => +/-2.5\%$ |
| | $2.1 < \theta < 2.8$ | +/-0.07* h _c /h _c | $\frac{2.8 - 2.4}{2.8} \approx \text{interval of } 14\% => +/-7\%$ |

Table 5-14 Graphical lower errors of the implicit parameter θ .

The graphical errors are only rough estimates of the inaccuracies in the relative-height-approach. The problem lies in the fact that the parameter θ is implicitly

incorporated. The approach using the relative structure height needs more data with different mobility parameters to achieve a clearer dependency on θ .

<u>Limitations of the use of the results for design aspects</u>

The simplification of the model tests compared with a situation in nature limits the validity of the test results.

Major simplifications compared to e.g. a North Sea situation (as mentioned earlier in this thesis) of the model are:

- The structures are attacked by waves described by a wave spectrum that is constant in time (in nature a spectrum changes during a storm) and attacks the structure perpendicularly.
- The structure is built on a flat non-eroding bottom.

The relevant dimensionless parameters must be similar in the model and in nature as already put forward in section 5.2. An erosion prediction for a North Sea situation based on the results of the model tests is more valid when the physical processes are similar. Demands can be considered in dimensionless form and are assumed to describe the borders of validity for the similarity of the model tests with a situation in nature. Possible demands for the comparison of the model tests results with environmental conditions in nature are:

| • | relative structure height | $h_c/h < 0.15$, |
|---|-------------------------------------------|--------------------------------|
| • | wave steepness (based on H _s) | $0.041 < s_p < 0.046$ |
| • | transitional water depth: | $1/20 < h/L_p < \frac{1}{2}$, |
| • | relative structure size: | $1 < h_c/B_c < 1.5$, |
| • | slope | n = 2.5, |
| • | relative crest length | $b_c/d_{n50} = 11,$ |
| • | mobility parameter | θ < 3.2, |
| • | mobility parameter with h _c | $\theta < 4.0$. |

The test results also could be valid outside the ranges of these dimensionless parameters, but as no tests are available for those conditions the prediction has less validity.

In the next section a situation in nature will be used to predict erosion of a near-bed structure. This will be done by a calculation example.

5.3.4 Example calculations based on the two approaches

For the calculations the characteristics of the hydraulic circumstances of measuring station YM6 in the Southern North Sea will be used. The two formulas derived from the two approaches in this section will be used for the example calculation:

Erosion parameter:
$$E \equiv \frac{A_e}{D_{n50}} = f(\theta_c, N)$$

Relative height:
$$E \equiv \frac{h_c'}{h_c} = f(\theta, N)$$

The probability aspect is important in the calculation. The following aspects are considered to govern the allowed failure chance:

- Design storm return period
- Accuracy of the deformation prediction formula
- Demanded safety margin and required lifetime of structure for the design

An important simplification for the calculation is that the hydraulic conditions are described by one design storm with a H_s and a wave steepness s_p . Also a value for the accuracy is assumed. The last aspects are demands from the designer; a larger safety margin and a smaller required lifetime result in a lower failure chance. The required lifetime can be translated into a value for the number of waves N from the design storm used for the calculation. When the value of N is larger, this can be seen as more storms. The chance that, within a required lifetime, more storms occur is smaller than when only one storm occurs.

Failure chance

In this thesis a probability analysis is not investigated, so an assumption is made based on a chosen H_s combined with a number of waves and the permitted failure chance for the lifetime period. Each parameter value can be reasonably assumed but their mutual relation in a probability function resulting in a chance value is not subject of investigation here. The length of a designed pipeline cover is for erosion prediction an important issue. A longer pipeline protection has a larger failure chance when a normal distribution describes the erosion. This aspect is not incorporated in the calculation.

For this example calculation a simple accumulative chance is calculated.

Assumptions for failure chance calculation:

- Required Life time: 30 years
- The output of the erosion prediction calculations will be increased with a factor 1.2 to ensure an exceedance chance of 5%.
- The design demand is a maximal failure chance of 5% with a hydraulic load with a minimal exceedance chance of 2%.

Calculations

The stone gradings have standard values which are available from a quarry. So a more practical example calculation will be with a stone grading characterised by a D_{n50} . Based on **Figure 3-14** the 50/150 mm grading has a D_{50} of approximately 110 mm, so a D_{n50} of 0.84*110 = 92 mm. For Δ a value of 1.65 will be used. Further data for the measuring station YM6 in the Southern North Sea are:

Water depth h: 25 m

Wave height H_s with Return period of 100 years: 7.6 m and $T_p = 13.5$ s $\rightarrow L_p = 192$ m and $S_p = 0.040$.

The assumed characteristics for the structure geometry are:

- $B_c=1.0 \text{ m}$
- slope steepness n = 2.5
- pipeline diameter: 0.5 m,
- minimal cover height above pipeline: 0.5 m

So a minimal structure height of 1.0 m is allowed at the end of the life time. Probability with a lifetime of 30 years, a return period of 100 years: with a Poisson distribution the chance would be 26%. If one storm lasts 6 hours this means for N: $6*3600/T_m$ (with $T_m = 0.85*T_p$) = 1900 waves.

Say now this storm will occur not once but three times in the life period. This reduces the exceedance chance (with one storm 26 % as pointed out) as the chance that three 100 year storms occur in a 30 year window. The exceedance chance must drop to maximal 2 %. The question is if one design storm with a return period of, say, 1000 years causes more deformation. The wave height, however, is bounded by the water depth. For these simple calculations it is assumed that three 100 year storms is the design situation for YM6.

Three storms means (3*1900 =) 5700 waves. With Poisson this results in an exceedance chance for the hydraulic conditions of around $0.26^3 \approx 2\%$. This was the maximal exceedance chance of the hydraulic load.

Calculation with the erosion parameter

As start for the iteration process a value of 1.3 m for the initial structure height h_c will be chosen for the numeric example.

The calculation where the parameters can be filled in in the following formulas:

$$\theta_c = \frac{\hat{u}_{\delta,c}^2}{g\Delta D_{n50}}$$

$$\hat{u}_{\delta,c} = \frac{\pi H_s}{T_p} \frac{1}{\sinh k(h - h_c)}$$
 (equation 5.8)

using the 0.2 error range from section 5.3.3:

$$\frac{S}{\log 5700}$$
 = (0.8+0.2)*2.85^{2.5} (equation 5.12):

results in
$$S = 61.2 = A_e / D_{n50}^2 \rightarrow A_e = 0.43 \text{ m}^2$$

With equation 5.14 the new height becomes: 1.07 m. This satisfies the demand of a minimal height of 1.0 m. With the same rock grading a calculation can be made for a

smaller water depth and which initial structure height would be needed then. The initial structure height needed can be found with an iteration process.

Calculation with the relative structure height

For the initial structure height h_c will be calculated directly with a minimal allowed h' of 1.0 m.

The calculation where the parameters can be filled in in the following formulas:

$$\theta = \frac{\hat{u}_{\delta}^{2}}{g\Delta D_{n50}}$$

$$\hat{u}_{\delta} = \frac{\pi H_{s}}{T_{p}} \frac{1}{\sinh k(h)}$$
 (equation 5.6)

$$h_{rel} \equiv \frac{h_c'}{h_c} = -aN + b$$
 for $N > 1500$ (equation 5.8)

with a value of 5.0*E-6 for a and for b a value depending on θ :

| | b (0 <b<1)[-]< th=""></b<1)[-]<> |
|--------------------------|----------------------------------|
| for $\theta < 1.8$ | > 0.82 |
| for $1.8 < \theta < 2.1$ | $-0.13*\theta+1.05$ |
| for $2.1 < \theta < 2.8$ | $-0.11*\theta+1.0$ |
| for $\theta > 2.8$ | < 0.70 |

This results in a value for h_{rel} of 0.71 and this leads to a needed initial structure height h_c of 1.4 m. When a margin based on the scatter in Figure 5-44 is used a save value might be 0.65 for h_{rel} and this means needed initial structure height h_c of 1.5 m. These values are larger than the calculation for the erosion parameter where a required initial structure height of 1.3 m was calculated to be sufficient.

5.4 Evaluation of deformation

This evaluation will treat the two main aspects of investigation; the time dependent erosion expressed with the number of waves N and the structure geometry expressed with h_a .

5.4.1 Duration of the wave load

The influence of the number of waves for near-bed structures under the tested conditions is clear. The logarithmic relation between erosion and time seems evident for near-bed structures. Also the time dependent erosion shows two different stages; first a relatively strong eroding structure and after 1000 to 1500 waves the erosion rate per time unit is much less and takes a more or less constant or slowly decreasing erosion rate per unit of time.

The boundary conditions for the wave breaking climate are very important for N. So the wave steepness s_p and the ratio between wave height and water depth H_s/h influence the hydraulic conditions and therefore N. When less breaking occurs, higher peaks are possible in a certain wave load duration. When the waves all tend to break on e.g. a too high steepness, then a limit is present for the hydraulic forces. For deformation depending on the number of waves this means that there isn't a larger probability for an extra large wave in the spectrum for a larger wave duration. So for these tests the dependency of the erosion on the number of waves has a less flat curve than a logarithmic relation.

5.4.2 Initial structure height

It can be seen in the erosion parameter approach as well as in the relative structure height approach that one structure height of 4 cm shows structurally more deviation to fit the relation than the rest of the data with values for the initial structure height around 5 and 6 cm do. So the relation as defined in equation 5.16 is accurate for 5 and 6 cm but not for 4 cm. It seems that there are two different regimes present that are influenced by the initial structure height. From these test results only two regimes can be identified; a regime with a higher level of mobility parameter (5 and 6 cm) and a regime with a lower level of mobility (4 cm). For a value of the initial structure height lower than 4 cm the height incorporated in the mobility parameter, gives significantly lower deformation values than the other crest levels. If the hypothesis of two different regimes is valid, this regime must be defined in a dimensionless way for the prediction of deformation in nature. The erosion results for the tests with different initial structure heights is assumed to be related to the stream line contraction as treated in section 5.2.3.

The basic idea is that for larger structure heights more streamline contraction of the flow occurs above the structure slope. When the stones of a structure protrude more in the orbital bottom motion around the structure, a higher load can be considered to be present. This protrusion in the flow is assumed to have some boundary level where the protrusion can grow but no larger hydraulic load occurs. The transition level

dependent on the initial structure height determines which regime is present. Two physical processes are treated here as possible causes for the two different regimes:

- relative boundary layer thickness,
- the ratio of the slope length and the water particle movement amplitude.

These two aspects can be an explanation for the different erosion results between the 4 cm structures on one hand and the 5 and 6 cm structures at the other. Both aspects will be analysed separately but the measured differences may also be a combination of both effects. The eroded stones are washed away (net) from the crest to the downhill slope, so this direction of the water movement is critical for the erosion process. Therefore only the uphill slope is considered when the water movement is in the direction away from the wave paddle.

Relative boundary layer thickness

When regarding the physical processes in Figure 5-34 a reason for a possible lower velocity at the crest of a 4 cm structure can be that the flow attacking the structure flowing parallel with the bottom isn't that parallel for the first 2 or 3 cm. Rotational flow as treated in section 2.1.3 can be present here. In a wave, the boundary layer can only grow during half the wave period and has to start from scratch again when the flow reverses. Values that are typical for the tests of T = 2 s and $\hat{u}_{\delta} = 0.4$ m/s, result in a boundary layer thickness of $\delta \approx 0.02$ m (equation 2.16). In this boundary layer the flow is highly rotational and the assumptions on which wave equations are based are not valid.

This would mean that the assumption that the complete height assists the higher velocity at the crest, through the contraction of horizontal flow lines above the slope, is uncertain. Once the height sticks out of this "turbulent height" only the part sticking out contributes to the velocity increase at the crest. To separate two regimes it is possible to define a parameter that has a critical value. This critical value determines if the "critical protrusion" through the boundary layer is present or not. The parameter suggested here is the relative boundary layer thickness parameter: δ/h_c . This parameter is dimensionless. So when the physical process identified is valid generally, the same ratio can be used in nature.

Based on the model tests the regime changes between an initial structure height of 4 and 5 cm. When a h_c of 4 cm is chosen as the transition height for these tests and a value of $\delta = 2$ cm as the example above is used, these values result in a critical value of $h_c/\delta \approx 2.0$.

When the measured situation has a value that is lower than this relative boundary layer thickness, then the used mobility parameter (in these tests θ or θ_c) has to be scaled down with a certain factor. The hydraulic conditions represented by θ or θ_c for $h_c/\delta > 2.0$ (for these tests the erosion results for the structures with 5 and 6 cm initial height), can be described by the prediction formulas in section 5.3.

The ratio of the slope length and the water particle movement amplitude.

Another critical parameter that can be used to express the difference between the 4 cm and 5/6 cm results, is the ratio of the slope length $(n*h_c)$ and the horizontal displacement amplitude of the water particles near the bottom (\hat{a}_{δ}) .

The threshold aspect can be made clear with the fact that a characteristic horizontal amplitude has a relation with the length of the slope (see Figure 5-47) that influences the extent of contraction of streamlines above the slope.

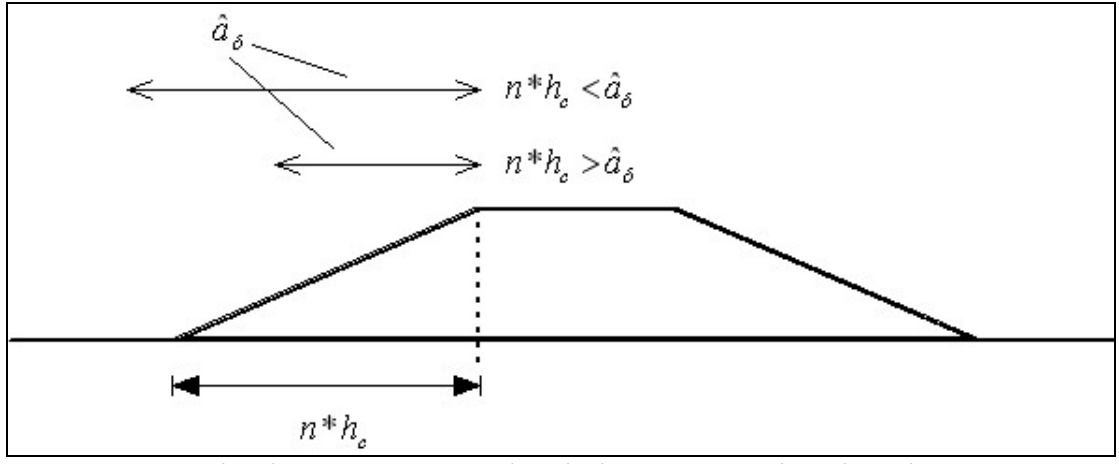


Figure 5-47. Orbital motion compared with the structure slope length.

When the slope length is larger than the horizontal movement $(n*h_c > \hat{a}_\delta)$, the streamline contraction has a maximal influence. When the initial structure height is lower than the (characteristic) horizontal movement, the extent of streamline contraction will become lower than the maximum or threshold value. The extent of contraction will then be a function of the initial structure height. A maximal value for the aspect of streamline contraction can be defined and can be based on the relative slope length:

$$\frac{n*h_c}{\hat{a}_{\delta}}$$

When this relative slope length is larger than the threshold value, the erosion will be independent of this relative slope length. When the relative slope length is smaller than the threshold value, the extent of contraction no longer has the maximum value and the extent of contraction is a function of the relative slope length. The threshold values for these tests are somewhere between the initial structure height of 4 cm and 5 cm. The transition seems also to be valid for all the tested hydraulic conditions (or \hat{a}_{δ}). The ratios for all the tests are shown in Table **5-15**.

| \hat{a}_{δ} n^*h_c | 4 cm structures 0.10 [m] | 5 cm structures 0.125 [m] | 6 cm structures 0.15 [-] |
|-----------------------------|--------------------------|------------------------------|--------------------------|
| 1a# 0.13 [m] | 0.77 | 0.96 | 1.15 |
| 2b# 0.11 [m] | 0.91 | 1.14 | 1.36 |

| 3c# 0.10 [m] | 0.98 | 1.23 | 1.47 |
|--------------|------|------|------|

Table 5-15. Relative slope length values $(n * h_c / \hat{a}_{\delta})$ for the tests.

Considering Table **5-15** the threshold value for $n*h_c/\hat{a}_\delta$ for these tests must be close to 0.96 (the value for test 1a5). The mobility parameter (θ or θ_c) for the conditions with the initial structure heights of 4 cm can be scaled down depending on the relative slope length. The values seem consistent with the deformation prediction as only the 4 cm tests (1a4, 2b4, 3c4) are below a value of 0.96, except the 3c4 test. But the 3c# tests don't have the significant lower value for the 3c4 test. When the value for $n*h_c/\hat{a}_\delta$ gets lower, as is the case for 1a# and 2b#, the difference should be larger with the 5 and 6 cm tests. This phenomenon can be seen in the deformation prediction figures.

5.4.3 Final remarks

When critical parameters, as treated in this section, are used based on test results, it is important that the values for the dimensionless boundary conditions defined in section 5.1.2 have similar values. The calculated values for the critical parameters are valid for these test conditions. For significantly different hydraulic conditions or structure geometry other values for the critical parameters proposed in this section are possible

A combination of the relative boundary layer thickness and the ratio of the slope length and the water particle movement amplitude can also be considered. A possible expression that combines the two aspects is the following:

$$\frac{n*(h_c-\delta)}{\hat{a}_{\delta}}$$

In this expression for the relative slope length the initial structure height is corrected with the boundary layer thickness.

The parameters that incorporate the initial structure height to estimate the extent of streamline contraction are derived from the test data available. For the relative slope length the parameter n is used, but only one slope steepness was tested, so it is difficult to say if this parameter is valid in general.

6 Conclusions and recommendations

In this chapter the general conclusions regarding the investigation on erosion of rubble mound near-bed structures under irregular waves are reviewed. In the second part of this chapter recommendations for further research on this subject are made. First the objective of the thesis, as described in section **1.3**, are repeated:

to investigate the deformation behaviour of near-bed structures under a long period of irregular waves and what aspects control this behaviour. An ultimate objective is to produce a rule or model to predict the deformation of such a near-bed structure.

The aim of this chapter is to see to what extent the objective is achieved. Only general remarks are stated in the conclusions and recommendations. More details and background information can be found in the relevant chapters.

Before presenting the conclusions and recommendations general observations from the tests are given:

Physical model test observations

- A non-linear behaviour of the waves was observed from the tests; sharp crests
 and long throughs. This was caused by the transitional or shallow water depth
 circumstances. For all tested conditions there was occasionally breaking and
 white capping of the waves caused by the interference of the irregular waves.
 The wave reflection caused by the structures was found to be very low.
- In general, at the beginning of a test, the stones started moving at the top of the structures. The movement of the stones could be described as rolling, sliding or making short jumps. The stones followed an oscillatory path where some stones travelled from the upstream slope over the crest to find the downstream slope. The opposite movement was observed less as the stones from the downstream slope remained on the crest or the upper part of the upstream slope.
- The eroded stones were deposited mainly on the downstream slope of the structure. The upstream slope lost a limited amount of stones but these occasionally created gaps in the slope. These gaps were filled with surrounding stones and stones rolling back from the crest. The border of the lower part of the upstream slope kept its slope angle. The net erosion or accretion of the lower part of the upstream slope is very low under the tested environment. Only a small amount of transport outside the structure boundaries (toes of the slopes) could be seen.
- A more stable situation for the tests was created after the first wave series (1000 waves). At the beginning of the second wave series (2000 waves) stones still moved to and fro over the crest of the structure. During this second wave

series the stone erosion and the deformation of the tested structures diminished significantly. A small level of erosion was present with a nearly constant structure height. When stones did move due to an extreme wave, they often moved as a group with 3 to 5 stones at a time. After the last wave series that a structure endured in a test, the compaction and interlocking forces were checked qualitatively under water by lightly stroking the crest of the structure with the finger tips. The structure showed a smoother surface.

6.1 Conclusions

Based on the observations of the model tests and the analysis of the tests the following conclusions are stated:

- "Paintal 2.5" (equation 2.32) seems to apply most as a general stone transport formula that can be used to estimate the erosion for near-bed structures. For design purposes it can not be used as it excludes the structure geometry and only determines the stability of a single stone. The formula by Van Gent and Wallast (2001), specifically derived for near-bed structures, seems to be the best prediction erosion formula available. It includes the wave load duration and the near-bed structure geometry aspect for erosion prediction.
- The incorporation of N with a logarithmic function gives a better prediction of the erosion results in these tests than the square root of N.
- There is a considerable variation of deformation within one test. The parallel lines show differences after identical hydraulic circumstances. This is caused by local turbulence of the fluid flow and the randomness of the positions of the stones and their individual sizes, shapes and densities.
- For the tested conditions the formulation in equation **5.12** with the structure height incorporated in the mobility parameter θ_c predicts the deformation reasonably well where the formula from Van Gent and Wallast (2001) generally overpredicts the erosion.
- The relative structure height parameter h_c'/h_c (equation **5.16**) indicates that the absolute decline of height is proportional to the initial structure height. This is mainly the case for the near-bed structure heights of 5 and 6 cm. The initial structure height h_c is incorporated in this parameter which describes the amount of deformation. However, the inaccuracy of the method with respect to the mobility parameter θ is high. This inaccuracy is also based on the limited variation of tested values for h_c and θ
- The structure height of 4 cm gives significantly lower erosion results than the 5 and 6 cm structures. A possible reason for this deviation is that there might be a certain threshold value value for hydraulic conditions related to the structure height. A larger structure height is thought to give more streamline

contraction. Suggestions for such a threshold are the relative slope length $n*h_c/\hat{a}_\delta$ and the relative boundary layer thickness h_c/δ .

6.2 Recommendations

The recommendations are separated in general recommendations for erosion prediction and recommendations with regard to the derived near bed velocity. These last recommendations are specifically for model tests where wave measurements are used and velocities are not directly measured.

General recommendations for erosion prediction:

- It is recommended to perform additional tests with different storms with different significant wave heights and research into the influence of a storm sequence. A question could be whether a rubble mound near-bed structure has better "armour" against an extreme storm when a less severe storm already has slightly deformed the structure.
- In general the validity of the near bed peak velocity \hat{u}_{δ} as characteristic value can be tested. Tests with longer wave periods and hence a smaller wave steepness but with similar peak velocities are a way to check this aspect. It is interesting to see what a longer lasting velocity does to a near-bed structure. The accelerations are smaller (which could result in less erosion) but there is a possibility that higher levels of erosion occur due to a longer lasting velocity. When tests are performed these hydraulic situations with larger wave periods can be considered as scale tests of swell waves on transitional water depth.
- Tests on a larger scale with bigger stones could be performed to check the validity of the incorporation of the mobility parameters θ or θ_c . For the relative structure height approach a larger range of mobility parameters is necessary to possibly increase the accuracy of the method or to find out whether the relative structure height parameter $h_c^{'}/h_c$ is an appropriate way to incorporate the influence of the initial structure height.
- When a larger range of mobility parameters and structure heights is tested, the
 influence of the relative structure slope length with the available data of these
 tests and new tests can be researched.
- The dynamic stability aspect can be recommended for further research. For the researched tests the structures underwent a transition after approximately 1500-2000 waves (in general for all test condition between 1000 and 3000 waves) and the erosion rate in time reduced significantly. In this investigation the maximal possible hydraulic conditions (wave paddle limitations) were used for the tests and it is considered here that it is usefull to do simular tests with larger mobility parameters. A hypothesis, based on the former, is that for some threshold value of the hydraulic load the structure can not arm itself

against the waves by interlocking forces and a smooth crest surface. The cause of this could be that the erosion is so strong that reposition of individual stones (so that they find a stable position) is impossible and a situation of continuous transport occurs.

• More research can be done on the aspect of interlocking forces with regard to near-bed structures. The crest area of a near-bed structure after wave loading can be investigated with regard to porosity of the top stone layers. The situation where the structure becomes stable can be compared with a situation of continuing erosion in time.

Recommendations with regard to the derived near bed velocity:

- The characteristic velocity \hat{u}_{δ} is estimated with linear wave theory. Higher order theories can be used in order to see whether the erosion prediction becomes more accurate. The variation within one measurement will not change as the same hydraulics are still present. When only these tests are evaluated the accuracy can not increase significantly as the variation within one measurement is relatively large. When only the data range of these tests is considered, the use of higher-order wave theories for the estimation of one characteristic velocity seems inappropriate. Higher-order wave theories are considered not to contribute to more accurate predictions for tests with irregular waves. For regular waves a prediction of the waves with higher-order wave theories could be useful as non-linear breaking processes, caused by interference of irregular waves, can be avoided. Probabilistic techniques can contribute more to erosion prediction under irregular waves than the use of higher-order wave theories.
- The incorporation of \hat{u}_{δ} can be derived from the spectrum or it can be considered to measure a velocity profile in time near (in front of) the structure. Direct velocity measurements near the bottom using Laser-Doppler velocimetry or other techniques can be used to estimate the hydraulic load on the structure. Measuring the wave time signal and then using characteristic parameters of the constructed spectrum can be used as an estimation of the hydraulic load.

References

Battjes, J.A. (1990), Lecture Notes b70, Vloeistofmechanica. Delft; Delft Faculty of Civil Engineering and Geosciences

Battjes, J.A. (1991), Lecture Notes CTWA 4320 Korte Golven. Delft; Delft Faculty of Civil Engineering and Geosciences

Booij, R. (1992), Lecture Notes CTWA 5312 Turbulentie in de waterloopkunde. Delft; Delft Faculty of Civil Engineering and Geosciences

Carling, P.A. et.al. (1992), Effect of Bed Roughness, Particle Shape and Orientation on Initial Motion Criteria, Dynamics of Gravel-bed Rivers, edited by P. Billi, R.D. Hey, C.R. Thorne & P. Tacconi, 1992, John Wiley & Sons Ltd, p. 23-39.

CUR/RWS Report 169 (2000), Manual on the use of Rock in Hydraulic Engineering. Gouda; CUR.

CIRIA/CUR report 154 (1991), Manual on the use of Rock in Coastal and Shoreline Engineering. Gouda: CIRIA/CUR.

Delft Hydraulics (1972), report M648/M863, Delft.

Hughes, G.J. (1993), Physical models and laboratory techniques in coastal Engineering, World scientific publishing Co Pte ltd, River East, USA.

Jonsson, I.G. (1966), Wave Boundary Layers and Friction Factors. Proceedings of the 10th Conference on Coastal Engineering, Vol 1, No. C4, pp.127-148.

Klomp, W.H.G. and Lomonaco, P. (1995), Pipeline cover stability. Proceedings of the 5th International Offshore and Polar Engineering Conference, pp.15-22, The Hague, The Netherlands.

Levit, M., M.R.A. Van Gent, W.W. Massie (1997), Stability of Pipeline Covers Under Waves and Currents, Proc. 8th Int. Conf on the Behaviour of Offshore Structures, Vol.1, pp.195-210, Delft.

Lomonaco, P. (1994), Design of rock cover for underwater pipelines, M.Sc.-thesis International Institute for Infrastructural, Hydraulic and Environmental Engineering, Delft.

Lomonaco, P. and W.H.G. Klomp (1997), Pipeline rock cover damage assessment, Proc. 8th Int. Conf on the Behaviour of Offshore Structures, Vol.1, pp.179-193, Delft.

Rance, P.J. and N.F. Warren (1968), The Threshold of motion of Coarse Material in Oscillatory flow, Proc. 11th Conf on Coastal Engineering, pp. 487-491, London.

Schiereck, G.J. (2001), Introduction to Bed, bank and shore protection. Delft; Delft University Press

Sleath J.F.A. (1978), Measurements of Bed Load in Oscillatory Flow, ASCE Journal of Waterway, Port, Coastal and Ocean Division. Vol 104, No. WW3, pp.291-307.

Sleath J.F.A. (1984), Sea bed Mechanics, John Wiley & Sons Inc., New York.

Tromp, M.M.A. (2004), M.Sc. Thesis The influence that fluid accelerations have on the threshold of motion. Delft: University of Technology (http://www.waterbouw.tudelft.nl/index.php?menu items id=65)

Van Gent, M.R.A. and I. Wallast. (2001), Stability of near-bed structures and bed protections; analysis of physical model tests with waves and currents, Delft Cluster report HC030204H3804, Delft Hydraulics, December 2001, Delft.

Velde, E Van der (2000), Lecture Notes CT5309 Coastal Engineering. Delft: Delft Faculty of Civil Engineering and Geosciences

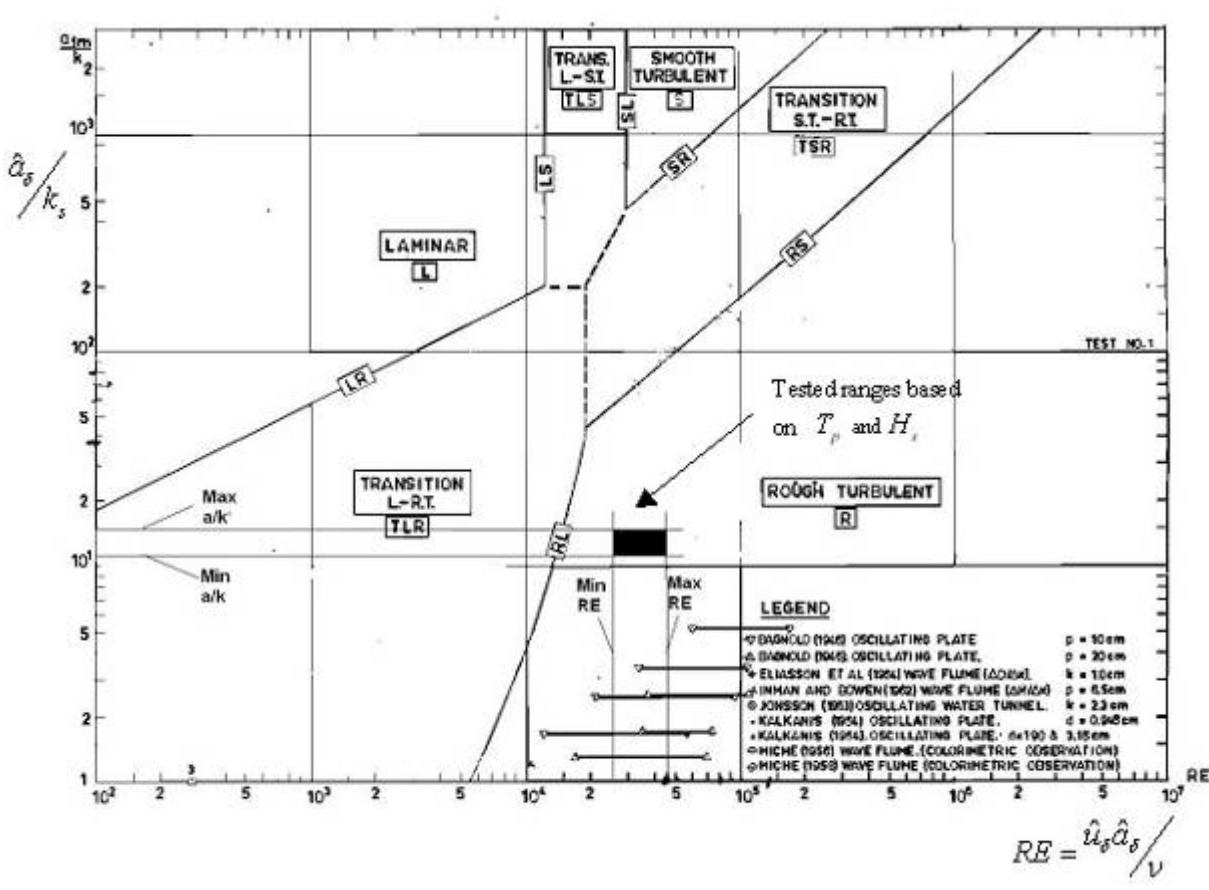
Vidal, C.I.J. Losada, F.L. Martin (1998), Stability of near-bed rubble mound structures, ASCE, Proc. ICCE 1998, Vol. 2, pp.1730-1743, Copenhagen.

Wiberg , P.L. Smith, J.D. (1987), Calculations of the Critical Shear Stress for Motion of Uniform and Heterogeneous sediments, Water Resources Research, Vol. 23, NO 8, pp. 1471-1480, August 1987

Appendix A: Flow regime and critical shear stress

Flow regimes under waves

The rough turbulent zone according to Jonsson (1966) must apply in the model to disregard viscous effects. In Appendix figure 1, a graph from the article of Jonsson can be found from which the flow regime can be derived.



Appendix figure 1. Chart for determining the flow regime under a wave (Jonsson, 1966).

In the figure characters can be found that define the flow regime areas. The definition of the characters is as follows:

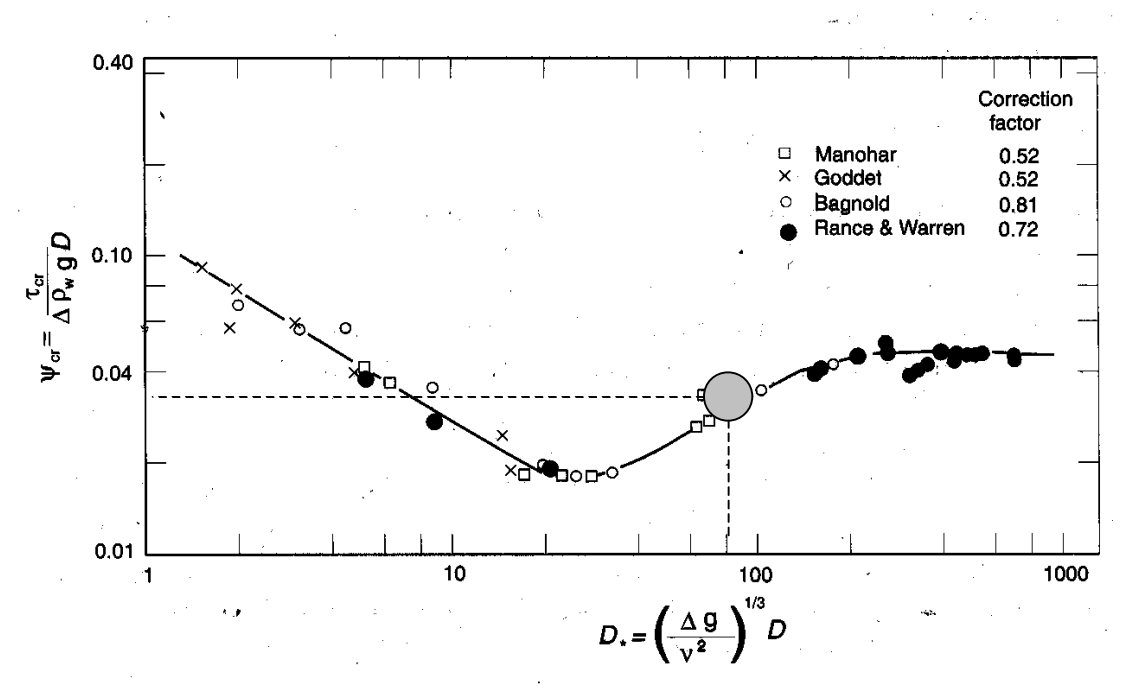
R = rough
S = smooth
T = turbulent
T = transition
L = laminair

The tested ranges based on the measured values of T_p and H_s are also shown in the Jonsson chart. These are in the Rough turbulent zone. There of course are lower velocities present as the Reynolds number in the chart is based on the maximum velocity of a T_p and H_s

combination, but only the situation of stone movement is interesting. So, for eroding stones it can be assumed that the physical processes are in the rough turbulent flow regime and that these processes are independent of viscous influences.

Critical shear stress under waves

For large stones the critical shear stress for stone movement under waves according to Sleath (1978) is independent of the stone size. This can be checked with the figure below: if the D_* on the horizontal axes is larger than about 150 the critical stress remains equal for larger stones.



Appendix figure 2. Modified Shields curve for unsteady flow (Sleath, 1978) with the tested stones and the resulting critical stress displayed in it.

With an assumed dynamic viscosity ν of $1.33*10^{-6}$ m²/s, a g of 9.81 m²/s, a D_{50} of 4.4 mm and a Δ of 1.56 results in a D_* of 90 in Appendix figure 2. So the tested stones have a smaller critical shear stress and will move relatively earlier than larger stones. For the tested situation the value for ψ_c is between 0.035-0.04. Whereas the critical mobility parameter for larger stones lies around 0.05 according to Sleath's chart. This means that the tested stones are considered to move earlier than larger stones in practise would.

Appendix B: Tables of the parameters of the tests

| | l_c std l_c [cm] | 0,09 | | 0,10 | | 0,05 | | | 0,13 | | | 0,08 | | | 0,12 | | | 0,10 | | | | | |
|----------------------------------------|----------------------------------------------------------|-------|-------|---------|------|------|------|------|-------|-------|-------|-------|-------|-------|---------|-------|-------|------|------|------|--------|------|------|
| | $egin{array}{c} {\sf mean} h_c \ {\sf [cm]} \end{array}$ | 5,98 | 5,98 | 2,96 | 5,96 | 4,48 | 4,48 | 4,48 | 4,94 | 4,94 | 4,94 | 6,37 | 6,37 | 6,37 | 5,96 | 5,96 | 5,96 | 4,20 | 4,20 | 4,20 | 6,04 | 6,04 | 0 |
| | std A_0 [cm 2] | 2,9 | | 3,3 | | 1,2 | | | 3,6 | | | 2,9 | | | 4,2 | | | 2,5 | | | | | |
| | mean $A_{\!\scriptscriptstyle 0}$ | 113,5 | | 112,8 | | 68,1 | | | 80,8 | | | 127,1 | | | 112,7 | | | 61,0 | | | 115.37 | | |
| | θ [-] | 2,37 | 2,37 | | | 2,75 | 2,75 | 2,75 | 2,75 | 2,75 | 2,75 | 2,75 | 2,75 | 2,75 | 2,75 | 2,75 | 2,75 | 1,95 | 1,95 | 1,95 | 1,95 | 1,95 | |
| | θ_c [-] | 3,10 | 3,10 | | | 3,41 | 3,41 | 3,41 | 3,49 | 3,49 | 3,49 | 3,76 | 3,76 | 3,76 | 3,68 | 3,68 | 3,68 | 2,39 | 2,39 | 2,39 | 2,57 | 2,57 | 0 |
| | Number of waves N [-] | 1096 | 3177 | 1052 | 3114 | 1052 | 3114 | 6196 | 1029 | 2820 | 5855 | 982 | 2941 | 5961 | 1015 | 3079 | 6296 | 1023 | 3063 | 6083 | 1052 | 3114 | 0.40 |
| | line 5 | | | | | | | | 0,70 | 0,66 | 0,65 | 0,72 | 0,66 | 0,65 | | | | | | | | | |
| | line 4 | | | | | | | | 0,70 | 99'0 | 0,64 | 0,71 | 0,70 | 0,68 | | | | | | | | | |
| , /h _c [- | line 3 | 0,70 | | 0,84 | 0,85 | 0,75 | 0,73 | 0,72 | 0,70 | 0,67 | 0,68 | 0,70 | 0,67 | 0,65 | 0,68 | 99'0 | | 0,79 | 0,78 | 0,75 | | | |
| neight h | le 2 | 0,70 | 0,67 | 0,85 | 0,83 | 0,81 | 0,77 | 0,75 | 0,73 | 0,69 | 0,68 | 0,71 | 0,68 | 0,65 | 0,68 | 99'0 | 0,64 | 0,86 | 0,81 | 0,78 | | | |
| Relative height h_c^\prime/h_c [-] | line 1 lin | 0,72 | 0,67 | 0,89 | 0,87 | 0,79 | 0,78 | 0,77 | 0,67 | 0,61 | 0,61 | 0,70 | 0,67 | 99'0 | 69'0 | 0,67 | 0,62 | 0,79 | 0,77 | 0,76 | 0,81 | 0,76 | 7 |
| | line 5 | | | | | | | | 79,9 | 96,8 | 98,3 | 109,6 | 155,0 | 162,4 | | | | | | | | | |
| D_{n50}^{2} [- | line 4 | | | | | | | | 81,7 | 102,0 | 107,4 | 120,4 | 127,5 | 135,9 | | | | | | | | | |
| $S = A_e /$ | line 3 | 110,4 | | 28,8 | 34,3 | 54,1 | 62,0 | 65,7 | 82,7 | 94,3 | 92,6 | 119,9 | 139,4 | 153,6 | 123,9 | 141,1 | | 41,8 | 44,0 | 53,1 | | | |
| number | line 2 | 115,1 | 129,2 | 43,5 | 41,1 | 37,9 | 49,9 | 55,6 | 71,1 | 90,5 | 93,4 | 111,2 | 129,1 | 149,8 | 120,0 | 130,6 | 140,9 | 23,9 | 33,8 | 41,7 | | | |
| Erosion number S = A_e/D_{n50}^2 [-] | line 1 | 98,0 | 127,1 | 40,7 | 46,5 | 43,4 | 48,0 | 51,5 | 102,1 | 132,1 | 132,7 | 124,7 | 141,8 | 150,8 | 113,0 | 127,9 | 160,3 | 37,8 | 44,1 | 45,8 | 26,7 | 78,9 | 900 |
| | Test codes | 0a6 | | 0a6s2.6 | | 1a4 | | | 1a5 | | | 1a6 | | | 1a6 her | | | 1b4 | | | 1b6 | | |

| 2a6 | 75,5 | 83,8 | 88,5 | | | 0,77 | 0,75 | 0,74 | | | 1034 | 3,13 | 2,25 | 114,6 | 0,2 | 6,02 | 0,00 |
|---------------|----------------------------------------|--------|-----------------|-----------------|--------|------------|-----------|------------------------------|------------|------|----------------------|--------------------|-------|-----------------------|------------------------------|-------------------|----------------|
| | 104,7 | 112,0 | 112,2 | | | 0,71 | 0,70 | 0,70 | | | 3184 | 3,13 | 2,25 | | | 6,02 | |
| | 114,7 | 116,8 | 118,5 | | | 0,70 | 0,69 | 0,69 | | | 6200 | 3,13 | 2,25 | | | 6,02 | |
| 2b4 | 25,7 | 23,2 | 38,1 | | | 0,85 | 0,86 | 0,79 | | | 1046 | 2,59 | 2,08 | 29,0 | 1,0 | 4,12 | 0,04 |
| | 33,5 | 25,9 | 37,7 | | | 0,81 | 0,84 | 0,80 | | | 3073 | 2,59 | 2,08 | | | 4,12 | |
| | 38,5 | 24,4 | 41,6 | | | 0,79 | 0,85 | 0,78 | | | 6128 | 2,59 | 2,08 | | | 4,12 | |
| 2b5 | 56,5 | 68,2 | 45,6 | 21,7 | 62,1 | 0,78 | 0,75 | 0,81 | 0,77 | 0,76 | 1104 | 2,74 | 2,08 | 85,1 | 2,8 | 5,09 | 0,10 |
| | 60,2 | 9,69 | 8,73 | 72,8 | 62,2 | 0,77 | 0,75 | 0,77 | 0,73 | 0,76 | 3330 | 2,74 | 2,08 | | | 5,09 | |
| | 67,5 | 82,5 | 9'99 | 73,7 | 64,4 | 0,75 | 0,72 | 0,75 | 0,73 | 0,75 | 6546 | 2,74 | 2,08 | | | 5,09 | |
| 5p6 | 54,9 | 57,1 | 71,4 | 46,7 | 50,1 | 0,82 | 0,81 | 0,78 | 0,84 | 0,82 | 1079 | 2,89 | 2,08 | 115,0 | 2,4 | 6,03 | 0,07 |
| | 51,2 | 57,3 | 74,9 | 49,2 | 81,8 | 0,83 | 0,81 | 0,77 | 0,83 | 0,75 | 3221 | 2,89 | 2,08 | | | 6,03 | |
| | 50,8 | 70,4 | 96,3 | 84,7 | 100,1 | 0,83 | 0,78 | 0,73 | 0,75 | 0,72 | 6369 | 2,89 | 2,08 | | | 6,03 | |
| 3c4 | 3,7 | 26,5 | 27,5 | 31,3 | 37,3 | | 0,84 | 0,84 | 0,83 | 0,80 | 066 | 2,30 | 1,78 | 62,1 | 2,5 | 4,25 | 0,10 |
| | 3,8 | 30,2 | 29,3 | 30,2 | 37,8 | | 0,83 | 0,84 | 0,84 | 0,80 | 2956 | 2,30 | 1,78 | | | 4,25 | |
| | 3,8 | 29,7 | 30,4 | 31,6 | 39,6 | 0,97 | 0,83 | 0,83 | 0,83 | 0,80 | 5921 | 2,30 | 1,78 | | | 4,25 | |
| 3c5 | 37,6 | 36,6 | 27,6 | 39,8 | 38,9 | 0,84 | 0,84 | 0,87 | 0,83 | 0,83 | 1014 | 2,44 | 1,78 | 8,78 | 4,2 | 5,18 | 0,14 |
| | 54,8 | 65,7 | 50,4 | 63,7 | 53,8 | 0,79 | 0,76 | 0,80 | 0,76 | 0,78 | 3112 | 2,44 | 1,78 | | | 5,18 | |
| | 59,4 | 58,0 | 43,9 | 8'09 | 55,9 | | 0,78 | 0,82 | 0,77 | 0,77 | 6028 | 2,44 | 1,78 | | | 5,18 | |
| 3c6 | 35,6 | 44,5 | 56,3 | 58,6 | 56,1 | 0,87 | 0,84 | 0,81 | 0,80 | 0,81 | 980 | 2,56 | 1,78 | 112,6 | 3,1 | 5,96 | 60'0 |
| | 36,9 | 51,9 | 6'09 | 58,0 | 58,0 | 0,86 | 0,82 | 0,80 | 0,81 | 0,80 | 2910 | 2,56 | 1,78 | | | 2,96 | |
| | 38,1 | 53,5 | 69,2 | | 60,1 | 0,86 | 0,82 | 0,78 | | 0,80 | 2962 | 2,56 | 1,78 | | | 5,96 | |
| 1d6 | 18,8 | 11,1 | 15,5 | 11,7 | 15,7 | 0,92 | 0,95 | 0,93 | 0,94 | 0,93 | 1036 | | | 109,9 | 2,9 | 5,88 | 60'0 |
| | 19,6 | 6,7 | 16,9 | 11,6 | 22,7 | 0,91 | 0,97 | 0,92 | 0,94 | 0,90 | 3185 | | | | | 5,88 | |
| Test codes | line 1 | line 2 | line 3 lir | line 4 lir | line 5 | line 1 | line 2 li | line 3 lir | line 4 lir | V V | Number of waves N [- | θ _c [-] | θ [-] | mean A_0 [cm 2] | std A_0 [cm ²] | $h_{_{\!c}}$ [cm] | std h_c [cm] |
| | Erosion number S = A_e/D_{n50}^2 [-] | number | $S = A_e / A_e$ | D_{n50}^2 [-] | | Relative I | height I | height $h_c^{'}/h_c^{'}$ [-] | | | | | | | | | |

| Test codes | [m] | H _s [m] | $T_p\left[\mathbf{s} ight]$ | $L_{ m 0p}$ [m] | $L_{0 m p}$ [m] $\left \hat{u}_{\delta} \left[m m/s ight] ight $ | \hat{a}_{δ} [m] | [-] as | $H_s/h[-]$ | $h/L_{ m 0p}$ [-] | $RE = \hat{u}_{\delta}\hat{a}_{\delta}/V$ | $H_{_{\mathrm{S}}}/h	ext{EJ} \left egin{array}{c} \hat{a}_{\delta} \hat{a}_{\delta} \\ h/L_{\mathrm{0p}}	ext{EJ} \end{array} ight RE = \hat{u}_{\delta} \hat{a}_{\delta} \sqrt{\left \left(k_{_{\mathrm{S}}} = 2.5D_{_{\mathrm{D50}}} ight) ight }$ |
|------------|------|--------------------|------------------------------|-----------------|-----------------------------------------------------------------------|------------------------|--------|------------|-------------------|-------------------------------------------|------------------------------------------------------------------------------------------------------------------------------------------------------------------------------------------------------------------------------------------------------------|
| 0a6 | 0,55 | 0,208 | 2,12 | 4,52 | 0,367 | 0,124 | 0,046 | 0,38 | 0,12 | 3,4E+04 | 13,37 |
| 0a6s2.6 | 0,55 | | | | | | | | | | |
| 1a4 | 0,50 | 0,209 | 2,14 | 4,39 | 0,395 | 0,134 | 0,046 | 0,42 | 0,11 | 4,0E+04 | 14,53 |
| 1a5 | 0,50 | 0,209 | 2,14 | 4,39 | 0,395 | 0,134 | 0,046 | 0,42 | 0,11 | 4,0E+04 | 14,53 |
| 1a6 | 0,50 | 0,209 | 2,14 | 4,39 | 0,395 | 0,134 | 0,046 | 0,42 | 0,11 | 4,0E+04 | 14,53 |
| 1a6 her | 0,50 | 0,209 | 2,14 | 4,39 | 0,395 | 0,134 | 0,046 | 0,42 | 0,11 | 4,0E+04 | 14,53 |
| 1b4 | 0,50 | 0,180 | 2,02 | 4,10 | 0,332 | 0,107 | 0,043 | 98'0 | 0,12 | 2,7E+04 | 11,54 |
| 166 | 0,50 | 0,180 | 2,02 | 4,10 | 0,332 | 0,107 | 0,043 | 0,36 | 0,12 | 2,7E+04 | 11,54 |
| 2a6 | 0,45 | 0,180 | 2,02 | 3,92 | 0,357 | 0,115 | 0,044 | 0,40 | 0,11 | 3,1E+04 | 12,40 |
| 2b4 | 0,45 | 0,173 | 2,02 | 3,92 | 0,343 | 0,110 | 0,042 | 0,38 | 0,11 | 2,8E+04 | 11,92 |
| 2b5 | 0,45 | 0,173 | 2,02 | 3,92 | 0,343 | 0,110 | 0,042 | 0,38 | 0,11 | 2,8E+04 | 11,92 |
| 2b6 | 0,45 | 0,173 | 2,02 | 3,92 | 0,343 | 0,110 | 0,042 | 0,38 | 0,11 | 2,8E+04 | 11,92 |
| 3c4 | 0,40 | 0,148 | 2,01 | 3,72 | 0,318 | 0,102 | 0,041 | 0,37 | 0,11 | 2,4E+04 | 10,98 |
| 3c5 | 0,40 | 0,148 | 2,01 | 3,72 | 0,318 | 0,102 | 0,041 | 0,37 | 0,11 | 2,4E+04 | 10,98 |
| 3c6 | 0,40 | 0,148 | 2,01 | 3,72 | 0,318 | 0,102 | 0,041 | 0,37 | 0,11 | 2,4E+04 | 10,98 |
| 1d6 | 0,50 | | | | | | | | | | |

Appendix C: Measured hydraulic conditions

This appendix shows the hydraulic conditions for the tests. The incident spectra and wave exceedance curves for the tests 0a6s2 and 2a6 are not available.

Here the following different wave spectra and exceedance curves are presented:

0a# representing: 0a6, 1a4, 1a5, 1a6,1a6 her

1b# representing: 1b4, 1b6 2b# representing: 2b4, 2b5, 2b6 3c# representing: 3c4, 3c5, 3c6.

Wave spectra

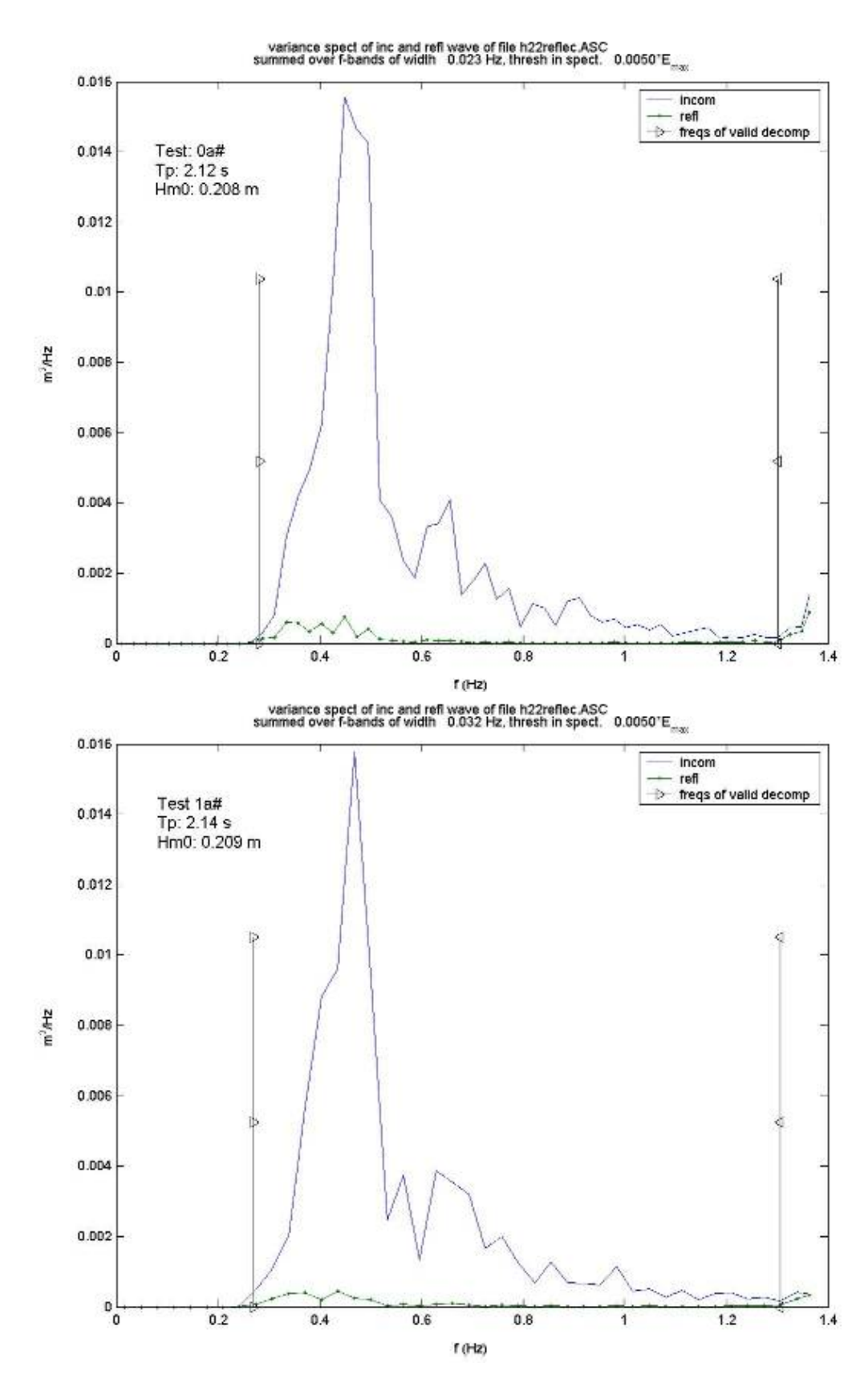
In the wave spectra the incoming wave spectrum and the reflected wave spectrum are displayed. The reflected waves are only generated at the end of the flume and not by the structure, as wave measurements in an empty flume gave identical incoming and reflected wave spectra.

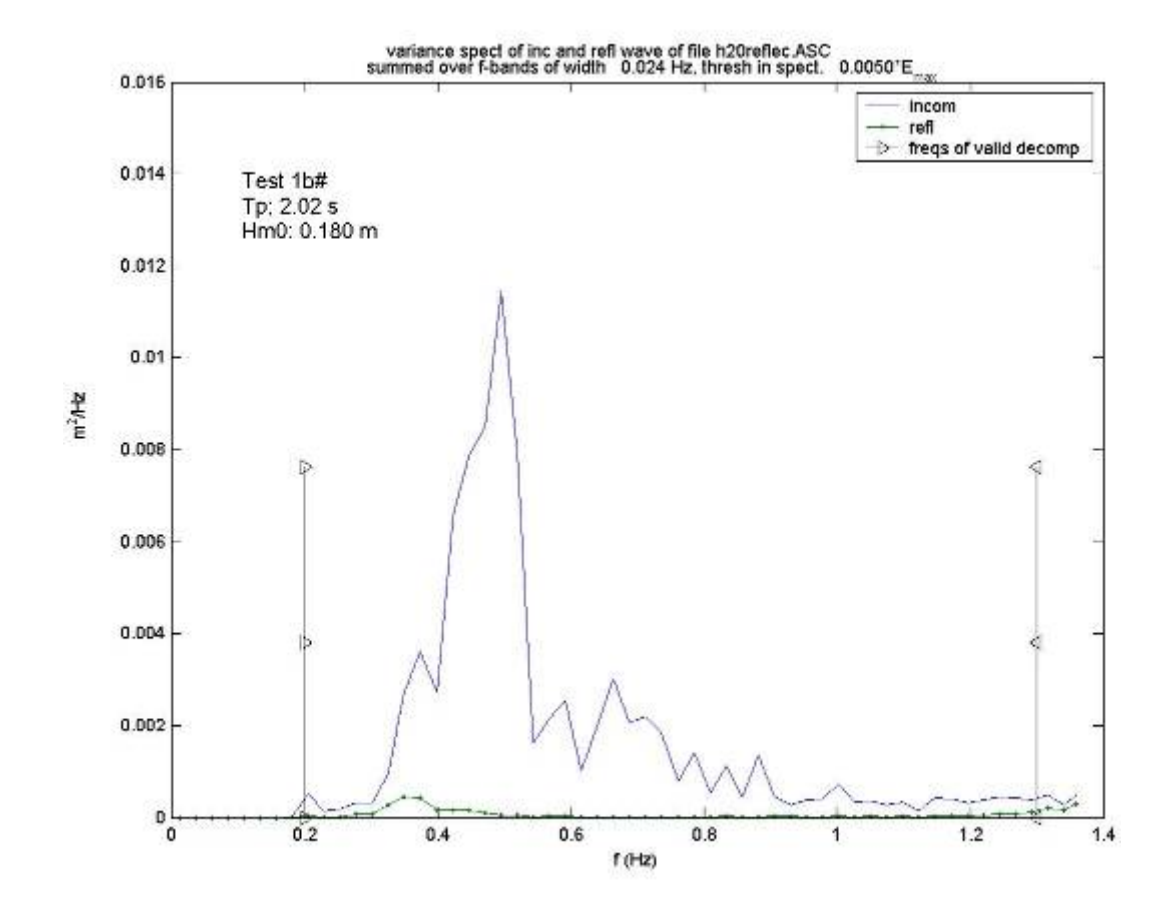
For the derivation of the hydraulic load in the tests only the incoming wave spectrum is used. The reflected spectrum can generate a different hydraulic load but is disregarded for the analysis of the tests. The reflected wave energy is relatively low as can be seen in the figures.

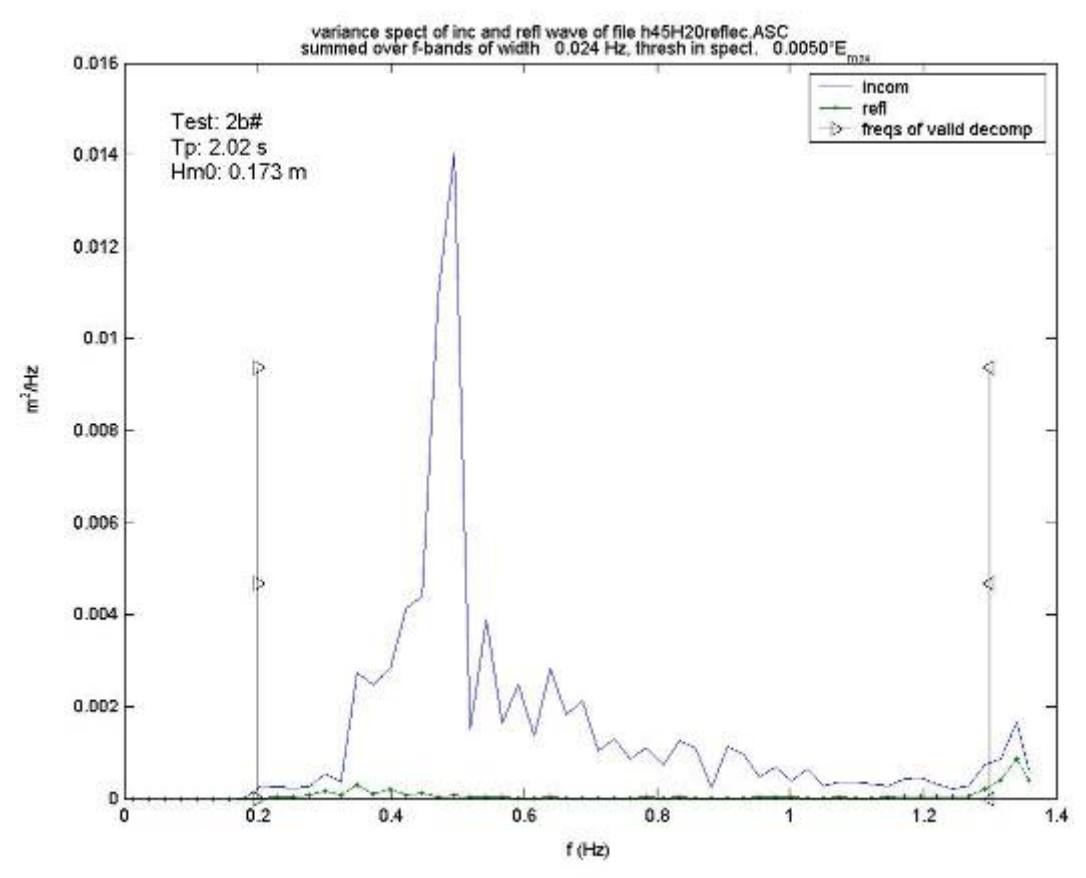
The presentation of the plots will start at the next page.

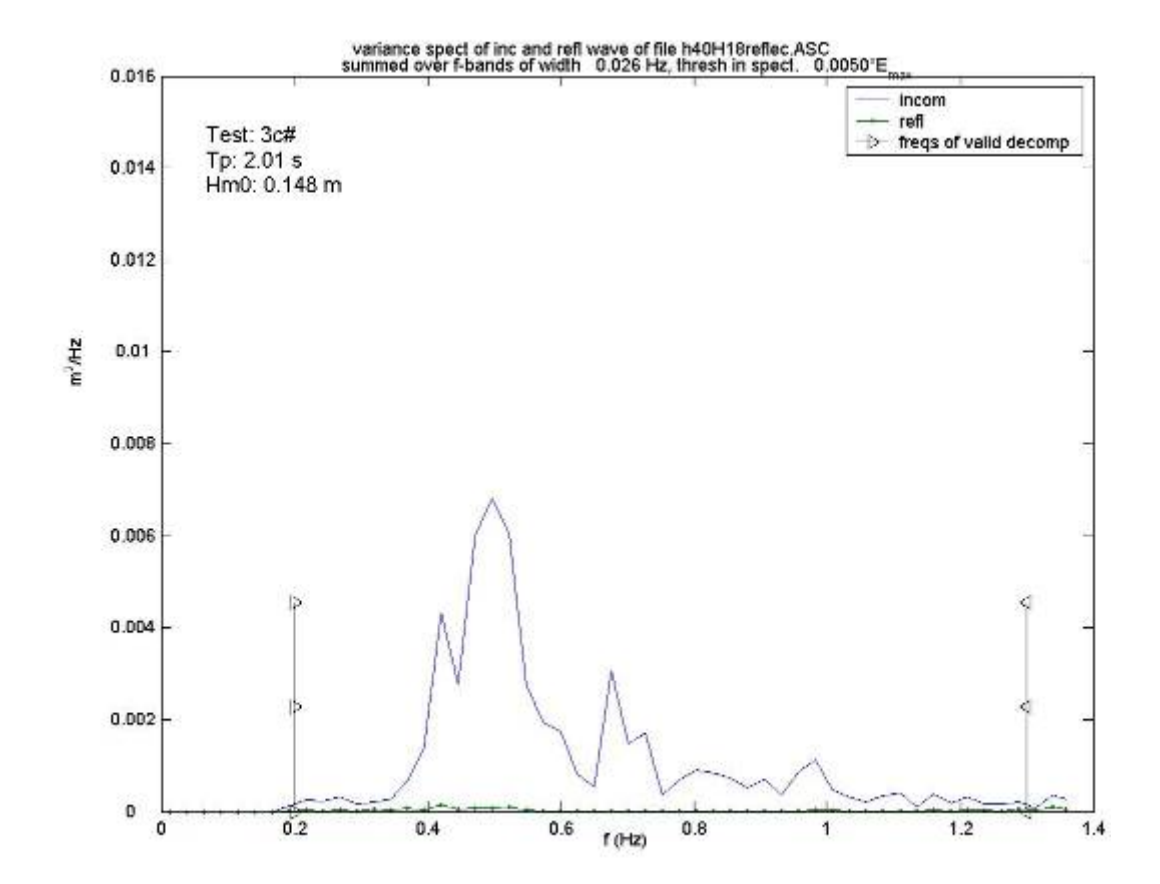
Wave spectra plots

The plots of the wave spectra 0a#, 1a#, 1b#, 2b# and 3c3 are given here.







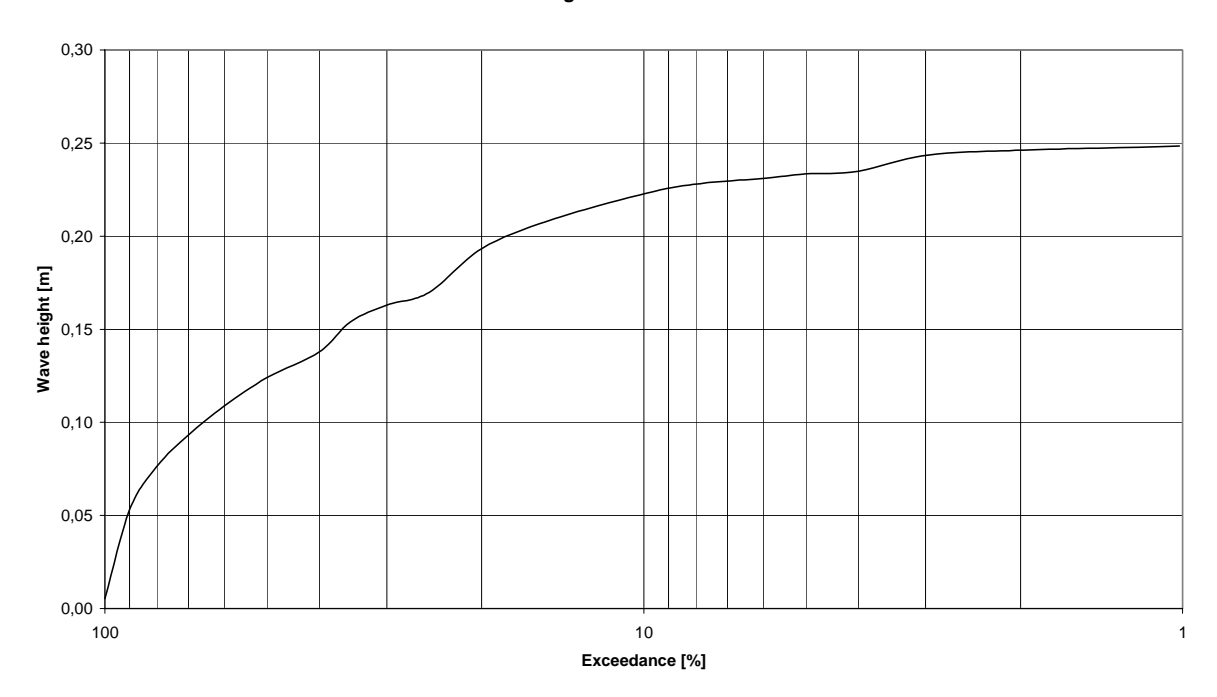


The spectra all have there peak at similar frequencies f_p ($T_p=1/f_p$). The characteristic estimated wave height is derived from the surface of the wave spectra. Only the shape of the 3c# tests differs from the rest in the way that the shape is blunter. There is less energy around a frequency of 0.5 Hz.

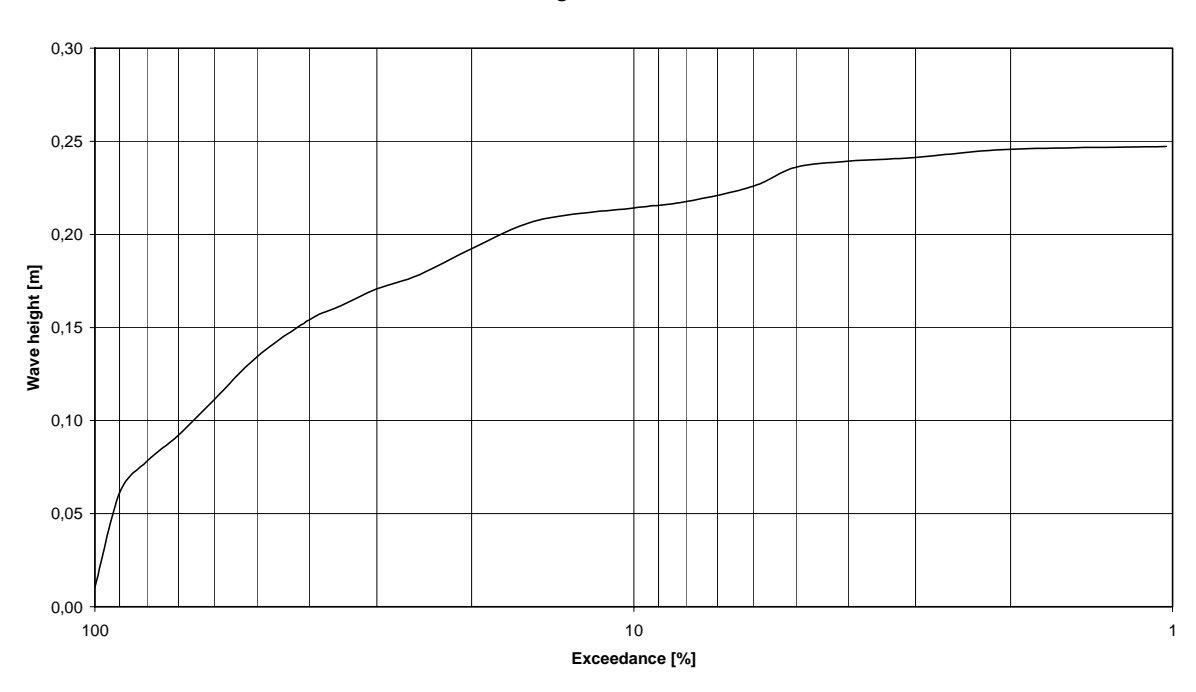
Wave exceedance curves

The wave signal from the wave gauge above the structure crest was used to produce a wave exceedance curve. The wave signal in time was used by the "Waves" program from the laboratory of fluid mechanics. The Hmax = 1.2* Hs. This is due to the intermediate water depth with relatively shallow circumstances; the peak waves generated by the wave board will break.

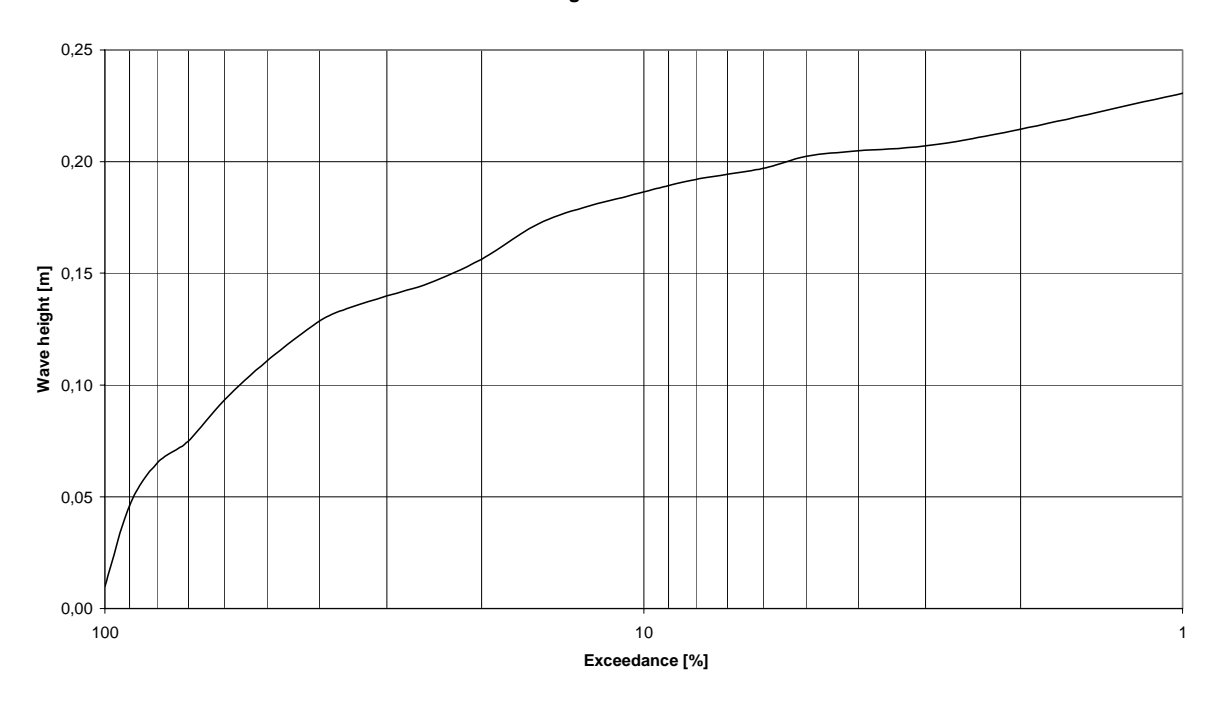
Wave Height Eexceedance 0a



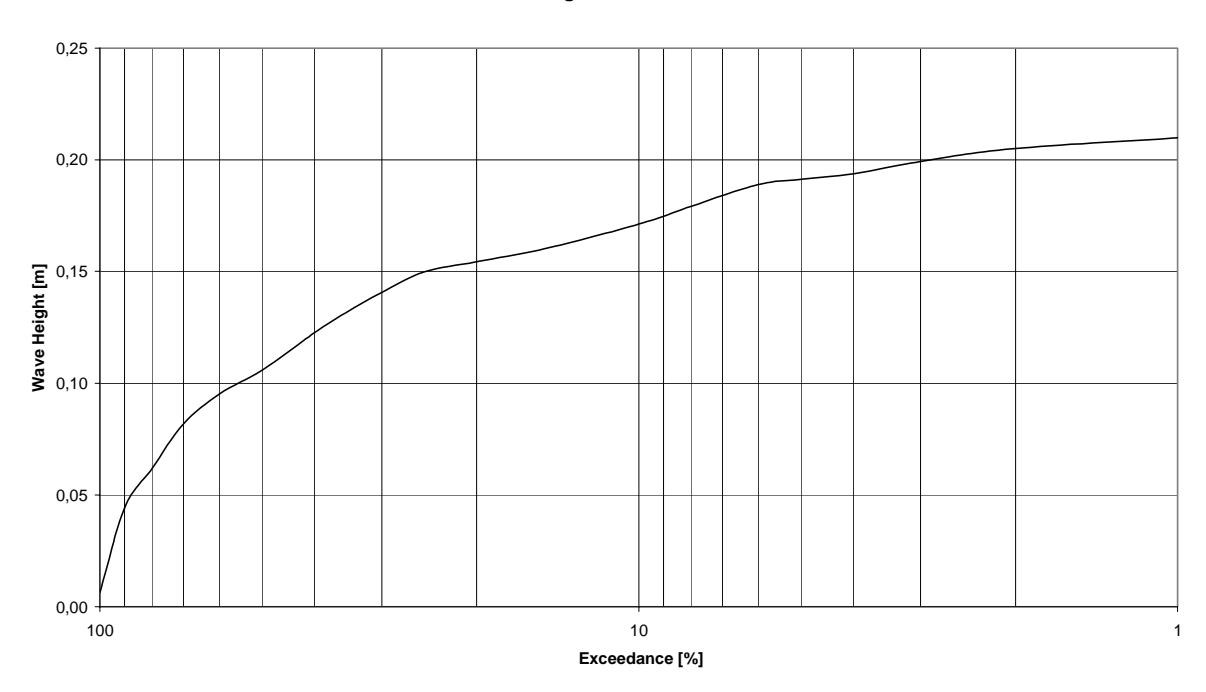
Wave Height Exceedance 1a



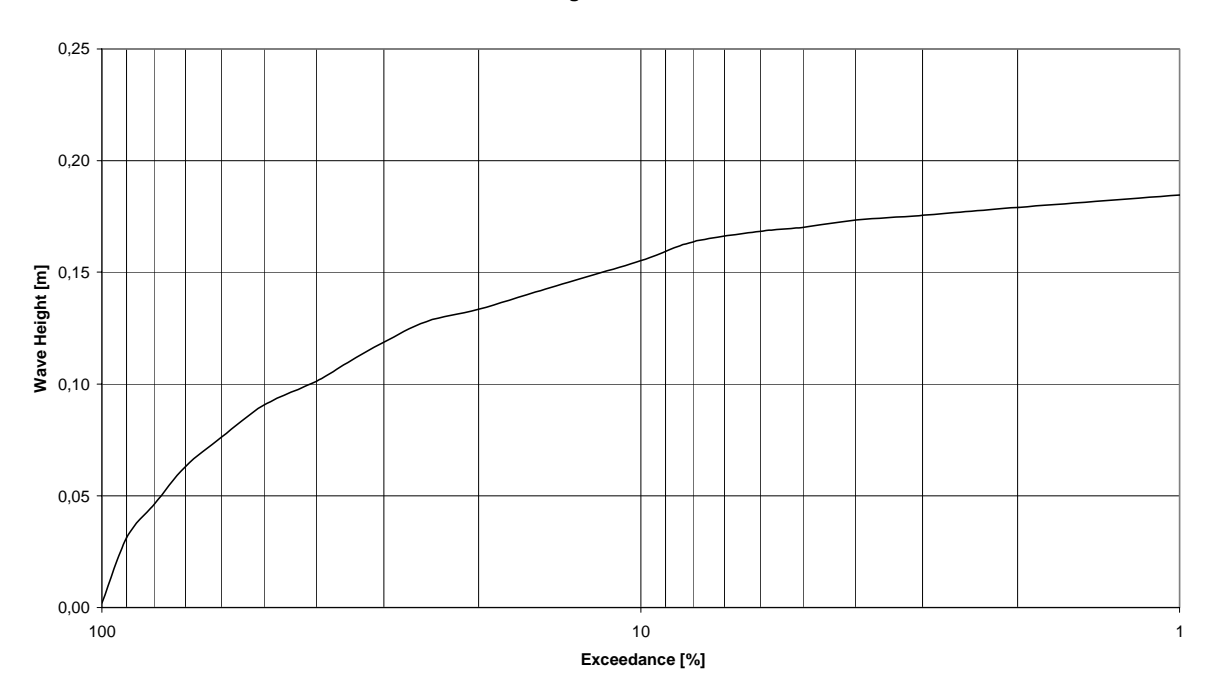
Wave Height Exceedance 1b



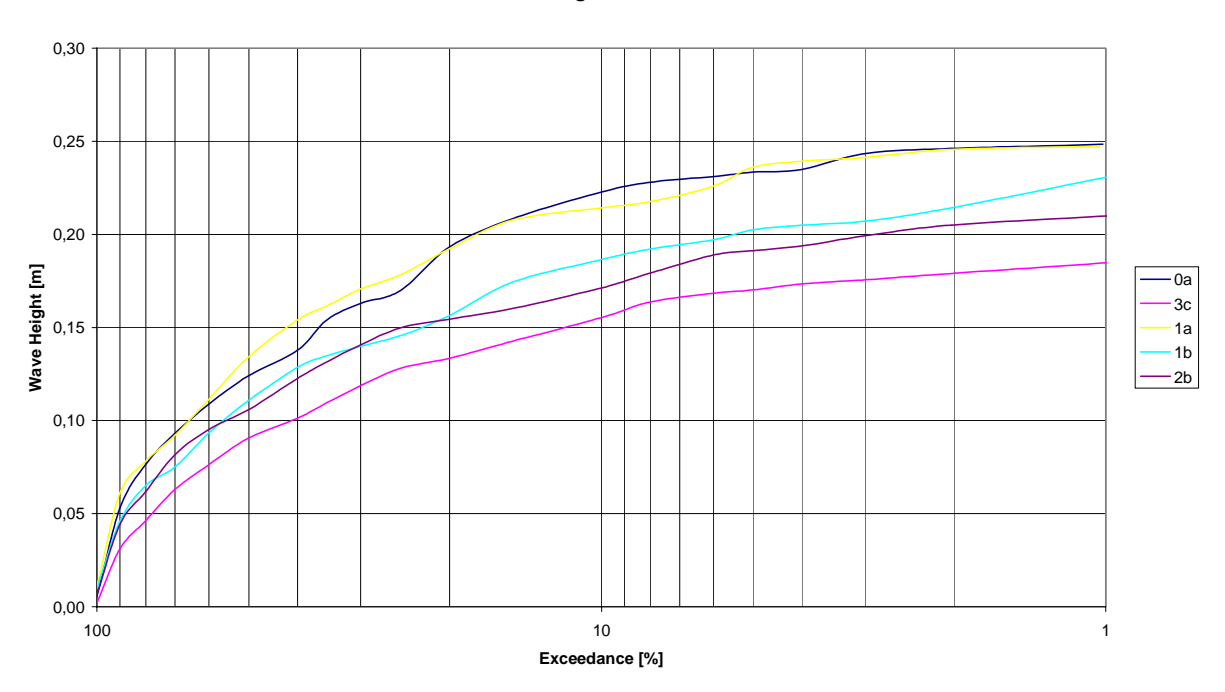
Wave Height Exceedance 2b







Wave Height Exceedance



In the overview of the wave height exceedance curves, can be that the wave height that is exceeded by 10% of the waves is not much bigger than the wave height that is exceeded by 1% of the waves. For the tests the value for the maximal occurring wave height $H_{\rm max}$ can be estimated by:

$$H_{\text{max}} \approx 1.2 * H_s$$

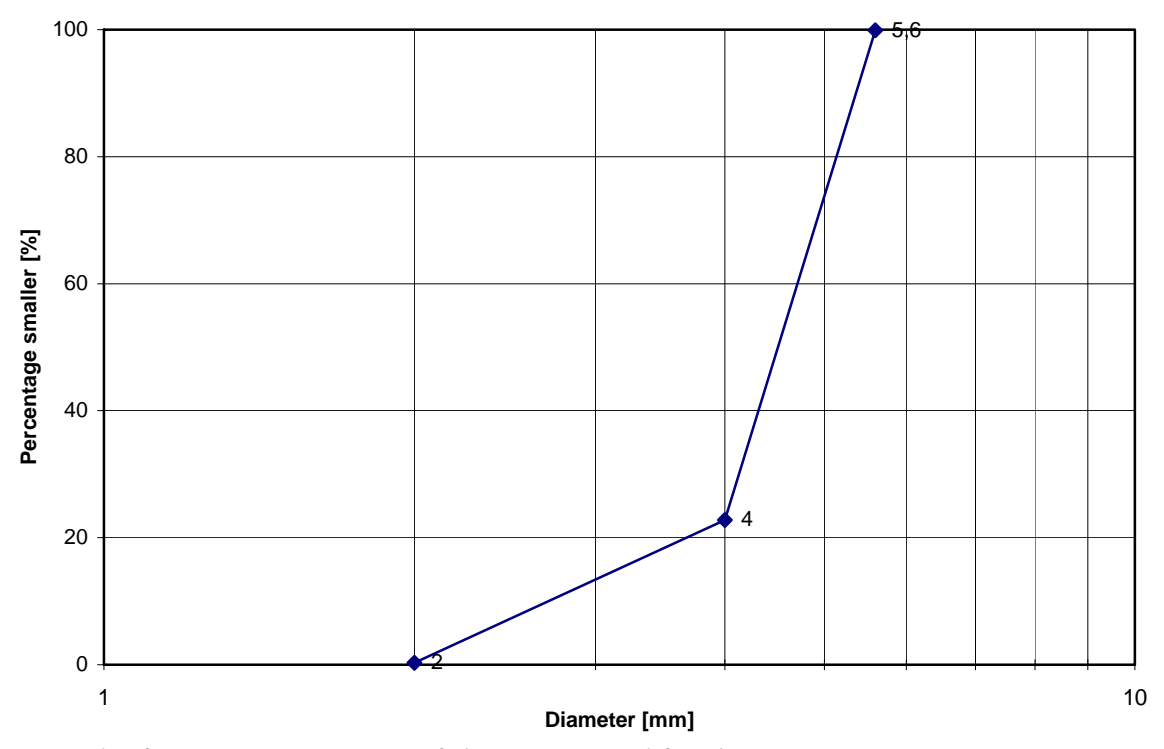
123

Appendix D : Data granular material

In this appendix the grading of the rocks used for the test will be given. Second the results of the stone density measurements will be given and finally a qualification will be made with regard to the stone shape of the used stones.

Rock grading

Interpolation of the straight line in Appendix figure 3 between the 4 mm sieve and the 5.6 mm sieve results in a D_{50} of 4.4 mm. The sieve curve is based on a mix between painted and unpainted stones. Sieve tests were done for painted and unpainted stones and gave similar curves within a margin of +/- 0.5 percent point.



Appendix figure 3. Sieve curve of the stones used for the tests.

Rock density

The results of the density measurements are shown in Appendix table 1 lead to the following characteristics:

Mean stone density 2,47 g/cm3 Stdev stone density 0,09 g/cm3

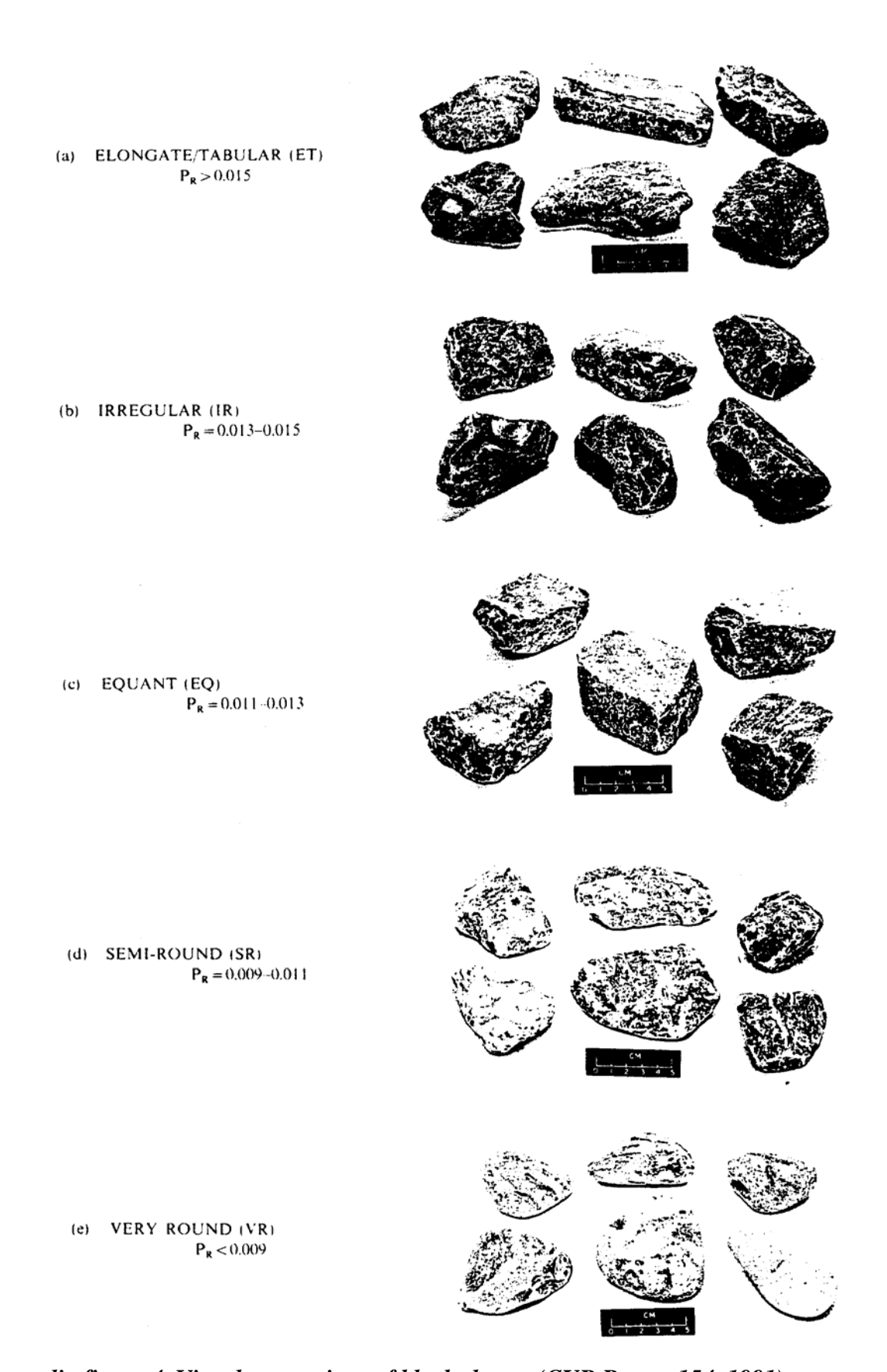
The maximum and minimal value of the stone density column have been disregarded. In the table one sample has an exceptionally high density value (marked red). This is assumed to be caused by an error in the measurement procedure.

| | | | Stone | characteristics | | |
|-------------|------|------------|-----------------|-----------------|--------------|----------------|
| | Nr. | Dry stone | Submerged | Disp water | Stone volume | Stone |
| Paint | INI. | weight [g] | stone weight[g] | weight [g] | [cm3] | density[g/cm3] |
| | 1 | 146.22 | 87.88 | 58.3400 | 58.3400 | 2.5063 |
| | 2 | 267.86 | 159.51 | 108.3500 | 108.3500 | 2.4722 |
| φ. | 3 | 205.18 | 121.87 | 83.3100 | 83.3100 | 2.4628 |
| White | 4 | 148.73 | 88.22 | 60.5100 | 60.5100 | 2.4579 |
| > | 5 | 243.86 | 145.25 | 98.6100 | 98.6100 | 2.4730 |
| | 6 | 220.34 | 133.75 | 86.5900 | 86.5900 | 2.5446 |
| | 7 | 223.05 | 135.09 | 87.9600 | 87.9600 | 2.5358 |
| | 8 | 214.85 | 130.26 | 84.5900 | 84.5900 | 2.5399 |
| | 9 | 241.80 | 146.91 | 94.8900 | 94.8900 | 2.5482 |
| | 10 | 206.12 | 125.11 | 81.0100 | 81.0100 | 2.5444 |
| | 11 | 205.08 | 124.47 | 80.6100 | 80.6100 | 2.5441 |
| | 12 | 198.94 | 120.76 | 78.1800 | 78.1800 | 2.5446 |
| | 13 | 175.91 | 100.43 | 75.4800 | 75.4800 | 2.3306 |
| Red | 14 | 174.84 | 113.13 | 61.7100 | 61.7100 | 2.8333 |
| Ř | 15 | 114.48 | 69.33 | 45.1500 | 45.1500 | 2.5355 |
| | 16 | 204.78 | 112.53 | 92.2500 | 92.2500 | 2.2198 |
| Black | 17 | 240.47 | 143.32 | 97.1500 | 97.1500 | 2.4752 |
| | 18 | 222.36 | 132.51 | 89.8500 | 89.8500 | 2.4748 |
| | 19 | 225.97 | 125.03 | 100.9400 | 100.9400 | 2.2387 |
| | 20 | 156.42 | 93.13 | 63.2900 | 63.2900 | 2.4715 |
| t | 21 | 221.17 | 133.38 | 87.7900 | 87.7900 | 2.5193 |
| No paint | 22 | 192.58 | 115.55 | 77.0300 | 77.0300 | 2.5001 |
| No | 23 | 158.40 | 94.88 | 63.5200 | 63.5200 | 2.4937 |

Appendix table 1. Stone characteristics of the stones used for the tests.

Rock shape

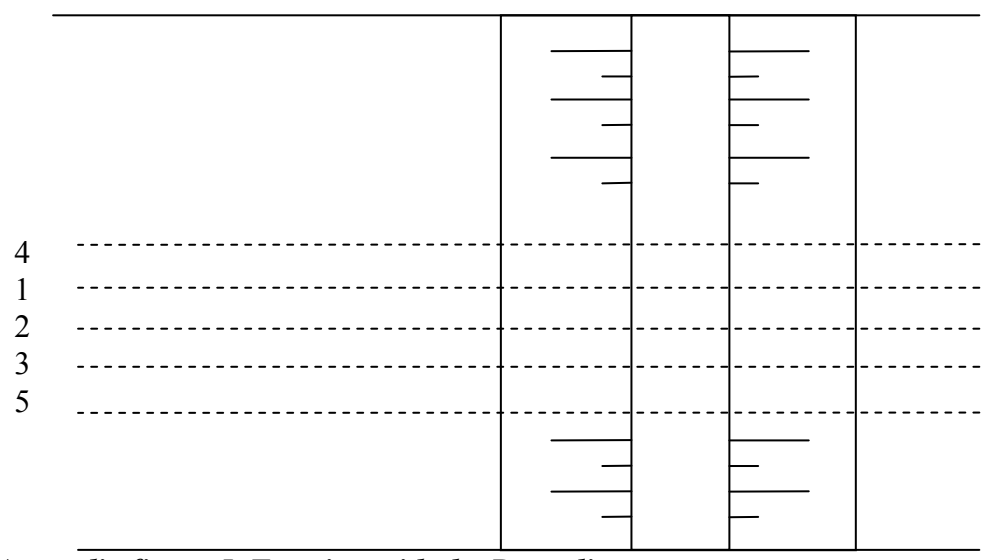
The rock shape of the stones used for the tests are characterized as: P_r =0.013-0.015 (in Appendix figure 4) This is a visual specification of the stone shape (page 92 of the CUR/CIRIA 'Manual on the use of rock in coastal and shoreline engineering')



Appendix figure 4. Visual comparison of block shapes (CUR Report 154, 1991)

Appendix E : Measured damage profiles

In this appendix all profile measurements for each test are plotted. The tests started with three Provo lines and at some point it was decided to work with 5 lines as there were quite some differences for the measurements and with 5 lines the statistical deviation can be estimated in a better way. For the positions of the measured lines with a top view at the structure see Appendix figure 5.



Appendix figure 5. Top view with the Provo lines.

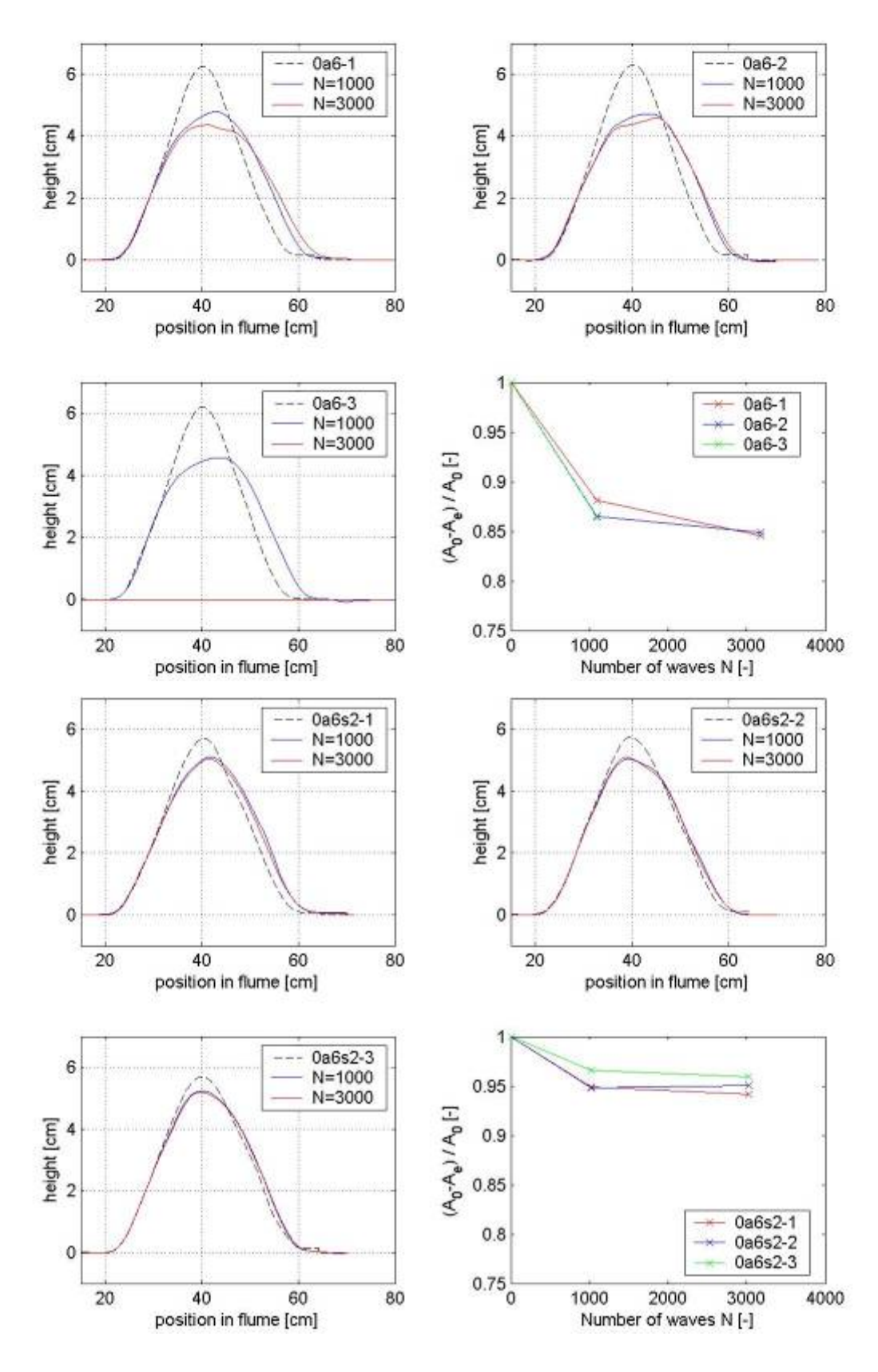
Line nr 2 was the line in the middle of the flume (width 0.8 m). The lines were measured with 5 cm between them.

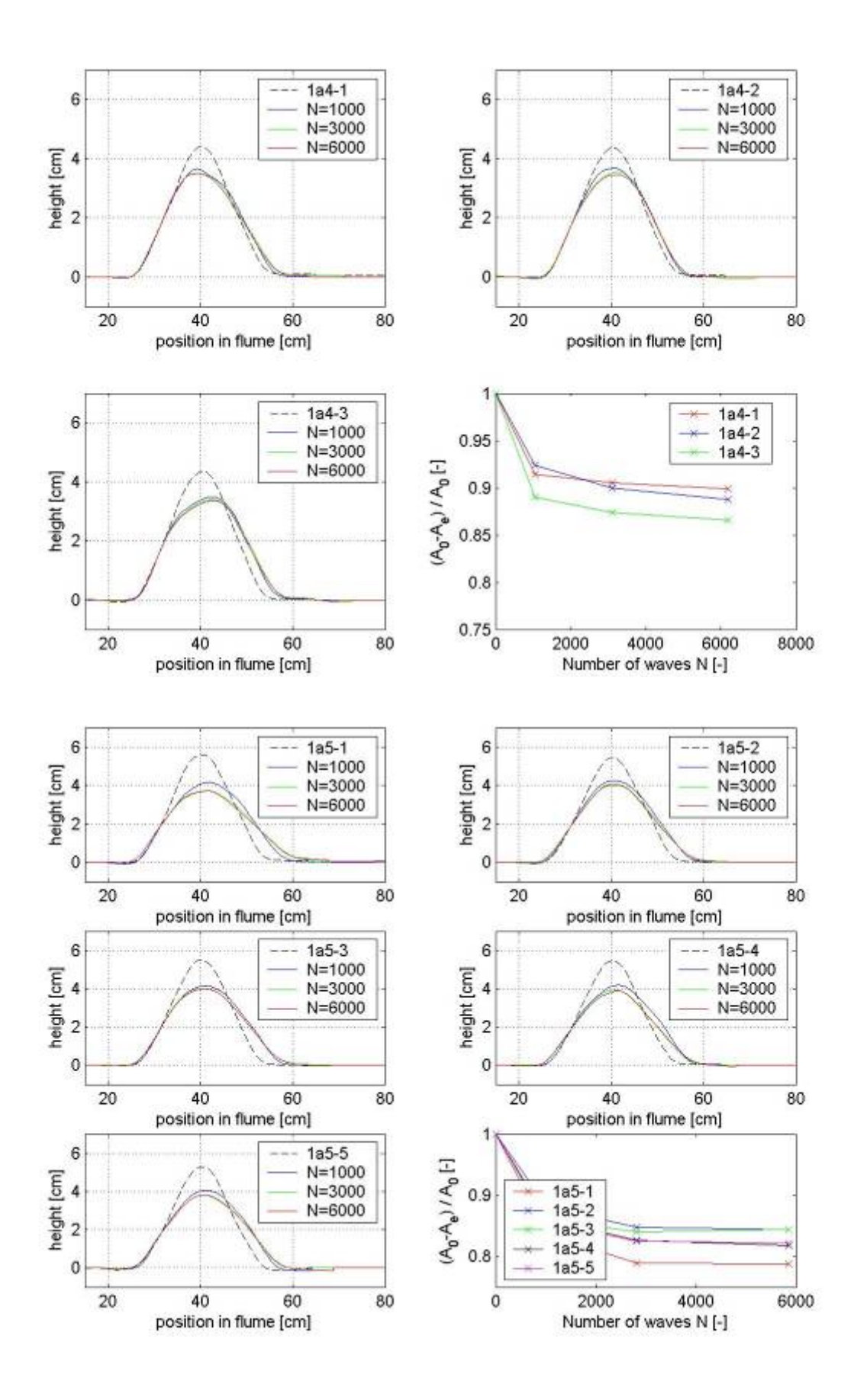
The profile line before waves is always dotted and the profiles after each wave series is plotted in the same figure. After the 3 or 5 profile lines in a test plot are given, the parameter A_{rel} is shown for each line. The Matlab procedure off acquiring them is shown in Appendix H.

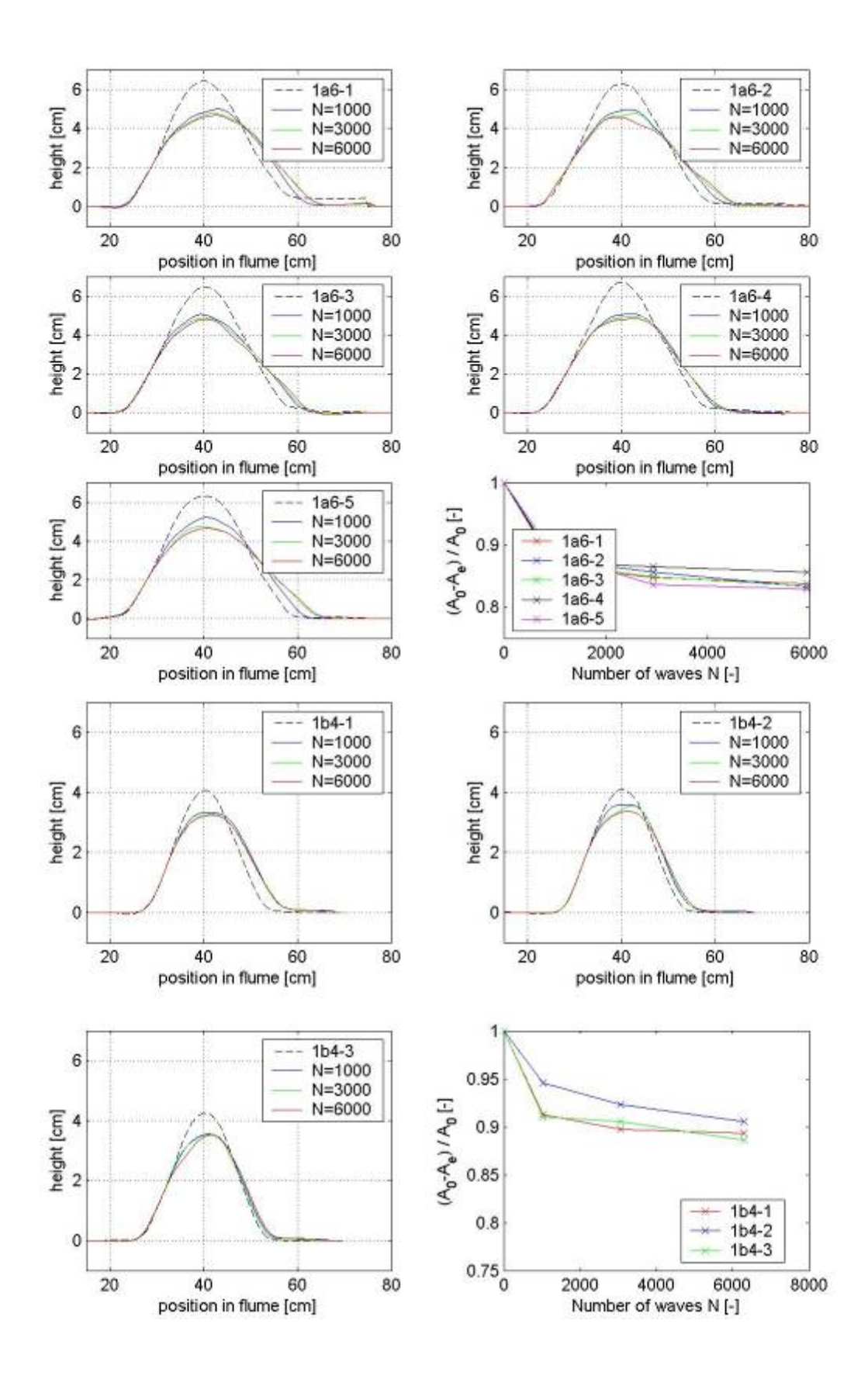
The presentation of the plots will start at the next page.

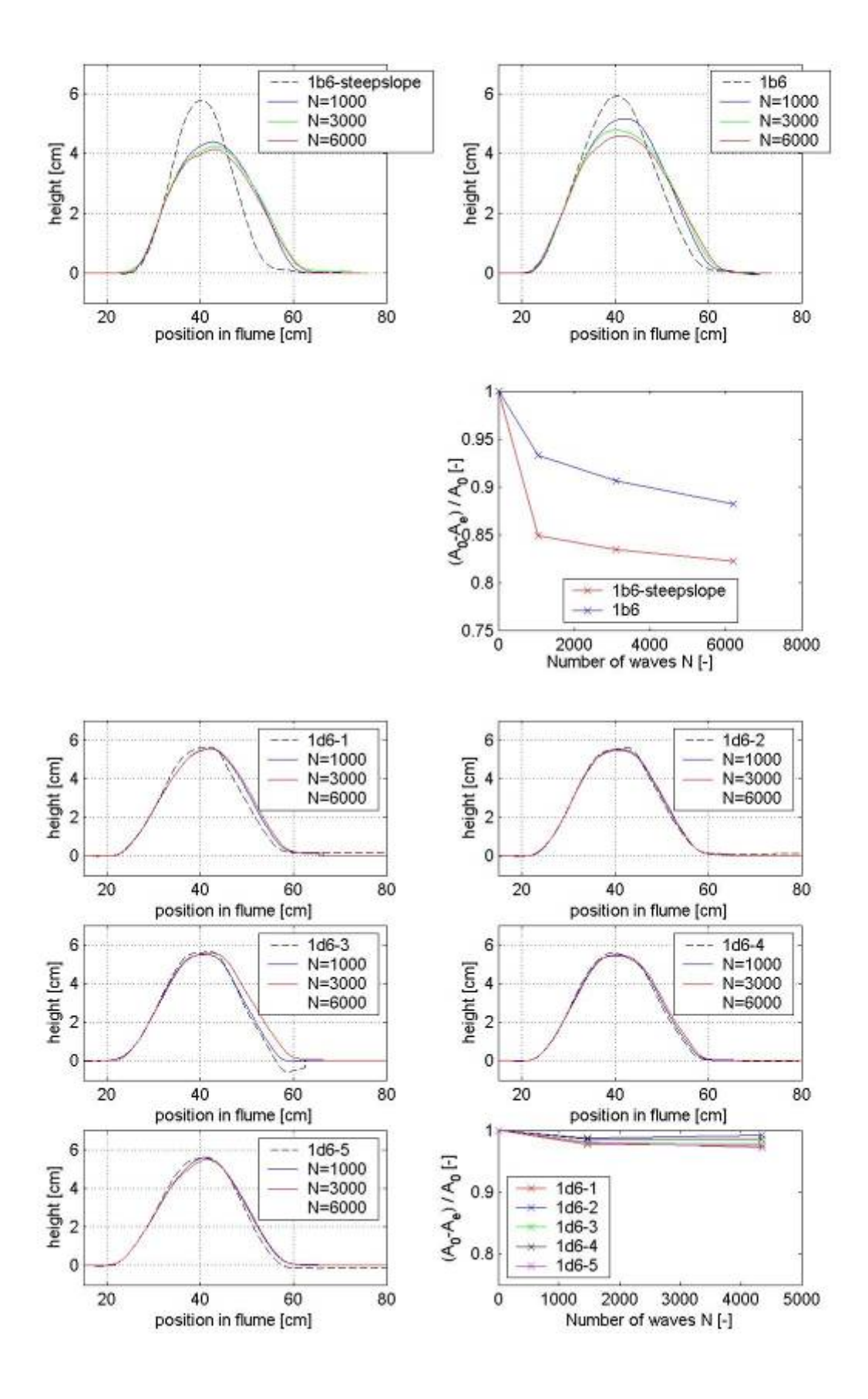
Test profile plots

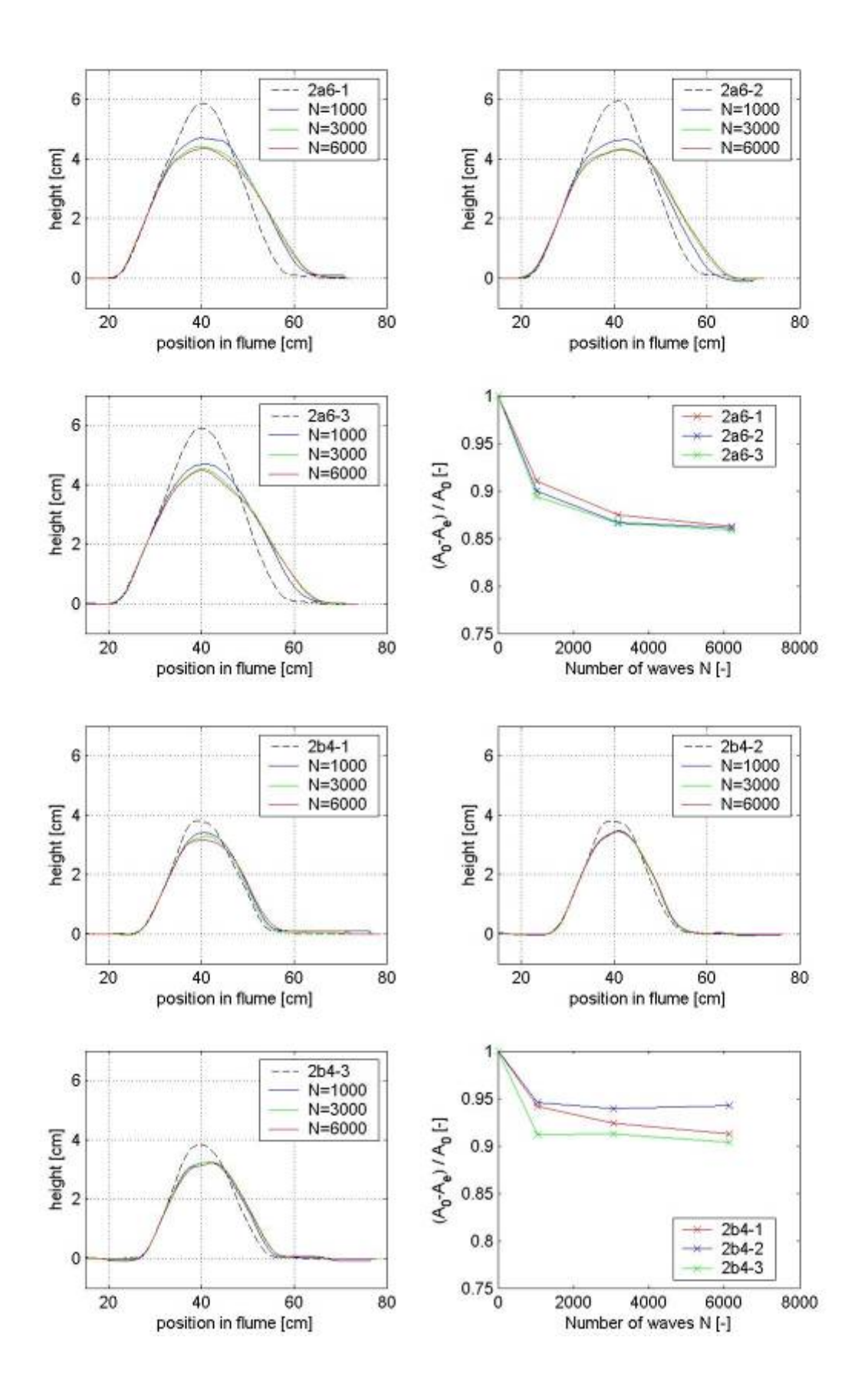
Here all the test plots are given. The test codes are: 0a6, 0a6s2, 1a4, 1a5, 1a6, 1b4, 1b6, 1d6, 2a6, 2b4, 2b5, 2b6, 3b4, 3b5, 3b6 and her1a6.

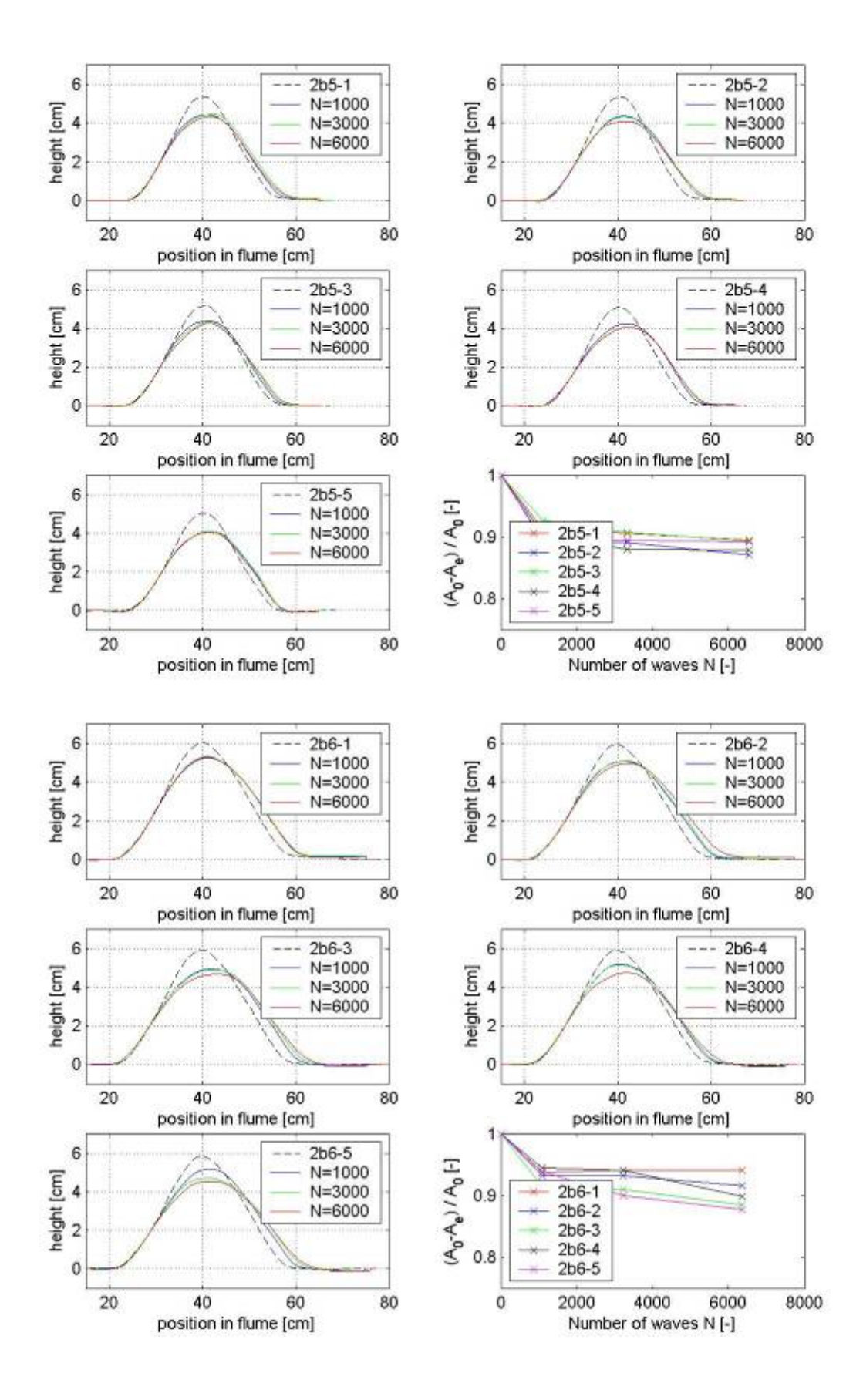


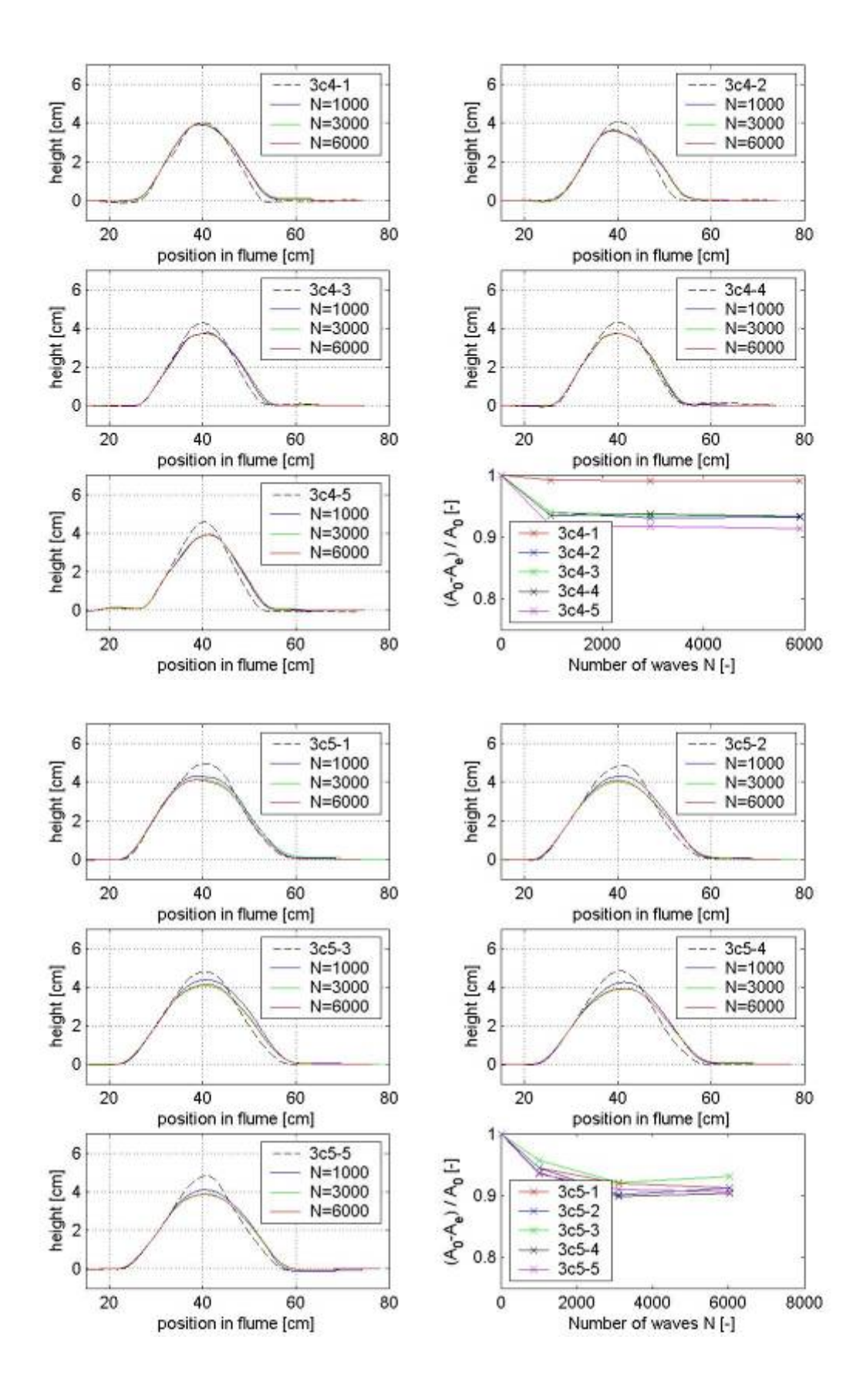


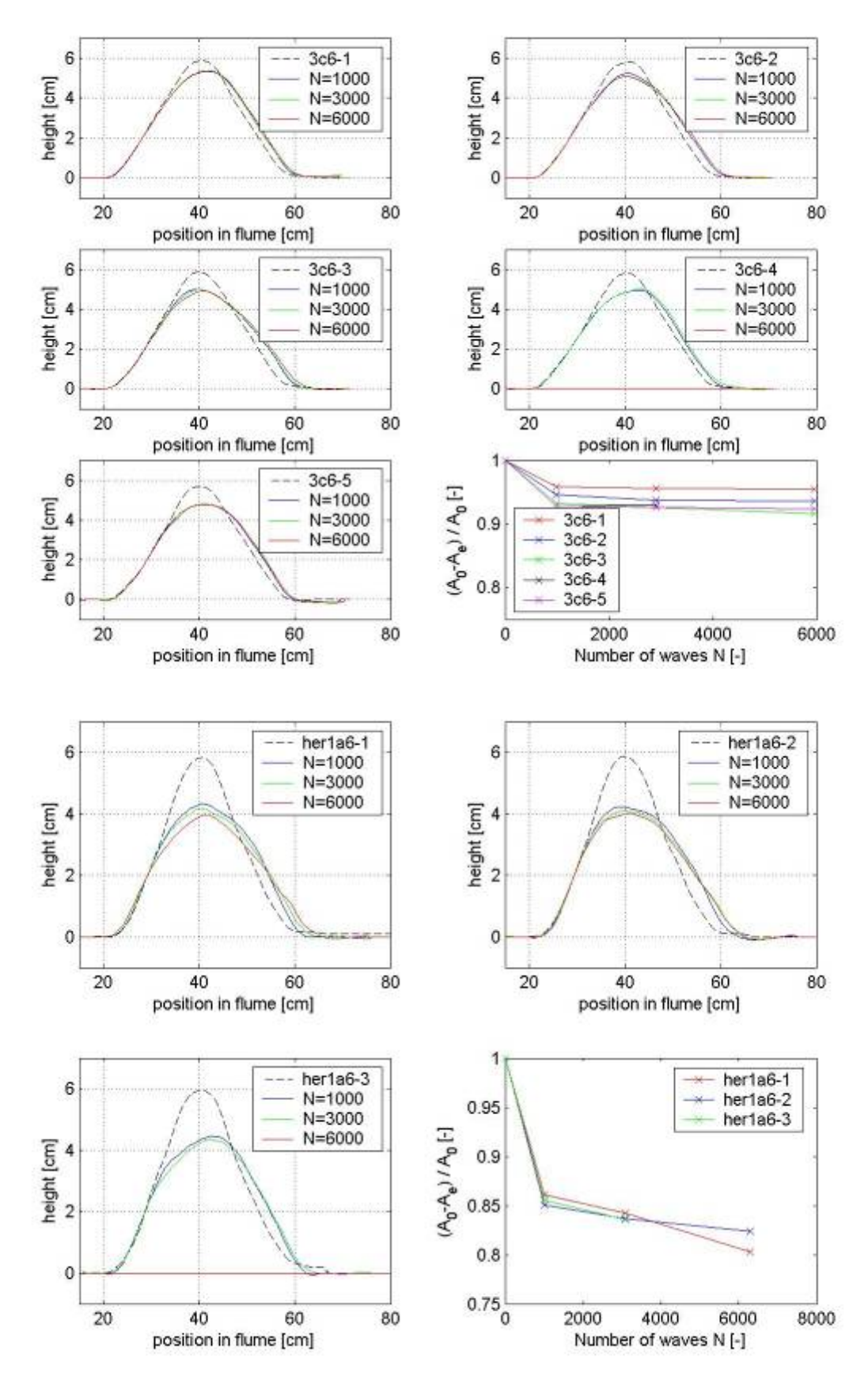












Final remark about the former plots: test 1b6-steepslope is not used for the analysis. Because of its steeper slope (around 1:2) it was found to be incomparable with the other tests.

Appendix F PROVO error analysis

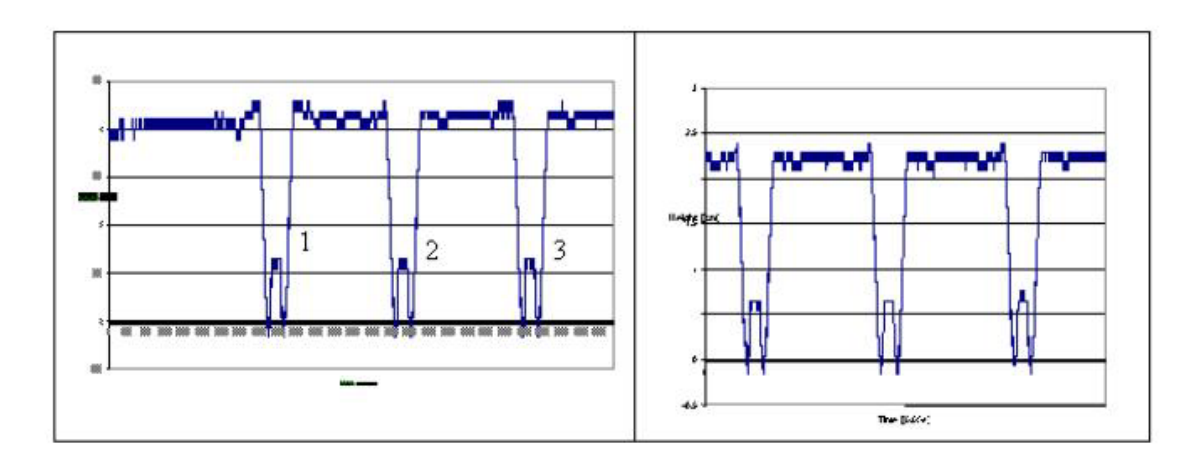
The precision (the difference between two identical profiles) and the accuracy (difference between the measurement and the real profile) are treated in this appendix.

PROVO precision

The precision for a test structure was evaluated by measuring the same structure multiple times. This was also for each test a calibration. The PROVO-lines are results from the right going carriage measurements. The PROVO measurements were very precise. As each profile after a wave series is an average profile over at least 3 lines (right going measuring carriage with as reference point the PVC-bar placed at a set position on the flume bottom after each wave series.

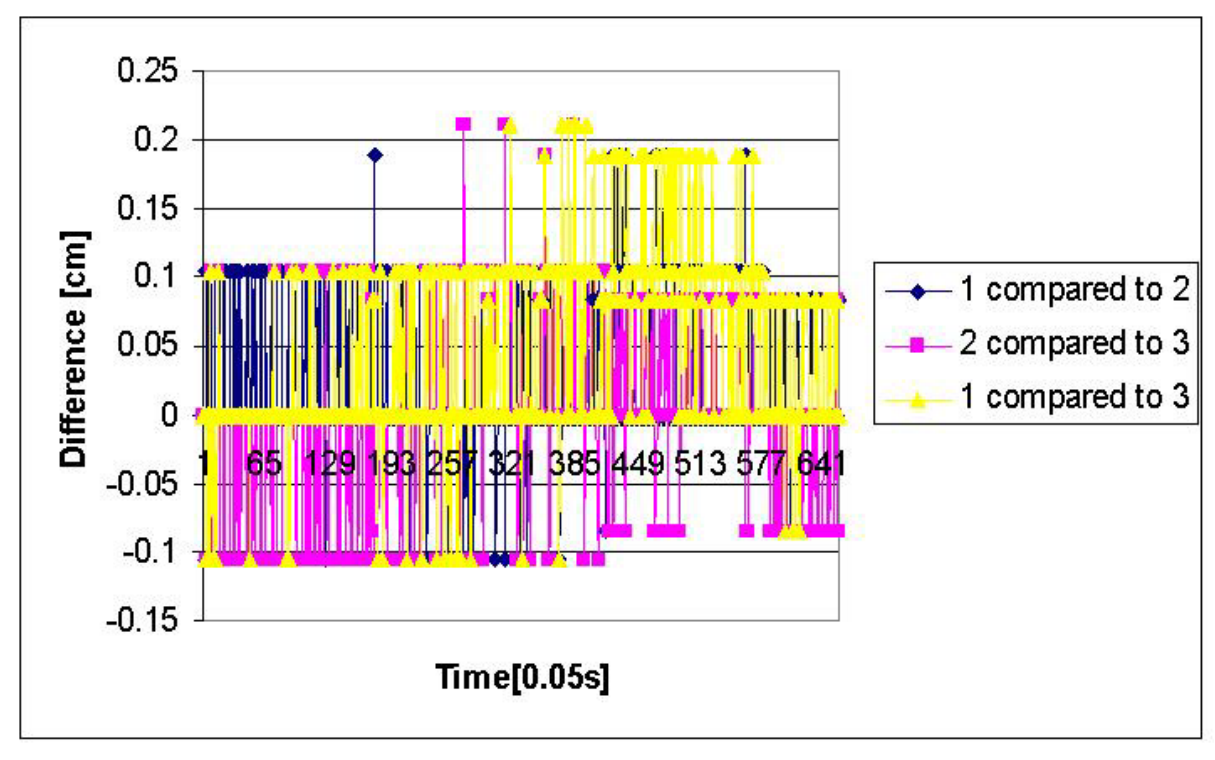
Determining accuracy with comparing identical profiles

The signal of the PROVO when the car init moving gives scatter or noise within a 1 mm bandwidth. This is for a not moving Provo and is the basic error range. When two profiles are compared (see Appendix figure 6), the accuracy of the PROVO-measuring system can be estimated. The results of the three comparisons of the three measured bumps (same bumps because of the back and forth going movement of the carriage) are shown in Appendix figure 6. Based on this figure the accuracy has a band width of 3 mm (+/- 1.5 mm). This agrees with what was seen form the data processing (the process of calculating the eroded area from the profiles before and after a wave series). For the tests between 5 and 10 profiles (the example in Appendix figure 6 shows only three) were averaged to create a representative profile. This 5-10 profiles, when plotted, were always within a 3 mm bandwidth.



Appendix figure 6. Two measurements of the same near-bed structure.

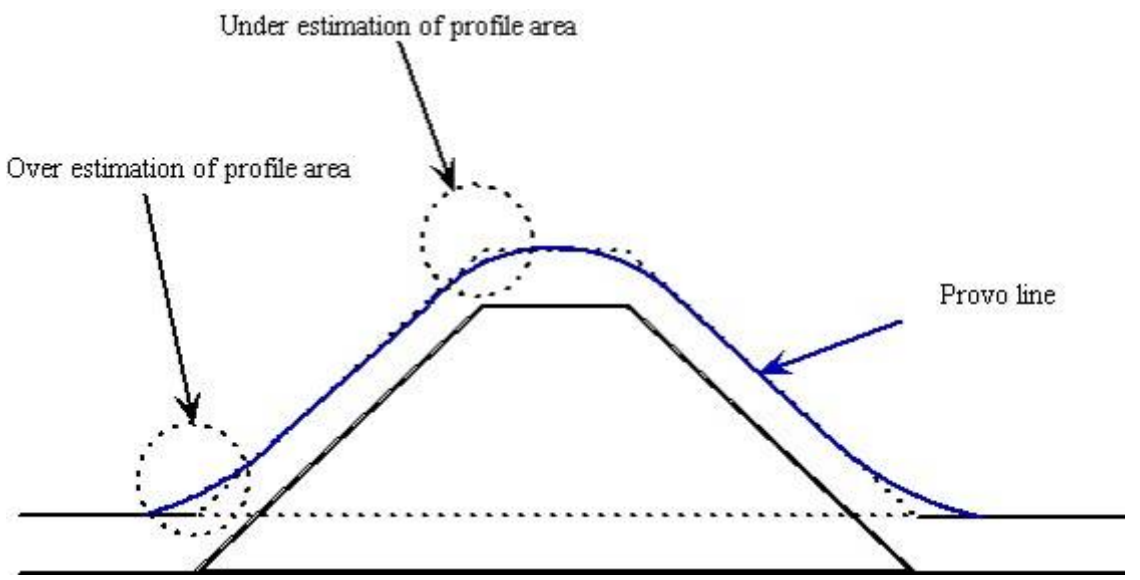
The differences of the two measurements of three identical near-bed-structure profiles (measured with turning points of the carriage in between) are shown in Appendix figure 7.



Appendix figure 7. Comparison between the "peaks" of Appendix figure 6.

Profile comparison accuracy

The accuracy of the Provo system can be validated when a known profile is measured. The difference between the known profile and the measured profile determines the accuracy. The accuracy was tested with a prism of PVC material. The prism shape is known within a range of 0,1 mm. The approach is schematically displayed in the following figure:



Appendix figure 8. PVC prism for the accuracy tests of the Provo system. Under and over estimated areas are shown.

From Appendix figure 8 can be seen that there are generally area that are over and under estimated. These errors reduce each other so that the combined error is considered to be small. The PVC prism shape was used for the calibration of the instruments. The Provo was calibrated with the known height of the prism and the carriage speed was then calibrated by comparing the measured area and the known prism area. During the tests it appeared that the measuring carriage showed unpredictable variations and each the carriage speed had to be calibrated for each individual test based on the measured profile data. The background information and the calibration method can be found in the next section.

Carriage speed estimation

Problems with measuring carriage speed

The input settings for the carriage speed were always the same: 0.6 cm/s. The carriage speed was chosen to be low to ensure less variation in the velocity change in time. During the tests became clear (with the PVC prism calibration) that the velocity showed large variation (up to 15%). The measured profiles were compared after each wave series. It was seen from profile plots that the profile after a wave series was shrunk or grown in the direction of the carriage speed. This means a different velocity because the distance step was based on the time step that a height with PROVO was registered and the carriage speed. Within one test there was hardly any variation. The profiles were compared with the aid of Matlab (for scripts see Appendix H) and were always within a 3mm band width after cutting and pasting on a reference point.

Solution with data calibration

The solution for the problem of the random variation of the speed of the measuring carriage was to calibrate each measurement. The Provo data was calibrated by estimating the carriage speed with two known reference points: one was the PVC bar in front of the structure and the

second one was the slope of the structure itself on the side of the wave paddle. It was found that this slope kept its position, at least on a level lower than half the structure height. From the know distance and the known elapsed time an estimation of the speed was made for each right going movement of the carriage. As each profile was measured several times also the carriage speed could be estimated several times and the average value was used.

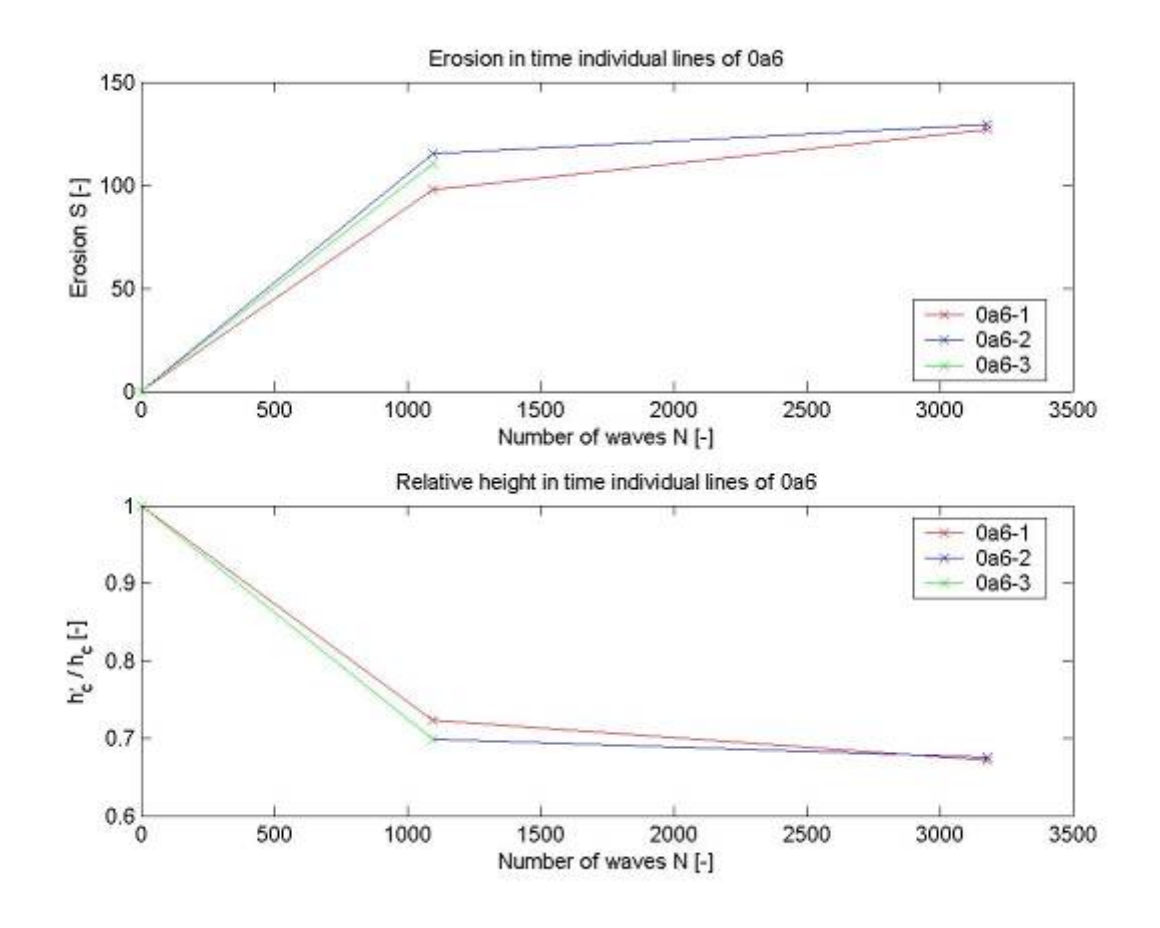
Appendix G: Erosion and relative height in time

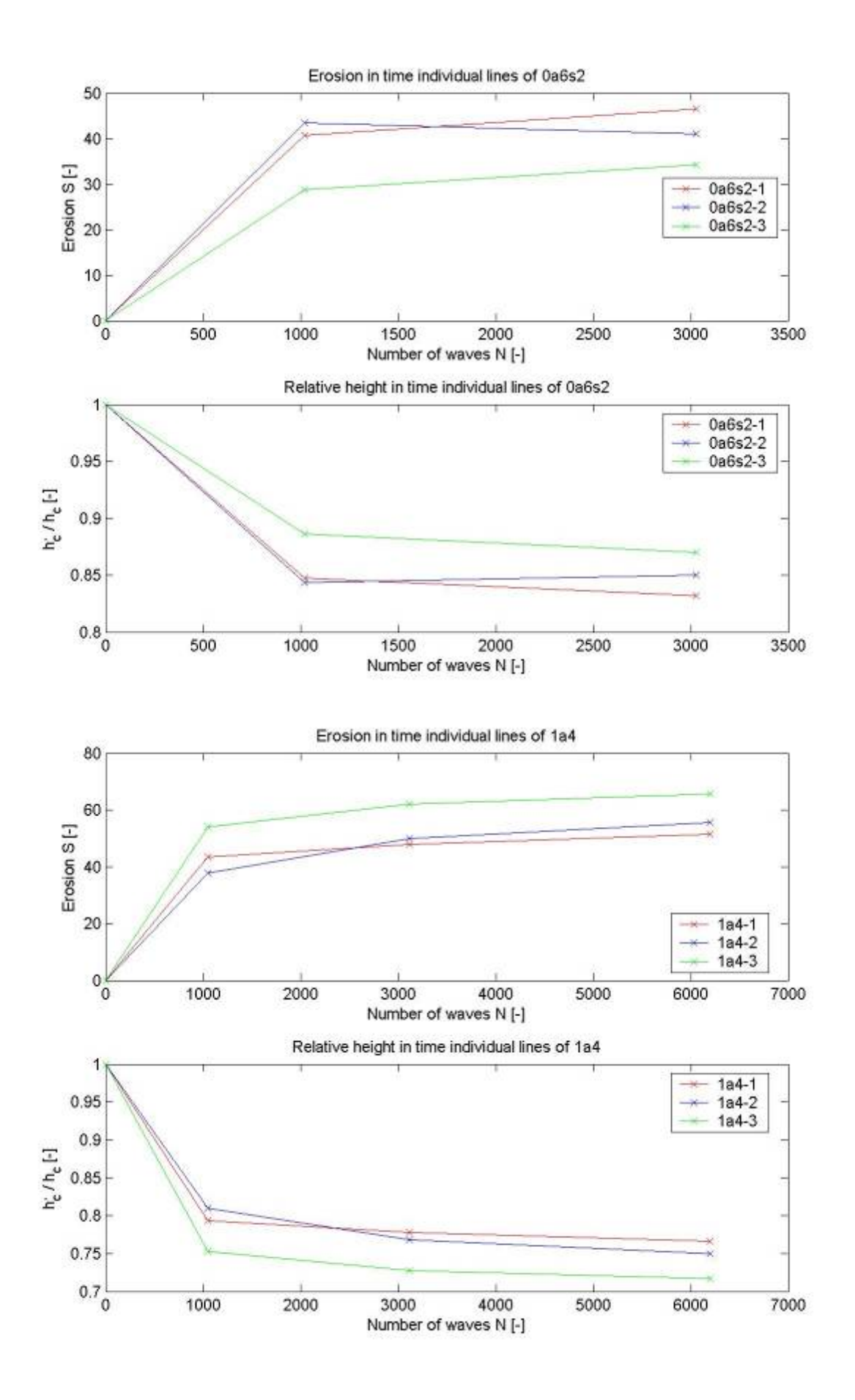
In this appendix all the data of the erosion number $S = A_e/D_{n50}^2$ and the relative height h_c/h_c are displayed against the number of waves for each test. For the erosion number the logarithmic relation between the erosion and the number of waves can be seen. The relative height is the identical graph as the graph for the second approach in section 5.3 but for each test and with the points connected (same profile position but after more waves).

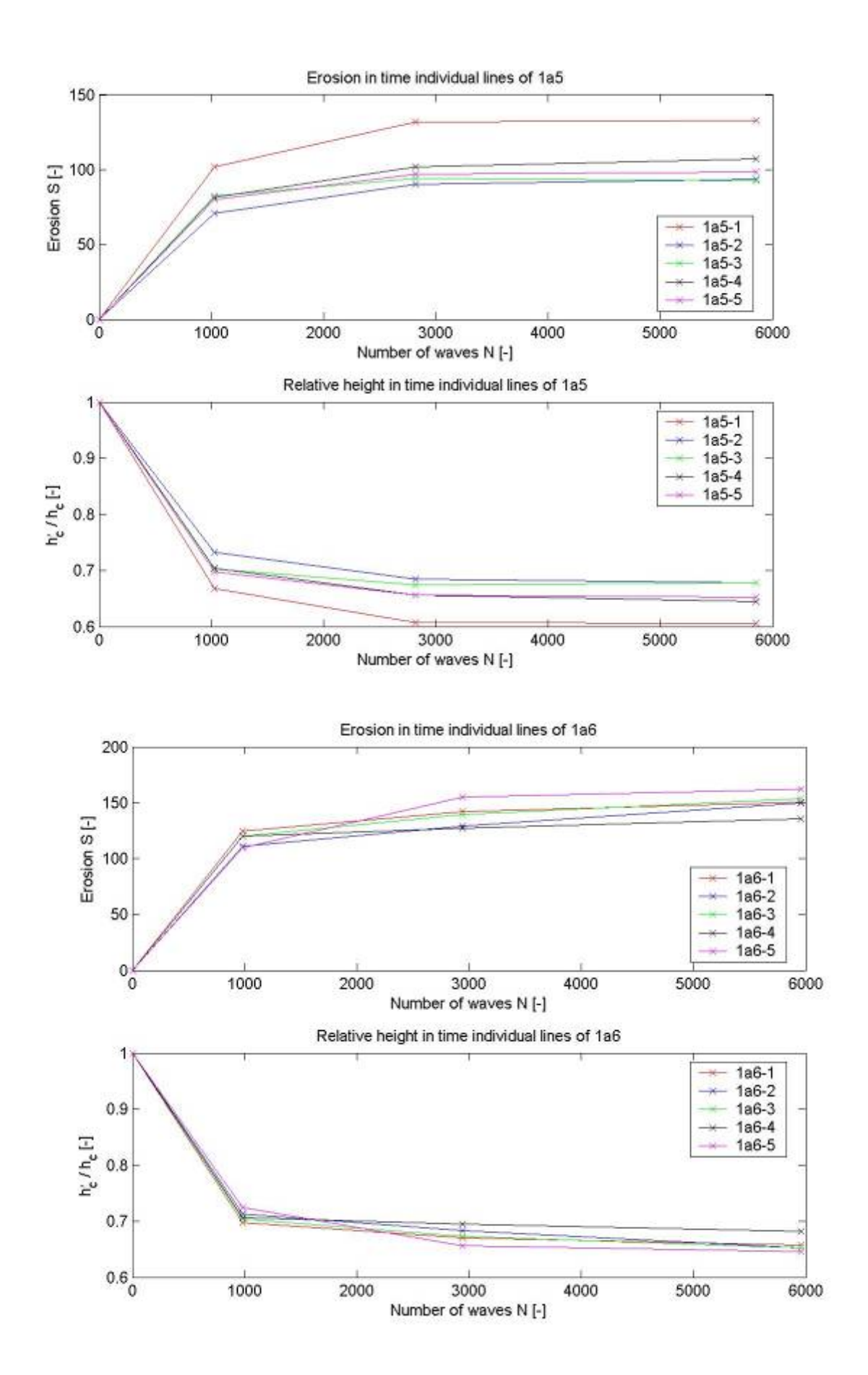
Plots of the erosion number and the relative height in time

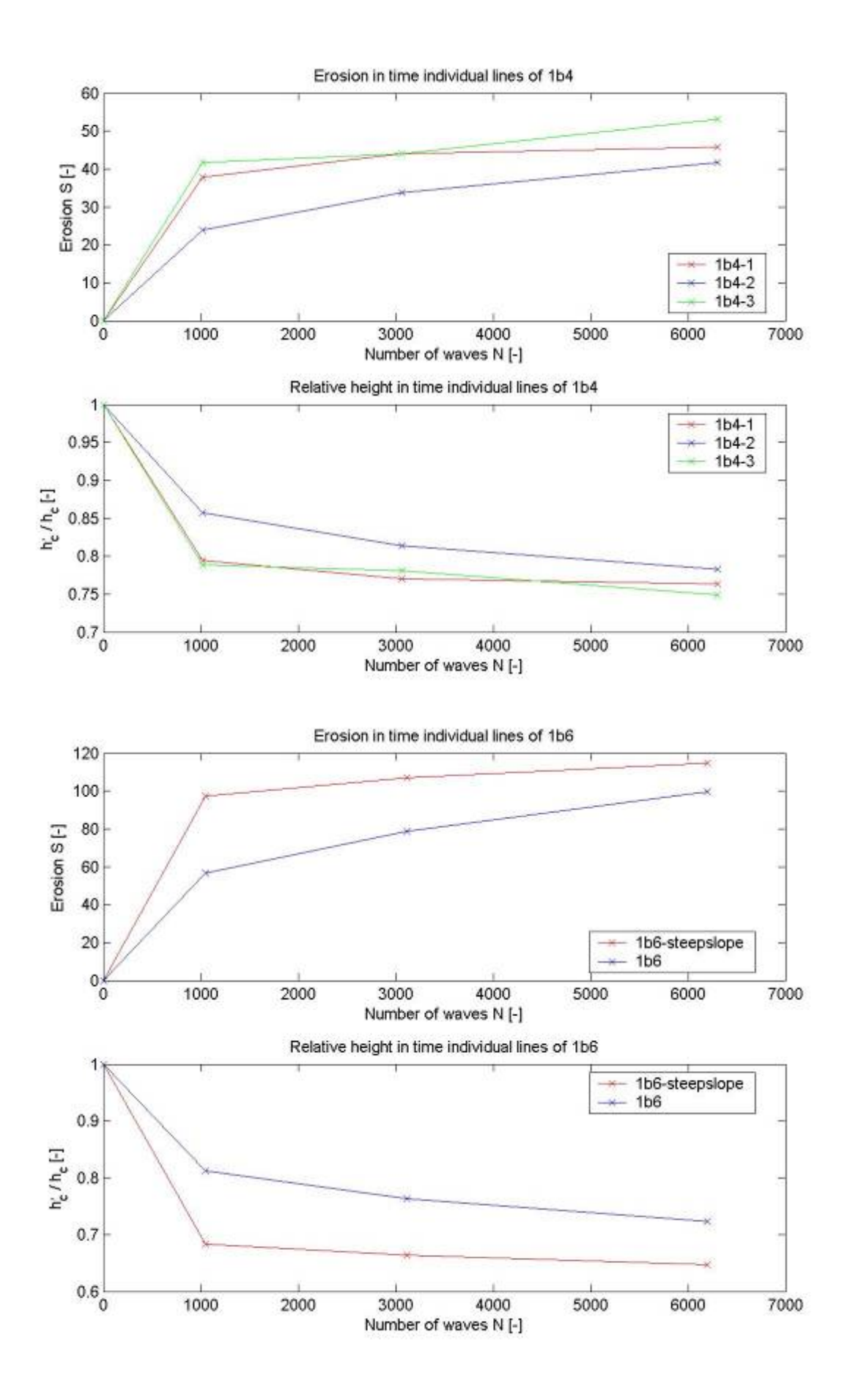
Here all the plots of the erosion and relative height in time are given for each test. The test codes are:

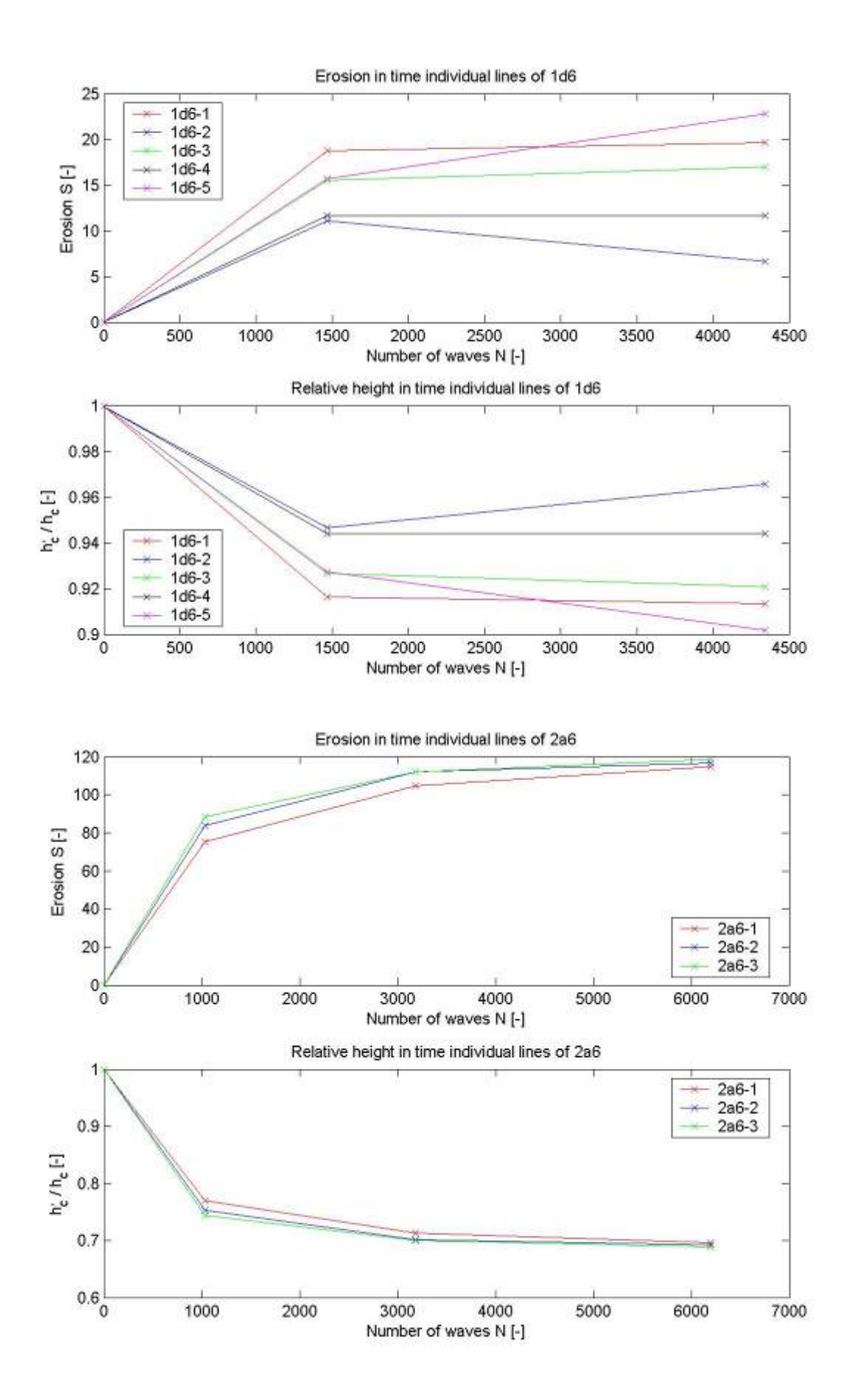
0a6, 0a6s2, 1a4, 1a5, 1a6, 1b4, 1b6, 1d6, 2a6, 2b4, 2b5, 2b6, 3b4, 3b5, 3b6 and her1a6.

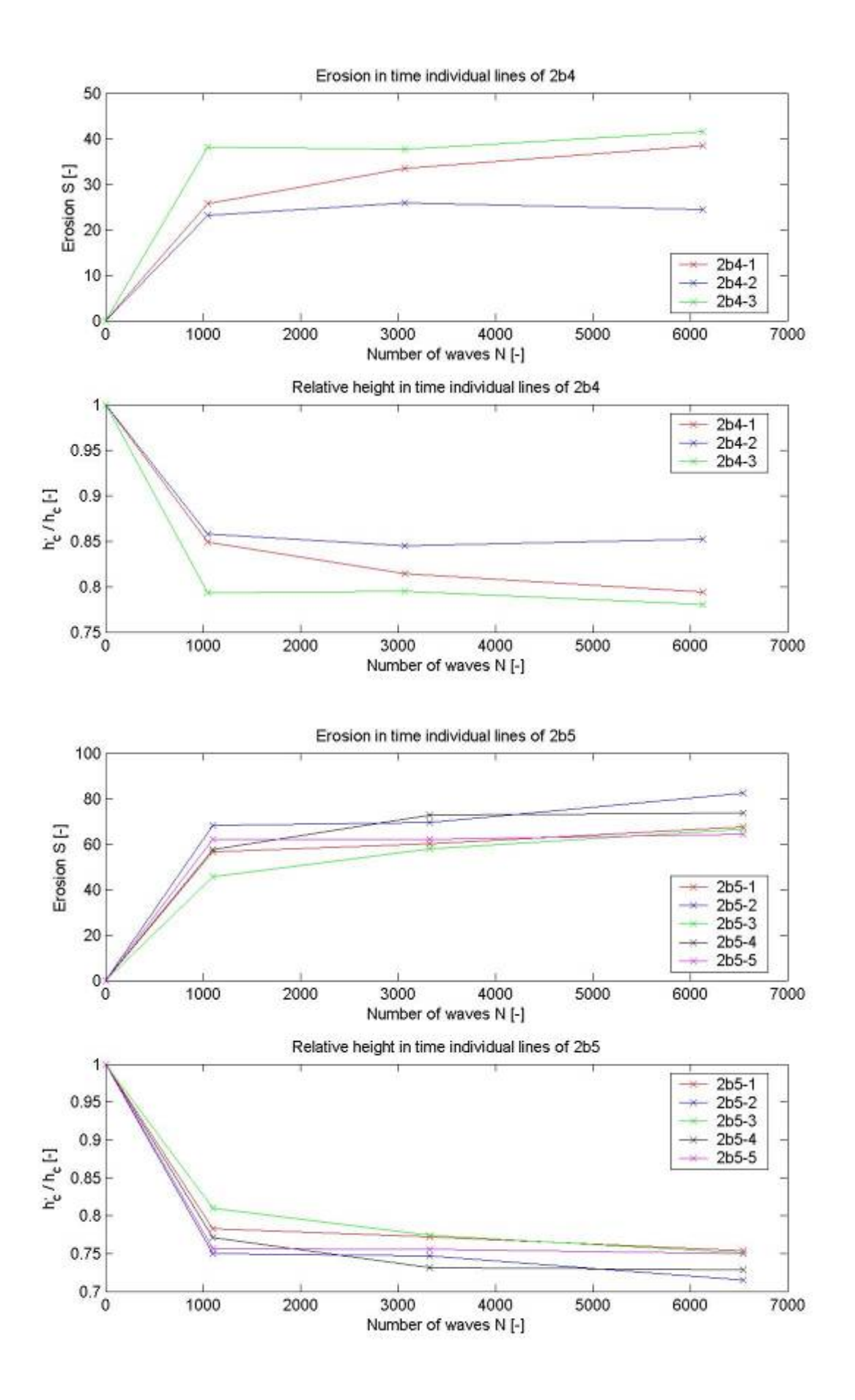


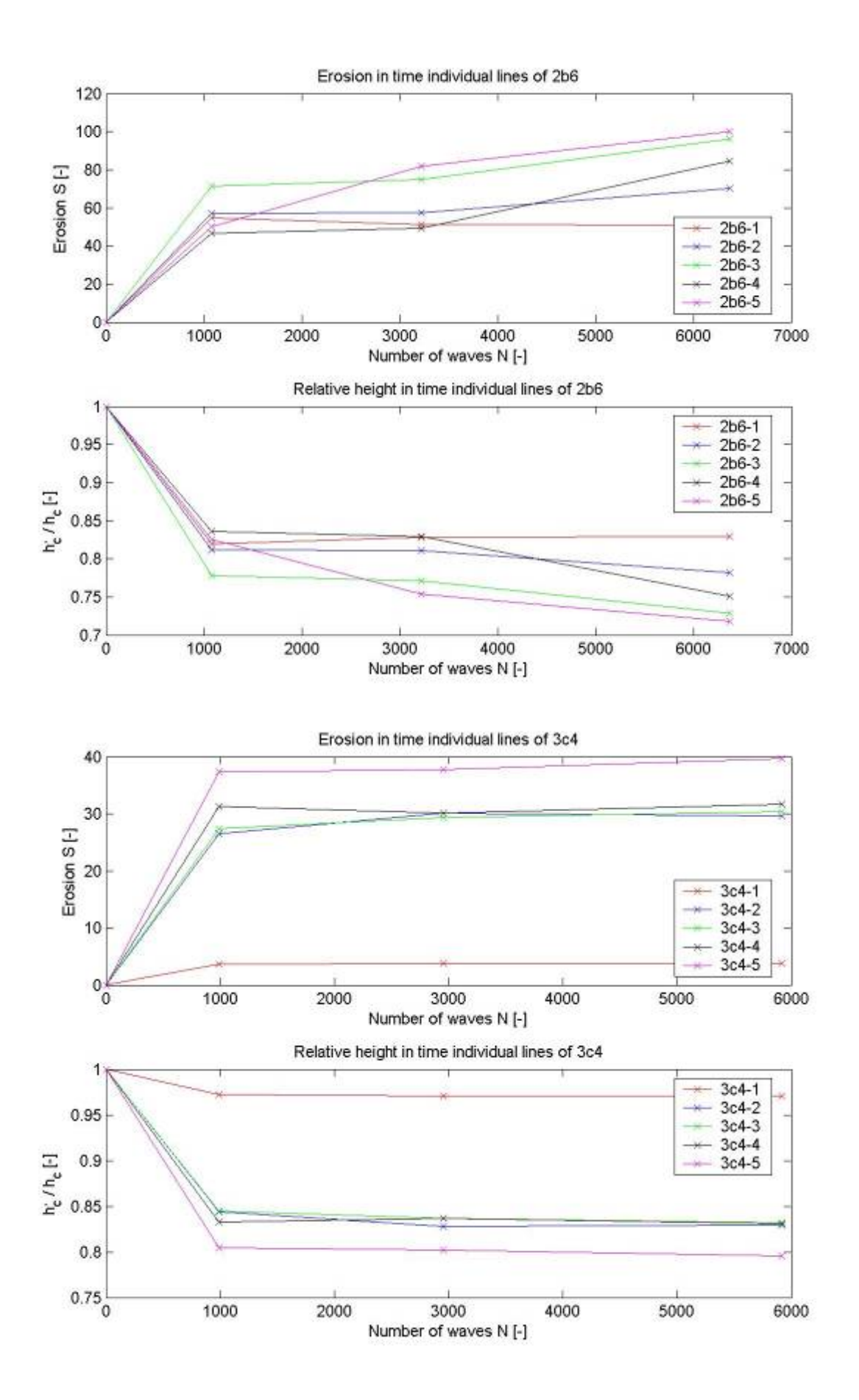


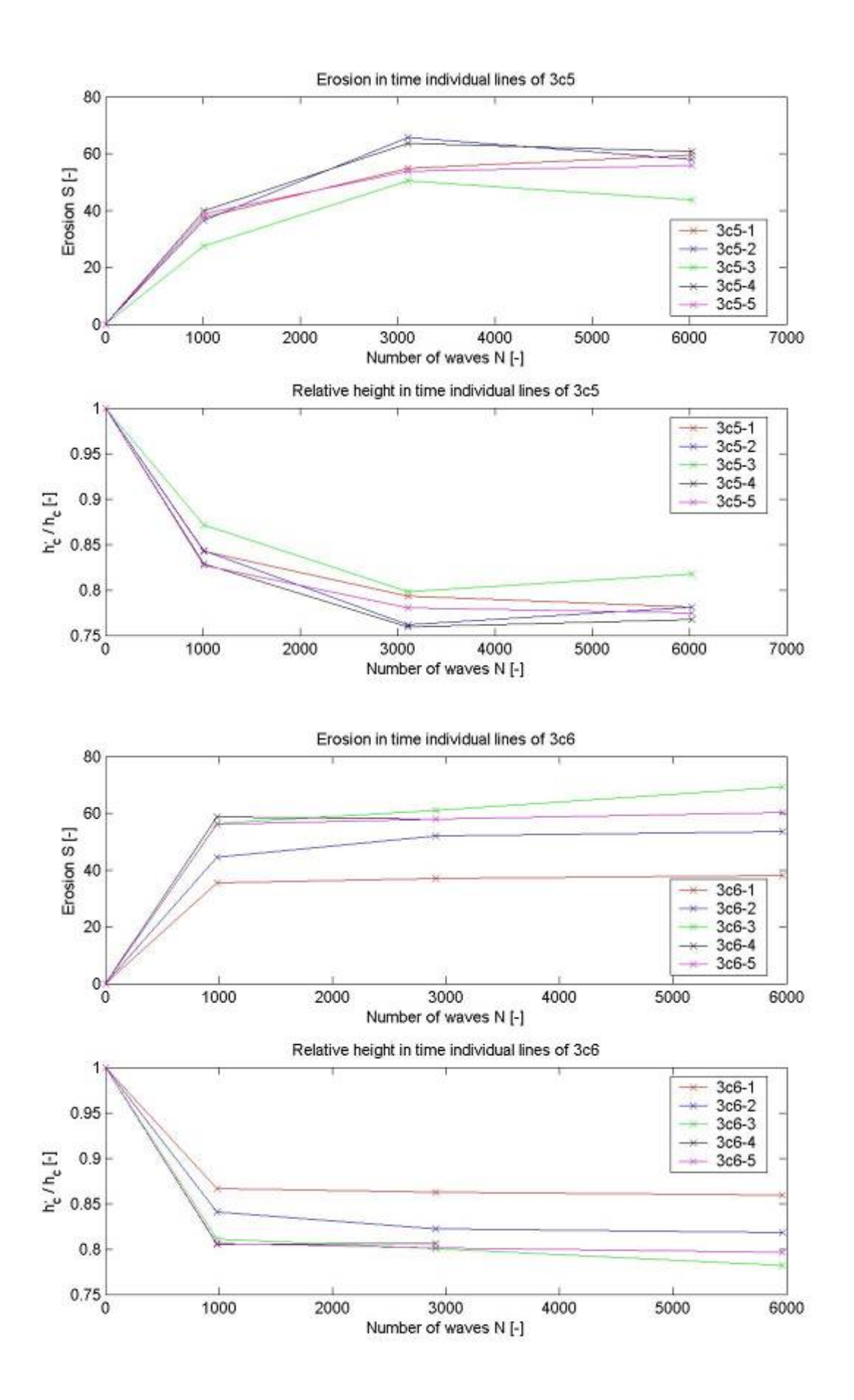


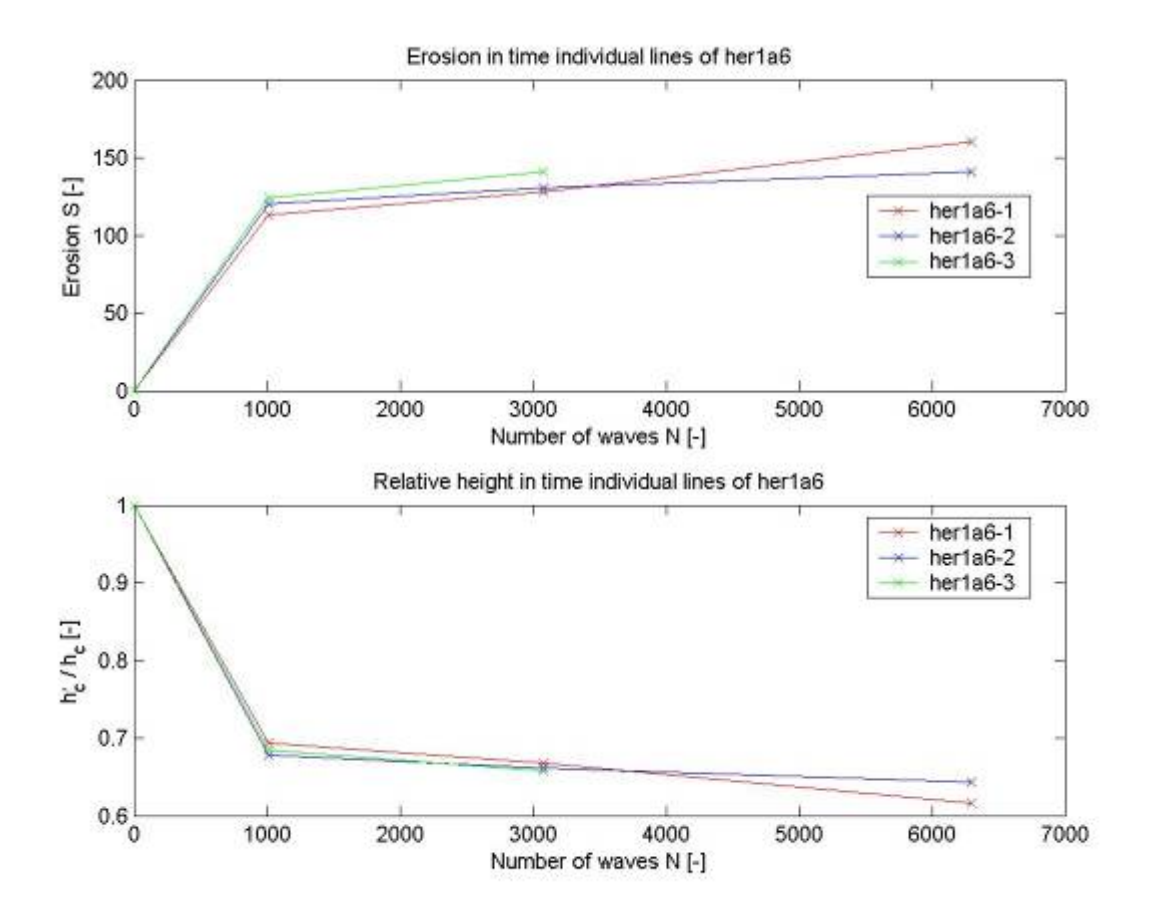












Remarks

In principle the erosion number is always growing in time. In 1d6 this is not the case because hardly any erosion took place and inaccuracies on the Provo measuring system give variation in the data. When damage occurs this variation will be relatively small.

When test 3c4 is concerned, one line gives low erosion compared to the other 3c4-lines. This can be a coincidence (outside a 95 % confidence interval). The hydraulic load for this test was small and the stones were almost stable and reached stable positions before 1000 waves as can be seen in the figure of 3c4. In this way a profile that is stable from the first wave is possible due to factors as favourable positioning of the stones compared to each other (interlocking and sheltering).

Appendix H: Matlab script listings

During the analysis of the experiment many Matlab files have been programmed in order to process the data. In this appendix the listings of some of those programs will be given. This will be done because after completion of this thesis someone else has to perform the same analysis, but then for different water depths. So sharing the m-files can help him.

Provo data calibration with the measuring carriage speed correction is done in the m-file Bepaalvkar (all M-files titles are marked gray and can be seen as Matlab scripts within the main script).

In this appendix the main Matlab script will be given for a test (e.g. 1a4). Of each M-file within the main file also a listing will be given. The M files in the main script are: Bepaalvkar, bepaalschade, golventellen and testplot2.

The Matlab script listings will be shown in the following part of this appendix.

Main Matlab script for a test

Here the listings of the main Matlab script for the example test 1a4 will be given.

```
%load file name
   close all;
   clear all;
   %load file name
   N=1;
   y=[]; [t y]=textread('0-1a4-1.asc','%f %f','headerlines',20); referentie;gemprofiel;
gemy01 = gemy; Y01=Y; gemy=[];
   y=[]; [t y]=textread('1-1a4-1.asc','%f %f','headerlines',20); referentie;gemprofiel;
gemy11 = gemy; Y11=Y; gemy=[];
   y=[]; [t y]=textread('2-1a4-1.asc','%f %f','headerlines',20); referentie;gemprofiel;
gemy21 = gemy; Y21=Y; gemy=[];
   y=[]; [t y]=textread('3-1a4-1.asc','%f %f','headerlines',20); referentie;gemprofiel;
gemy31 = gemy; Y31=Y; gemy=[];
   y=[]; [t y]=textread('0-1a4-2.asc','%f %f','headerlines',20); referentie; gemprofiel;
gemy02 = gemy; Y02=Y; gemy=[];
   y=[]; [t y]=textread('1-1a4-2.asc','%f %f','headerlines',20); referentie; gemprofiel;
gemy12 = gemy; Y12=Y; gemy=[];
   y=[]; [t y]=textread('2-1a4-2.asc','%f %f','headerlines',20); referentie;gemprofiel;
gemy22 = gemy; Y22=Y; gemy=[];
   y=[]; [t y]=textread('3-1a4-2.asc','%f %f','headerlines',20); referentie;gemprofiel;
gemy32 = gemy; Y32=Y; gemy=[];
```

```
y=[]; [t y]=textread('0-1a4-3.asc','%f %f','headerlines',20); referentie;gemprofiel;
gemy03 = gemy; Y03=Y; gemy=[];
   y=[]; [t y]=textread('1-1a4-3.asc','%f %f','headerlines',20); referentie; gemprofiel;
gemy13 = gemy; Y13=Y; gemy=[];
   y=[]; [t y]=textread('2-1a4-3.asc','%f %f','headerlines',20); referentie; gemprofiel;
gemy23 = gemy; Y23=Y; gemy=[];
   y=[]; [t y]=textread('3-1a4-3.asc','%f %f','headerlines',20); referentie; gemprofiel;
gemy33 = gemy; Y33=Y; gemy=[];
   %invoer van rij van aantal golven
   %eerst gelijk knippen gemy's
   gemy01(length(gemy01):N)=zeros;
   gemy11(length(gemy11):N)=zeros;
   gemy21(length(gemy21):N)=zeros;
   gemy31(length(gemy31):N)=zeros;
   gemy02(length(gemy02):N)=zeros;
   gemy12(length(gemy12):N)=zeros;
   gemy22(length(gemy22):N)=zeros;
   gemy32(length(gemy32):N)=zeros;
   gemy03(length(gemy03):N)=zeros;
   gemy13(length(gemy13):N)=zeros;
   gemy23(length(gemy23):N)=zeros;
   gemy33(length(gemy33):N)=zeros;
   %laden van profielmatrix
   A=[];
   A(1,1,:)=gemy01;
   A(1,2,:)=gemy11;
   A(1,3,:)=gemy21;
   A(1,4,:)=gemy31;
   A(2,1:)=gemy02:
   A(2,2,:)=gemy12;
   A(2,3,:)=gemy22;
   A(2,4,:)=gemy32;
   A(3,1,:)=gemy03;
   A(3,2,:)=gemy13;
   A(3,3,:)=gemy23;
   A(3,4,:) = gemy33;
   %bepaal snelheid kar met provo en daaruit direct per test de delta x
   %bepalen.
```

bepaalvkar;

```
%Schade matrix S alleen oppervlak later dimensieloos maken
S=[];
S=zeros(3,1);
for i=1:3;
  for j=1:3;
    bepaalschade;
    k=0:
    while k < length(schade)
         k=k+1;
         if schade(k)<0
           schade(k)=0;
            if k>700
              schade(k:length(schade))=0;
              k= length(schade);
            end
         end
    end
    S(i,j+1)=sum(schade);
  end
end
%Volumematrix
%neem einde gewoon 2400 hier
hulp=zeros(3,4);
for i=1:3;
  % maal individuele dx:
  V(i,1:4) = sum(A(i,1,600:2400)) * A(i,1,1);
  %volumebehoud tabel:
  for j=1:4
  Volumebehoud(i,j)=sum(A(i,j,600:2400)) * A(i,j,1);
  %hooge matrix maken met abc-formule
  hoogte(i,1:4)= ((4^2+10*V(i,1))^5 - 4)/5;
  %nu schade oppervlak erafhalen met abc formule
    for j=1:3
    for k=2:4
       hulp(j,k) = ((4^2+10*S(j,k))^5.5-4)/5;
    end
  end
end
hoogte=hoogte-hulp;
hoogte(3+1,:)=mean(hoogte);
for i=1:4
```

```
hoogte(3+2,i)=std(hoogte(1:3,i));
   end
   hoogterelatief=[];
   for i=1:4;
   hoogterelatief(i,:) = hoogte(i,:) / hoogte(i,1);
   end
   V=V-S;
   V(3+1,:)=mean(V);
   V(3+2,:)=std(V(1:3,:));
   S(3+1,:)=mean(S);
   %relatieve volume matrix maken
   Vrelatief=[];
   for i=1:4;
     Vrelatief(i,:) = V(i,:) / V(i,1);
   end
   %dan schade dimensieloos maken met dn50. d50 = 0.44cm, dn50 = 0.84*0.44 = 0.37
cm
   %dus S = S * 1/0.37^2 = maat voor aantal stenen binnen 1 profiel.
   S = S * (1/0.37^2);
   %gemiddelde toevoegen aan profielen
   A(3+1,:,:)=mean(A);
   % creatie beginvolumes en hoogtes in tabel vorm
   [Q,M]=size(V);
   begingemiddeldenher1a6=V(Q-1:Q,1)';
   [O,M]=size(hoogte);
   begingemiddeldenher1a6(3:4)=hoogte(Q-1:Q,1)';
   %------plotblok-----
   % creatie tabel met aantal golven en schade
   golventellen;
   [Q,M]=size(Ng);
   Nk=Ng(1:M-1);
   testplot2;
```

```
Schadetabel=S';
[Q,M]=size(Schadetabel);
Schadetabel(1,:)=[];
Schadetabel(:,M)=[];
aantalgolven=Ng';
aantalgolven(1)=[];
Schadetabel(:,M)=[aantalgolven];
```

Listings of the M-files within of the main Matlab script

The parts of the main Matlab scripts called subscripts (Bepaalvkar, bepaalschade, golventellen, testplot2) will be displayed here.

Bepaalvkar;

```
vkar=[];
[RijA,KolomA, N] = size(A);
vkar=zeros(RijA,KolomA);
for k=1:KolomA
for i=1:RijA
if k==1
  top = 3/4 * max(A(i,k,:));
  j=2;
  while j \le N
     if A(i,k,j-1) \le top \& A(i,k,j) > top
       punt1=i;
     elseif A(i,k,j-1) \ge top & A(i,k,j) \le top
        punt2=j;
       j=N;
     end
     j=j+1;
  end
  %snelheid kar=afstand gedeeld door benodigde tijd dus in cm per sec:
  %alleen geldend voor de eerste kolom
  vkar(i,1)=(40.3/(0.05*(punt1+punt2)/2))';
else
     refpunt = 1/3 * max(A(i,1,:));
  j=2;
  while i < N
     if A(i,1,j-1) \le \text{refpunt & } A(i,1,j) > \text{refpunt}
       punt1=j;
       j=N;
     end
     j=j+1;
  end
  j=2;
  while j < N
     if A(i,k,j-1) \le \text{refpunt } \& A(i,k,j) > \text{refpunt}
       punt2=j;
       j=N;
     end
     j=j+1;
  end
```

```
%snelheid kar als nominale snelheid maal factor
          vkar(i,k) = vkar(i,1) * (punt1/punt2);
       end
       end
       end
       dxmatrix = vkar*0.05;
       %snelheid van de kar plaatsen in totaal matrix
       A(:,:,1) = dxmatrix;
bepaalschade;
       schade=[];
       y=[];
       xfactor = A(i,j+1,1)/A(i,1,1);
       a=[];
       a = reshape(A(i,1,:),[N,1]);
       b = reshape(A(i,j+1,:),[N,1]);
       %bepaal einde
       einde = length(a)-100;
       if x factor < 1
         einde = (length(a)*xfactor) -100;
       end
       for tellera = 2:floor(einde)
         realxb = tellera / xfactor;
         k=floor(realxb);
         %nu interpoleren met x2-x1=1 en valt dus weg
         y = b(k) + ((b(k+1)-b(k)) * (realxb-k));
         schade(tellera) = a(tellera) - y;
       end
       schade = schade * A(i,1,1);
       schade(1:750)=[];
golventellen;
       hmin=1.0;
       Nher1a6=[];
       Nher1a6(1)=0;
```

```
for j=1:3
```

figure(5)

```
GHM=[]; [onzin onzin onzin GHM]=textread(['C:\Documents and
   Settings\saers.WAVL\Bureaublad\Wouter\Metingen wouter\1a4\GHM\1a4-' num2str(j)
   '.ASC'],'%f %f %f %f','headerlines',20);
       %consequent de 3e GHM boven constructie nemen
       h=GHM;
       h=h-mean(h);
       [Q,M]=size(h);
       %knippen van tijdsignaal
       i=1;
       while i<Q;
         if h(i)>hmin;
           begin=i;
           i=Q;
         end
        i=i+1;
       end
       i=Q;
       while i>2;
         if h(i)>hmin;
           eind=i;
           i=1;
         end
         i=i-1;
       % tellen van golven binnen geknipt stuk
       N=0;
       for i=begin:eind;
         if h(i) \le 0.5 \& h(i+1) > 0.5;
                N = N+1;
              end
       end
       Nher1a6(j+1)= Nher1a6(j)+N;
       end
       Ng=Nher1a6
testplot2;
       [Q,M,N]=size(A);
```

```
for i=1:3
    for j=1:3
       subplot(3,2,i);
       a=[];
       a = reshape(A(i,j,:),[N,1]);
       t=[];
       t=0:a(1):a(1)*(N-1);
       plot(t,a);
       xlim([15 80])
       ylim([-1 7])
       if i == 1
          hold;
       end
    end
    a=[];
     a = reshape(A(i,3,:),[N,1]);
     t=[];
     t=0:a(1):a(1)*(N-1);
     plot(t,a, 'r');
     title(['verloop lijn' num2str(i)]), grid
     ylabel('hoogte [cm]');
     xlabel('afstand in goot [cm]');
  end
subplot(3,2,4);
plot(Ng, Vrelatief(1,:), 'rx-', Ng, Vrelatief(2,:), 'bx-', Ng, Vrelatief(3,:), 'gx-')
legend('lijn 1','lijn 2','lijn 3',0);
title('relatief volume individuele lijnen 1a4');
xlabel('N (aantal golven) [-]');
ylabel('V / Vbegin [-]');
ylim([0.55 1]);
subplot(3,2,5);
plot(Ng,S(1,:),'rx-',Ng,S(2,:),'bx-',Ng,S(3,:),'gx-')
legend('lijn 1','lijn 2','lijn 3',0);
title('schade verloop individuele lijnen 1a4');
xlabel('N (aantal golven) [-]');
ylabel('Schade [-]');
       ylim([0\ 200])
subplot(3,2,6);
plot(Ng,hoogterelatief(1,:),'rx-',Ng,hoogterelatief(2,:),'bx-',Ng,hoogterelatief(3,:),'gx-')
legend('lijn 1','lijn 2','lijn 3',0);
title('relatieve hoogte individuele lijnen 1a4');
xlabel('N (aantal golven) [-]');
ylabel('hoogte / hoogtebegin [-]');
```

ylim([0.55 1])

 $saveas (5, C: \Documents\ and\ Settings \saers. WAVL \Bureaublad \Verwerk tedata \1a4 \overzicht -1a4.pdf', 'pdf')$